GRADUATE COLLEGE

STUDIES ON SELECTED ENZYMES OF THE α-AMINOADIPATE PATHWAY FOR LYSINE BIOSYNTHESIS IN *Saccharomyces cerevisiae*

A Dissertation

SUBMITTED TO THE GRADUATE FACULTY

In partial fulfillment of the requirement for the

Degree of

Doctor of Philosophy

By

BABAK ANDI
Norman, Oklahoma
2005

Downloaded from SHAREOK. Persistent Handle URL: https://hdl.handle.net/11244/944

UMI Number: 3203304

UMI®

UMI Microform 3203304

Copyright 2006 by ProQuest Information and Learning Company.
All rights reserved. This microform edition is protected against
unauthorized copying under Title 17, United States Code.

ProQuest Information and Learning Company
300 North Zeeb Road
P.O. Box 1346
Ann Arbor, MI 48106-1346

STUDIES ON SELECTED ENZYMES OF THE α-AMINOADIPATE PATHWAY FOR LYSINE BIOSYNTHESIS IN *Saccharomyces cerevisiae*

A Dissertation APPROVED FOR THE
DEPARTMENT OF CHEMISTRY AND BIOCHEMISTRY

BY

Paul F. Cook, Ph.D.

Ann H. West, Ph.D.

Phillip E. Klebba, Ph.D.

Ralph A. Wheeler, Ph.D.

Roger G. Harrison Jr.,Ph.D.

© Copyright by BABAK ANDI 2005
All Rights Reserved

The Prologue to *Bertrand Russell's Autobiography

What I Have Lived For

Three passions, simple but overwhelmingly strong, have governed my life: the longing for love, the search for knowledge, and unbearable pity for the suffering of mankind. These passions, like great winds, have blown me hither and thither, in a wayward course, over a great ocean of anguish, reaching to the very verge of despair.

I have sought love, first, because it brings ecstasy - ecstasy so great that I would often have sacrificed all the rest of life for a few hours of this joy. I have sought it, next, because it relieves loneliness--that terrible loneliness in which one shivering consciousness looks over the rim of the world into the cold unfathomable lifeless abyss. I have sought it finally, because in the union of love I have seen, in a mystic miniature, the prefiguring vision of the heaven that saints and poets have imagined. This is what I sought, and though it might seem too good for human life, this is what--at last--I have found.

With equal passion I have sought knowledge. I have wished to understand the hearts of men. I have wished to know why the stars shine. And I have tried to apprehend the Pythagorean power by which number holds sway above the flux. A little of this, but not much, I have achieved.

Love and knowledge, so far as they were possible, led upward toward the heavens. But always pity brought me back to earth. Echoes of cries of pain reverberate in my heart. Children in famine, victims tortured by oppressors, helpless old people a burden to their sons, and the whole world of loneliness, poverty, and pain make a mockery of what human life should be. I long to alleviate this evil, but I cannot, and I too suffer.

This has been my life. I have found it worth living, and would gladly live it again if the chance were offered me.

*Bertrand Russell (1872-1970) won the Nobel prize for literature for his *History of Western Philosophy* and was the co-author of *Principia Mathematica*.
(http://www.users.drew.edu/%7Ejlenz/prolog.html)

ACKNOWLEDGEMENTS

First I would like to express my heartiest gratitude to Dr. Paul. F. Cook and Dr. Ann H. West for allowing me to join their research groups and being my advisors and for everything they have taught me during my period of graduate research. I am greatly honored to be able to work with these two outstanding scientists, receiving valuable opportunities, excellent ideas, encouragement and freedom throughout. I will never forget their kindness, enthusiasm, good-will and above all their friendship.

I am also grateful to all members of my graduate committee, at the University of Oklahoma for admitting me to candidacy and for their advice, guidance and encouragement throughout my graduate education. My committee includes the following professors: Dr. Bruce A. Roe, Dr. Helen I. Zgurskaya, Dr. Phillip E. Klebba, Dr. Ralph A. Wheeler, and Dr. Roger G. Harrison Jr, who have always served their best for my success from the moment of my proposal defense to the moment of defending my dissertation.

It has been enormous pleasure to have worked with my colleagues in Dr. Cook's and Dr. West's research groups. My special thanks go to Dr. William E. Karsten and his wife Dr. Lillian Chooback for teaching me most of the biochemical methods for enzyme kinetics and protein crystallization. I massively appreciate their kindness and approachability. I am thankful to Dr. Eric Enwall and D. Bryan Prince for their great assistance on X-ray data collection. I would like to remember Dr. Wael Rabeh and Dr.

Corey M. Johnson with gratitude, for their technical assistance on analytical methods and data analysis. I am also grateful to Daniel Copeland for his technical assistance for macromolecular model building. I wish to extend my appreciation to Dr. Fabiola Janiak Spens, Dr. Stace Porter and Hui (Toni) Tan for their discussions about molecular biology experiments. It's my pleasure to acknowledge Jean Keil for helping me through all of the paperwork and administrative issues.

I indeed enjoyed the friendly and cheerful atmosphere in Dr. Cook's and Dr. West's labs. All members in these labs, Deniz Aktas, Mamar Baizid, Alla Dubrovska, Devi Ekanayake, Jennifer Gray, Rong Guan, Lei Li, Dali Liu, Jinghua (Edmond) Qian, Ashwani Vashishtha, and Hengyu (Carina) Xu, are gratefully appreciated for being so nice, supportive and helpful.

I also wish to thank many others, whom I may have never met in person or knew their names, but shared their thoughts and experiences with me by different ways and means helping me anonymously through all the different stages of my research project.

It is my pleasure to remember all my sincere friends at the University of Oklahoma, who gave me friendship, company and care. I would like to thank Timothy M. Click for helping me on Linux computer operating system. Also, Mohammad

Hajjari and Amin Parnian are deeply appreciated for giving care and offering me their help whenever it was needed.

I am very much obliged to my cousin Maryam Rangbast and my cousins-in-laws Babak Hooshiarnejad and Mohammad Mahmoodifar for their continuing support and encouragement given to me and also for being with me, sharing all my ups and downs whenever needed.

Finally, I am infinitely grateful to my life's greatest blessings, my adorable parents Esfandiar Andi and Raheleh Rangbast and also my loving sister and brother, Bahareh and Mehrdad for their immense love, encouragement and never-ending support. I am ever indebted to all devotions they have done so far, while cheering me up, and keeping up my good spirits with the noble aim of creating a well-accomplished future for me. This dissertation would be a mission-impossible without them being a part of my life.

All the work in this dissertation were supported by a grant in aid from the Office of the Research and Administration at the University of Oklahoma to P.F.C. and A.H.W., a grant from NIH to P.F.C. and A.H.W. (GM 071417) and by the Grayce B. Kerr endowment to the University of Oklahoma for the research of P.F.C.

TABLE OF CONTENTS

Prologue **iv**
Acknowledgements **v**
Table of Contents **viii**
List of Tables **xii**
List of Illustrations **xiii**
List of Schemes **xvi**
List of Abbreviations **xvii**
Abstract **xx**

CHAPTER 1 Introduction **1**

1-1. Amino acid biosynthesis in brief 1
1-2. Biosynthesis of lysine 2
1-2-1. Diaminopimelate pathway of L-Lysine biosynthesis 2
1-2-2. α-Aminoadipate pathway of L-Lysine biosynthesis 3
1-2-3. Significance of the α-aminoadipate pathway 8
1-2-4. Regulation of the α-Aminoadipate pathway 8
1-2-4-1. Genetic regulation 9
1-2-4-2. Regulation of enzyme activity 11
1-3. Enzymes of the α-aminoadipate pathway 12
1-3-1. Enzyme-catalyzed Claisen condensation of AcCoA and α-ketoacids 12
1-3-2. Homocitrate synthase 15
1-3-2-1. Location of HCS 15
1-3-2-2. Expression, purification, and characterization 15
1-3-2-3. Kinetic mechanism 17
1-3-3. Homoaconitase 18
1-3-4. Homoisocitrate dehydrogenase 18
1-3-5. α-Aminoadipate aminotransferase 18
1-3-6. α-Aminoadipate reductase 19
1-3-7. Saccharopine reductase 22
1-3-7-1. Expression, purification, and characterization 22
1-3-7-2. Structure 24
1-3-7-3. Chemical mechanism 26
1-3-8. Saccharopine dehydrogenase 28
1-3-8-1. Expression, purification, and characterization 28
1-3-8-2. Kinetic mechanism 28
1-3-8-3. Chemical mechanism 30
1-4. Summary 32
References 34

CHAPTER 2 Stabilization and characterization of homocitrate synthase 45

2-1. Introduction 45
2-2. Materials and methods 47
2-2-1. Chemicals 47
2-2-2. Cell growth and protein expression 48
2-2-3. Enzyme assay 49
2-2-4. Stoichiometry of the reaction of DCPIP with CoASH 49
2-2-5. Stabilization of HCS 50
2-2-6. Size exclusion chromatography – HPLC 51
2-2-7. Fluorescence studies of HCS 51
2-2-8. Circular dichroism studies 55
2-2-9. Ultraviolet spectra 55
2-3. Results and discussion 56
2-3-1. Cell growth and protein expression 56
2-3-2. Enzyme assay 57
2-3-3. Stoichiometry of the reaction of DCPIP with CoASH 59
2-3-4. Stabilization of HCS 59
2-3-5. Size exclusion chromatography – HPLC 62
2-3-6. Fluorescence studies of HCS 64
2-3-7. Circular dichroism studies 68
2-3-8. Ultraviolet spectra 69
2-4. Conclusion 70
2-5. Acknowledgements 70
References 71

CHAPTER 3 Kinetic mechanism of homocitrate synthase 74

3-1. Introduction 75
3-2. Materials and methods 75
3-2-1. Materials 75
3-2-2. Assays of homocitrate synthase activity 76
3-2-3. Initial velocity studies 77
3-2-4. Inhibition studies 78
3-2-5. Fluorescence determination of the HCS-ligand dissociation constant 79
3-2-6. Data analysis 80
3-3. Results 81
3-3-1. Initial velocity studies 81
3-3-2. Product inhibition studies 83
3-3-3. Dead-end inhibition studies 83
3-3-4. Fluorescence Studies 85
3-4. Discussion 87
3-4-1. Quantitative analysis of inhibition data 88
3-4-2. Fluorescence binding studies 92

3-4-3. Active site specificity and kinetic mechanism 93
3-5. Acknowledgements 95
References 95

CHAPTER 4 Regulatory mechanism of homocitrate synthase: I 97

4-1. Introduction 97
4-2. Materials and methods 99
4-2-1. Materials 99
4-2-2. Assays of homocitrate synthase activity 99
4-2-3. Initial velocity studies 100
4-2-4. Fluorescence binding studies 101
4-2-5. Effect of monovalent and divalent cations on HCS activity 102
4-2-6. Data analysis 103
4-3. Results 104
4-3-1. Initial rate studies of lysine inhibition 104
4-3-2. Initial rate studies of sodium inhibition and activation 108
4-3-3. Effect of lysine and Na^+ 110
4-3-4. Fluorescence determination of the HCS-ligand dissociation constant 110
4-3-5. Effect of monovalent and divalent cations on HCS activity 110
4-4. Discussion 116
4-4-1. Inhibition by lysine 116
4-4-2. The Na^+ effect 118
4-4-3. Interaction of Na^+ and lysine 122
4-4-4. Effect of other monovalent cations and divalent cations on HCS activity 124
4-4-5. Physiologic significance 125
4-5. Acknowledgements 126
References 126

CHAPTER 5 Regulatory mechanism of homocitrate synthase: II 129

5-1. Introduction 129
5-2. Materials and methods 129
5-2-1. Data analysis and simulation 129
5-3. Theory 129
5-4. Results and discussion 143
References 156

CHAPTER 6 Crystal structure of saccharopine reductase 158

6-1. Introduction 158
6-2. Materials and methods 160
6-2-1. Materials 160
6-2-2. Construction of the saccharopine reductase expression plasmid 160

6-2-3. Expression and purification of saccharopine reductase 161
6-2-4. Enzyme assay 162
6-2-5. Protein crystallization 162
6-2-6. Data collection and processing 163
6-2-7. Molecular replacement, model building, structure refinement 163
6-2-8. Molecular graphics 165
6-3. Results 165
6-3-1. Expression and purification of saccharopine reductase 165
6-3-2. Proteine crystallization 165
6-3-3. Activity 166
6-3-4. Data collection and processing 166
6-3-5. Molecular replacement, model building, structure refinement 168
6-3-6. Overall structure 169
6-4. Discussion 173
6-5. Acknowledgements 181
References 181

APPENDIX **185**

LIST OF TABLES

CHAPTER 1 Introduction **1**

Table 1-1. Genes and enzymes involved in the α–aminoadipate pathway in *S. cerevisiae* 4

CHAPTER 2 Stabilization and characterization of homocitrate synthase **45**

Table 2-1. Matrix of co-solute combinations used to determine optimum conditions for stabilization of HCS 53
Table 2-2. Kinetic parameters for homocitrate synthase (graphical analysis) 58
Table 2-3. Fluorescence quenching parameters for homocitrate synthase 66

CHAPTER 3 Kinetic mechanism of homocitrate synthase **74**

Table 3-1. Kinetic parameters for HCS 82
Table 3-2. Inhibition kinetic constants for product and dead-end inhibitors of HCS 84
Table 3-3. Dissociation constants of ligand-HCS complexes from fluorescence titration 85

CHAPTER 4 Regulatory mechanism of homocitrate synthase: I **97**

Table 4-1. Kinetic parameters for inhibition patterns of HCS 107
Table 4-2. Dissociation constants of ligand-HCS complexes by fluorescence titration 114

CHAPTER 5 Regulatory mechanism of homocitrate synthase: II **129**

Table 5-1. Rate equations for HCS enzymatic activity in extreme cases 142

CHAPTER 6 Crystal structure of the saccharopine reductase **158**

Table 6-1. Summary of data collection statistics 167
Table 6-2. Results of molecular replacement 168
Table 6-3. Summary of the refinement statistics for the $P3_121$ space group 169
Table 6-4 Hydrogen bond interactions in homodimer interface 173

LIST OF ILLUSTRATIONS

CHAPTER 1 Introduction **1**

Figure 1-1. The enzymes of the lysine DAP biosynthetic pathway 2
Figure 1-2. The enzymes of the lysine AAA biosynthetic pathway 5
Figure 1-3. General reaction for a Claisen condensation 13
Figure 1-4. Three dimensional structure of saccharopine reductase from *Magnaporthe grisea* 24
Figure 1-5. Proposed chemical mechanism for saccharopine reductase 27
Figure 1-6. Proposed chemical mechanism for saccharopine dehydrogenase 31

CHAPTER 2 Stabilization and characterization of homocitrate synthase **45**

Figure 2-1. α-Aminoadipate pathway for the synthesis of lysine 45
Figure 2-2. SDS-PAGE of HCS stained with Coomassie brilliant blue 56
Figure 2-3. Analytical HPLC trace 59
Figure 2-4 Elution profile of the HCS 63
Figure 2-5. Fluorescence, CD and UV spectra of HCS 65
Figure 2-6. Modified Stern-Volmer plot for KI, CsCl and Acrylamide 67

CHAPTER 3 Kinetic mechanism of homocitrate synthase **74**

Figure 3-1. Initial velocity double-reciprocal plot for the HCS reaction 81
Figure 3-2. Determination of the K_d for CoA and AcCoA via fluorescence titration 86
Figure 3-3. Proposed kinetic mechanism for the HCS 88

CHAPTER 4 Regulatory mechanism of homocitrate synthase: I **97**

Figure 4-1. Initial rate studies of lysine inhibition 105
Figure 4-2. Secondary and tertiary replots of the data in Fig. 4-1 106
Figure 4-3. Tertiary replots of the data for Na^+ inhibition and activation studies 109
Figure 4-4. Interactive effects of Na^+ and lysine at low AcCoA 112
Figure 4-5. Interactive effects of Na^+ and lysine at high AcCoA 113
Figure 4-6. Fluorescence titration of HCS with lysine 114
Figure 4-7. Effect of monovalent and divalent cations on HCS activity 115
Figure 4-8. Initial velocity pattern for HCS suggesting a competitive substrate inhibition by AcCoA 120

CHAPTER 5 Regulatory mechanism of homocitrate synthase: II **129**

Figure 5-1. Tertiary replot of slope of slope for the inhibition and activation by Na^+ 146
Figure 5-2. Tertiary replot of slope of intercept for the inhibition and activation by Na^+ 146
Figure 5-3. Predicted slope of slope (SOS) replot for Na^+ activation and inhibition as a function of NaCl, K_{act} and K_i 150
Figure 5-4. Predicted slope of intercept (SOI) replot for Na^+ activation and inhibition as a function of NaCl and K_{act} 151
Figure 5-5. Percentage of HCS activity as a function of NaCl and substrate concentration 152
Figure 5-6. Predicted slope for Na^+-lysine activation-inhibition as a function of lysine at low and high AcCoA 154
Figure 5-7. Predicted intercept for Na^+-lysine activation-inhibition as a function of lysine at low and high AcCoA 155

CHAPTER 6 Crystal structure of the saccharopine reductase **158**

Figure 6-1. Saccharopine reductase from *S. cerevisiae* 171
Figure 6-2. Dimer interface of the SR enzyme 172
Figure 6-3. Stereoview of structural superposition of the apo-SR molecules from *M. grisea* and *S. cerevisiae* 174
Figure 6-4. Structural superposition of the apo-SR molecules from *M. grisea* and *S. cerevisiae* focusing on the positions of Trp173 and Trp174 175
Figure 6-5. Structural superposition of the apo-SR molecules from *M. grisea* and *S. cerevisiae* focusing on the residues around the active site 177
Figure 6-6. Stereo diagram of the structural superposition of the apo SR molecule from *S. cerevisiae* with the NADPH:Saccharopine:SR ternary complex from *M. grisea* 178
Figure 6-7. Electron density of a sulfate molecules in the vicinity of Arg246 180
Figure 6-8. Location of the non-conserved residues between SRs from *S. cerevisiae* vs. *M. grisea* 180

APPENDIX **185**

Figure A-1. Stoichiometry of the reaction of DCPIP with CoA 185
Figure A-2. Effects of the different stabilization buffers on homocitrate synthase activity 186
Figure A-3. Activity of the homocitrate synthase in the absence and presence of the stabilization buffer as the function of day 187
Figure A-4. Initial velocity double-reciprocal plot for the HCS reaction

using OAA as substrate 187
Figure A-5. Inhibition of HCS by lysine 188
Figure A-6. Initial rate studies of Na^+ inhibition and activation 189
Figure A-7. Secondary replots of the data in Fig. A-6 190
Figure A-8. PCR for the *LYS9* gene (1341 bp) from *Saccharomyces cerevisiae* 191
Figure A-9. *LYS9*-pUC12 cloning vector (4060 bp) 192
Figure A-10. Construction of the *LYS9*-pUC12 cloning vector 193
Figure A-11. *LYS9*-pET-16b expression vector (7065 bp) 194
Figure A-12. Sequencing of the *LYS9* fragment of the *LYS9*-pET-16b expression vector 195
Figure A-13. Purification of the SR using Ni-NTA resin 196
Figure A-14. Single crystals of SR from *Saccharomyces cerevisiae* 197
Figure A-15. Dimensions of the SR crystal used for data collection 198
Figure A-16. Reflection images of the SR crystals 199
Figure A-17. Schematic diagram for the regulation mechanism of HCS by Na^+ and lysine 200

LIST OF SCHEMES

CHAPTER 4 Regulatory mechanism of homocitrate synthase: I **97**

Scheme 4-1. Kinetic mechanism for activation and inhibition by Na^+ 121
Scheme 4-2. Kinetic mechanism for interactive Na^+ and lysine effects 123

CHAPTER 5 Regulatory mechanism of homocitrate synthase: II **129**

Scheme 5-1. Kinetic mechanism for activation by Na^+ 132
Scheme 5-2. Kinetic mechanism for interaction between Na^+ and lysine 143

LIST OF ABBREVIATIONS

AAA	α-aminoadipate acid
AAS	α-aminoadipate semialdehyde
Ac	acetate
AcCoA	acetyl-CoA
ADH	alcohol dehydrogenase
ADP	adenosine diphosphate
AMP	adenosine monophosphate
ATP	adenosine triphosphate
Bis-Tris	bis (2-hydroxyethyl) imino-tris (hydroxymethyl) methane
bp	base pair
C	competitive
CD	circular dichroism
CoA	coenzyme A
CoASH	coenzyme A
DAP	diaminopimelate
DCPIP	dichlorophenol indophenol
DTT	dithiothreitol
EDTA	ethylenediaminetetraacetic acid
Gdm	guanidinium
Hc	homocitrate
HCS	homocitrate synthase

Hepes	4-(2-hydroxyethyl)-1-piperazine-ethanesulfonic acid
HPLC	high-performance liquid chromatography
IPTG	isopropyl-β-D-1-thiogalactopyranoside.
kDa	kilodaltons
α-Kg	α-ketoglutarate
MPD	2-methyl-2,4-pentanediol
NAD^+	nicotinamide adenine dinucleotide
$NADP^+$	nicotinamide adenine dinucleotide phosphate
NC	noncompetitive
Ni-NTA	nickel-nitrilotriacetic acid
NMN^+	nicotinamide mononucleotide
OAA	oxaloacetic acid
PCR	polymerase chain reaction
PDB	protein data bank
PEG	polyethylene glycol
PEP	phosphoenolpyruvate
PMSF	phenylmethanesulfonyl fluoride
P_i	inorganic phosphate
PP_i	inorganic pyrophosphate
RMS	root mean square
rTEV	recombinant tobacco etch virus
SDH	saccharopine dehydrogenase (L-Lys forming)

SDS	sodium dodecyl sulfate
SDS-PAGE	sodium dodecyl sulfate-polyacrylamide gel electrophoresis
SOI	slope of intercept
SOS	slope of slope
SR	saccharopine reductase
TCA	tricarboxylic acid
Tris	tris-(hydroxymethyl) aminomethane
UC	uncompetitive
UV	ultraviolet

Amino acids (Standard one-letter and three-letter amino acid abbreviations):

A=Ala=Alanine, C=Cys=Cysteine, D=Asp=Aspartic acid, E=Glu=Glutamic acid, F=Phe=Phenylalanine, G=Gly=Glycine, H=His=Histidine, I=Ile=Isoleucine, K=Lys=Lysine, L=Leu=Leucine, M=Met=Methionine, N=Asn=Asparagine, P=Pro=Proline, Q=Gln=Glutamine, R=Arg=Arginine, S=Ser=Serine, T=Thr=Threonine, V=Val=Valine, W=Trp=Tryptophan, and Y=Tyr=Tyrosine.

ABSTRACT

Homocitrate synthase (HCS) catalyzes one of the regulated steps of the α-aminoadipate pathway for Lys biosynthesis in fungi. His-tagged HCS from *Saccharomyces cerevisiae* was purified to about 98% using a Ni-NTA resin and stabilized. The enzyme, in the absence of reactants, self associates, as suggested by size exclusion chromatography. Fluorescence and circular dichroic spectra suggested a partially exposed Trp residue and a mixed (α/β) secondary structure for the enzyme. Fluorescence quenching studies with KI, CsCl, and acrylamide, suggest that the microenvironment around the single Trp residue of the enzyme has some positive charge.

Kinetic data have been collected suggesting a preferred sequential ordered kinetic mechanism for the His-tagged HCS from *S. cerevisiae* with α-Kg binding before AcCoA and CoA released before Hc. In agreement with the ordered kinetic mechanism desulfo-CoA is uncompetitive and citrate is competitive vs α-Kg. Varying AcCoA, citrate is a noncompetitive inhibitor as predicted, but CoA is noncompetitive vs AcCoA suggesting binding of CoA to E:Hc and E:α-Kg. The product CoA behaves identical to desulfo-CoA, suggesting an E:α-Kg:CoA dead-end complex. Data further suggest an irreversible reaction overall. Fluorescence titration data show finite binding of CoA and AcCoA to free enzyme, suggesting the mechanism may be random with a high degree of synergism of binding between the reactants.

The kinetic mechanism of regulation of HCS from *S. cerevisiae* by Na^+ and the feedback inhibitor Lys was studied by measuring the initial rate in the absence and

presence of the effectors. Data suggest that Na^+ is an activator at low concentrations and an inhibitor at high concentrations, and these effects occur as a result of the monovalent ion binding to two different sites in the free enzyme. Inhibition and activation by Na^+ can occur simultaneously. The inhibition by Na^+ is eliminated at high concentrations of AcCoA, the second substrate bound, but the activation remains. Fluorescence binding studies indicate Lys binds with high affinity to its binding site as an inhibitor. The inhibition by Lys is competitive and linear vs α-Kg. The effects of Na^+ and Lys are independent of one another. A model is developed for regulation of HCS that takes into account all of the effects discussed above. The rate equations that predict the regulatory kinetic behavior of HCS are also derived, and simulation of the predicted behavior is carried out over a range of values for the kinetic parameters. Data obtained allow application of the resulting expressions to enzyme systems that exhibit activation and inhibition as a result of the interaction of the effectors at multiple sites in free enzyme. The HCS is used as an example, in terms of its activation by Na^+ binding to the active enzyme conformer at an allosteric site, inhibition by binding to the active site, and inhibition by Lys binding to the less active enzyme conformer.

In the case of saccharopine reductase (SR), the three-dimensional structure of the enzyme from *S. cerevisiae*, was determined to 1.7 Å resolution in the apo form using molecular replacement. The enzyme monomer consists of three domains. Comparative fold alignment with the enzyme from *Magnaporthe grisea* suggests that domain I binds to NADPH, domain II binds to saccharopine and is involved in dimer formation.

Domain III is involved in closing the active site of the enzyme once substrates are bound. Structural comparison of the SR enzymes from *S. cerevisiae* and *M. grisea* indicates that domain II has the highest number of conserved residues suggesting that it plays an important role in substrate binding and in spatially orienting domains I and III.

CHAPTER 1

Introduction

"Reproduced in part with automatic permission from [Xu, H., Andi, B., Qian, J., West, A. H., and Cook, P. F. (2005) The α-aminoadipate pathway for lysine biosynthesis in fungi, *Cell Biochem. Biophys.,* In press] Copyright [2005] Humana Press, Inc."

1-1. Amino acid biosynthesis

In general, most of the living organisms use 20 common amino acids to make their protein pools. Biosynthesis of these amino acids can be categorized into six major families as follows: 1) the glutamate family for the biosynthesis of Glu, Gln, Pro, and Arg; 2) the serine family for the biosynthesis of Ser, Gly and Cys; 3) the aspartate family for the biosynthesis of Asp, Asn, Lys, Met, Thr, Ile; 4) the pyruvate family for the biosynthesis of Ile, Leu, Val and Ala; 5) the aromatic family for the biosynthesis of Phe, Tyr and Trp; and 6) the histidine biosynthetic pathway (*1*).

Biosynthetic regulation of the aforementioned amino acids occurs at two distinct levels. The first level of regulation occurs at the level of enzyme activity and metabolite flow that is the subject of enzymologic studies. The second level of regulation occurs via regulation of gene expression that is the subject of molecular genetics. Most of the studies of regulation of amino acid biosynthesis have been performed in *Escherichia coli* and *Salmonella typhimurium* (*1*).

The focus of this dissertation is on the α-aminoadipate pathway for lysine biosynthesis which is unique to fungi.

1-2. Biosynthesis of lysine

L-lysine is an essential amino acid for humans and animals and can only be obtained from protein in the diet. It can be synthesized *de novo* in bacteria, lower eukaryotes, and some plants. Among the 20 common proteinogenic amino acids, L-lysine is the only one known to have two distinct biosynthetic pathways: the diaminopimelate (DAP) pathway in plants, bacteria and lower fungi, and the α-aminoadipate (AAA) pathway in euglenoids and higher fungi (*2*). Unlike the pathways for lysine synthesis, pathways for other amino acid synthesis are similar in bacteria and fungi (*1, 3*).

1-2-1. Diaminopimelate pathway of L-lysine biosynthesis

The diaminopimelate pathway is found in most plants, bacteria, and lower fungi, and consists of seven enzyme-catalyzed reactions (Fig. 1-1) (*1, 5*).

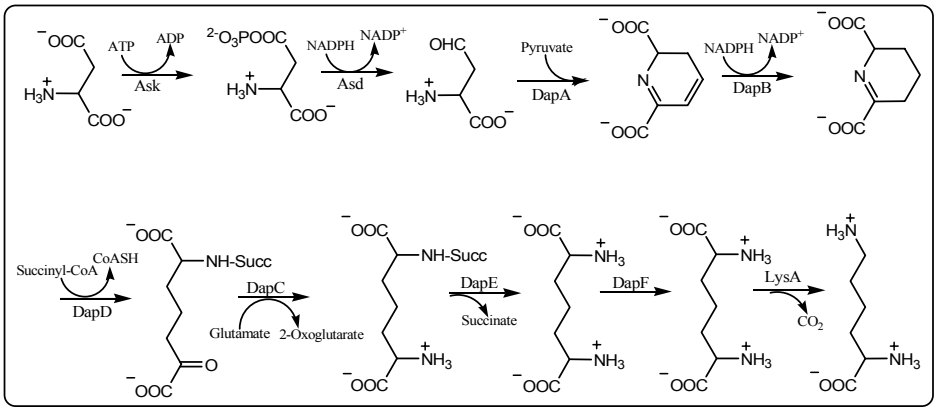

Fig. 1-1: The enzymes of the lysine DAP biosynthetic pathway are as follows: (1) Aspartate kinase (Ask, E.C. 2.7.2.4), (2) Aspartate semialdehyde dehydrogenase (Asd, E.C. 1.2.1.11), (3) Dihydrodipicolinate synthase (DapA, E.C. 4.2.1.52), (4) Dihydrodipicolinate reductase (DapB, E.C. 1.3.1.26), (5) Tetrahydrodipicolinate acyltransferase (DapD, E.C. 2.3.1.117), (6) N-succinyl-α-amino-ε-ketopimelate-glutamate aminotransaminase (DapC, E.C. 2.6.1.17), (7) N-acyldiaminopimelate deacylase (DapE, E.C. 3.5.1.18, E. C. 3.5.1.47), (8) Diaminopimelate epimerase (DapF, E.C. 5.1.1.7), (9) Diaminopimelate decarboxylase (LysA, E. C. 4.1.1.20).

It belongs to the aspartate family of amino acid biosynthesis with aspartate as the common precursor. This pathway is the source of the diaminopimelate and lysine that are incorporated into bacterial cell wall peptidoglycan and transpeptidative cross-linking. Enzymes in the DAP pathway are therefore targets for developing new antibacterial agents (*6*).

The pathway begins with the phosphorylation of aspartate by aspartokinase to give aspartyl-β-phosphate followed by an NADPH-dependent reduction to give aspartate β-semialdehyde. Aldol condensation of aspartate semialdehyde with pyruvate yields, upon rearrangement, 2,3-dihydrodipicolinate, which is then reduced by NADPH to Δ^1-piperideine-2, 6-dicarboxylate. Succinylation (or acetylation) opens the ring to give N-succinyl (or acetyl) α-amino-ϵ-ketopimelate. After transamination, the acyl group is removed to yield L, L-diaminopimelate, which can be incorporated directly into the peptidoglycan, or racemized to the *meso* compound prior to incorporation. Racemization to the *meso* form is required, since this is the precursor to L-lysine, once it is decarboxylated.

1-2-2. α-Aminoadipate pathway of L-Lysine biosynthesis

The presence of the α-aminoadipate pathway for lysine biosynthesis has been demonstrated in several yeasts and molds, including *Saccharomyces cerevisiae* (*4, 7*), *Yarrowia lipolytica* (*8*), *Schizosaccharomyces pombe* (*9*), *Rhodotorula glutinis* (*10*), *Candida maltosa* (*11*), *Neurospora crassa* (*12*), *Penicillium chrysogenum* (*13*), human pathogenic fungi, such as *Candida albicans* (*14*), *Cryptococcus neoformans* (*15*),

Aspergillus fumigatus (*15*), and plant pathogens, including *Magnaporthe grisea* (*1, 15*). The enzymes from *S. cerevisiae* are highly similar to their closest homologs from *C. albicans* and *A. fumigatus*. Multiple sequence alignment shows >60% identity for all but one (aminotransferase) of the enzymes in the pathway from those organisms.

The α-aminoadipate pathway is present only in euglenoids and higher fungi (*3-4, 16-17*), with α-ketoglutarate serving as the precursor for L-lysine. This pathway is a member of the glutamate family of amino acid biosynthesis, and resembles the pathway from glutamate to ornithine in bacterial arginine biosynthesis (*18-19*). Enzymes involved in the fungal α-aminoadipate pathway are unique to lysine synthesis (*1, 4*).

The *Saccharomyces cerevisiae* genome has been completely sequenced (*20-22*). Extensive genetic, enzymatic, and regulatory studies of the lysine biosynthetic pathway are being carried out in *S. cerevisiae* (*14*). Seven enzymes, eight steps and more than 12 non-linked genes are responsible for the biosynthesis of lysine in *S. cerevisiae* (*4, 23-24*). Genes and their encoded enzymes involved in the AAA pathway are listed in Table 1-1. The pathway for the *de novo* synthesis of lysine in fungi is shown in Fig. 1-2, and the enzymatic steps are briefly described below.

Table 1-1: Genes and enzymes involved in the α–aminoadipate pathway in *S. cerevisiae*.

Enzyme	Gene
Homocitrate synthase	*LYS20* (cytosol), *LYS21* (mitochondria)
Homoaconitase	*LYS4 (LYS7)*
Homoisocitrate dehydrogenase	*LYS10*
α-Aminoadipate aminotransferase	General aminotransferase
α -Aminoadipate reductase (phosphopantetheinyl transferase)	*LYS2* (*LYS5*)
Saccharopine reductase	*LYS9* (regulated by *LYS14*)
Saccahropine dehydrogenase	*LYS1*

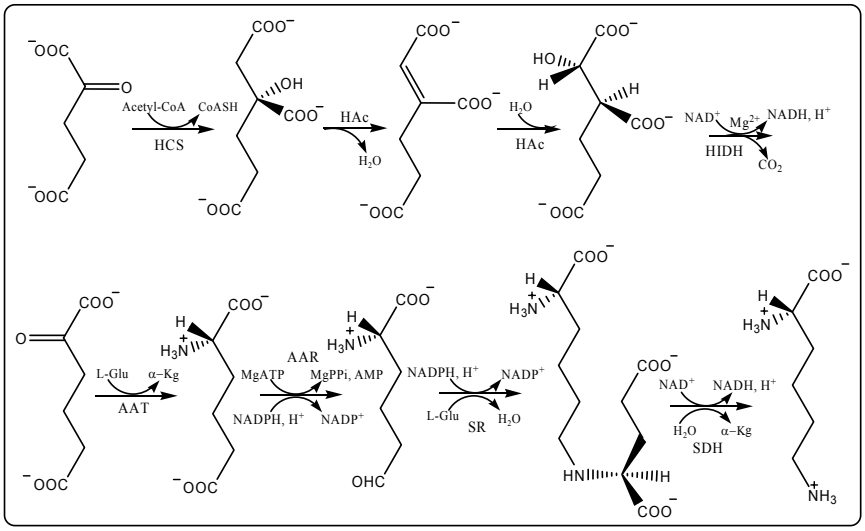

Fig. 1-2: The enzymes of the lysine AAA biosynthetic pathway are as follows: (1) Homocitrate synthase (HCS, E.C. 4.1.3.21), (2) Homoaconitase (HAc, E.C. 4.2.1.36), (3) Homoisocitrate dehydrogenase (HIDH, E.C. 1.1.1.87), (4) α-aminoadipate aminotransferase (AAT, E.C. 2.6.1.39), (5) α-aminoadipate reductase (AAR, E.C. 1.2.1.31), (6) Saccharopine reductase (SR, E.C. 1.5.1.10), (7) Saccharopine dehydrogenase (SDH, E.C. 1.2.1.31).

The first half of the pathway, formation of α–aminoadipate from AcCoA and α–ketoglutarate, takes place in the mitochondrion (*25*). The pathway is initiated by the homocitrate synthase (HCS)-catalyzed condensation of AcCoA and α-ketoglutarate to give the enzyme-bound intermediate homocitryl-CoA, which is hydrolyzed by the same enzyme to give homocitrate. Homocitrate synthase catalyzes the first and committed step in the pathway, is highly regulated to economize the use of resources and its reaction is believed to be the rate-limiting step in the pathway.

Homoaconitase (HAc), an enzyme containing an FeS cluster, catalyzes the interconversion of homocitrate and homoisocitrate via the intermediate homoaconitate. The enzyme is a member of the aconitase superfamily, which includes isopropylmalate isomerase (a member of the leucine biosynthetic pathway in bacteria

and fungi) and aconitases. This is the first documented evolutionary link between the α-aminoadipate pathway in fungi and non-fungal organisms (*26*).

The resulting homoisocitrate is then oxidatively decarboxylated by the pyridine-nucleotide linked homoisocitrate dehydrogenase (HIDH) to give α-ketoadipate. This enzyme belongs to the pyridine nucleotide-linked β–hydroxyacid oxidative decarboxylase family, which is a well-studied class of enzymes (*27*).

α–Aminoadipate is then formed via a PLP-dependent aminotransferase (AAT) using L-glutamate as the amino donor. Although the first half of the pathway takes place in the mitochondrion, the aminotransferase is thought to be present in both mitochondrion and cytoplasm. The aminotransferase reaction is also a branch point to secondary metabolism including the *de novo* synthesis of β–lactam antibiotics. In addition, the product α–aminoadipate can serve as the sole nitrogen source for *Filobasidiella neoformans*, *S. pombe*, *C. albicans*, and *A. fumigatus* (*28*).

In the cytoplasm, the α-aminoadipate reductase (AAR) then reduces α-aminoadipate to 2-aminoadipate-6-semialdehyde (AAS) via an adenosylated derivative, a unique process involving both adenylation and reduction that is found only in fungi. However, this enzyme has to be activated by a phosphopantetheinyl transferase (PPT). This unique two component system represents a novel reaction in fungal amino acid metabolism. In addition, phylogenetic studies and BLAST results show that the α-aminoadipate reductase in fungal lysine synthesis is evolutionarily related to some bacterial antibiotic peptide synthetases (*29*). The reductase-catalyzed reaction is believed to be the key to evolution of fungal lysine synthesis (*29*).

Once the semialdehyde is formed, it is condensed with α-ketoglutarate, and the imine is reduced by NAD(P)H to L-saccharopine catalyzed by saccharopine reductase (SR). Finally, saccharopine dehydrogenase (SDH) catalyzes the oxidative deamination of saccharopine to give L-lysine. It is of interest that saccharopine is a stable intermediate and pyridine nucleotides, rather than a vitamin B_6 – dependent transamination of the semialdehyde is used by fungi. The last two enzymes have very little sequence homology at the amino acid level, but both enzymes are fungi specific and catalyze very similar reactions. Since NADPH and NADH are used as coenzymes by these two enzymes respectively, a high NADPH to NADH ratio may favor the synthesis of lysine from aminoadipate semialdehyde, whereas a low ratio would discourage such synthesis and favor the reverse reactions.

The pathway occurs in two compartments. One of the reasons may be due to the availability of NAD(P)H and ATP, of allosteric regulators, or the proper environment to give the active site residues of the enzymes an optimum protonation state in order to catalyze the reactions involved along the pathway. The split between two compartments may also contribute to a better overall regulation of the whole pathway, or a secondary metabolic pathway.

It has been reported that an α-aminoadipate-like pathway is present in *Thermus thermophilus* and *Pyrococcus horikoshii* (*30-31*). However, this pathway is not the same as that found in fungi. The first half of the pathway is similar to that presented above, but α-aminoadipate is first converted to N-acetyl-α-aminoadipate, which is phosphorylated at the ε–carboxylate, and then reductively dephosphorylated to the ε–

aldehyde. The aldehyde is then transaminated to N-acetyl-L-lysine, which is deacetylated to give L-lysine (*18, 29*).

1-2-3. Significance of the α-aminoadipate pathway

A number of fungal alkaloids or peptides have lysine as a structural element or biosynthetic precursor. In addition, several α-aminoadipate pathway intermediates are incorporated into secondary metabolites. The best example is α-aminoadipate as an essential precursor for penicillins in the synthesis of ACV (L-δ-(α-aminoadipoyl)-L-cysteinyl-D-valine) tripeptide (*32*).

The uniqueness of the α-aminoadipate pathway makes it a target for the rapid detection and control of pathogenic yeasts and molds. Selective inhibition of the enzyme(s) of this pathway by (an) appropriate substrate analog(s) may control or eradicate the growth of fungal pathogens *in vivo* (*9, 14*). To date, however, there are only a few novel compounds designed to target early steps in the pathway, specifically those steps involving the synthesis of (*R*)-homocitrate and (2*R*, 3*S*)-homoisocitrate (*33*).

1-2-4. Regulation of the α-aminoadipate pathway

The α-aminoadipate pathway for the biosynthesis of lysine is highly regulated at the level of both enzyme synthesis and activity (*4*).

1-2-4-1. Genetic regulation

The pathway is regulated by the general mechanism for the control of amino acid biosynthesis as well as a pathway-specific coinducer-dependent transcriptional activation (*25, 34-36*). The coinducer is α-aminoadipate semialdehyde (AAS), which is an intermediate of the pathway (*34*). In *S. cerevisiae*, expression of the lysine genes can be stimulated by Lys14p in the presence of its coinducer AAS (*34*). Production of the coinducer is also under the control of the metabolic flux mediated by feedback inhibition by lysine of the first enzyme in the pathway, homocitrate synthase (*37-38*). Thus, lysine can repress the expression of its biosynthetic genes. Excess lysine also acts as a repressor of six of the enzymes of the pathway (*25, 39*). Lysine inhibits its own biosynthesis by feedback inhibition of HCS, which decreases the concentration of AAS, and eliminates induction by Lys14p. Several mutants were identified that were insensitive to lysine inhibition (*40*), and the loss of sensitivity was shown to result from mutagenesis of the HCS gene (*LYS20* or *LYS21*). A 4- to 10- fold increase in lysine production was observed upon transformation of the mutant genes. These results support the role of HCS in the repression of the lysine biosynthetic enzymes.

Two unlinked genes, *LYS9* (saccharopine reductase) and *LYS14* (transcriptional activator) are required for the production of saccharopine in *S. cerevisiae* (*23*). Strains mutated in these genes accumulate AAS and show a significant reduction in saccharopine reductase activity. Mutation of *LYS9* results in lysine auxotrophy and no reductase activity. Mutation of *LYS14* causes yeast to grow slowly in the absence of lysine with a low level of reductase activity. Lys14p is required for the expression of

the *LYS9* gene and it has a regulatory role with AAS as the coinducer of transcriptional activation. Therefore, a low level of reductase activity in the *LYS14* mutants is because of the weak expression of the *LYS9* gene in the absence of the semialdehyde coinduction (*2, 34*).

Lys14p is a 90 kDa (790 amino acids) protein that participates in a complicated network of protein-protein interactions with 65 other proteins (Biomolecular Interaction Network Database, available at www.bind.ca). Lys14p contains a DNA binding domain similar to the Zn_2Cys_6 binuclear cluster of other fungal transcriptional activators like Gal4p and Ppr1p (*41-42*). Promoters of genes responding to this type of transcriptional activator usually contain an upstream activating sequence (UAS) that, in most instances, consists of two CGG triplets that are separated by a specific number of bases dependent on the specific activator. In the case of Gal4p and Ppr1p, the intervening sequence consists of 11 and 6 base pairs, respectively. These proteins bind as a dimer to the target sequence (UAS) with each of the zinc clusters binding to a CGG triplet (*43-44*).

Using a deletion and insertion approach, a UAS responsible for binding Lys14p has been identified in the promoter regions of the *LYS1* (saccharopine dehydrogenase) and *LYS9* genes from *S. cerevisiae* which differs slightly from the above-mentioned consensus sequence (*36*). The UAS for the transcriptional activation of the *LYS1* and *LYS9* genes consists of a TCC and GGA triplet separated by 3 base pairs. One or several copies of this nine bp sequence has been found in the promoter of at least four other *LYS* genes, including *LYS20* (cytosolic homocitrate synthase), *LYS21*

(mitochondrial homocitrate synthase), *LYS2* (α-aminoadipate reductase), and *LYS4* (homoaconitase). *LYS5* (phosphopantetheinyl transferase), which does not respond to the Lys14p transcriptional activation, does not contain the UAS element (*36*).

In *S. cerevisiae* one cannot exclude the possibility that some other enzyme-catalyzed step(s) may be rate-limiting step(s) and acts in a manner similar to HCS in the regulation of lysine synthesis. For example, in *P. chrysogenum*, overexpression of HCS does not lead to an increase in α-aminoadipate even in a strain in which the *LYS2* gene, which encodes α-aminoadipate reductase, is disrupted. These results suggest the presence of at least one additional rate-limiting step between the HCS and the α-aminoadipate reductase catalyzed reactions (*46*).

1-2-4-2. Regulation of enzyme activity

The activity of HCS is highly regulated. It can be feedback inhibited by lysine, the end-product of the pathway. The K_i for lysine inhibition of HCS in *T. thermophilus* and *P. chrysogenum* is only around 9 μM (*13, 47*). In *P. chrysogenum*, the synthesis of penicillin is regulated by lysine through the inhibition of homocitrate synthase (*48-49*), which results in a decrease in the concentration of α-aminoadipic acid, the branch point for the biosynthesis of penicillin and lysine. The effect of lysine can be reversed by addition of aminoadipic acid and other intermediates of the pathway such as α-ketoadipate and homocitrate (*48-49*). The inhibition by lysine is partial in *P. chrysogenum* (*13*). Luengo *et al*. (*50*) suggest the partial inhibition is essential for maintaining a steady state level of α-aminoadipate for penicillin production.

It has also been found that the inhibition of HCS by lysine is pH dependent in *P. chrysogenum* (*13*). Inhibition could not be detected at pH 6.6 to 7.0 with 0.5 mM lysine, while a K_i of 8 μM for lysine was measured at pH 8.0. In *P. chrysogenum*, the cytosolic pH is controlled by a proton gradient, generated by a cytoplasmic membrane ATPase. A decrease in the ATP concentration will result in a decreased cytosolic pH and an increase in HCS activity, allowing the fungus to use intermediates from the lysine biosynthetic pathway to produce secondary metabolites.

Kohlhaw *et al*. (*51-54*) reported that CoA, the product of the HCS reaction, can inactivate the enzyme from *S. cerevisiae* and this could be prevented by lysine and α-ketoglutarate. The inactive enzyme could not be reactivated by addition of AcCoA (*51*). A similar inactivation was also observed for α-isopropylmalate synthase and β-hydroxy-β-methylglutaryl-CoA reductase, both of which also use AcCoA as a substrate (*55-56*).

1-3. Enzymes of the α-aminoadipate pathway

1-3-1. Enzyme-catalyzed Claisen condensation of AcCoA and α-keto acids

A Claisen condensation is a base-catalyzed condensation of a carbon α to an ester carbonyl and another carbonyl containing compound, e.g., a ketone or aldehyde (*57*). An example is shown in Fig. 1-3, where the nucleophilic carbon is generated by enolization of the ester, catalyzed by a general acid or base. The carbanion then adds to the electrophilic carbonyl carbon of the ketone to generate the β-hydroxy ester.

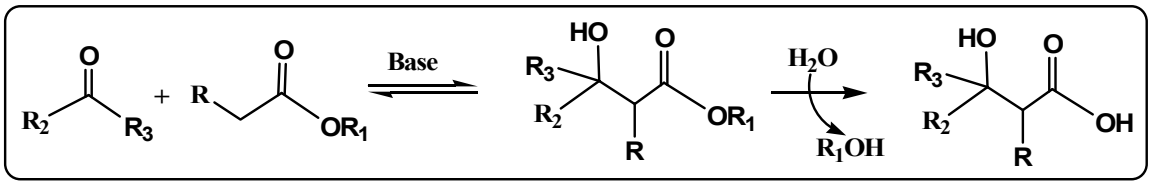

Fig. 1-3: General reaction for a Claisen condensation

The reaction is reversible but the product can be trapped by ester hydrolysis. The enzyme-catalyzed Claisen reactions catalyzed by the following enzymes are between a carbon α to a thioester (AcCoA) and a α-keto acid: homocitrate synthase, α-isopropylmalate synthase, methylthioalkylmalate synthase, citramalate synthase, citrate synthase and malate synthase. These enzymes are bifunctional in that they catalyze the reversible formation of the β-hydroxy ester and the subsequent hydrolysis of the thioester.

Citrate synthase is the most thoroughly studied of the enzymes that catalyze this type of reaction. The enzyme is a dimeric protein that does not require a divalent cation for catalysis. There are thought to be three different steps in the overall reaction catalyzed by this class of enzyme: enolization of the thioester to generate the α-carbanion, condensation to form the acyl-CoA, and hydrolysis of the acyl-CoA. In the citrate synthase reaction, enolization of AcCoA is thought to be the rate-limiting step (*58-61*).

In the citrate synthase reaction, OAA binds to enzyme first and His320 forms a hydrogen bond to its keto-oxygen, making it more electrophilic and susceptible to the nucleophilic attack by the methyl of AcCoA. AcCoA then binds to the enzyme-OAA

complex, with its methyl near Asp375 and its thioester hydrogen-bonded to His274. Enolization of AcCoA then occurs with His274 protonating the thioester oxygen and Asp375 accepting a proton from the methyl. C2 of the enolate then attacks the carbonyl carbon of OAA, and His320 donates a proton resulting in the intermediate citryl-CoA. Formation of the intermediate results in inversion of configuration of the protons of the attacking methyl group. At this point the reaction is reversible. With the help of the general acid Asp375, citryl-CoA is then hydrolyzed to yield citrate and CoA.

Malate synthase catalyzes the condensation of glyoxylate and AcCoA to form malate and CoA. It differs from citrate synthase in its overall structure, but uses a similar catalytic strategy for its reaction. Opposed to citrate synthase, malate synthase is a Mg-containing metalloenzyme. The Mg^{2+} ion takes the place of the imidazole that hydrogen-bonds the carbonyl of OAA in the citrate synthase reaction and also functions in positioning the glyoxylate in a suitable orientation for reaction. In the formation of the enolate intermediate of AcCoA, an Asp residue acts as the general base and an Arg residue is thought to stabilize the enolate intermediate. Thus, although the overall reaction is the same as that catalyzed by citrate synthase, the mechanism is quite different (*62-64*). α-Isopropylmalate synthase, which catalyzes the reaction between α-ketoisovalerate and AcCoA, is a Zn-metalloenzyme, with the Zn^{2+} thought to participate in a role similar to Mg^{2+} in the malate synthase reaction (*65*). Although the reactions catalyzed by this class of enzyme are similar, their mechanisms differ.

1-3-2. Homocitrate synthase

1-3-2-1. Location of HCS

Using cell fractionation techniques, Tracy *et al.* (*51*) proposed that most of the HCS activity in *S. cerevisiae* was located in mitochondria (80%) with the remainder in cytosol. Ramos *et al.* (*37*) suggested 70% of HCS activity is cytosolic, due to Lys20p and the remainder, resulting from Lys21p was located in mitochondria. Using monoclonal antibodies and immunofluorescence, Chen *et al*. (*66*) showed that both isoenzymes are also located in the nucleus. Results were subsequently corroborated using HCS-GFP fusion proteins (*40*). Upon deletion of the two HCS genes, no phenotype was found other than lysine auxotrophy. Neither isoenzyme has a signal sequence for targeting to mitochondria, or a canonical sequence for nuclear localization. These interesting findings raise questions concerning why HCS is located in nucleus. The localization of HCS in *P. chrysogenum* has also been studied recently (*67*). Using HCS-GFP fusion protein, HCS was localized in the cytoplasm and mitochondria with the majority in the cytoplasm; the same result was obtained by cell fractionation techniques (*13*).

1-3-2-2. Expression, purification, and characterization

In 1995, Verhasselt *et al.* (*68*) reported that the sequence of open reading frame D1298 (YDL 182w) in chromosome IV of *S. cerevisiae* had a significant sequence similarity with the *NifV* gene from *Azotobacter vinelandii* which encodes HCS. Homocitrate is a component of the FeMo cofactor which is contained in nitrogenase

for nitrogen fixation in *A. vinelandii* (*69-70*). Disruption of this gene in *S. cerevisiae* gave a three-fold decrease in HCS activity (*37*). A 10-fold increase in HCS activity was observed when a strain was transformed with a plasmid containing the putative HCS genes, given the name *LYS20*. The *LYS20* gene product accounts for almost 70% of lysine synthesis, and is subject to repression by lysine. Disruption of the *LYS20* gene did not inhibit cell growth on minimal medium and significant HCS activity was still measurable, suggesting there are at least two HCS isoenzymes in *S. cerevisiae*.

As early as 1972, two isoenzymes of homocitrate synthase were identified in *S. cerevisiae*, both of which could be inhibited by lysine (*38*). Using monoclonal antibodies, Chen *et al.* showed that two isoenzymes of HCS, 47,000 Da and 49,000 Da, respectively, are located in the nucleus (*66*), and the 47,000 Da HCS corresponded to Lys20p. The 49,000 Da HCS was the product of a separate gene named *LYS21*. The gene and protein sequences of the two enzymes shared 90% identity, and are located on Chromosome IV in *S. cerevisiae*, suggesting they originated from gene duplication. Deletion of the *LYS20* and *LYS21* genes in *S. cerevisiae,* resulted in the elimination of HCS activity.

In order to obtain 50% inhibition of HCS activity, 1 mM and 0.15 mM lysine are required for Lys20p and Lys21p, respectively (*40*). This explains why Lys20p accounts for most of the lysine synthesized. The sensitivity of Lys21p to lysine is such that it is predominantly inactive, and may only be active under conditions of extreme lysine deficiency.

The subunit composition of HCS has been studied in several organisms. The HCS in *A. vinelandii* is a dimer, while that from *T. thermophilus* is thought to be a monomer, and that from *P. chrysogenum* is reported to have multiple subunits (*13, 47, 70*). It appears the organization of HCS in bacteria is simpler than that in fungi. This is consistent with the more complex allosteric regulation of HCS in fungi (*47*).

Homocitrate synthase is not stable as isolated. Crude HCS from *Saccharomycopsis lipolytica* is stable for a week at 4 °C (*71*), but 50% of the HCS activity from *A. vinelandii* was lost within 2 hr when exposed to air (*70*). The enzyme from *P. chrysogenum* loses 65% of its activity upon storage at 4-6 °C for 48 hrs, even in the presence of 20% glycerol (*13*).

1-3-2-3. Kinetic mechanism

An ordered kinetic mechanism has been proposed for the HCS from *S. lipolytica* with α-ketoglutarate binding before AcCoA (*71*). The authors reported a sigmoid saturation curve for AcCoA. A sigmoid saturation curve for AcCoA was also reported for the enzyme from *P. chrysogenum* (*13*). It has been also demonstrated that the HCS from *T. thermophilus* is capable of catalyzing the reaction using oxaloacetate in place of α-ketoglutarate as a substrate, and thus behaves as a citrate synthase (*47*). Virtually nothing is known of the chemical mechanism of the HCS and the structure is currently not available.

1-3-3. Homoaconitase

Homoaconitase (E.C. 4.2.1.36) also known as homoaconitate hydratase, encoded by the *LYS4* gene in *S. cerevisiae*, catalyzes the interconversion of homocitrate and homoisocitrate via the intermediacy of *cis*-homoaconitate. The enzyme is a member of the aconitase superfamily. It is a mitochondrial enzyme that is repressed by both lysine and glucose. The enzyme from *Aspergillus nidulans* is 55% sequence identical to that from *S. cerevisiae*, with the greatest similarity in the region attributed to binding of an FeS cluster (*2*). However, little is known of the mechanism of the homoaconitase, but its mechanism may be similar to that of aconitase (*72*).

1-3-4. Homoisocitrate dehydrogenase

Homoisocitrate dehydrogenase (3-carboxy-2-hydroxyadipate dehydrogenase; E.C. 1.1.1.87) catalyzes the NAD^+-dependent conversion of homoisocitrate to α-ketoadipate. Other than its sequence, almost nothing is known about the mechanism of this enzyme. Based on the general mechanism of the pyridine nucleotide-linked β–hydroxyacid oxidative decarboxylases (*27*), the mechanism may be similar to that of isocitrate dehydrogenase (*73*). Whether the enzyme requires a divalent metal ion to catalyze its reaction as does isocitrate dehydrogenase will have to be determined.

1-3-5. α-Aminoadipate aminotransferase

α-Aminoadipate aminotransferase (E.C.2.6.1.39) is a PLP-dependent enzyme responsible for the conversion of α–ketoadipate to α–aminoadipate using L-glutamate

as the amino donor, and generating α–ketoglutarate as the second product. The aminotransferase reaction is also a branch point to secondary metabolism including the *de novo* synthesis of β–lactam antibiotics.

In *S. cerevisiae*, two isozymes of the aminotransferase have been isolated (*2, 74-75*). Isozyme I is localized in the mitochondrion, is inhibited by α–ketoglutarate, and utilizes either L-glutamate or L-aspartate as the amino donor, but exhibits only weak activity with α–aminoadipate as the amino donor. Isozyme II is localized in the cytosol, has a strict requirement for L-glutamate as the amino donor, and is not inhibited by α–ketoglutarate. Neither isoform is inhibited by lysine, but the activity of isozyme II is repressed by α–aminoadipate and slightly repressed by glucose. Only the cytosolic isoform appears to be specific for the α–aminoadipate pathway. Its mechanism is expected to be ping pong on the basis of ample precedence from other aminotransferases, but its specific mechanism will have to await future studies.

1-3-6. α-Aminoadipate reductase

α-Aminoadipate reductase (E.C.1.2.1.31), also known as α–aminoadipate semialdehyde dehydrogenase catalyzes the reduction of α-aminoadipate to α–aminoadipate δ-semialdehyde in the cytoplasm, a unique reaction involving both adenylation and reduction. On the basis of early investigations (*76-77*), the AAR-catalyzed reaction is believed to be a three-step process, with the amino acid first reacting with ATP to form an adenylyl derivative, followed by the reduction of the adenylyl derivative of α-aminoadipate by NADPH, followed by cleavage of the

reduced adenylyl derivative of the amino acid to form α-aminoadipate-δ-semialdehyde. The first and second steps require MgATP and NADPH, respectively, while the third step requires no cofactors. The product of the first step was successfully isolated and identified as an δ-5′-adenylyl-L-α-aminoadipate by Bhattacharjee's group, while the product of the second step was too unstable to be identified (*78*). Formation of the δ-5′-adenylyl-L-α-aminoadipate, rather than phosphorylation of the substrate by ATP makes this reaction a unique process.

The enzymatic conversion of α–aminoadipate to the δ-semialdehyde requires expression of two genes in *S. cerevisiae*, *LYS2* and *LYS5*. The reductase, encoded by *LYS2*, contains domains for ATP hydrolysis, thioester formation with a 4-phosphopantetheine binding consensus sequence and an active site serine residue. The reductase is feedback inhibited by lysine and thialysine (*2, 79*). The active form of the reductase requires an additional activity catalyzed by Lys5p, a member of the phosphopantetheinyl transferase (PPTase) family (*80*). It has recently been shown that Lys5p is a posttranslational modification catalyst, which uses coenzyme A (CoASH) as a cosubstrate to phosphopantetheinylate Ser880 of AAR, activating it for catalysis (*81*). Thus, the phosphopantetheinyl transferase and the α–aminoadipate reductase (Lys2p/Lys5p heterodimer) represent a two component system with the transferase covalently priming the reductase, a novel mechanism for fungal amino acid metabolizing enzymes. A human homolog of the α–aminoadipate reductase-phosphopantetheinyl transferase gene has been identified (*82*). The posttranslational

activation of the *LYS2* encoded α-aminoadipate reductase from *C. albicans* has also been investigated (*83*).

A mechanism for the reductase from *S. cerevisiae* has been proposed by Walsh's group (*81*). The reductase is first activated by phosphopantetheinylation using the transferase. The activated reductase then catalyzes the adenylation of the δ-carboxylate of α–aminoadipate via the adenylation (A) domain, followed by acyl transfer of the aminoadipoyl moiety to the thiol of the phosphopantetheine to generate the thioester of the phosphopantetheinyl cleavage protein (PCP) domain. Hydrolysis of the $MgPP_i$ product of the adenylation reaction is used to drive the reaction toward the adenylated intermediate. The covalent thioester intermediate is reduced by NADPH to regenerate reduced phosphopantetheine and the final semialdehyde product. The latter reaction is similar to the reverse of glyceraldehyde 3-phosphate dehydrogenase reaction. Each of the partial reactions of the overall reaction can be studied independently, but mechanistic details will have to await future studies.

The *S. cerevisiae* α–aminoadipate reductase is evolutionarily related to some of the bacterial antibiotic peptide synthetases (*30*). Multienzyme complexes also exist for adenylation and partner-protein-specific posttranslational activation of non-ribosomal peptide synthetases (NRPS) in the synthesis of antibiotics, *e.g.* bacitracin, cyclosporine, penicillin, and vancomycin (*80*). However, the yeast AAR has two unusual features as a non-ribosomal peptide synthetase type catalyst, an unusual organization with a reductase domain fused down-stream of the prototypic adenylation/peptidyl carrier protein domains, and an unusual regiospecific activation

of its amino acid substrate (*81*). Nonetheless, the homology of adenylation and posttranslational modification of AAR to those of NRPS suggests the reductase-catalyzed reaction is the key to the evolution of fungal lysine synthesis. The link between AAR and NRPS may be useful for the design of antifungal agents since Lys2p and Lys5p are essential for fungal growth.

1-3-7. Saccharopine reductase

Saccharopine reductase (SR) (E.C. 1.5.1.10), also known as aminoadipate semialdehyde-glutamate reductase or saccharopine dehydrogenase (N6-(L-1, 3-dicarboxypropyl)-L-lysine: $NADP^+$ oxidoreductase (L-glutamate-forming)), is the penultimate enzyme of the α-aminoadipate pathway for lysine biosynthesis (*3, 12, 87*). The enzyme catalyzes the synthesis of saccharopine via the reversible condensation of α-aminoadipate-δ-semialdehyde with L-glutamate using NADPH as the reducing agent.

1-3-7-1. Expression, purification, and characterization

The enzyme from *S. cerevisiae* has a monomer M.W. of 50,000 by SDS-PAGE and is stable for several weeks when stored at -70 °C in Tris, pH 8.0 containing 1 mM PMSF, 10 mM 2-mercaptoethanol and 5 mM EDTA (*88*). A molecular weight of 67,000 was reported from gel filtration chromatography (*88*), close to a value of 73,000 estimated from sucrose density gradient centrifugation (*89*). The difference between M. W. obtained under native and denaturing conditions was attributed to an

unusual protein conformation (*88*). Additional studies gave a M.W. of 70,000-90,000 under native conditions suggesting a dimeric structure in solution for the fungal enzymes (*4*). A M.W. of 84,000 was obtained by gel-filtration chromatography for the enzyme from *Magnaporthe grisea* suggesting a dimeric structure in agreement with structural studies (*84, 90*).

pH optima of 7.0 for the saccharopine formation reaction (*88*), and 9.5-9.75 for the α-aminoadipate-δ-semialdehyde formation reaction were reported for the enzyme from *S. cerevisiae* (*88-89*). The enzyme is unstable above 34 °C (*88*). Estimates of K_m values for L-saccharopine, $NADP^+$ and NAD^+ were estimated at 2.3 mM, 0.022 mM and 0.054 mM, respectively (*88-89*). It has been reported that NADPH is far more effective than NADH in the forward reaction (*12, 89*). Because α-aminoadipate-δ-semialdehyde is not readily available, the enzyme is typically assayed in the reverse reaction direction (*2*).

Carbonyl reagents such as hydroxylamine, isoniazid and semicarbazide have no effect on enzyme activity, but some metal chelators such as 2, 2-bipyridine and 1, 10-phenanthroline inhibit the enzyme (*88*). The enzyme may require a sulfhydryl group for activity as suggested by complete inhibition in the presence of mercuric chloride (*88*) or *p*-hydroxymercuribenzoate (*12, 88*). The inactivation is attributed to modification of Cys155 in the *S. cerevisiae* enzyme, which is in the proximity of the saccharopine binding site, but not positioned to participate in the reaction (*84*).

1-3-7-2. Structure

The crystal structure of the saccharopine reductase from *M. grisea* has been

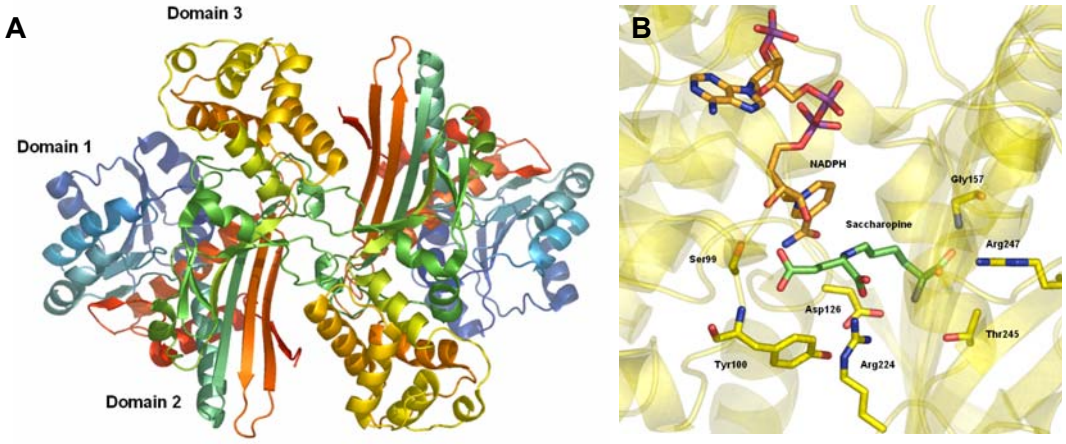

Fig. 1-4: Three dimensional structure of saccharopine reductase from *Magnaporthe grisea* (*84*). A. Ribbon diagram of the dimer. Color depiction is based on the dimer symmetry. PDB accession number is 1E5L. B. Close up view of the active site of the saccharopine reductase from *M. grisea* with NADPH and saccharopine bound. PDB accession number is 1E5Q. Figures produced using PyMOL (www.pymol.org).

solved (*84, 90*). *M. grisea* is a pathogenic fungus of grass species and it is responsible for enormous losses in the rice crop annually (*84, 91*). The purified saccharopine reductase from *M. grisea* was crystallized, and structure of the apo enzyme and ternary E:NADPH:saccharopine complex were solved to 2.0 Å and 2.1 Å, respectively. The apo enzyme and ternary complex structures were homodimeric with each subunit binding one NADPH and one saccharopine molecule (*84*). A ribbon diagram of the apo structure of SR is shown in Fig. 1-4A.

The polypeptide chain of the saccharopine reductase from both *M. grisea* folds into three domains. The first domain is a variant of the dinucleotide-binding Rossmann fold (*92*) that binds to $NADP^+$ or NADPH. The second domain is an α/β fold known as the saccharopine reductase fold. This domain consists of a central seven-stranded

mixed β-sheet. The third domain is an all-helical domain that moves upon binding of substrates. The active site is in a deep cleft that forms between domains one and two (*84*).

One common interacting surface exists between the monomeric units in all structures solved, and it was thus identified as the dimer interface. The two subunits in the homodimer are related by two-fold symmetry. The dimer interface contains 45% polar and 55% nonpolar residues. The majority of the residues at the subunit interface of the fungal enzymes are conserved, while they vary for enzymes from plants and mammals, suggesting there may be a different type of subunit interaction for the fungal organisms (*84*).

Binding of the ligands to the saccharopine reductase from *M. grisea* induces a conformational change that includes a rotation of domain three by 17.7° and a translation of -0.93 Å compared to the structure of the apo enzyme, making the active site less accessible to solvent. NADPH binds in an extended conformation to the Rossmann fold that contains a β-α-β motif with a conserved sequence of GXGXXG (where X is any amino acid). The nicotinamide ring is deeply buried in the cleft and is not accessible to solvent. The carboxamide side chain of NAD(P)H is anchored to the protein by several main chain hydrogen bonds that determine the orientation of the ring and the *pro*-R (A-side) stereospecificity of hydride transfer. Saccharopine is held by a combination of hydrogen bonds, salt-bridges and hydrophobic interactions to the protein, Fig. 1-4B (*84*).

1-3-7-3. Chemical mechanism

A chemical mechanism can be written using the general mechanism for amino acid dehydrogenases and is shown in Fig. 1-5, path A. An imine is formed by attack of the α-amine of glutamate on the δ-aldehyde of α-aminoadipate semialdehyde, likely facilitated by a general acid-base catalyst. Based on the three-dimensional structure of the ternary complex, the general acid-base catalyst is likely Asp126, since there are no other residues in the vicinity of saccharopine that could facilitate proton transfer. Reduction of the imine then gives the product saccharopine. A second possibility involves the cyclic imine formed by attack of the α-amine of AAS on its δ-aldehyde, Fig. 1-5, path B. In this case, the α-amine of glutamate attacks the imine carbon in a transimination reaction, generating the same imine intermediate (in the dashed box) as shown in path A. Similar acid-base chemistry is used, but the physical rearrangement to generate the common imine may not be accommodated in the saccharopine reductase active site. The conformation of saccharopine as bound in the E:NADPH:saccharopine structure favors path A (*84*). In addition, the principle of microscopic reversibility requires the imine be formed as the product in the reverse reaction, which is unlikely. Nevertheless, this mechanism cannot be ruled out at present.

The structure of the saccharopine reductase shows a high structural similarity to enzymes of the diaminopimelate pathway (members of the aspartate family of amino acid biosynthetic pathways), despite the lack of overall amino acid sequence homology. In general, the structure of domain 1 (Rossmann fold) is highly conserved,

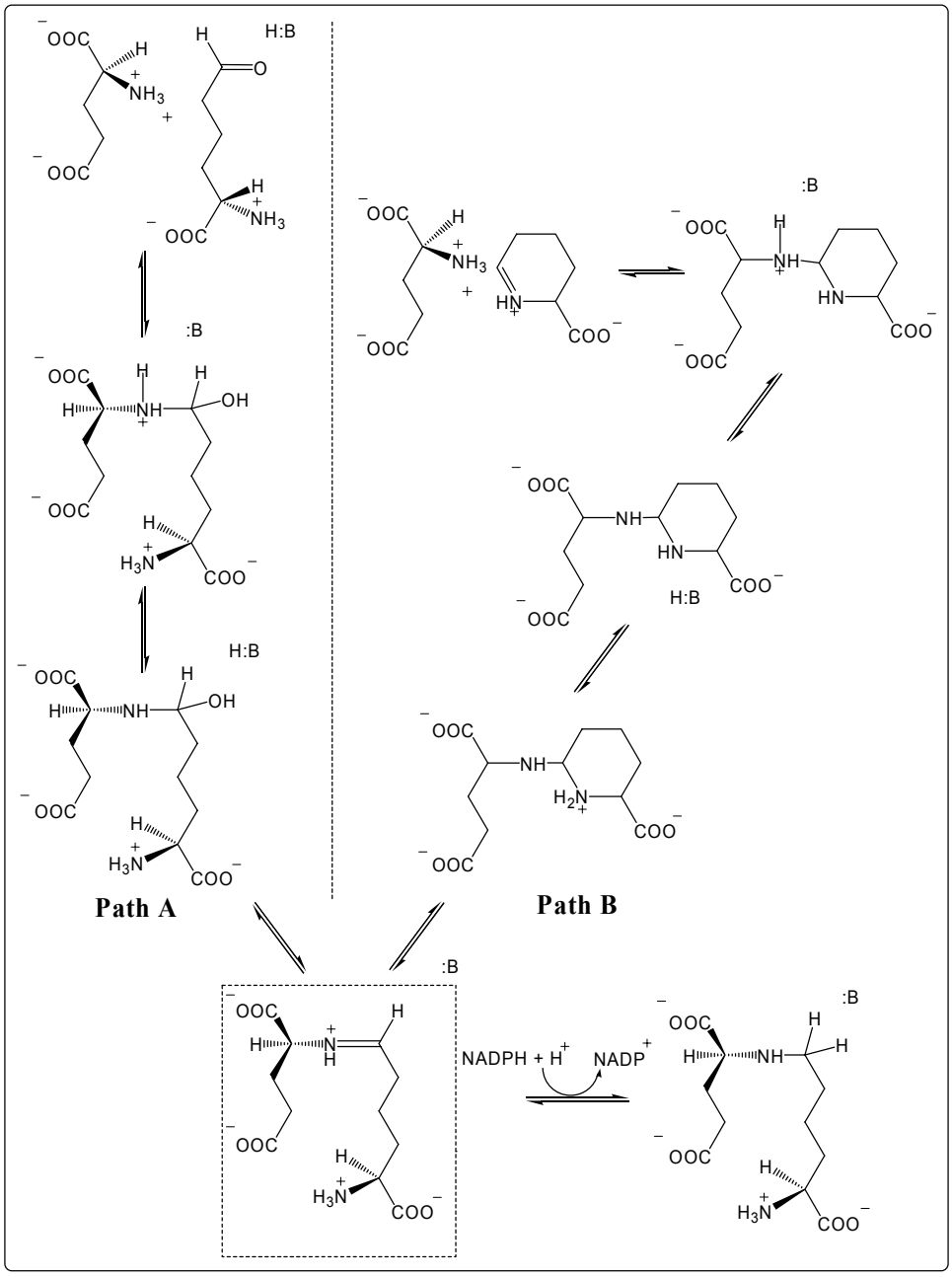

Fig. 1-5: Proposed chemical mechanism for saccharopine reductase.

while the domains 2 and 3 structures are less conserved. Since the AAA and DAP pathways belong to two different amino acid biosynthetic families, the structural similarity may suggest an evolutionary relationship between these two pathways, with

some of the enzymes evolving from a common ancestor (*84*). However, the evolutionary history of this unique fungal lysine pathway is not well established.

1-3-8. Saccharopine dehydrogenase

Saccharopine dehydrogenase (N6-(glutaryl-2)-L-lysine: NAD^+ oxidoreductase (L-lysine forming); (EC 1.5.1.7)) is the last enzyme in the α-aminoadipate pathway for lysine biosynthesis. It catalyzes the reversible pyridine nucleotide-dependent oxidative deamination of saccharopine to generate α-ketoglutarate and lysine using NAD^+ as an oxidizing agent.

1-3-8-1. Expression, purification, and characterization

A monomeric subunit structure was reported for the enzyme from *S. cerevisiae* with a molecular weight of 39,000 Da (*93*). It is a basic protein with a pI of 10.1, and is stable for months at -20 °C at concentrations ≥ 0.1 mg/ml and a pH of 5-8 (*93*). It contains 4 cysteine residues but no disulfide bonds, and one binding site for reactants per molecule of enzyme (*94*). The *LYS1* gene has been cloned from *C. albicans* (*14*) and *S. pombe* (*95*).

1-3-8-2. Kinetic mechanism

The overall reaction catalyzed by SDH is reversible. The *S. cerevisiae* enzyme has an optimum pH in the direction of lysine formation of 10, while in the direction of saccharopine formation it is 7 (*2, 96*). The K_m values for NAD^+, saccharopine, lysine,

α-ketoglutarate, and NADH were estimated as 0.1 mM, 1.7 mM, 2 mM, 0.55 mM, and 0.089 mM, respectively (*2*). SDH from *S. cerevisiae* shows very strict substrate specificity with respect to its amino acid and keto acid substrates (*97-98*). Only pyruvate has been observed as an alternative substrate in the direction of ε–N-(L-propionyl-2)-L-lysine formation (*99*). In addition, the enzyme exhibits a high degree of coenzyme specificity (*97, 100*). It does utilize NADPH as a poor substrate, but with a much lower affinity compared to NADH (*96*). Furthermore, binding of NADPH causes an increase in the K_m values for α-ketoglutarate and lysine (*96*). Coenzyme fragments, such as AMP, ADP, ADP-Ribose, and ATP, inhibit the enzyme activity, but no inhibition is observed by adenine, 3′-AMP, 2′-deoxy-5′-AMP, IMP, GMP, pyrimidine nucleotides, NMN^+, and NMNH (*96*). Data suggest that the AMP moiety of NAD^+ is responsible for majority of the binding energy. The lack of inhibitory effect of 2′-deoxy-5′-AMP and low affinities of NADPH suggests that the interaction of the oxygen at the 2′ position of the adenosine moiety with the enzyme is important in binding (*96*). No binding of lysine or α-ketoglutarate to free enzyme was detected.

A number of pyridine nucleotide dehydrogenases that have an ordered kinetic mechanism exhibit substrate inhibition. SDH was reported to exhibit inhibition by high concentrations of α-ketoglutarate and lysine in the direction of saccharopine formation, but not by saccharopine in the oxidative direction (*101*).

Hydrophobic amino acids with 5 and 6 carbon atoms, leucine, norleucine, and norvaline, were potent inhibitors, while branched-chain isomers, valine, isoleucine, and α-aminobutyrate inhibited weakly, and no inhibition was observed by aspartate,

glutamate, or α-aminoadipate (*98*). It appears that a hydrophobic interaction between the side chain of an amino acid and the enzyme is important in binding the amino acid reactant. Inhibition observed with keto acid analogues was more complicated. Noncompetitive inhibition was observed with oxalacetate, pyruvate, α-ketobutyrate, α-ketovalerate, and α–ketocaproate whether NADH, α-ketoglutarate, or lysine was the varied substrate, inconsistent with the proposed kinetic mechanism. Data suggested combination of the dead-end inhibitors with more than one enzyme form, but this aspect will have to await future studies (*98*).

An ordered Bi-Ter kinetic mechanism was proposed for the SDH with NAD^+ binding first, followed by saccharopine, and products released in the order of lysine, α-ketoglutarate, and NADH (*2, 98, 102*). Since all substrates must add to the enzyme before any product is released, the enzyme may be considered to have separate binding sites for the coenzyme, keto and amino substrates. With pyruvate as a substrate, data also suggest an ordered ter-reactant mechanism in the direction of ε–N-(L-propionyl-2)-L-lysine formation, but with the order NAD^+, ε–N-(L-propionyl-2)-L-lysine, pyruvate, lysine, and NADH (*103*). The reversal in the release of lysine and the keto acid suggests that there may be randomness in substrate binding.

1-3-8-3. Chemical mechanism

SDH is a *pro*-R specific for hydride transfer from C2 of the saccharopine glutaryl moiety to the nicotinamide ring of NAD^+ (*85-86*). A series of chemical modification experiments suggested the presence of essential cysteine (*94*), histidine (*104*), lysine

(*105*), and arginine residues (*106*) that may be involved in substrate-binding and/or catalysis. A chemical mechanism for the enzyme has been proposed on the basis of pH-rate profiles and product and dead end inhibition studies, Fig. 1-6 (*86*). Saccharopine is first oxidized to the ε–glutaminyl-L-lysine. A general base then

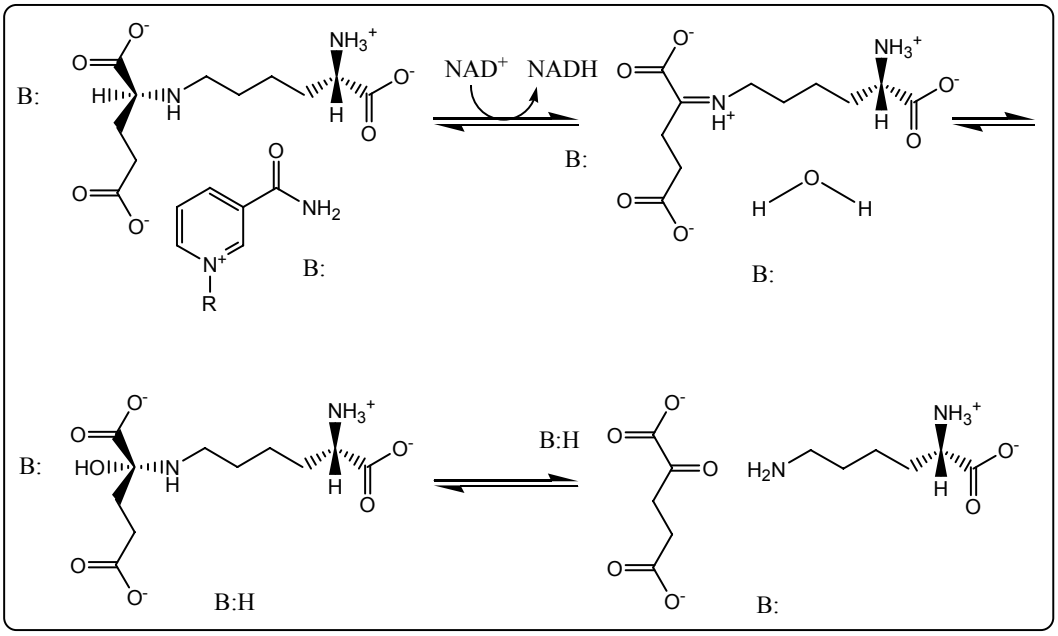

Fig. 1-6: Proposed chemical mechanism for saccharopine dehydrogenase.

activates water for attack to form a carbinolamine intermediate, which collapses to give the products, L-lysine and α–ketoglutarate using general acid, general base chemistry.

In the direction of saccharopine formation, the pH dependence of V/K_{lysine} exhibits a p*K* of 6.3 for a group that must be unprotonated, and a p*K* of 8.0 for a group that must be protonated for activity (*86*). Temperature and solvent perturbation studies are consistent with these groups being histidines. The $V/K_{\alpha\text{-kg}}$ pH profile exhibits a single p*K* of 8.4 for a group that must be protonated for α–ketoglutarate binding (*86*).

In the direction of saccharopine cleavage, the V/K_{sacch} pH profile shows two p*K*s of 6.0 and 7.1 that must both be unprotonated for catalysis and/or binding of saccharopine (*86*). Although the mechanism proposed in Fig. 1-6 is certainly consistent with the data, studies are incomplete and the identity of the groups involved is based on the observed p*K* values, their temperature dependence, and chemical modification studies; all are notoriously inaccurate.

1-4. Summary

Although mechanistic precedence for each of the enzyme-catalyzed reactions discussed above is available, none of the mechanisms of the enzymes in the first half of the α-aminoadipate pathway is known with any certainty. However, some information is available for enzymes in the second half of the pathway. A general mechanism has been proposed for the α-aminoadipate reductase, but all mechanistic detail is lacking. For the saccharopine reductase, only structural information is available, with virtually nothing known of its mechanism. Significant, but incomplete, mechanistic data have been collected for the saccharopine dehydrogenase, but no structural information is available. Regulation of the pathway at the enzyme level is not completely clear and little is known about the mechanism of regulation.

Our understanding of the α-aminoadipate pathway for lysine synthesis at the molecular level has been increasing dramatically, together with a growth in genomic information. However, a complete understanding of the gene-enzyme relationship, mechanisms of the enzymes, regulation of the α-aminoadipate pathway, as well as a

comparative study of the cloned genes would help to gain an understanding of the functions of the biosynthetic and catabolic genes and enzymes. Knowledge gained using biochemical and molecular techniques with *S. cerevisiae* can be applied to pathogenic fungi to gain a basic understanding of the metabolism of fungal pathogens. Systemic fungal infections are among the most difficult infectious diseases to treat and are life-threatening for individuals who are immune-suppressed, including those with AIDS and other autoimmune diseases, those undergoing chemotherapy, and those who have undergone a transplant. All of the presently available antifungal drugs have side effects, including nausea, vomiting, and diarrhea, toxicities including hepatotoxicity and renal insufficiency, and drug interactions. It is thus important to develop new antifungal drugs that are more effective and less toxic. The metabolic pathway for the biosynthesis of lysine in fungi is for the most part unique to these organisms, which has prompted speculation that the enzymes involved in the pathway may be viable targets for selective antifungal agents. Selective inhibition of the enzyme(s) by an appropriate substrate analog(s) may control the growth of fungal pathogens *in vivo*. Similarly, the novelty of several genes in the pathway may permit them to serve as a molecular marker to facilitate rapid identification of fungal pathogens.

In this dissertation, extensive kinetic data about homocitrate synthase and the crystal structure of the saccharopine reductase from *S. cerevisiae* is presented. In chapter two, we describe for the first time the stabilization of the unstable cytosolic HCS using the artificial chaperone-assisted renaturation strategy. The stabilized enzyme has also been characterized with respect to its physical properties. In chapter

three, we report the kinetic mechanism of the HCS from *S. cerevisiae* using initial velocity, product and dead-end kinetic studies. In chapter four, we make use of steady state kinetic and fluorescence binding studies to probe the kinetics of regulation of the cytosolic HCS by Na^+ and lysine. In chapter five, a theory is developed for regulation by multiple effectors on the basis of studies presented in chapter four. Also, rate equations are derived to predict the regulatory effects of Na^+ and lysine on the activity of HCS, on the basis of experimental data presented in chapter four. The simulated data suggest that the activity of the HCS in the presence of Na^+ is simultaneously inhibited and activated and the Na^+ effect is independent of lysine. Finally, in chapter six, we report the crystal structure of the apo-histidine-tagged saccharopine reductase from *S. cerevisiae*. A comparative structural analysis with an emphasis on the active site is presented.

References

[1] Umbarger, H. E. (1978) Amino acid biosynthesis and its regulation. *Annu Rev Biochem 47*, 532-606.

[2] Zabriskie, T. M. and Jackson, M. D. (2000) Lysine biosynthesis and metabolism in fungi. *Nat. Prod. Rep. 17*, 85-97.

[3] Bhattacharjee, J. K. (1985) α-Aminoadipate pathway for the biosynthesis of lysine in lower eukaryotes. *Crit. Rev. Microbiol. 12*, 131-151.

[4] Bhattacharjee, J. K. (1992) Evolution of α-aminoadipate pathway for the synthesis of lysine in fungi, in handbook of Evolution of metabolic function, (Mortlock, R. P., ed.), CRC Press, Boca Raton, Fla, pp. 47-80.

[5] Vogel, H. J. (1960) Two modes lysine synthesis among lower fungi: evolutionary significance. *Biochim. Biophys. Acta. 41*, 172-174.

[6] Berges, D. A., DeWolf, W. E., Jr., Dunn, G. L., Grappel, S. F., Newman, D. J., Taggart, J. J., and Gilvarg, C. (1986) Peptides of 2-aminopimelic acid: antibacterial agents that inhibit diaminopimelic acid biosynthesis. *J. Med. Chem. 29*. 89-95.

[7] Bhattacharjee, J. K. and Strassman, M. (1967) Accumulation of tricarboxylic acids related to lysine biosynthesis in a yeast mutant. *J. Biol. Chem. 242*, 2542-2546.

[8] Gaillardin, C. M., Ribert, A. M., and Heslot, H. (1982) Wild type and mutant forms of homoisocitric dehydrogenase in the yeast *Saccharomycopsis lipolytica*. *Eur. J. Biochem. 128*, 489-494.

[9] Ye, Z. H. and Bhattacharjee, J. K. (1988) Lysine biosynthesis pathway and biochemical blocks of lysine auxotrophs of *Schizosaccharomyces pombe*. *J. Bacteriol. 170*, 5968-5970.

[10] Glass, J. and Bhattacharjee, J. K. (1971) Biosynthesis of lysine in *R. glutinis*: accumulation of homocitric, homoaconitic, and homoisocitric acids in a leaky mutant. *Genetics 67*, 365-376.

[11] Kunze, G., Bode, R., Schmidt, H., Samsonova, I. A., and Birnbaum D. (1987) Identification of a *lys2* mutant of *C. maltosa* by means of transformation. *Curr. Genet. 11*, 385-391.

[12] Broquist, H. P. (1971) Lysine biosynthesis (yeast). *Methods Enzymol. 17*, 112-129.

[13] Jaklitsch, W. M. and Kubicek, C. P. (1990) Homocitrate synthase from *Penicillium chrysogenum*. Localization, purification of the cytosolic isoenzyme, and sensitivity to lysine. *Biochem. J. 269*, 247-253.

[14] Garrad, R. C. and Bhattacharjee, J. K. (1992) Lysine biosynthesis in selected pathogenic fungi: characterization of lysine auxotrophs and the cloned *LYS1* gene of *Candida albicans*. *J. Bacteriol. 174*, 7379-7384.

[15] Andi, B., West, A. H., and Cook, P. F. (2004) Stabilization and characterization of histidine-tagged homocitrate synthase from *Saccharomyces cerevisiae*. *Arch. Biochem. Biophys. 421*, 243-254.

[16] Strassman, M. and Weinhouse, S. (1953) Biosynthetic pathways. III. The biosynthesis of lysine *Torulopsis utilis*. *J. Am. Chem. Soc. 75*, 1680-1684.

[17] Vogel, H. J. (1965) Lysine biosynthesis and evolution, in handbook of Evolving genes and proteins (Bryson, V., ed.), Academic Press, New York, pp. 25-40.

[18] Nishida, H., Nishiyama, M., Kobashi, N., Kosuge, T., Hoshino, T., and Yamane, H. (1999) A prokaryotic gene cluster involved in synthesis of lysine through the aminoadipate pathway: a key to the evolution of amino acid biosynthesis. *Genome Res. 9*, 1175-1183.

[19] Cunin, R., Glandsorff, N., Pierard, A., and Stalon, V. (1986) Biosynthesis and metabolism of arginine in bacteria. *Microbiol. Rev. 50*, 314-352.

[20] Jacq, C., Alt-Morbe, J., Andre, B., Arnold, W., Bahr, A., Ballesta, J. P.,Bargues, M., Baron, L., Becker, A., Biteau, N., Blocker, H., Blugeon, C., Boskovic, J., Brandt, P., Bruckner, M., Buitrago, M. J., Coster, F., Delaveau, T., del Ray, F., Dujon, B., Eide, L. G., Garcia-Cantalejo, J. M., Goffeau, A., Gomez-Peris, A., Zaccaria, P., and al, e. (1997) The nucleotide sequence of *Saccharomyces cerevisiae* chromosome IV. *Nature 387*, 75-78.

[21] Philippsen, P., Kleine, K., Pohlmann, R., Dusterhoft, A., Hamberg, K., Hegemann, J. H., Obermaier, B., Urrestarazu, L. A., Aert, R., Albermann, K., Altmann, R., Andre, B., Baladron, V., Ballesta, J. P., Becam, A. M., Beinhauer, J., Boskovic, J., Buitrago, M. J., Bussereau, F., Coster, F., Crouzet, M., D'Andelo, M., Dal Pero, F., De Antoni, A., Hani, J. and al, e. (1997) The nucleotide sequence of *Saccharomyces cerevisiae* chromosome XIV and its evolutionary implications. *Nature 387*, 93-98.

[22] Tettelin, H., Agostoni Carbone, M. L., Albermann, K., Albers, M., Arroyo, J., Backes, U., Barreiros, T., Bertani, I., Bjourson, A. J., Bruckner, M., Bruschi, C. V., Carignani, G., Castagnoli, L., Cerdan, E., Clemente, M. L., Coblenz, A., Coglievina, M., Coissac, E., Defoor, E., Del Bino, S., Delius, H., Delneri, D., de Wergifosse, P., Dujon, B., Kleine, K. and al, e. (1997) The nucleotide sequence of *Saccharomyces cerevisiae* chromosome VII. *Nature 387*, 81-84.

[23] Borell, C. W., Urrestarazu, L.A., and Bhattacharjee, J. K. (1984) Two unlinked lysine genes (*LYS9* and *LYS14*) are required for the synthesis of saccharopine reductase in *Saccharomyces cerevisiae*. *J. Bacteriol. 159*, 429-432.

[24] Wang, L., Okamoto, S., and Bhattacharjee, J. K. (1989) Cloning and physical characterization of linked lysine genes (*LYS4*, *LYS15*) of *S. cerevisiae*. *Curr. Genet. 16*, 7-12.

[25] Urrestarazu, L. A., Borell, C. W., and Bhattacharjee, J. K. (1985) General and specific controls of lysine biosynthesis in *Saccharomyces cerevisiae. Curr. Genet. 9*, 341-344.

[26] Irvin, S. D. and Bhattacharjee, J. K. (1998) A unique fungal lysine biosynthesis enzyme shares a common ancestor with tricarboxylic acid cycle and leucine biosynthetic enzymes found in diverse organisms. *J. Mol. Evol. 46*, 401-408.

[27] Karsten, W. E. and Cook, P. F. (2000) Pyridine nucleotide-dependent β-hydroxyacid oxidative decarboxylases: an overview. *Protein and Peptide Letters 7*, 281-286.

[28] Ye, Z. H., Garrad, R. C., Winston, M. K, and Bhattacharjee, J. K. (1991) Use of alpha-aminoadipate and lysine as sole nitrogen source by *Schizosaccharomyces pombe* and selected pathogenic fungi. *J Basic Microbiol. 31*(2), 149-56.

[29] Nishida, H. and Nishiyama, M. (2000) What is characteristic of fungal lysine synthesis through the α-aminoadipate pathway? *J. Mol. Evol. 51*, 299-302.

[30] Kosuge, T. and Hoshino T. (1998) Lysine is synthesized through the α-aminoadipate pathway in *Thermus thermophilus*. *FEMS Microbiol. Lett. 169*, 361-367.

[31] Kobashi, N., Nishiyama, M., and Tanokura, M. (1999) Aspartate kinase-independent lysine synthesis in an extremely thermophilic bacterium, *Thermus thermophilus*: lysine is synthesized via α-aminoadipic acid not via diaminopimelic acid. *J. Bacteriol. 181*, 1713-1718.

[32] Baldwin, J. E., Shiau, C., Byford, M., and Schofield, C. J. (1994) Substrate specificity of L-delta-(alpha-aminoadipoyl)-L-cysteinyl-D-valine synthetase from *Cephalosporium acremonium*: demonstration of the structure of several unnatural tripeptide products. *Biochem. J. 301*, 367-372.

[33] Palmer D. R., Balogh, H, Ma, G., Zhou, X., Marko, M., and Kaminskyj, S. G. (2004) Synthesis and antifungal properties of compounds which target the alpha-aminoadipate pathway. *Pharmazie. 59*, 93-98.

[34] Ramos, F., Dubois, E., and Piérard, A. (1988) Control of enzyme synthesis in the lysine biosynthetic pathway of *Saccharomyces cerevisiae.* Evidence for a regulatory role of gene *LYS14. Eur. J. Biochem. 171*, 171-176.

[35] Wolfner, M., Yep, D., Messenguy, F., and Fink, G. R. (1975) Integration of amino acid biosynthesis into the cell cycle of *Saccharomyces cerevisiae*. *J. Mol. Biol. 96*, 273-290.

[36] Becker, B., Feller, A., El Alami, M., Dubois, E., and Pierard, A. (1998) A nonameric core sequence is required upstream of the *LYS* genes of *Saccharomyces cerevisiae* for Lys14p- mediated activation and apparent repression by lysine. *Mol. Microbiol. 29*, 151-163.

[37] Ramos, F., Verhasselt, P., Feller, A., Peeters, P., Wach, A., Dugois, E., and Volckaert, G. (1996) Identification of a gene encoding a homocitrate synthase isoenzyme of *Saccharomyces cerevisiae*. *Yeast 12*, 1315-1320.

[38] Tucci, A. F. and Ceci, L. N., (1972) Homocitrate synthase from yeast. *Arch. Biochem. Biophys. 153*, 742-750.

[39] Ramos, F., and Wiame, J. M. (1985) Mutation affecting the specific regulatory control of lysine biosynthetic enzymes in *Saccharomyces cerevisiae*. *Mol. Gen. Genet. 200*, 291-294.

[40] Feller, A., Ramos, F., Piérard, A., and Bubois, E. (1999) In *Saccharomyces cerevisiae,* feedback inhibition of homocitrate synthase isoenzymes by lysine modulates the activation of *LYS* gene expression by Lys14p. *Eur. J. Biochem. 261*, 163-170.

[41] Harrison, S. C. (1991) A structural taxonomy of DNA-binding domains. *Nature 353*, 715-719.

[42] Vallee, B. L., Coleman, J. E., and Auld, D. S. (1991) Zinc fingers, zinc clusters, and zinc twists in DNA-binding protein domains. *Proc. Natl. Acad. Sci.* USA *88*, 999-1003.

[43] Marmorstein, R., Carey, M., Ptashne, M., and Harrison, S. C. (1992) DNA recognition by *GAL4*: structure of a protein-DNA complex. *Nature 356*, 408-414.

[44] Marmorstein, R., and Harrison, S. C. (1994) Crystal structure of a PPR1-DNA complex: DNA recognition by proteins containing a Zn_2Cys_6 binuclear cluster. *Genes Dev. 8*, 2504-2512.

[45] Schjerling, P. and Holmberg, S. (1996) Comparative amino acid sequence analysis of the C_6 zinc cluster family of transcriptional regulators. *Nuc. Acid. Res. 24*, 4599-4607.

[46] Bañuelos, O., Casqueiro, J., Gutiérrez, S., and Martín, J. F. (2000) Overexpression of the *lys1* gene in *Penicillium chrysogenum*: homocitrate synthase levels, α-aminoadipic acid pool and penicillin production. *Appl. Microbiol. Biotechnol. 54*, 69-77.

[47] Wulandari, A. P., Miyazaki, J., Kobashi, N., Nishiyama, M., Hoshino, T., and Yamane, H. (2002) Characterization of bacterial homocitrate synthase involved in lysine biosynthesis. *FEBS Lett. 522*, 35-40.

[48] Friedrich, C. G. and Demain, A. L. (1977) Homocitrate synthase as the crucial site of the lysine effect on penicillin biosynthesis. *J. Antibiot. 30*, 760-761.

[49] Somerson, N. L., Demain, A. L., and Nunheimer, T. D. (1961) Reversal of lysine inhibition of penicillin production by α-aminoadipic acid. *Arch. Biochem. Biophys. 93*, 238-241.

[50] Luengo, J. M., Revilla. G., López, M. J., Villanueva, J. R., and Martín, J. F. (1980) Inhibition and repression of homocitrate synthase by lysine in *Penicillium chrysogenum. J. Bacteriol. 144*, 869-976.

[51] Tracy, J. W. and Kohlhaw, G. B. (1975) Reversible, Coenzyme-A-medidated inactivation of biosynthetic condensing enzymes in yeast: a possible regulatory mechanism. *Proc. Nat. Acad. Sci.* USA *72*, 1802-1806.

[52] Hampsey, D. M. and Kohlaw, G. B. (1981) Inactivation of yeast α-isopropyl malate synthase by CoA. *J. Biol. Chem. 256*, 3791-3796.

[53] Tracy, J. W. and Kohlhaw, G. B. (1977) Evidence for two distinct CoA binding sites on yeast α-isopropylmalate synthase. *J. Biol. Chem. 252*, 4085-4091.

[54] Kohlhaw, G. B. (2003) Leucine biosynthesis in fungi: entering metabolism through the back door. *Microbiol. Mol. Biol. Rev. 67*, 1-15.

[55] Tan-Wilson, A. and Kohlhaw, G. B. (1978) Specific, reversible inactivation of yeast β-hydroxy-β-methylglutaryl-CoA reductase by CoA. *Biochem. Biophys. Res. Commun. 85*, 70-76.

[56] Gilbert, H. F. and Stewart, M. D. (1981) Inactivation of hydroxymethylglutaryl-CoA reductase from yeast by coenzyme A disulfide. *J. Biol. Chem. 256*. 1782-1785.

[57] Li, J. J. (2003) Name Reactions: A collection of detailed reaction mechanism (II ed.), Springer-Verlag, Berlin, Heidelberg, pp. 73.

[58] Alter, G. M., Casazza, J. P., Zhi, W., Memeth, P., Srere, P. A., and Evans, C. T. (1990) Mutation of essential catalytic residues in pig citrate synthase. *Biochemistry 29*, 7557-7563.

[59] Karpusas, M., Branchaud, B., and Remington, S. J. (1990) Proposed mechanism for the condensation reaction of citrate synthase: 1.9 Å structure of the ternary complex with oxaloacetate and carboxymethyl coenzyme A. *Biochemisty 29*, 2213-2219.

[60] Mulholland, A. J., Lyne, P. D., and Karplus, M. (2000) Ab initio QM/MM study of the citrate synthase mechanism: a low-barrier hydrogen bond is not involved. *J. Am. Chem. Soc. 122*, 534-535.

[61] Evans, C. T., Kurz, L. C., Remington, S. J., and Srere, P. A. (1996) Active site mutants of pig citrate synthase: effects of mutations on the enzyme catalytic and structural properties. *Biochemistry 35*, 10661-10672.

[62] Simth, C. V., Huang, C.-C., Miczak, A., Russell, D. G., Sacchettini, J, C., and Höner zu Bentrup, K. (2003) Biochemical and structural studies of malate synthase from *Mycobacterium tuberculosis*. *J. Biol. Chem. 278*, 1735-1743.

[63] Anstrom, D. M., Kallio, K., and Remington, S. J. (2003) Structure of the *Escherichia coli* malate synthase G:pyruvate:acetyl-coenzyme A abortive ternary complex at 1.95 Å resolution. *Protein Sci. 12*, 1822-1832.

[64] Howard, B. R., Endrizzi, J. A., and Remington, S. J. (2000) Crystal structure of *Escherichia coli* malate synthase G complexed with magnesium and glyoxylate at 2.0 Å resolution: mechanistic implications. *Biochemistry 39*, 3156-3168.

[65] Koon, N., Squire, C. J., and Baker, E. N. (2004) Crystal structure of LeuA from *Mycobacterium tuberculosis*, a key enzyme in leucine biosynthesis. *Proc. Nat. Acad. Sci.* USA *101*, 8295-8300.

[66] Chen, S., Brockenbrough, J. S., Dove, J. E., and Aris, J. P. (1997) Homocitrate synthase is located in the nucleus in the yeast *Saccharomyces cerevisiae. J. Biol. Chem. 272*, 10839-10846.

[67] Bañuelos, O., Casqueiro, J., Steidl, S., Gutiérrez, S., Brakhage, A., and Martin, J. F. (2002) Subcellular localization of the homocitrate synthase in *Penicillium chrysogenum. Mol. Genet. Genomics. 266*, 711-719.

[68] Verhassselt, P., Voet, M., and Volckaert, G. (1995) New open reading frames, one of which is similar to the *nifV* gene of *Azotobacter vinelandii,* found on a

12.5 kbp fragment of chromosome IV of *Saccharomyces cerevisiae*. *Yeast 11*, 961-966.

[69] Shah, V. K. and Brill, W. J. (1977) Isolation of an iron-molybdenum cofactor from nitrogenase. *Proc. Natl. Acad. Sci.* USA *74*, 3249-3253.

[70] Zheng, L. M., White, R. H., and Dean, D. R. (1997) Purification of the *Azotobacter vinelandii nifV*-encoded homocitrate synthase. *J. Bacteriol. 179*, 5963-5966.

[71] Gaillardin, C. M., Poirier, L., and Heslot, H. (1976) A kinetic study of homocitrate synthase activity in the yeast *Saccharomycopsis lipolytica. Biochim. Biophys. Acta. 422*, 390-406.

[72] Beinert, H., Kennedy, M. C., and Stout, C. D. (1996) Aconitase as iron-sulfur protein, enzyme, and ironregulatory protein. *Chem. Rev. 96*, 2335-2373.

[73] Grodsky, N. B., Soundar, S., and Colman, R. F. (2000) Evaluation by site-directed mutagenesis of aspartic acid residues in the metal site of pig heart NADP-dependent isocitrate dehydrogenase. *Biochemistry 39*, 2193-2200.

[74] Matsuda, M. and Ogur, M. (1969) Separation and specificity of the yeast glutamate-α-ketoadipate transaminase. *J. Biol. Chem.* 244, 3352-3358.

[75] Matsuda, M. and Ogur, M. (1969) Enzymatic and physiological properties of the yeast glutamate-α-ketoadipate transaminase. *J. Biol. Chem. 244*, 5153-5158.

[76] Sagisaka, S. and Shimura, K. (1962) Studies in lysine biosynthesis. IV. Mechanism of activation and reduction of α–aminoadipic acid. *J. Biochem. 52*, 155-161.

[77] Larson, R. L., Sandine, W. D., and Broquist, H. P. (1963) Enzymatic reduction of α-aminoadipic acid: relation to lysine biosynthesis. *J. Biol. Chem. 238*, 275-282.

[78] Sinha, A. K. and Bhattacharjee, J. K. (1971) Lysine biosynthesis in *Saccharomyces*, conversion of α-aminoadipate into α-aminoadipic δ-semialdehyde. *Biochem. J. 125*, 743-749.

[79] Suyarna, K., Seah, L., Bhattacharjee, V., and Bhattacharjee, J. K. (1998) Molecular analysis of the *LYS2* gene of *Candida albicans*: homology to peptide antibiotic synthetases and the regulation of the α-aminoadipate reductase. *Curr. Genet. 33*, 268-275.

[80] Lambalot, R. H., Gehring, A. M., Flugel, R. S., Zuber, P., LaCelle, M., Marahiel, M. A., Reid, R., Khosla, C., and Walsh, C. T. (1996) A new enzyme superfamily -- the phosphopantetheinyl transferases. *Chem. Biol. 3*, 932-936.

[81] Ehmann, D. E., Gehring, A. M, and Walsh, C. T. (1999) Lysine biosynthesis in *Saccharomyces cerevisiae*: mechanism of α–aminoadipate reductase (*LYS2*) involves posttranslational phosphopantetheinylation by *LYS5*. *Biochemistry 38*, 6171-6177.

[82] Praphanphoj, V., Sacksteder, K. A., Gould, S. J., Thomas, G. H., and Geraghty, M. T. (2001) Identification of the α-aminoadipic semialdehyde dehydrogenase-phosphopantetheinyl transferase gene, the human ortholog of the yeast *LYS5* gene. *Mol. Genet. Metab. 72*, 336-342.

[83] Guo, S., Evans, S. A., Wilkes, M. B., and Bhattacharjee, J. K. (2001) Novel posttranslational activation of the *LYS2*-encoded α–aminoadipate reductase for biosynthesis of lysine and site-directed mutational analysis of conserved amino acid residues in the activation domain of *Candida albicans. J. Bacteriol. 183*, 7120-7125.

[84] Johansson, E., Steffens, J. J., Lindqvist, Y., and Schneider, G. (2000) Crystal structure of saccharopine reductase from *Magnaporthe grisea*, an enzyme of the α-aminoadipate pathway of lysine biosynthesis. *Structure Fold. Des. 8*, 1037-1047.

[85] Fujioka, M. and Takata, Y. (1979) Stereospecificity of hydrogen transfer in the saccharopine dehydrogenase reaction. *Biochim. Biophys. Acta. 570*, 210-212.

[86] Sugimoto, K. and Fujioka, M. (1984) Chemical mechanism of saccharopine dehydrogenase (NAD^+, L-lysine-forming) as deduced form initial rate pH studies. *Arch. Biochem. Biophys. 230*, 553-559.

[87] Jones, E. W. and Fink, G. R. (1982) Regulation of amino acid and nucleotide synthesis in yeast, in molecular biology of the yeast *Saccharomyces*, metabolism and gene regulation (Strathern, J. N., Jones, E. W. and Broach, J. R., ed.), Cold spring harbor laboratory, Cold spring harbor, NY, pp. 181-299.

[88] Storts, D. R. and Bhattacharjee, J. K. (1987) Purification and properties of saccharopine dehydrogenase (glutamate forming) in the *Saccharomyces cerevisiae* lysine biosynthetic pathway. *J. Bacteriol. 169*, 416-418.

[89] Jones, E. E. and Broquist, H. P. (1966) Saccharopine, an intermediate of the aminoadipic acid pathway of lysine biosynthesis. III. Aminoadipic semialdehyde-glutamate reductase. *J. Biol. Chem. 241*, 3430-3434.

[90] Johansson, E., Steffens, J. J., Emptage, M., Lindqvist, Y., and Schneider, G. (2000) Cloning, expression, purification and crystallization of saccharopine reductase from *Magnaporthe grisea. Acta Crystallogr.* D *Biol. Crystallogr. 56*, 662-664.

[91] Talbot, N. J. (1995) Having a blast: exploring the pathogenicity of *Magnaporthe grisea*. *Trends Microbiol. 3*, 9-16.

[92] Rossmann, M. G., Liljas, A., Branden, C. I., and Banaszak, L. J. (1975) Evolutionary and structural relationship among dehydrogenases. *Enzymes 11*, 51-102.

[93] Ogawa, H. and Fujioka, M. (1978) Purification and characterization of saccharopine dehydrogenase from baker's yeast. *J. Biol. Chem. 253*, 3666-3670.

[94] Ogawa, H., Okamoto, M. and Fujioka, M. (1979) Chemical modification of the active site sulfhydryl group of saccharopine dehydrogenase (L-lysine-forming). *J. Biol. Chem*. *254*, 7030-7035.

[95] Ford, R. A. and Bhattacharjee, J. K. (1995) Molecular properties of the *lys1+* gene and the regulation of α-aminoadipate reductase in *Schizosaccharomyces pombe*. *Curr. Genet. 28*, 131-137.

[96] Fujioka, M. and Nakatani, Y. (1974) Saccharopine dehydrogenase, a kinetic study of coenzyme binding. *J. Biol. Chem. 249*, 6886-6891.

[97] Saunders, P. P. and Broquist, H. P. (1966) Saccharopine, an intermediate of the aminoadipic acid pathway of lysine biosynthesis, saccharopine dehydrogenase. *J. Biol. Chem. 241*, 3435-3440.

[98] Fujioka, M. and Nakatani, Y. (1972) Saccharopine dehydrogenase, interaction with substrate analogues. *Eur. J. Biochem. 25*, 301-307.

[99] Fujioka, M. and Tanaka, M. (1978) Enzymic and chemical synthesis of ε–N-(L-propionyl-2)-L-lysine. *Eur. J. Biochem. 90*, 297-300.

[100] Cleland, W. W. (1963) The kinetics of enzyme-catalyzed reactions with two or more substrates. *Biochim. Biophys. Acta. 67*, 173-187.

[101] Fujioka, M. (1975) Saccharopine dehydrogenase, substrate inhibition studies. *J. Biol. Chem. 250*, 8986-8989.

[102] Fujioka, M. and Nakatani, Y. (1970) A kinetic study of saccharopine dehydrogenase reaction. *Eur. J. Biochem. 16*, 180-186.

[103] Sugimoto, K. and Fujioka, M. (1978) The reaction of pyruvate with saccharopine dehydrogenase. *Eur. J. Biochem. 90*, 301-307.

[104] Fujioka, M., Takata, Y., Ogawa, H., and Okamoto, M. (1979) The inactivation of saccharopine dehydrogenase (L-lysine-forming) by diethyl pyrocarbonate. *J. Biol. Chem. 255*, 937-942.

[105] Ogawa, H. and Fujioka, M. (1980) The reaction of pyridoxal-5′-phosphate with an essential lysine residue of saccharopine dehydrogenase (L-lysine-forming). *J. Biol. Chem. 255*, 7420-7425.

[106] Fujioka, M. and Takata, Y. (1981) Role of arginine residue in saccharopine dehydrogenase (L-lysine-forming) from baker's yeast. *Biochemistry 20*,468-472.

CHAPTER 2

Stabilization and characterization of homocitrate synthase

"Reproduced with automatic permission from [Andi, B., West A. H., and Cook, P. F. (2004) Stabilization and characterization of Histidine-tagged Homocitrate Synthase from *Saccharomyces cerevisiae*, *Arch. Biochem. Biophys. 421*, 243-254] Copyright [2003] Elsevier Inc."

2-1. Introduction

Lysine is the only essential amino acid known to have two distinct anabolic pathways for its biosynthesis. The diaminopimelate pathway is found in plants, bacteria and lower fungi and begins with the phosphorylation of aspartate by

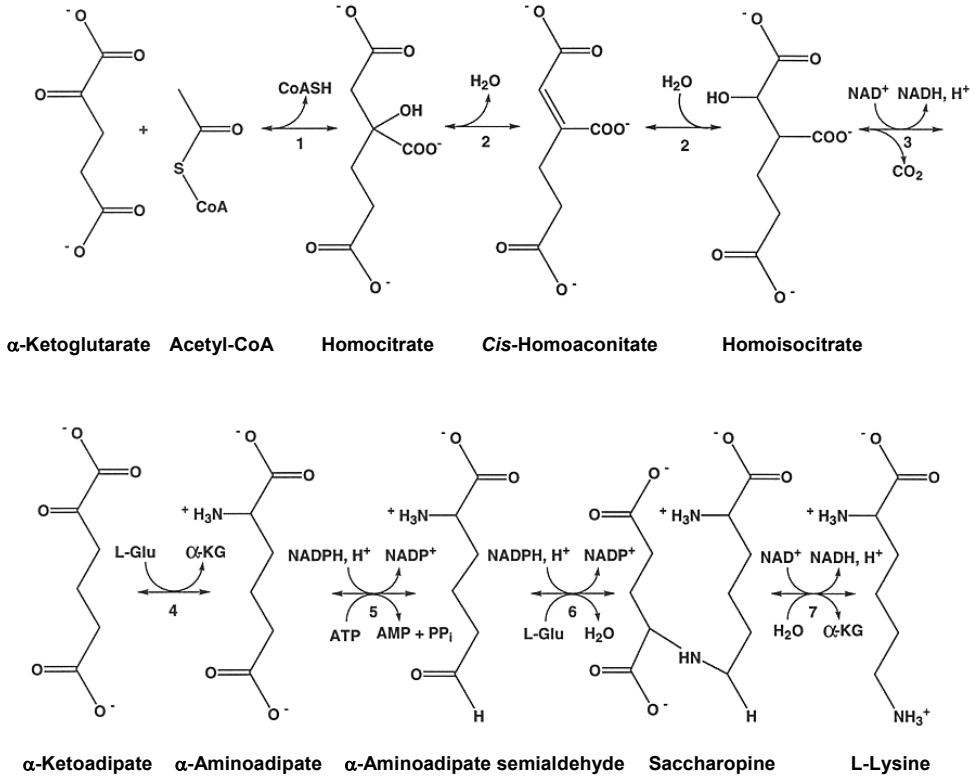

Fig. 2-1: α-Aminoadipate pathway for the synthesis of lysine. Homocitrate synthase catalyses the first and committed step of the pathway. The enzymes of the pathway are as follows: (1) Homocitrate synthase, (2) Homoaconitate hydratase, (3) Homoisocitrate dehydrogenase, (4) α-Aminoadipate aminotransferase, (5) α-Aminoadipate reductase, (6) Saccharopine dehydrogenase (L-Glu forming), (7) Saccharopine dehydrogenase (L-Lys forming).

aspartokinase. Human pathogenic fungi such as *Candida albicans*, *Cryptococcus neoformans* and *Aspergillus fumigatus* and plant pathogens like *Magnaporthe grisea* use the α-aminoadipate pathway for the synthesis of the lysine (Fig. 2-1). The human pathogens represent a major health threat for patients with cancer, transplant patients and AIDS patients undergoing immunosuppressive treatment. In addition, *Magnaporthe grisea* is among the most destructive pathogens in crop plants. The uniqueness of the α-aminoadipate pathway makes it a potential target for new antifungal drugs (*1-6*).

Homocitrate synthase (HCS) [2-hydroxybutane-1,2,4-tricarboxylate 2-oxoglutarate-lyase (CoA-acetylating), EC 2.3.3.14] catalyzes the first and committed step of the pathway (Fig. 2-1) which involves the condensation of α-ketoglutarate with acetyl-CoA to yield homocitrate and coenzyme A (*1, 7-9*). The first half of the α-aminoadipate pathway has been reported to be located in the mitochondria (*10*). There are two isozymes of homocitrate synthase (cytosolic and mitochondrial) from *Saccharomyces cerevisiae* that are subject to feedback inhibition by lysine. Expression of the cytosolic isozyme can be strongly repressed by lysine (*7*). It has been also reported that CoA is capable of regulating the enzyme activity in the presence of divalent metal ions (*8*).

Homocitrate synthase is an unstable enzyme as isolated. As reported in the case of the *Penicillium chrysogenum* enzyme, storage at 4-6 °C for 48 hrs in the presence of 20% glycerol results in a 65% loss of activity; after freezing and thawing, 50% of the initial activity remained (*9*). In *Saccharomycopsis lipolytica*, the enzyme has been

reported to be stable for one week at 4°C (*10*). In another study, the crude enzyme from *Saccharomyces cerevisiae* was only stable for 4 days at 0 °C (*11*).

Using the artificial chaperone-assisted renaturation strategy (*12-13*), in this paper we describe for the first time stabilization of the cytosolic homocitrate synthase from *Saccharomyces cerevisiae*. The stabilized enzyme has been characterized with respect to its physical properties.

2-2. Materials and methods

2-2-1. Chemicals

All chemicals were of the highest grade commercially available. The Ni-NTA agarose resin was from Qiagen, imidazole was from Research Organics, and the rTEV protease was from Invitrogen. Acetyl-CoA, α-ketoglutarate, dichlorophenol indophenol (DCPIP), CoASH, sucrose, sorbitol, glutamic acid, α-cyclodextrin, PMSF and chloramphenicol were obtained from Sigma. $(NH_4)_2SO_4$, PEG-1500 and 2-methyl-2,4-pentanediol (MPD) were from Fluka. GdmCl, glycerol and NH_4Cl were obtained from Fisher Scientific. Hepes and kanamycin were from Amresco. Gdm sulfate was purchased from TCI America. Urea, DTT, IPTG and SDS were from Gibco BRL, Boehringer Mannheim Biochemicals, Gold BioTechnology, Inc. and Bio-Rad, respectively.

Acetyl-CoA was prepared freshly prior to each assay and the concentration was adjusted spectrophotometrically ($\varepsilon_{260\ nm}$, 16.4 $mM^{-1}cm^{-1}$). The average percent hydrolysis of the acetyl-CoA preparations as deduced by spectrophotometric

measurements (calculated using the ratio of $A_{260\ nm}$ and $A_{232\ nm}$) was about 5% (Maximum 10%). The concentration of DCPIP preparations was also adjusted spectrophotometrically ($\varepsilon_{600\ nm}$, 19.1 $mM^{-1}cm^{-1}$).

2-2-2. Cell growth and protein expression

B834 (DE3) RIL/P31-TEV carrying the *LYS20* gene (kindly provided to us by Dr. F.W. Studier from Brookhaven National Laboratory) was used to express the HCS. The RIL plasmid (pACYC-based) confers chloramphenicol resistance and supplies extra copies of rare tRNAs. The P31-TEV plasmid is a derivative of pET-28 and confers kanamycin resistance. The *E.coli* strain B834 (DE3) contains a gene for T7 RNA polymerase and requires methionine for growth. The P31 protein has a 25 amino acid insertion at the N-terminal carrying a 6His-tag that is cleavable by rTEV protease.

The strain was grown in LB medium containing chloramphenicol (25 μg/ml) and kanamycin (10 μg/ml) and induction by 0.6 mM IPTG (final concentration) was accomplished once an $OD_{600\ nm}$ of 0.6-0.8 was reached. Growth was then continued at 30 °C for 3.5 h.

After centrifugation, the harvested cells were suspended in 20 mM Hepes, pH 7.5 containing 300 mM KCl and disrupted using either sonication or French press. After removing the cell debris by centrifugation at 12000*g* for 10 min, the collected supernatant was mixed with the Ni-NTA resin at 4 °C, washed with 20 mM imidazole and then eluted with buffer containing 200 mM imidazole.

For rTEV protease cleavage, 30 µg HCS was mixed with 10 U rTEV protease in a total volume of 100 µl using rTEV buffer (50 mM Tris-HCl, pH 8.0 and 0.5 mM EDTA) and the mixture incubated overnight at 4 °C.

2-2-3. Enzyme assay

A typical assay for the HCS using the DCPIP method contained in a final volume of 1 ml; 50 mM Hepes, pH 7.5 (adjusted by KOH; Na^+ is an inhibitor of HCS), 20 mM α-ketoglutarate, 0.5 mM acetyl-CoA and 0.1 mM DCPIP. All assays were carried out at 31 °C. All of the reagents, with the exception of enzyme were incubated for five minutes in a water bath for thermal equilibration and to allow for completion of the reaction of CoA (in the acetyl CoA solution) with DCPIP.

Immediately after addition of the enzyme the reduction in blue color of DCPIP was monitored for 10 min at 600 nm using a Beckman DU-640 spectrophotometer equipped with a circulating water bath to maintain the temperature of the cell compartment. The linear portion of the time course following the lag to establish steady state (usually in the range of 2-4 min) was used to estimate the steady state rate.

2-2-4. Stoichiometry of the Reaction of DCPIP with CoASH

A Beckman analytical HPLC system Gold Nouveau equipped with model 168 detector and model 126 solvent module and operated by GOLD Nouveau 1.7 software was used to analyze the reaction of DCPIP with CoASH. The mobile phase buffer was a solution of tetrabutylammonium dihydrogen phosphate, pH 7.5, used at a flow rate

of 1 ml/min. The column was an Alltech Adsorbosphere HS C18 7µ hydrophobic column. A 100µl mixture of DCPIP and CoASH (0.25 mM and 0.75 mM, respectively) was loaded onto the column and the components were eluted using a gradient of the running buffer with acetonitrile from 35-85% for 30 min. The same experiment was carried out with DCPIP and CoASH separately as controls. The decrease in the blue color of DCPIP upon reaction with CoASH in a ratio of 2:1 was followed spectrophotometrically in a separate reaction to monitor reaction progress.

2-2-5. Stabilization of HCS

A variety of solvents and additives at different concentrations, alone and in combination, were added to the storage buffer, and the solutions (in 250 µl aliquots) were then stored at 4 °C. The effect of the additives on enzyme stability was checked by daily enzyme assay for one week. Enzyme activity was also determined for some frozen (-20 °C and -80 °C) and thawed samples. Co-solutes and their final concentrations are shown in Table 2-1. In this table, X indicates addition of one or two co-solutes at the concentrations given. A Y in a row is an indicator that all of the possible combinations of the three or four co-solutes at the concentrations shown were used. For example, row 16 contains 6 Ys and thus nine combinations of three co-solutes were used for the experiment at the concentrations given. Mathematically, these combinations can be shown as follow: a (b + c + d) (e + f + g) where a is 0.1 M GdmCl, b, c and d are 30, 60 and 120 mM α-cyclodextrin and e, f and g are 0.1, 0.3 and 0.6 M $(NH_4)_2SO_4$, respectively. A Z is used in a column in a manner similar to Y

in a row. α-Cyclodextrin begins to form a precipitate under the above conditions at temperatures less than 30 °C (especially at 4 °C). Enzyme solutions can be incubated in a water bath (30 °C) to just dissolve the precipitate, but not longer, since the enzyme begins to lose activity.

2-2-6. Size exclusion chromatography - HPLC

The Beckman analytical HPLC system was used to analyze the HCS physical size. The running buffer was a solution of 100 mM KH_2PO_4 and 100 mM K_2SO_4, pH 7.5. The flow rate was set to 0.25 ml/min. The column used was a PVC-column, LKB-3000, TSK G3000SW with a M_r fractionation range of 10,000-500,000. A 50 µl (7 mg/ml) sample of HCS (50 kDa/monomer) was loaded onto the column and 30 fractions were collected over a chromatogram time of one hour. The standards for molecular mass determination were blue dextran (2000 kDa), alcohol dehydrogenase (ADH) from yeast (150 kDa), bovine serum albumin (BSA) (66 kDa), and carbonic anhydrase from rabbit erythrocytes (29 kDa). Samples of 50 µl of each were loaded at the following concentrations: 20 mg/ml, 8.8mg/ml, 6.5 mg/ml and 12 mg/ml, respectively. Elution was monitored at 280 nm.

2-2-7. Fluorescence studies of HCS

Fluorescence spectra were measured as indicated for quenching studies. The emission monochromator was scanned either from 290-400 nm or from 310-400 nm

(with the excitation monochromator fixed at either 278 or 298 nm). Excitation spectra were measured from 220-320 nm at a fixed emission wavelength of 350 nm.

Table 2-1: Matrix of co-solute combinations used to determine optimum conditions for stabilization of HCS.

	Co-solutes and additives[a]	α-Cyclodextrin (30 mM)	α-Cyclodextrin (60 mM)	α-Cyclodextrin (100 mM)	α-Cyclodextrin (120 mM)	α-Ketoglutarate (20 mM)	$(NH_4)_2SO_4$ (0.1 M)	$(NH_4)_2SO_4$ (0.3 M)	$(NH_4)_2SO_4$ (0.6 M)	MPD (10%)	DDT (0.1 mM)	DDT (1 mM)	Gdm sulfate (0.1 M)	Gdm sulfate (0.2 M)	Gdm sulfate (0.3 M)	Gdm sulfate (0.4 M)	GdmCl (0.1 M)	GdmCl (0.2 M)	Glutamic acid (0.3 M)	Glycerol (10%)	Glycerol (20%)	KCl (30 mM)	KCl (150 mM)	KCl (300 mM)	NH_4Cl (0.1 M)	NH_4Cl (0.3 M)	PEG-1500 (7%)	SDS (0.01%)	Sorbitol (0.5 M)	Sucrose (0.5 M)	Urea (0.1 M)
1	α-Cyclodextrin (30 mM)												X		X																
2	α-Cyclodextrin (60 mM)												X		X																
3	α-Cyclodextrin (100 mM)			X				Y					Z				Y														Z
4	α-Cyclodextrin (120 mM)												X		X																
5	α-Ketoglutarate (20 mM)					X																									
6	$(NH_4)_2SO_4$ (0.1 M)																X	X													
7	$(NH_4)_2SO_4$ (0.3 M)							X									X	X													Z
8	$(NH_4)_2SO_4$ (0.6 M)																														
9	MPD (10%)									X											X										
10	DTT (0.1 mM)										X																				
11	DTT (1 mM)											X																			
12	Gdm sulfate (0.1 M)			Y				Y					X									Y	Y	Y							
13	Gdm sulfate (0.2 M)													X																	
14	Gdm sulfate (0.3 M)																														
15	Gdm sulfate (0.4 M)															X															
16	GdmCl (0.1 M)	Y	Y	X	Y		Y	Y	Y				Z				X														
17	GdmCl (0.2 M)																														
18	Glutamic acid (0.3 M)																		X											X	
19	Glycerol (10%)																			X											
20	Glycerol (20%)																				X										
21	KCl (30 mM)			Y				Y	Y				Z				Y						Y	Y							
22	KCl (150 mM)												Z										X								
23	KCl (300 mM)			Y				Y					Z									Y	Y								Y
24	NH_4Cl (0.1 M)																X	X													
25	NH_4Cl (0.3 M)																X	X													
26	PEG-1500 (7%)																													X	
27	SDS (0.01%)			X																											
28	Sorbitol (0.5 M)							X																							
29	Sucrose (0.5 M)																													X	
30	Urea (0.1 M)			Y									Y									Y	Y	Y							

[a]For definitions of X, Y and Z, see page 47.

Spectra were recorded on a Shimadzu RF-5301 PC spectrofluorometer equipped with a special cuvette holder for maintaining the temperature at 25 °C using a circulating water bath. A 1 ml quartz cuvette with a path length of 1 cm was used to take both the sample (1 ml) and blank spectra. The excitation slit width was set to the minimum 1.5 nm and that of the emission was set to 5 nm. Blank spectra contained all components except the enzyme (220 μg/ml) and were subtracted from sample spectra. Peak heights were obtained after smoothing the spectrum using the available software for operating the fluorometer.

For fluorescence quenching studies, a typical final buffer composition used to measure the spectra contained 55 mM Hepes (adjusted to pH 7.5 with KOH), 150 mM $(NH_4)_2SO_4$, 25 mM GdmCl, 25 mM α-cyclodextrin, 8 mM KCl and 5 mM imidazole. All samples contained enzyme at a concentration of 55 μg/ml. Compounds used for quenching studies were KI (anionic quencher), CsCl (cationic quencher) and acrylamide (neutral quencher). Quenchers were added sequentially from low to high concentration to both the blank and sample from a stock solution of 2 M for KI, 7.5 M for CsCl and 2 M for acrylamide. The final total dilution in each case was 1.09 (KI), 1.12 (CsCl) and 1.10 (acrylamide). The stock solution of the enzyme used for fluorescence quenching studies contained 100 mM α-cyclodextrin, 600 mM $(NH_4)_2SO_4$, 100 mM GdmCl, 30 mM KCl, 20 mM imidazole, 22 mM Hepes, pH 7.5 and 220 μg/ml HCS. The first three components of the stock solution are required to stabilize the enzyme. A final dilution of 4 with 50 mM Hepes is required to dissolve the precipitated α-cyclodextrin and to decrease inner filter effects.

2-2-8. Circular dichroism studies

Circular dichroic spectra were measured at room temperature using an upgraded AVIV 62DS CD spectrometer. Spectra were obtained in a 0.2 cm quartz cuvette with a sample volume of 0.5 ml. The HCS concentration was 250 µg/ml (5 µM enzyme protomer) in a buffer containing 20 mM KH_2PO_4, pH 7.5 and 300 mM KCl. The blank contained all the components except the enzyme. The time constant and bandwidth were maintained at 100 ms and 3 nm, respectively. An average of eight scans were analyzed (four samples were scanned with two scans per sample). The averaging and dwell time were set at 1 s. The spectra were measured from 180-250 nm at 1 nm intervals.

2-2-9. Ultraviolet spectra

Ultraviolet absorption spectra were recorded at 25 °C on a Beckman DU-640 spectrophotometer. The HCS concentration was 830 µg/ml in Ni-NTA elution buffer (20 mM Hepes pH 7.5, 300 mM KCl and 200 mM imidazole). Addition of GdmCl (4.8 M final) was used to denature the enzyme for 5 minutes at 45 °C. The native and denatured HCS samples were scanned from 400 nm to 240 nm and the difference spectrum was obtained. The Blank contained all components except the enzyme.

2-3. Results and discussion

2-3-1. Cell growth and protein expression

The expression of HCS is very good under conditions used to induce expression. The HCS produced in the expression system is about 20% of the total soluble proteins. After washing with 20 mM imidazole, the enzyme is eluted from the Ni-NTA column from 60 to 180 mM imidazole with the highest concentration eluting at 60 - 90 mM. The purity of the eluted HCS from the Ni-NTA column is ≥ 80% (by densitometric scanning). The amount of the enzyme obtained is 8 – 10 mg from 500 mg wet cell pellet (200 ml cell culture). As shown in Fig. 2-2, if the column is initially washed with 50 mM imidazole the enzyme can be further purified to 98% without any significant decrease in yield. On the basis of several purifications, the fold purification

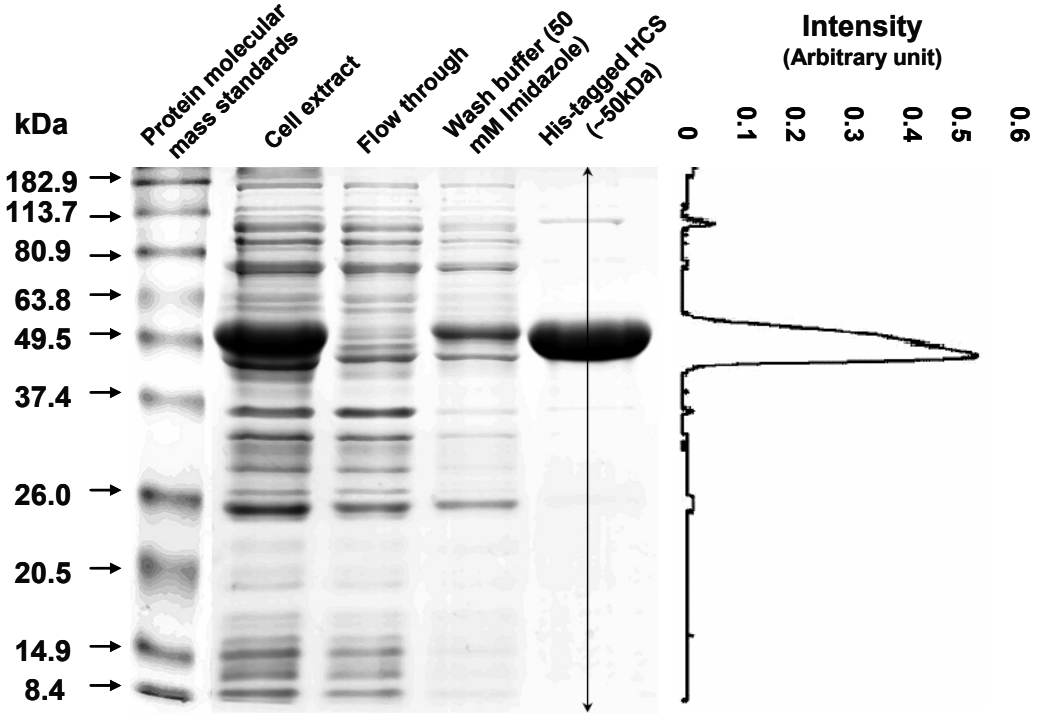

Fig. 2-2: SDS-PAGE of HCS stained with Coomassie brilliant blue (left). Densitometry scanning (right) shows that the enzyme is about 98% pure.

is 2-5 with a yield 60-120% (the value >100% suggests there may be inhibitors of the HCS in the crude extract). Although HCS has a histidine tag, it is still active. The histidine tag is readily cleaved by rTEV protease as shown by SDS-PAGE (data not shown). However, inhibitors (EDTA, DTT and Triton X-100) present in the protease storage buffer interfered with HCS activity. The buffer was exchanged with HCS buffer making use of the His-tag on the protease. The rTEV protease still cleaved the His-tag of the HCS, but also gave nonspecific proteolysis of the enzyme. The resulting enzyme was still active but with reduced activity compared to the His-tagged enzyme (see below).

2-3-2. Enzyme assay

The most common assay for enzymes that produce CoASH as a product makes use of a disulfide exchange reaction between DTNB and CoASH, which yields 5′-thio-2-nitrobezoate ($\varepsilon_{412\ nm}$ = 13.6 $mM^{-1}cm^{-1}$). However, preincubation of HCS with DTNB for 15 min, results in a complete inactivation of the enzyme. On the other hand, the DCPIP method is a good continuous monitor of HCS activity (*11*) and the activity is a linear function of enzyme concentration in the range of 0-0.3 dA/min (data not shown). Preincubation of HCS with DCPIP for 15 min has no effect on activity. A solution of DCPIP can be used up to 3 weeks, after which inhibitors/inactivators are present in the solution. The small amount of Na^+ in the acetyl-CoA and DCPIP solutions has no effect on enzyme activity for the concentrations used in the assay.

Kinetic parameters for the HCS are summarized in Table 2-2. The range of K_m(α-kg) and K_m(AcCoA) values for HCS from other sources are 2.2 - 11.8 and 0.06 - 0.2 mM, respectively (*14*). The k_{cat} for HCS from *Thermus thermophilus* is 75 min^{-1} (*14*). As shown in Table 2-2, the one year old stabilized HCS still has about 50% of its activity when isolated, while the His-tag-cleaved enzyme has lost 90% of its activity. However, the K_m values for all enzymes are identical within error suggesting a loss of active enzyme, with the remaining active enzyme behaving in a manner identical to the freshly isolated and stabilized His-tagged enzyme. It thus appears that 1) less active conformers of the HCS are unlikely, and 2) the His-tag has no influence on the activity of the HCS.

Table 2-2: Kinetic parameters for homocitrate synthase (graphical analysis).

Enzyme[a]	Substrate	K_m (mM)	k_{cat} (min^{-1})	Specific Activity (mU/mg)
1	α-ketoglutarate	4.6	37	730
	acetyl-CoA	0.014		
2	α-ketoglutarate	1.3	37	730
	acetyl-CoA	0.024		
3	α-ketoglutarate	0.7	17	350
	acetyl-CoA	0.021		
4	α-ketoglutarate	1.8	3	45
	acetyl-CoA	0.026		

[a]1. HCS without stabilization buffer; 2. HCS plus stabilization buffer; 3. 2 after 1 yr storage at 4°C; 4. His tag-cleaved HCS. Standard errors of the parameters are ≤10%.

2-3-3. Stoichiometry of the reaction of DCPIP with CoASH

Spectrophotometric measurements showed that the stoichiometry of the reaction of DCPIP (*15*) with CoASH is 1:1 (see Appendix – Fig. A-1). The analytical HPLC results showed the formation of an unidentified CoA species as the result of the reaction (Fig. 2-3). The unidentified form of the CoA may be an oxidized form of the CoA-S-S-CoA molecule or a DCPIP-CoA adduct. The above will require additional study.

2-3-4. Stabilization of HCS

Protein stability depends on a subtle interaction of the protein with water and

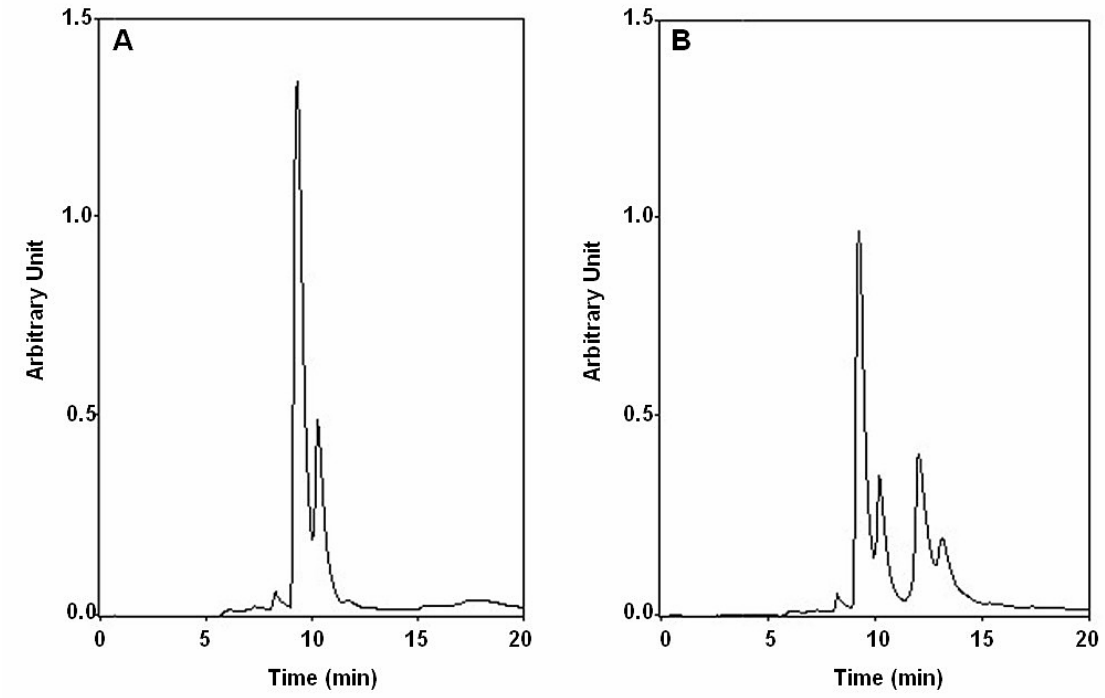

Fig. 2-3: (A) Analytical HPLC trace of 1.5 mM CoASH. The first peak is the linear CoASH and the second peak is likely the cyclic (thiazoline) form of the CoASH (*30*) (B) Trace of the reaction mixture of 0.75 mM CoASH and 0.25 mM DCPIP. The second two peaks are the two new forms of the oxidized CoASH dimer.

other solute molecules, including ionic interactions between the surface of the protein and water dipoles, hydrophobic interactions with other solute molecules, and hydrogen bonding with water and other solute molecules. In designing a protocol to determine conditions to stabilize a protein, different classes of co-solutes capable of affecting one of the interactions listed above were chosen (*16*). Polyols and sugars like sorbitol and sucrose can stabilize the lattice structure of water and also increase the viscosity. Polymers like PEG prevent protein aggregation by increasing solvent viscosity. Amino acids like glutamic acid are capable of increasing the surface tension of water and give also electrostatic interaction with polar groups on the protein surface. Ionic compounds like $(NH_4)_2SO_4$ are useful for surface charge shielding, while denaturing agents like urea stabilize the unfolded state of the protein, providing a better opportunity for the proper refolding. GdmCl is a chaotrophic agent that disrupts hydrogen bonds and the hydration shell around protein. DTT can be used to maintain free sulfhydryls in a reduced state, while PMSF and EDTA are protease inhibitors (*16*).

Cyclodextrins (and their derivatives) are of particular interest. The 3D structure of these molecules suggests a cone that has a hydrophobic interior and a hydrophilic exterior. α-Cyclodextrin is capable of binding to hydrophobic areas of the protein to render it more hydrophilic. In equilibration with denaturing agents, α-cyclodextrin also acts as an adsorbent that gradually adsorbs the denaturing agents from the surface of the protein and provides the protein with proper local conformational refolding.

This mechanism is similar to chaperone-assisted renaturation that has been used to renature some proteins from the denatured state (*12-13*).

Experiments to determine conditions that will stabilize the highly unstable enzyme were quite successful. Sucrose, glutamic acid, sorbitol, glycerol and α-ketoglutarate have no effect on HCS stability, and α-cyclodextrin and $(NH_4)_2SO_4$ also have no effect if used alone. Combinations of $(NH_4)_2SO_4$ and sorbitol, sucrose and PEG-1500, sucrose and glutamic acid, GdmCl and $(NH_4)_2SO_4$, or GdmCl and α-cyclodextrin also have no effect on stability. 2-Methyl-2, 4-pentanediol alone or in combination with other co-solutes inactivates the enzyme. Dithiothreitol at a concentration of 1 mM inactivates the enzyme, while a concentration of 0.1 mM gives only slight inactivation. Preincubation of HCS with 1 mM PMSF for five minutes decreases the activity of enzyme by 20%, while 100 mM α-cyclodextrin plus 0.01% SDS stabilizes the enzyme to some extent.

Preliminary studies showed that a combination of 100 mM α-cyclodextrin, 300 mM $(NH_4)_2SO_4$ and 100 mM GdmCl gives the best stability. More detailed experiments showed that in this combination $(NH_4)_2SO_4$ and GdmCl can not be replaced by NH_4Cl and urea, respectively. In addition, Gdm sulfate is not a replacement for GdmCl and $(NH_4)_2SO_4$, and surprisingly Gdm sulfate is a potent destabilizing agent. Data suggest a role for NH_4^+ in stabilizing HCS. Therefore, it is concluded that the combination of three co-solutes (100 mM α-cyclodextrin, 100 mM GdmCl and 600 mM $(NH_4)_2SO_4$) is needed for HCS stability and stabilization is optimum at higher concentration of these co-solutes.

Screening against different concentrations of KCl showed that in the presence of 600 mM $(NH_4)_2SO_4$, 300 mM KCl has a destabilizing effect, but lower concentrations of KCl stabilize (See Appendix – Fig. A-2). Other components of the stabilization stock solution are 30 mM KCl, 20 mM imidazole and 22 mM Hepes, pH 7.5 (from the Ni-NTA column elution buffer). Upon storage at 4 °C, the enzyme is stable up to 50 days, with very little decrease in activity (See Appendix – Fig. A-3). The half lives of the stabilized and non-stabilized HCS are 180 and 5 days, respectively.

2-3-5. Size exclusion chromatography – HPLC

Results showed that the enzyme elutes from the column over a broad range and is fractionated into several peaks. Activity is found in most of the fractions with the highest activity in the lowest molecular mass form. Comparison of the elution profile with that of the standards suggests that HCS may be present in a number of different forms including the monomer, dimer, tetramer and higher molecular mass aggregates (Fig. 2-4). The higher molecular mass forms are likely aggregates, suggesting the enzyme has a high potential for self-association at higher concentration. The exact M_r of the different forms of the HCS enzyme was not obtained as a result of interaction of the enzyme with the column. Estimation of the molecular mass of the different species

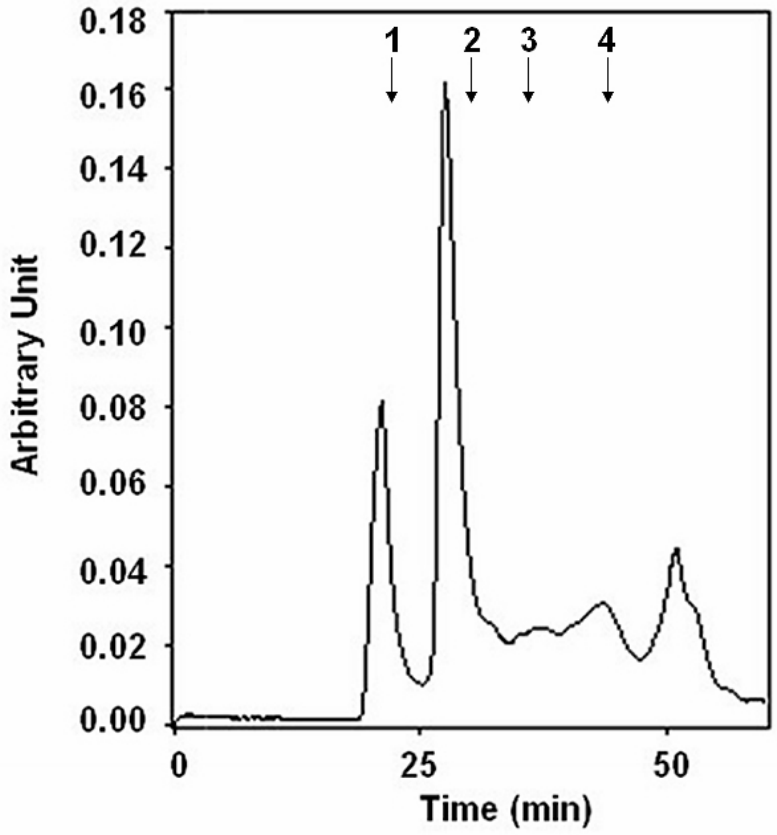

Fig. 2-4: Elution profile of the HCS suggests the enzyme may be present in a number of different self-associated forms. The position of standards for molecular mass determination has been shown as arrows. From left to right arrows 1 to 4 are Blue dextran (2000 kDa) (23.0 min), ADH from yeast (150 kDa) (31.3 min), BSA from bovine (66 kDa) (36.7 min), and carbonic anhydrase from rabbit erythrocytes (29 kDa) (44.0 min), respectively.

eluting from the gel filtration column, on the basis of the elution profile of the standards, gives the following estimated molecular mass at the retention time listed: 4 kDa (51.3 min), 18 kDa (43.6 min), 68 kDa (37.6 min), 270 kDa (31.5 min), 550 kDa (27.7 min) and 2200 kDa (21.4 min). The peaks show a preferred multiplicity of four suggesting a trend in the self-association properties. A non-spherical or highly asymmetric three dimensional structure may contribute to the interaction of the HCS with the column. These studies will be followed up using the analytical ultracentrifuge.

2-3-6. Fluorescence studies of HCS

The excitation spectrum of the HCS shows the typical ultraviolet absorption spectrum of tryptophan suggesting that the spectrum of the HCS is dominated by contribution of the tryptophan residue (*17*). The fluorescence emission spectrum, with excitation at 278 nm, shows a λ_{max} of 337 nm and a shoulder at 307 nm, Fig. 2-5A. Normalization of the emission spectrum with excitation at 298 nm to the same intensity of the emission spectrum obtained upon excitation at 278 nm shows that tyrosine residues contribute about 35% to the total fluorescence in the blue region of the emission spectrum; Fig. 2-5A, and the remainder of the fluorescence is from the single tryptophan residue (data not shown). The 298 nm emission spectrum, originating from the single Trp, shows a λ_{max} at 337 nm. According to Burstein, who has classified the emission properties of tryptophan residues in proteins (*18-20*), the position of the λ_{max} for emission spectra of the tryptophan residues in proteins varies from 307 to 353 nm (five spectral classes A, S, I, II and III). The blue extreme (307 nm) or tryptophan spectral form A indicates an unperturbed indole chromophore in a nonpolar environment inside the protein. The red extreme (353 nm) or tryptophan spectral form III corresponds to the indole chromophore at the surface of the protein in contact with free water molecules. The HCS emission spectrum belongs to the spectral form II that corresponds to the emission of the indole chromophore near the surface of the protein. The tryptophan residue is assumed to be in contact with the bound water (not free water molecules) and other polar groups of the protein.

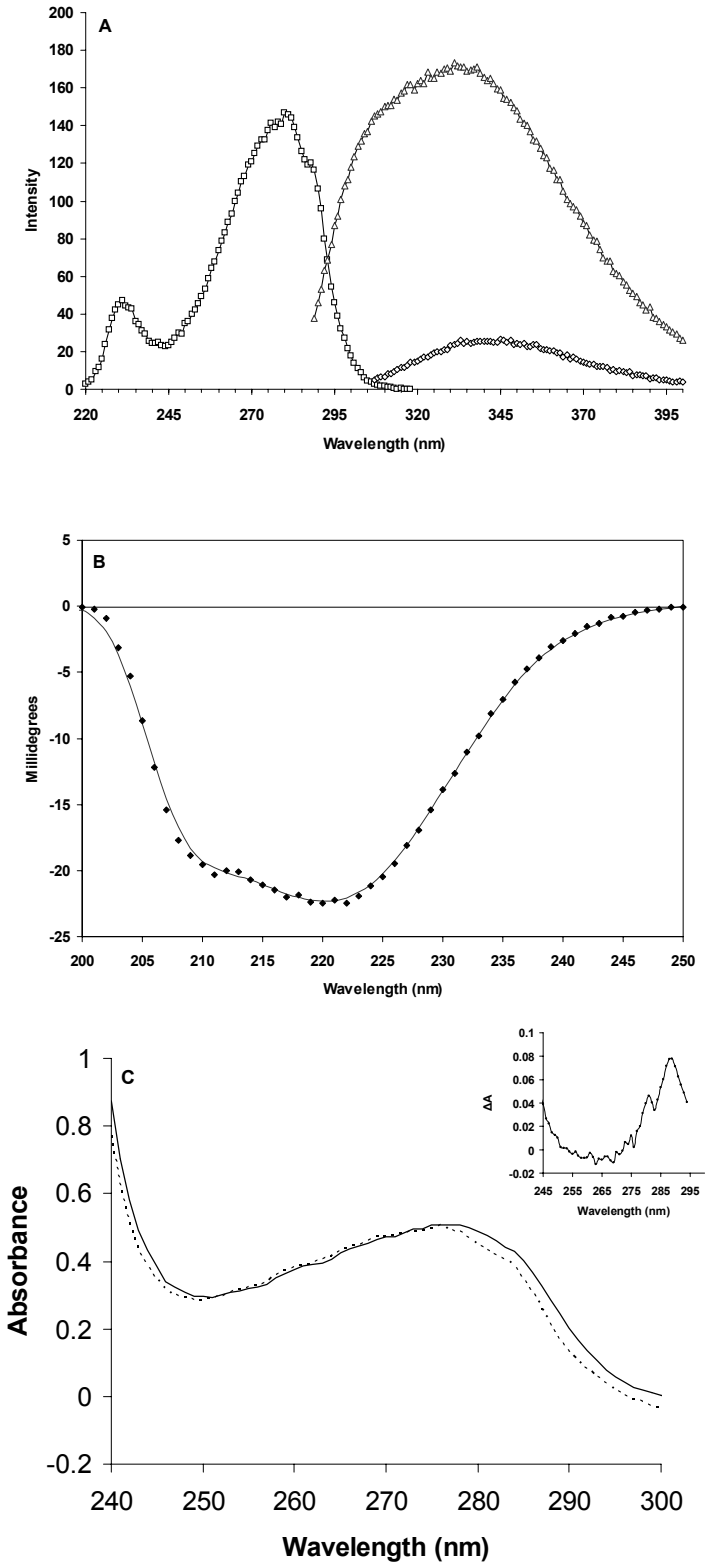

Fig. 2-5: (A) Fluorescence excitation spectrum of HCS (❑) taken at fixed emission wavelength of 350 nm and emission spectra of HCS taken at excitation wavelength of 278 nm (Δ) and 298 nm (◊). (B) CD spectrum of HCS. (C) U.V. spectrum of native (—) and denatured (---) HCS. Difference spectrum between native and unfolded HCS is shown in inset.

Fluorescence quenching data were analyzed using the Stern-Volmer plot (F_0/F

vs.[Q]) and the modified Stern-Volmer plot ($F_0/\Delta F$ vs. 1/[Q]) (Fig. 2-6). The modified Stern-Volmer equation is $F_0/\Delta F = (f_a K_{SV}[Q])^{-1} + (f_a)^{-1}$ where F_0 is the fluorescence intensity in the absence of quencher, ΔF is the change in fluorescence intensity in the presence of quencher, K_{SV} is the Stern-Volmer constant, [Q] is the concentration of quencher and f_a is the fraction of the total fluorescence of the enzyme that is accessible to quenching (*21*). The K_{SV} and f_a values are shown in Table 2-3. The K_{SV} and f_a were determined by monitoring the fluorescence spectra measured upon excitation at 298nm. These data are the most reliable because the emission results from the single Trp of HCS alone.

Table 2-3: Fluorescence quenching parameters for homocitrate synthase

Quencher	K_{SV}
KI (25 °C)	K_{SV} = 10.3 M^{-1}, f_a = 34%
KI (35 °C)	K_{SV} = 7.8 M^{-1}, f_a = 40%
CsCl (25 °C)	K_{SV} = 5.6 M^{-1}, f_a = 11%
CsCl (35 °C)	K_{SV} = 1.1 M^{-1}, f_a = 23%
Acrylamide (25 °C)	K_{SV} = 6.2 M^{-1}, f_a = 59%
Acrylamide (35 °C)	K_{SV} = 3.7 M^{-1}, f_a = 77%

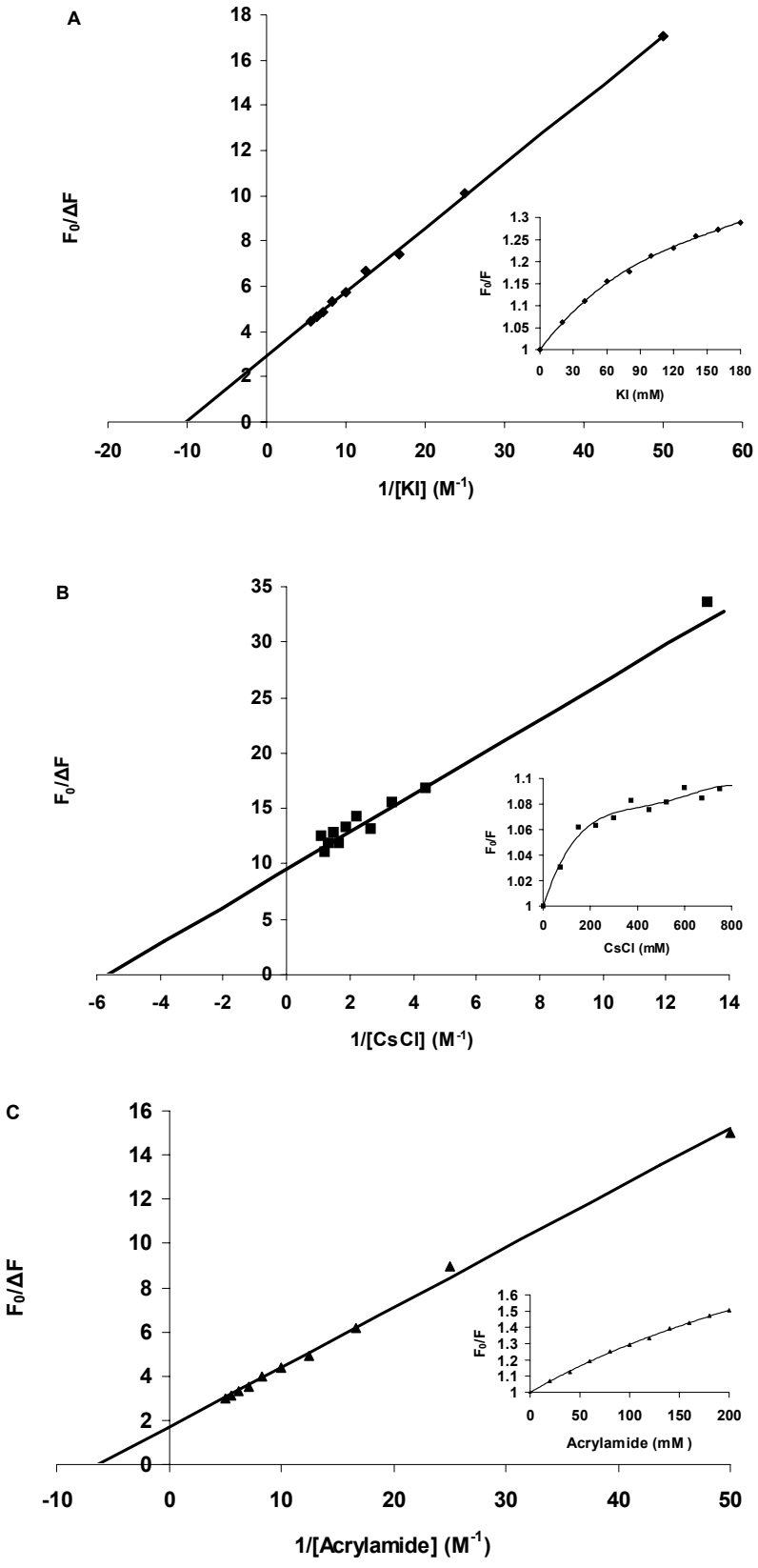

Fig. 2-6: Modified Stern-Volmer plot for KI (A), CsCl (B) and Acrylamide (C) at 25 °C. X-intercept = - K_{SV}, Y-intercept = f_a^{-1} and the slope is equal to $(f_a K_{SV})^{-1}$. Stern-Volmer plots are shown in insets.

An upward curvature in the Stern-Volmer plot results from a combination of static and dynamic quenching and has two possibilities regarding the K_D (dynamic quenching constant) and K_S (static quenching constant) values. However, fluorescence lifetime measurements are needed to elucidate the real K_D and K_S. A downward curvature in the Stern-Volmer plot results from a combination of two different conformers that differ in their accessibility of the fluorophores to the quencher (*21*). By definition $(K_{SV})^{-1}$ is the quencher concentration at which 50% of the fluorescence intensity is quenched. Although Cs^+ is smaller than I^- (ionic radii are 165 and 220 pm, respectively (*22*)), I^- is the best quencher and it suggests that the microenvironment around tryptophan is positively charged. Quenching of HCS by KI, CsCl and acrylamide shows a downward curvature in the Stern-Volmer plot and a decrease in the K_{SV} values upon increasing the temperature, but fluorophore lifetime measurements are needed to distinguish between static and dynamic quenching because of the nonlinear dependence of the quenching on quencher concentration.

2-3-7. Circular dichroism studies

The CD spectrum of HCS, Fig. 2-5B, shows a typical protein spectrum with minima at 222 nm and 208 nm suggesting the presence of α and β secondary structural components. The protein type seems to be α/β because the 208 nm band is of lower intensity than 222 nm band (in α + β proteins the 208 nm band is of higher intensity than 222 nm band (*23*)), consistent with multiple sequence alignment data that suggest a TIM barrel fold at the N-terminal part of the HCS (*24*). The C-terminal part of the

HCS is likely to possess a regulatory cyclin-like, EF-hand-like fold and may possess a DNA-binding motif as indexed using the 3D-PSSM program (*25*). However, precise conclusions await the determination of the structure.

Experimental data could not be collected at wavelengths less than 200 nm due to absorbance of the stabilizing buffer. As a result, deconvolution of the spectrum into its components could not be carried out. Predicted secondary structure composition using the PROF (Profile network prediction heidelberg) network prediction (*26-27*) shows that the original HCS (without histidine tag) contains 41% α-helix, 17% β-sheet and 42% coil structure, while the His-tagged HCS contains 38% α-helix, 17% β-sheet and 45% coil structure. Estimation of the α-helical content of the His-tagged HCS on the basis of the mean residue ellipticity at 222 nm (fraction α-helix = $(- [\theta]_{222\ nm} + 3000)/39000$) (*28*) gives a value of 20%. The low mean residue rotation of the HCS may be due to a small amount of periodic secondary structure or cancellation of β-sheet and random coil contributions (*29*).

2-3-8. Ultraviolet spectra

U.V. spectra of native and denatured HCS are shown in Fig. 2-5C. The difference spectrum between native and unfolded HCS is shown in the inset. The prominent peaks at 281 and 289 nm in the difference spectrum are due to solvent exposure of the tyrosine and tryptophan residues, respectively, suggesting that the HCS is easily denatured on the basis of the conditions used for denaturation. The theoretical extinction coefficient of the denatured His-tagged HCS at 280 nm was calculated to be

24090 $M^{-1}cm^{-1}$ using the ProtParam tool at the ExPASy website (http://us.expasy.org/tools/protparam.html). The experimental $\varepsilon_{280\ nm}$ for denatured and native His-tagged HCS was calculated as 26800 and 29200 $M^{-1}cm^{-1}$, respectively.

2-4. Conclusion

The purified homocitrate synthase (HCS) from *Saccharomyces cerevisiae* can be stabilized using a combination of guanidine hydrochloride, α-cyclodextrin and ammonium sulfate. The histidine tag at the N-terminal of the HCS can be used to purify the enzyme and is cleavable by rTEV protease. The fluorescence and CD spectra suggest a partially exposed tryptophan residue and a mixed secondary structure. The fluorescence quenching studies suggest a positively charged microenvironment around the single tryptophan residue.

2-5. Acknowledgements

We gratefully thank Dr. F. W. Studier at Brookhaven National Laboratory for the gift of the strain containing the cloned HCS. We thank Drs. W. E. Karsten, and L. Chooback and Wael Rabeh for technical assistance. We also thank Dr. Helen I Zgurskaya for providing us with the spectrofluorometer.

References

[1] E. Johansson, J. J. Steffens, Y. Lindqvist, and G., Schneider (2000) Crystal structure of saccharopine reductase from *Magnaporthe grisea*, an enzyme of the alpha-aminoadipate pathway of lysine biosynthesis, *Struct. Fold Des. 8*, 1037-1047

[2] J. K. Bhattacharjee (1992) in: R. P. Mortlock (Ed.), *Evolution of Metabolic Function*, CRC Press, Boca Raton, pp. 47-80.

[3] J. K. Bhattacharjee (1985) α-Aminoadipate pathway for the biosynthesis of lysine in lower eukaryotes, *Crit. Rev. Microbiol. 12*, 131-151.

[4] H. E. Umbarger (1987) Amino acid biosynthesis and its regulation, *Annu. Rev. Biochem. 47*, 532-606.

[5] H. J. Vogel (1960) Two modes of lysine biosynthesis among lower fungi: evolutionary significance, *Biochim. Biophys. Acta 41*, 172-173.

[6] S. Chen, J. S. Brockenbrough, J. E. Dove and J. P. Aris (1997) Homocitrate synthase is located in the nucleus in the yeast *Saccharomyces cerevisiae*, *J. Biol. Chem. 272*, 10839-10846

[7] F. Ramos, P. Verhasselt, A. Feller, P. Peeters, A. Wach, E. Dubois and G. Volckaert (1996) Identification of a gene encoding a homocitrate synthase isoenzyme of *Saccharomyces cerevisiae*, *Yeast 12*, 1315-1320.

[8] J. Tracy and G. Kohlhaw (1975) Reversible, coenzyme-A-mediated inactivation of biosynthetic condensing enzymes in yeast: a possible regulatory mechanism, *Proc. Natl. Acad. Sci. USA 72*, 1802-1805.

[9] W. M. Jaklitsch and C. P. Kubicek (1990) Homocitrate synthase from Penicillium chrysogenum. Localization, purification of the cytosolic isoenzyme, and sensitivity to lysine, *Biochem. J. 269*, 247-253.

[10] G. M. Gaillardin, L. Poirier and H. Heslot (1976) A kinetic study of homocitrate synthetase activity in the yeast *Saccharomycopsis lipolytica*, *Biochim. Biophys. Acta 422*, 390-406.

[11] G. S. Gray and J. K. Bhattacharjee (1976) Biosynthesis of lysine in Saccharomyces cervisiae: properties and spectrophotometric determination of homocitrate synthase activity, *Can. J. Microbiol. 22*, 1664-1667.

[12] D. Rozema and S. H. Gellman (1996) Artificial chaperone-assisted refolding of carbonic anhydrase B, J. *Biol. Chem. 271*, 3478-3487.

[13] D. L. Daugherty, D. Rozema, P. E. Hanson and S. H. Gellman (1998) Artificial chaperone-assisted refolding of citrate synthase, *J. Biol. Chem. 273*, 33961-33971.

[14] A.P. Wulandari, J. Miyazaki, N. Kobashi, M. Nishiyama, T. Hoshino and H. Yamane (2002) Characterization of bacterial homocitrate synthase involved in lysine biosynthesis, *FEBS Letters 522*, 35-40.

[15] R. E. Basford and F. M. Huennekens (1955) Studies on Thiols. I. Oxidation of Thiol Groups by 2,6-Dichlorophenol Indophenol, *J. Am. Chem. Soc. 77*, 3873-3 877.

[16] C. H. Schein (1990) Solubility as a function of protein structure and solvent components, *Biotechnology 8*, 308-317.

[17] T. E. Creighton (1989) in : T.E. Creighton (Ed.), *Protein Structure a practical approach*, IRL Press, Oxford University Press, pp. 251-285.

[18] E. A. Burstein, N. S. Vedenkina, M. N. Ivkova (1973) Fluorescence and the location of tryptophan residues in protein molecules, *Photochem. Photobiol. 18*, 263-279.

[19] E. A. Burstein (1977) in: E. A. Burstein (Ed.), *Equilibrium Dynamics of Native Structure of Protein*, ONTI NCBI, Pushchino, pp. 60-83.

[20] A.S. Ladokhin (2000) in: R. A. Meyers (Ed.), *Encyclopedia of Analytical chemistry*, John Wiley & sons Ltd, Chichester, pp. 5762-5779.

[21] J. R. Lakowicz (1999) in: *Principles of Fluorescence Spectroscopy*, Kluwer Academic/Plenum, New York, 2nd ed.

[22] J. Emsley (1998) *The Elements*, Clarendon Press, Oxford, 3rd ed.

[23] J. T. Pelton and L. R. McLean (2000) Spectroscopic methods for analysis of protein secondary structure, *Analytical Biochemistry 277*, 167-176.

[24] R. R. Copley and P. Bork (2000) Homology among $(\beta\alpha)_8$ barrels: implications for the evolution of metabolic pathways, *J. Mol. Biol. 303*, 627-640.

[25] L. A. Kelly, R. M. MacCallum and M. J. E. Sternberg (2000) Enhanced genome annotation using structural profiles in the program 3D-PSSM, *J. Mol. Biol. 299*, 499-520.

[26] B. Rost (1996) PHD: predicting one-dimensional protein structure by profile-based neural networks, *Methods in Enzymology 266*, 525-539.

[27] B. Rost and C. Sander (1993) Prediction of protein secondary structure at better than 70% accuracy, *J. Mol. Biol. 232*, 584-599.

[28] J. A. Morrow, M. L. Segall, S. Lund-Katz, M. C. Phillips, M. Knapp, Bernhard Rupp and K. H. Weisgraber (2000) Differences in stability among the human apolipoprotein E isoforms determined by the amino-terminal domain, *Biochemistry 39*, 11657-11666.

[29] N. Greenfield and G. D. Fasman (1969) Computed circular dichroism spectra for the evaluation of protein conformation, *Biochemistry 8*, 4108-4116.

[30] R. E. Basford and F. M. Huennekens (1955) Studies on Thiols. II. Multiple Forms of Coenzyme A, J. *Am. Chem. Soc. 77*, 3878-3882.

CHAPTER 3

Kinetic mechanism of homocitrate synthase

"Reproduced with permission from [Andi, B., West A. H., and Cook, P. F. (2004) Kinetic Mechanism of Histidine-Tagged Homocitrate Synthase from *Saccharomyces cerevisiae*, *Biochemistry 43*, 11790-11795] Copyright [2004] American Chemical Society."

3-1. Introduction

Homocitrate synthase (HCS) [2-hydroxybutane-1,2,4-tricarboxylate 2-oxoglutarate-lyase (CoA-acetylating), EC 2.3.3.14] is the first and regulated enzyme of the α-aminoadipate pathway for the biosynthesis of lysine. The pathway is unique to higher fungi such as the human pathogens *Candida albicans*, *Cryptococcus neoformis* and *Aspergillus fumigatus* and the plant pathogen *Magnaporthe grisea*. The uniqueness of the α-aminoadipate pathway makes it a potential target for the design of the highly specific antimycotic agents (*1*-*5*).

The pathway begins with the condensation of α-ketoglutarate with AcCoA to yield homocitrate and coenzyme A with the intermediacy of a homocitryl-CoA intermediate (*2*-*5*). There are two isozymes of HCS from *Saccharomyces cerevisiae* (cytosolic and mitochondrial), and both are feedback inhibited by lysine, the pathway end product, and the expression of the cytosolic isozyme is repressed by lysine (*6*). HCS activity may also be regulated by divalent metal ions in the presence of CoA (*7*).

There are few studies on the kinetic mechanism of the HCS. An ordered kinetic mechanism has been proposed for the HCS from *Saccharomycopsis lipolytica* with α-ketoglutarate binding before AcCoA (*8*). The authors reported a sigmoid saturation

curve for AcCoA. A sigmoid saturation curve for AcCoA was also reported for the enzyme from *Penicillium chrysogenum* (*9*). It has been also demonstrated that the HCS from *Thermus thermophilus* is capable of catalyzing the reaction using oxaloacetate in place of α-ketoglutarate as a substrate, and thus behaves as a citrate synthase (*10*).

The HCS from *Saccharomyces cerevesiae* is unstable as isolated (*11*). Stabilization of the HCS from *S. cerevisiae* provided us with an enzyme with a longer half-life (*11*) making it possible to carry out detailed kinetic studies. In this paper, we report the kinetic mechanism of the HCS from *S. cerevisiae*.

3-2. Materials and methods

3-2-1. Materials

All chemicals were of the highest grade commercially available. α-Ketoglutarate, oxaloacetate, citrate, dichlorophenol indophenol (DCPIP), AcCoA, CoA, desulfo-CoA, α-cyclodextrin, L-glutamate, succinic acid and γ-ketopimelate were obtained from Sigma. KCl, GdmCl and glycerol were purchased from Fisher Scientific. $(NH_4)_2SO_4$ was obtained from Fluka and Hepes was from Amresco. Imidazole was obtained from Research Organics.

The concentrations of AcCoA, CoA and desulfo-CoA were adjusted spectrophotometrically (ε_{260}, 16.4 $mM^{-1}cm^{-1}$). A solution of AcCoA in ddH_2O is stable, without any significant hydrolysis, for at least a month if kept at -21°C. The

concentration of DCPIP preparations was also adjusted spectrophotometrically (ε_{600}, 19.1 $mM^{-1}cm^{-1}$).

3-2-2. Assays of homocitrate synthase activity

Cell growth, HCS expression and purification were performed as previously described (*11*). A typical assay for the HCS using the DCPIP method (monitoring the decrease in absorbance at 600 nm upon DCPIP reduction) is as described with slight modifications (*11*). The final volume of the assay was 0.5 mL and contained 50 mM Hepes, pH 7.5 (adjusted by KOH), and variable concentrations of α-Kg and AcCoA (~K_m or ~20K_m) and 0.1 mM DCPIP. All assays were carried out at 25 °C. Reactions were thermally equilibrated to allow for completion of the reaction between the small amount of CoA in the AcCoA solution and DCPIP before adding the enzyme to the reaction mixture. It should be noted that inhibition patterns for CoA could not be studied using DCPIP assay. Therefore, the disappearance of absorbance at 232 nm (reflecting the thioester bond of AcCoA) was monitored in these cases (*11*). The decrease in absorbance at 232 nm ($\Delta\varepsilon_{232}$ = 4.5 $mM^{-1}cm^{-1}$) was monitored upon addition of the HCS using the 0.4 cm path length cuvette (NSG Precision Cells, Inc.).

In order to dissolve the precipitated α-cyclodextrin in the stabilized HCS suspension (*11*) glycerol was added to a final concentration of 10%. A dilute enzyme solution prepared using this method is stable at room temperature up to three hours after which, the enzyme begins to lose activity.

3-2-3. Initial velocity studies

As described in the enzyme assay section, the DCPIP method was used to study initial velocity patterns with the exception of those in which CoA was present. The initial rate was measured as a function of AcCoA concentration (0.0125-0.125 mM) and a fixed concentration of α-Kg and the experiment was then repeated at several additional α-Kg concentrations (1-10 mM). A similar experiment was carried out with OAA (10-50 mM) in place of α-Kg using the same variable concentrations of AcCoA at different fixed concentrations of OAA. Data in both cases were fitted to Eq. 1 for a sequential mechanism as represented using Cleland's nomenclature (*12*).

$$v = \frac{\mathbf{VAB}}{K_{ia}K_b + K_a\mathbf{B} + K_b\mathbf{A} + \mathbf{AB}} \qquad (1)$$

where v and V are initial and maximum rates, **A** and **B** are reactant concentrations, K_{ia} is the dissociation constant for A, and K_a and K_b are the Michaelis constants for **A** and **B**, respectively.

A point that must be considered when carrying out inhibition studies is related to the effect of monovalent ions on the HCS reaction. The behavior of HCS is complicated in the presence of monovalent and divalent cations (see Chapter 4). The major source of these ions is from the titrant used to adjust the pH of buffer and carboxylic acid substrate solutions. In addition, the presence of NH_4^+ in the stabilization buffer for HCS (*11*) is a source of monovalent ions. The activating effect

of the NH_4^+ is obvious in Figure 3-1 at the lowest α-Kg concentration where the reciprocal values of the experimental data points are lower than the predicted values (solid line). This effect introduces some (manageable) error in data analysis. In general, when monovalent cations are not a subject of kinetic studies, their concentration should not exceed 50 mM.

3-2-4. Inhibition studies

Inhibition patterns were obtained by measuring the initial rate at different concentrations of one reactant, a fixed concentration of the second reactant equal to K_m, and a fixed concentration of the inhibitor. The experiment was then repeated at several different fixed concentrations of the inhibitor (including zero). Dependent on whether the inhibition was competitive, noncompetitive or uncompetitive, data were fitted to Eqs. 2-4.

$$v = \frac{\mathbf{VA}}{K_a\left(1+\frac{\mathbf{I}}{K_{is}}\right)+\mathbf{A}} \tag{2}$$

$$v = \frac{\mathbf{VA}}{K_a\left(1+\frac{\mathbf{I}}{K_{is}}\right)+\mathbf{A}\left(1+\frac{\mathbf{I}}{K_{ii}}\right)} \tag{3}$$

$$v = \frac{\mathbf{VA}}{K_a+\mathbf{A}\left(1+\frac{\mathbf{I}}{K_{ii}}\right)} \tag{4}$$

In Eqs. 2-4 K_{is} and K_{ii} are slope and intercept inhibition constants, respectively, **I** is the concentration of inhibitor, and all other terms are as defined above.

3-2-5. Fluorescence determination of the HCS-ligand dissociation constant

Fluorescence spectra were measured as previously described (*11*). Emission spectra were measured from 310-400 nm with the excitation monochromator fixed at 298 nm. Spectra were recorded on a Shimadzu RF-5301 PC spectrofluorometer equipped with circulating water bath to maintain the temperature at 25°C. Fluorescence quartz cuvettes with a volume of 1 mL and a path length of 1 cm were used to measure sample and blank spectra. Excitation and emission slit widths were set to 1.5 nm and 5 nm, respectively. Because all of the reagents and buffer components have no absorbance above 310 nm, the inner filter effect is negligible under conditions used for taking the spectra.

The final buffer composition used to measure the spectra contained 55 mM Hepes (adjusted to pH 7.5 with KOH), 150 mM $(NH_4)_2SO_4$, 25 mM GdmCl, 25 mM α-cyclodextrin, 8 mM KCl and 5 mM imidazole. All samples contained enzyme at a concentration of 55 μg/mL. Compounds used for fluorescence studies were α-Kg, OAA, AcCoA and CoA that were added sequentially from low to high concentration to both the blank and sample from a stock solution of 1 M for α-Kg, 100 mM for OAA, 5 mM for AcCoA and 8.6 mM for CoA. The final total dilution in each case was 1.07 (α-Kg), 1.08 (OAA), 1.10 (AcCoA) and 1.06 (CoA), and all the data were corrected for dilution.

To calculate the K_d based on the fluorescence intensity, data were fitted to the equation for a rectangular hyperbola shown in Eq. 5

$$\Delta F = \frac{\Delta F_{\max} \mathbf{L}}{K_d + \mathbf{L}} \quad (5)$$

where ΔF is the change in intrinsic tryptophan fluorescence upon addition of ligand to enzyme, $\Delta F_{\max}$ is the maximum change in fluorescence at infinite ligand concentration, **L** is the ligand concentration and K_d is the dissociation constant for the enzyme-ligand complex.

3-2-6. Data analysis

Initial rates and fluorescence intensity changes were plotted as reciprocal plots vs. substrate or ligand concentration, and all plots and replots were linear. Data were fitted using the appropriate equations and the Marquardt-Levenberg algorithm supplied with the EnzFitter program from BIOSOFT, Cambridge, UK. Rate, kinetic and dissociation constants and their corresponding standard errors were estimated using a simple robust weighing method for the activity or affinity of the enzyme by fitting the curves to the data either in the absence or presence of inhibitors or ligands.

3-3. Results

3-3-1. Initial velocity studies

The initial velocity pattern obtained varying the concentration of α-Kg at different fixed concentrations of AcCoA is shown in Fig. 3-1. The lines intersect to the left of the vertical axis consistent with the sequential Bi Bi mechanism (*13*). Data could not be obtained in the reverse reaction direction because of the irreversibility of the reaction (see below). However, the inhibition patterns provide a great deal of information about the sequential mechanism.

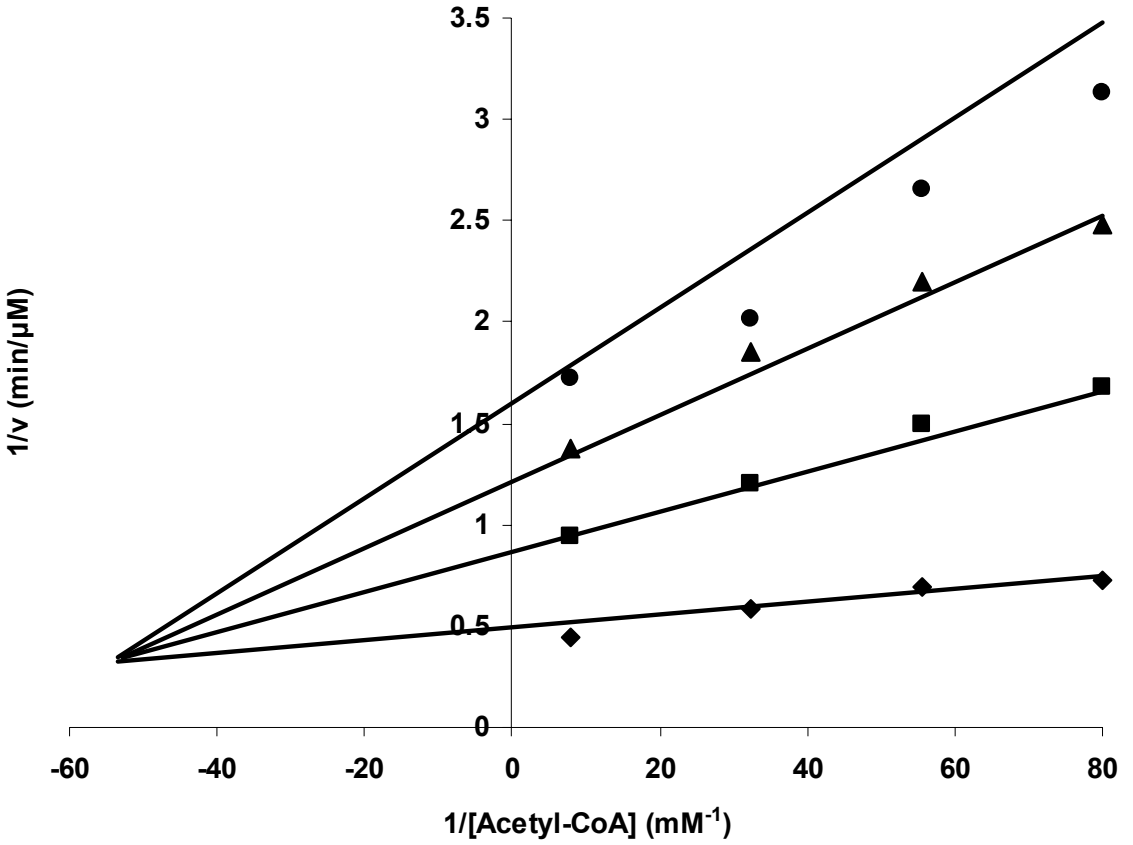

Fig. 3-1: Initial velocity Double-reciprocal Plot for the HCS reaction. The concentrations of AcCoA are as plotted, while α-Kg is fixed at 10 mM (◆), 2.5 mM (■), 1.46 mM (▲), and 1 mM (●). The solid lines are theoretical data based on the fit to equation 1, while the points are experimental. Note that the experimental values measured using 1 mM α-Kg are higher than the predicted values due to the activating effect of monovalent cations on the HCS (see Chapter 4).

An intersecting pattern is also observed when OAA is used as a α-Kg substrate analog (see Appendix – Fig. A-4). Thus, HCS is capable of catalyzing a reaction that is specific to citrate synthase from the TCA cycle, although homocitrate synthase has no homology to citrate synthase in terms of sequence and probably three-dimensional structure (citrate synthase has an all-helical structure while the structure of homocitrate synthase is predicted to contain an α/β TIM barrel domain (*11*, *14*)). Kinetic parameters for HCS using either α-Kg or OAA are shown in Table 3-1.

Table 3-1: Kinetic parameters for HCS.

Parameter	A = α-Kg	A = OAA
K_a (mM)	3.3 ± 0.2	25.5 ± 0.1
K_b (μM)	2.4 ± 0.2	1.30 ± 0.01
K_{ia} (mM)	25.1 ± 2.5	140 ± 1
V/E_t (s^{-1})	0.60 ± 0.03	0.30 ± 0.02
V/K_aE_t ($M^{-1}\cdot s^{-1}$)	180 ± 14	9.8 ± 0.7
V/K_bE_t ($M^{-1}\cdot s^{-1}$)	$(2.5 \pm 0.2) \times 10^5$	$(2.0 \pm 0.1) \times 10^5$

The V/E_t values obtained with α-Kg and OAA are very similar, but V/KE_t values differ by more than an order of magnitude with $V/K_{\alpha\text{-Kg}}E_t > V/K_{OAA}E_t$. There is no difference in terms of specificity of the HCS for AcCoA using either α-Kg or OAA.

3-3-2. Product inhibition studies

The only product inhibition patterns obtained were with CoA, which is UC vs. α-Kg and NC vs. AcCoA, Table 3-2. The K_i of 20 μM for CoA suggests it still binds with reasonably high affinity without the acetyl group.

3-3-3. Dead-end inhibition studies

Based on preliminary studies, HCS did not show any detectable inhibition by 10 mM L-glutamate, 50 mM γ-ketopimelate, or 50 mM succinate (data not shown).

Dead-end inhibitors are invaluable in establishing order of binding in an enzyme mechanism (*13*). Desulfo-CoA was used as a dead-end analog of AcCoA, and is NC against AcCoA, and UC against α-Kg. The uncompetitive inhibition against α-Kg suggests an ordered mechanism with α-Kg binding prior to AcCoA. The noncompetitive inhibition by CoA and desulfo-CoA suggest two combinations by the two inhibitors, one identical to the enzyme form to which AcCoA combines, and a second on the product side of the reaction, likely the E:Hc form of the enzyme. The lack of a slope effect in the case of the inhibition by CoA with α-Kg varied at a low AcCoA concentration suggests an irreversible reaction consistent with the downhill nature of the reaction as a result of the hydrolysis of the intermediate homocitryl-CoA.

Citrate was used as a dead-end analog of α-Kg, and is C vs. α-Kg and NC vs. AcCoA. Data are consistent with the proposed ordered addition of α-Kg before AcCoA with a dead-end E:α-Kg:CoA complex. All kinetic constants are summarized in Table 3-2.

Table 3-2. Inhibition kinetic constants for product and dead-end inhibitors of HCS.

Varied substrate	Fixed substrate	Inhibitor	K_{is} (mM)	K_{ii} (mM)	Inhibition pattern
α-Kg	AcCoA (0.031 mM)	Citrate	13.5 ± 1.0		C
AcCoA	α-Kg (5 mM)	Citrate	19 ± 2 (17 ± 2)	200 ± 60 74 ± 24	NC
α-Kg	AcCoA (0.031 mM)	Desulfo-CoA		0.021 ± 0.001	UC
AcCoA	α-Kg (5 mM)	Desulfo-CoA	0.014 ± 0.002 (0.0023 ± 0.0004)	0.18 ± 0.05 (0.11 ± 0.03)	NC
α-Kg	AcCoA (0.031 mM)	CoA		0.0240 ± 0.0005	UC
AcCoA	α-Kg (5 mM)	CoA	0.008 ± 0.002 (0.0013 ± 0.0003)	0.033 ± 0.009 (0.020 ± 0.006)	NC

The values in parentheses are the corrected for the fixed reactant where applicable.

3-3-4. Fluorescence studies

In order to further test the proposed kinetic mechanism, fluorescence titrations were utilized to estimate the dissociation constants for enzyme-reactant complexes. Table 3-3 gives a list of the dissociation constants measured. All of the ligands quench the fluorescence emission of the single tryptophan of HCS with the exception of CoA, which gives a slight enhancement of fluorescence (*11*). Although AcCoA binds to free HCS, its K_d (450 μM) (Fig. 3-2) is much higher than its K_m (2 μM). The K_d for E:α-Kg, however, is identical within error to the K_{ia} value reported in Table 3-1. Although CoA binds better to E than does AcCoA (3-fold), it still has a weaker affinity than it does to the E:Hc complex (8-9-fold). Interestingly, the presence of CoA (3-times its K_d) decreases the affinity of α-Kg by 4-fold, while OAA binds better to free HCS than does α-Kg (7-fold).

Table 3-3. Dissociation constants of ligand-HCS complexes from fluorescence titration.

Ligand	K_d (mM)
α-Kg	26 ± 1
α-Kg (+0.5 mM CoA)	111 ± 1
OAA	3.70 ± 0.02
CoA	0.17 ± 0.01
AcCoA	0.45 ± 0.01

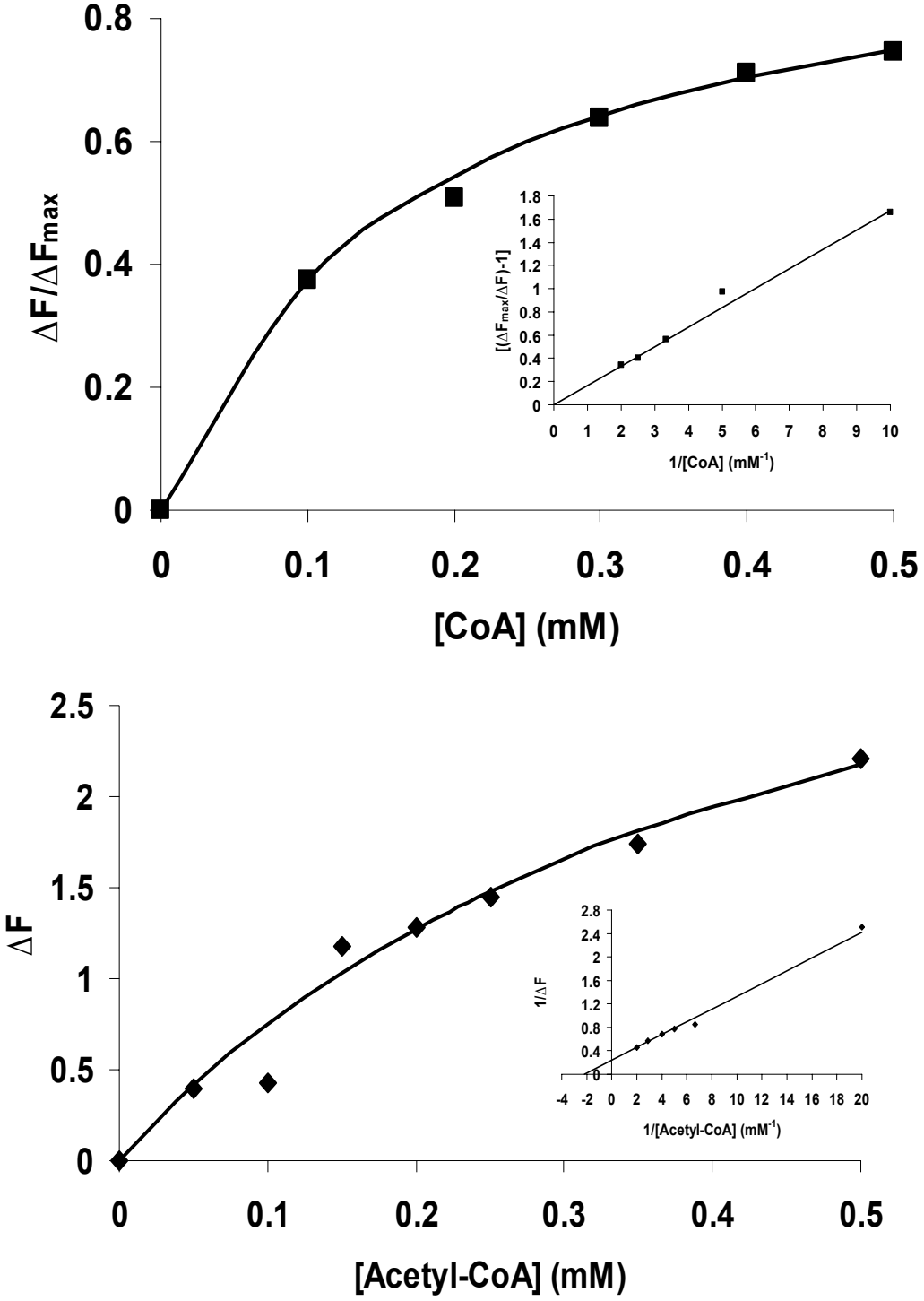

Fig. 3-2: (A) Determination of the K_d for AcCoA via fluorescence titration. A plot of ΔF vs. the concentration of AcCoA is shown. The inset shows a double reciprocal plot of the data, with the x-intercept equal to $-1/K_d$. (B) Determination of the K_d for CoA via fluorescence titration. The curves are theoretical based on a fit to eq. 5, while points are experimental in both cases.

3-4. Discussion

The initial velocity pattern gives a family of lines that intersect to the left of the ordinate suggesting a sequential kinetic mechanism for HCS. The ordered nature of the mechanism is suggested by the UC inhibition by desulfo-CoA and CoA vs. α-Kg. In both cases these inhibitors are NC vs. AcCoA, the substrate they mimic structurally. Data thus indicate the inhibitors combine with two separate enzyme forms, one the same as that to which AcCoA binds, the E:α-Kg complex, and a second, likely the normal product complex to which CoA binds, E:homocitrate. In a reversible reaction binding of CoA to the E:Hc complex would give NC inhibition vs. both substrates in an ordered mechanism as a result of reversal of the reaction. In this case, however, equilibrium is far to the right as a result of hydrolysis of the intermediate homocitryl CoA, and the reaction is practically irreversible. (Homocitrate and CoA are products since the absorbance of the thioester bond decreases as AcCoA is used up and the appearance of CoA can be monitored using the DCPIP assay (*11*).) Both CoA and desulfo-CoA can thus be treated as dead-end inhibitors. An analog of the first substrate bound in an ordered mechanism would be expected to be C vs. α-Kg and NC vs. AcCoA, as is observed for citrate. A kinetic mechanism can thus be proposed as shown in Figure 3-3. The mechanism is ordered with α-Kg binding before AcCoA and with CoA released before Hc. The reaction is practically irreversible and the product CoA can bind to the E:α-Kg and E:Hc complexes.

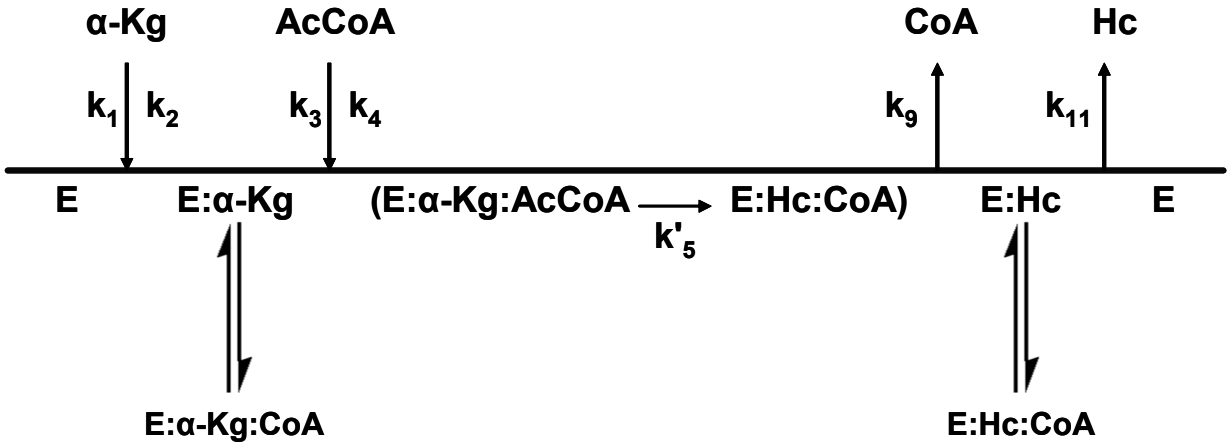

Fig. 3-3: Proposed kinetic mechanism for the HCS. E represents the HCS. Kinetic data suggest that the reaction is irreversible in agreement with the thermodynamics of the reaction. CoA (and desulfo-CoA) can bind to both E:α-Kg and E:Hc forms of the enzyme, while citrate binds to E. k'_5 is the net catalysis rate and is defined as $k_5k_7/(k_6+k_7)$.

3-4-1. Quantitative analysis of inhibition data

Since all inhibitors, including CoA, can be treated as dead-end inhibitors, correction of the observed K_i values for the fixed variable substrate should give the same true K_i values whichever of the substrates is varied. The competitive inhibition by citrate vs. α-ketoglurate gives the true K_i for the inhibitor for the E:citrate complex, 14 mM. With AcCoA varied, however, the observed K_{is} and K_{ii} values must be corrected for the concentration of the fixed substrate. Given the rate equation for the ordered kinetic mechanism, Eq. 1, the presence of the inhibitor adds a $(1 + \mathbf{I}/K_i)$ terms to each of the denominator terms representing free enzyme, $K_{ia}K_b$ and K_aB to give Eq. 6, where K_i is the intrinsic dissociation constant for EI.

$$v = \frac{\mathrm{VAB}}{(K_{ia}K_b + K_a\mathbf{B})\left(1 + \frac{\mathbf{I}}{K_i}\right) + K_b\mathbf{A} + \mathbf{AB}} \quad [6]$$

With **B** varied, Eq. 6 in double reciprocal form is given by Eq. 7.

$$\frac{1}{v} = \left[\left(\frac{K_{ia}K_b}{\mathrm{VA}}\right)\left(1 + \frac{\mathbf{I}}{K_i}\right) + \frac{K_b}{\mathrm{V}}\right]\left(\frac{1}{\mathbf{B}}\right) + \left(\frac{K_a}{\mathrm{VA}}\right)\left(1 + \frac{\mathbf{I}}{K_i}\right) + \frac{1}{\mathrm{V}} \quad [7]$$

The observed or appK_i is then obtained from the expressions for slope and intercept vs. I when the slope is zero. As an example, the expression for the slope inhibition constant is derived below.

$$\text{Slope} = \left(\frac{K_{ia}K_b}{\mathrm{VA}} + \frac{K_b}{\mathrm{V}}\right) + \left(\frac{K_{ia}K_b}{\mathrm{V}K_i\mathbf{A}}\right)\mathbf{I} \quad [8]$$

and with slope equal to zero

$$\mathbf{I} = \text{app}K_i = -K_i\left(1 + \frac{\mathbf{A}}{K_{ia}}\right) \quad [9]$$

where appK_i is the measured K_{is} value given in Table 3-2. The expression for K_{ii} can be derived in a similar manner, and the true K_i can be calculated. The calculated K_i

values of 13 mM and 17 mM agree very well, Table 3-2 (values in parentheses). Although, the corrected K_{is} and K_{ii} values for the inhibition by citrate vs. B (Table 3-2) are different, they are the same order of magnitude, and the value obtained from K_{ii} has a high error associated with it.

Inhibition by desulfo-CoA or CoA results from binding to E:α-Kg, represented by the K_bA term, and a form of the enzyme present at saturating concentrations of both reactants, represented by the AB term. Equation 1 can thus be modified as follows to give the rate equation for inhibition by either desulfo-CoA or CoA.

$$v = \frac{V\mathbf{AB}}{K_{ia}K_b + K_a\mathbf{B} + K_b\mathbf{A}\left(1+\frac{\mathbf{I}}{K_{i1}}\right) + \mathbf{AB}\left(1+\frac{\mathbf{I}}{K_{i2}}\right)} \qquad [10]$$

In eq. 10, K_{i1} is the intrinsic K_i for E:α-Kg:I, but K_{i2} is an apparent K_i with a value determined by the amount of the E:Hc complex that builds up in the steady state at saturating substrate concentrations. Values for K_{i1} and K_{i2} can be evaluated as above, from the noncompetitive inhibition vs. AcCoA, giving 1 μM and 20 μM, respectively, for CoA, and 2μM and 110 μM, respectively, for desulfo-CoA. Thus, CoA binds better by a factor of 2 to E:α-Kg.

The observed K_{ii} from the UC inhibition pattern obtained for CoA or desulfo-CoA vs. α-Kg cannot so easily be evaluated. The expression for K_{ii} is given in Eq. 11.

$$K_{ii} = \frac{\left(1 + \frac{K_b}{\mathbf{B}}\right)}{\left(\frac{1}{K_{i2}} + \frac{K_b}{\mathbf{B}K_{i1}}\right)} \qquad [11]$$

Substituting values for **B**, K_b, and the calculated values for K_{i1} and K_{i2} from Table 3-2 in Eq. 11, gives K_{ii} values of 25 μM and 19 μM for desulfo-CoA and CoA, respectively, in excellent agreement with the measured values of 21 μM and 24 μM, respectively. Data are consistent with the proposed ordered kinetic mechanism.

If the assumption is made that $K_{i1} = K_{i2}$, perhaps reasonable due to the similarity in the structures of the desulfo-CoA to CoA and AcCoA, the amount of E:Hc that builds up in the steady state can be estimated. The ratio K_{i1}/K_{i2} is directly proportional to the amount of E:Hc that builds up in the steady state. Estimates that are obtained from CoA and desulfo-CoA are 2-5% suggesting a significant but small contribution of the release of homocitrate to overall rate limitation under V_{max} conditions. A reasonable kinetic mechanism for HCS under V_{max} conditions is given below:

$$\text{E:}\alpha\text{-Kg:AcCoA} \underset{k_6}{\overset{k_5}{\rightleftharpoons}} \text{E:HcCoA} \xrightarrow{k_7} \text{E:Hc:CoA} \xrightarrow{k_9} \text{E:Hc} \xrightarrow{k_{11}} \qquad [12]$$

where HcCoA is homocitryl-CoA, k_5 and k_6 represent formation of HcCoA and its decomposition to reactants α-Kg and AcCoA, k_7 represents hydrolysis of HcCoA to products Hc and CoA, and k_9 and k_{11} represents release of CoA and Hc, respectively.

The expression for V_{max} is then given below in terms of enzyme forms that build up in the steady state.

$$V = \frac{E_t}{\frac{k_6 + k_7}{k_5 k_7} + \frac{1}{k_7} + \frac{1}{k_9} + \frac{1}{k_{11}}} = \frac{\mathbf{E_t}}{\mathbf{E:\alpha - Kg:AcCoA + E:HcCoA + E:Hc:CoA + E:Hc}}$$

[13]

If E:Hc is 2-5% of the total enzyme at saturating substrates, the remaining 95-98% is made up of some combination of the remaining enzyme forms. The determination of distribution will have to await further studies including those using isotope effects to probe the chemical steps.

3-4-2. Fluorescence binding studies

The dissociation constant for the E:α-Kg complex obtained from steady state kinetic studies (K_{ia} in Table 3-1) is identical to that obtained from fluorescence titration, Table 3-3. However, fluorescence data, Table 3-3, indicate finite binding of AcCoA and CoA to free enzyme. The K_d for E:AcCoA (450 μM), Table 3-3, is more than 200 times higher than the K_m for AcCoA (2 μM), Table 3-1. In addition, the K_d for E:CoA, (170 μM), Table 3-3, is almost 100 times higher than its K_i for the E:α-Kg:CoA complex (1 μM), Table 3-2. It is thus possible that the kinetic mechanism of HCS is random with a high degree of synergism of binding between α-Kg and AcCoA (There is a similar but less pronounced difference in the dissociation constant for

enzyme-α-Kg complex and its K_m). Since the ordered mechanism suggested for HCS may arise as a result of a high degree of synergism (*13*) as described above, we suggest a preferred ordered mechanism. Although one would expect NC inhibition by CoA vs. α-Kg in this case, the concentration of CoA used in these studies would not be sufficient to generate a significant slope effect as a result of CoA binding to E at low α-Kg.

Interestingly, the binding of CoA (in contrast to AcCoA) to the HCS enhances the intrinsic fluorescence of the HCS suggesting a conformational change that alters the microenvironment of the strategically located single tryptophan residue of the enzyme toward an increased hydrophobicity. The reasoning for this phenomenon may be the closure of the active site upon binding of the CoA to the free enzyme or E:α-Kg complex, consistent with the increased K_d of E:α-Kg:CoA, Table 3-3.

3-4-3. Active site specificity and kinetic mechanism

Based on the inhibition studies and data obtained with the alternative substrate OAA, some information can be provided on the active site of HCS. As shown in Table 3-3, the dissociation constant (K_d) of E:OAA (3.7 mM) is less than that for E:α-Kg (25 mM) suggesting that the binding of OAA is favored by about 1.1 kcal/mol. On the other hand the second order rate constant (V/KE_t) is a factor of 16 higher for α-Kg than for OAA. This reflects a kinetic preference for binding of α-Kg of about 1.7 kcal/mol. (The V/K for the first substrate in an ordered mechanism is its rate constant for combination with enzyme. For a simple, single step binding process this rate

constant would be expected to equal the diffusion limit of 10^8 $M^{-1}s^{-1}$. The low values observed for both substrates suggest a multi-step binding process with the first reactant inducing a conformational change in enzyme to facilitate binding of the second substrate.)

The value of K_a/K_{ia} is almost the same for both α-Kg and OAA, and the crossover point for the intersecting initial velocity pattern is above the horizontal axis for both substrates due to be less than unity of the K_a/K_{ia} ratio. The kinetically determined K_{ia} for E:α-Kg is the same as fluorescently determined K_d. However, this is not the case for OAA. This discrepancy may be explained by some randomness in the kinetic mechanism in which OAA can bind productively to the E:AcCoA complex (preliminary data agree with this suggestion). It is also possible that with OAA as a substrate, some nonproductive binding is observed. However, in this case a decrease in K_m and V_{max} would be expected for OAA compared to α-Kg and this is not observed.

The low K_d for OAA binding relative to α-Kg, see above, and inability of the enzyme to accommodate the carboxyethyl moiety of the γ-ketopimelate suggests that α-Kg, when bound, may be somewhat strained, i.e. it does not bind in an extended conformation, and the shorter OAA may fit better in the active site. The fact that succinate is not an effective inhibitor suggests that α-carbonyl group is important for binding, as expected since the carbonyl oxygen must be protonated as homocitryl CoA is formed. In the case of HCS from *T. thermophilus*, α-ketoadipate and α-ketoisovalerate have no effect on enzyme activity as reported (*10*), so that chains

longer than 5 carbons or with bulkier side chains are not accommodated. Additional kinetic experiments are required to better understand active site specificity.

3-5. Acknowledgements

We thank Dr. W. E. Karsten for his insightful discussion of the results. We also thank Dr. Elena Zgurskaya for the use of the spectrofluorometer.

References

[1] Johansson, E., Steffens, J. J., Lindqvist, Y., and Schneider, G. (2000) Crystal structure of Saccharopine reductase from *Magnaporthe grisea*, an enzyme of the α-aminoadipate pathway of lysine biosynthesis, *Structure 8*, 1037-1047.

[2] Bhattacharjee, J. K. (1992) Evolution of α-aminoadipate pathway for the synthesis of lysine in fungi, in *Evolution of Metabolic Function* (Mortlock, R. P., Ed.), pp 47-80, CRC Press, Boca Raton.

[3] Bhattacharjee, J. K. (1985) α-aminoadipate pathway for the biosynthesis of lysine in lower eukaryotes, *Crit. Rev. Microbiol. 12*, 131-151.

[4] Umbarger, H. E. (1987) Amino acid biosynthesis and its regulation, *Annu. Rev. Biochem. 47*, 532-606.

[5] Vogel, H. J. (1960) Two modes of lysine synthesis among lower fungi: evolutionary significance, *Biochim. Biophys. Acta 41*, 172-173.

[6] Ramos, F., Verhasselt, P., Feller, A., Peeters, P., Wach, A., Dubois, E., and Volckaert, G. (1996) Identification of a gene encoding a homocitrate synthase isoenzyme of *Saccharomyces cerevisiae*, *Yeast 12*, 1315-1320.

[7] Tracy, J., and Kohlhaw, G. (1975) Reversible, coenzyme-A-mediated inactivation of biosynthesis condensing enzymes in yeast: A possible regulatory mechanism, *Proc. Natl. Acad. Sci. USA 72*, 1802-1805.

[8] Gaillardin, G. M., Poirier, L. and Heslot, H. (1976) A kinetic study of homocitrate synthase activity in the yeast *Saccharomycopsis lipolytica*, *Biochim. Biophys. Acta 422*, 390-406.

[9] Jaklitsch W. M., and Kubicek, C. P. (1990) Homocitrate synthase from *Penicillium chrysogenum*, localization, purification of the cytosolic isoenzyme, and sensitivity to lysine, *Biochem. J. 269*, 247-253.

[10] Wulandari, A. P., Miyazaki, J., Kobashi, N., Nishiyama, M., Hoshino T., and Yamane, H. (2002) Characterization of bacterial homocitrate synthase involved in lysine biosynthesis, *FEBS Letters 522*, 35-40.

[11] Andi, B., West, A. H., and Cook, P. F. (2004) Stabilization and characterization of histidine-tagged homocitrate synthase from *Saccharomyces cerevisiae*, *Arch. Biochem. Biophys. 421*, 243-254.

[12] Cleland, W. W. (1963) The kinetics of enzyme-catalyzed reactions with two or more substrates or products I. Nomenclature and rate equations, *Biochim. Biophys. Acta 67*, 104-137.

[13] Cleland, W. W. (1977) Determining the chemical mechanisms of enzyme-catalyzed reactions by kinetic studies, *Adv. Enzymol. 45*, 273-387.

[14] Berman, H. M., Westbrook, J., Feng, Z., Gilliland, G., Bhat, T. N., Weissig, H., Shindyalov, I. N., and Bourne, P.E. (2000) The protein data bank, *Nucleic Acids Research 28*, 235-242.

CHAPTER 4

Regulatory mechanism of homocitrate synthase: I. KINETIC STUDIES

"Reproduced with automatic permission from [Andi, B., West A. H., and Cook, P. F. (2005) Regulatory Mechanism of Histidine-tagged Homocitrate Synthase from *Saccharomyces cerevisiae* I. KINETIC STUDIES, *J. Biol. Chem. 280*, 31624-31632] Copyright [2005] The American Society for Biochemistry and Molecular Biology, Inc."

4-1. Introduction

There are two distinct pathways for the biosynthesis of the essential amino acid lysine. The diaminopimelate pathway is common among plants, bacteria and lower fungi (Phycomycetes or algal fungi). Homocitrate synthase (HCS) [2-hydroxybutane-1,2,4-tricarboxylate 2-oxoglutarate-lyase (CoA-acetylating), EC 2.3.3.14] is the first and committed enzyme of the α-aminoadipate pathway for the biosynthesis of lysine that is unique to higher fungi (Ascomycetes and Basidomycetes). Pathogenic fungi such as *Candida albicans*, *Cryptococcus neoformis* and *Aspergillus fumigatus* (human pathogens) and *Magnaporthe grisea* (a plant pathogen) use the α-aminoadipate pathway for lysine biosynthesis. The uniqueness of the α-aminoadipate pathway makes it a potential target for the design of antifungal drugs to protect immunocompromised patients (transplant, AIDS and cancer patients) against opportunistic fungi (*1–6*).

The α-aminoadipate pathway begins with the condensation of α-ketoglutarate with AcCoA to yield homocitrate and coenzyme A (*1–6*). There are two isozymes of homocitrate synthase in *Saccharomyces cerevisiae*, cytosolic and mitochondrial, and

both isozymes are feedback inhibited by lysine and the expression of the cytosolic isozyme is repressed by lysine (*7*). However, HCS is a physiologically complex enzyme, and in addition to its role in lysine biosynthesis, the localization of this enzyme in the nucleus (*8*) and its interaction with a number of nuclear proteins (BIND: Biomolecular Interaction Network Database) (www.bind.ca) suggest possible additional function in the nucleus and complex regulation.

There are few studies of the regulation of the HCS. In *Saccharomycopsis lipolytica* it has been shown that the HCS activity is completely inhibited by lysine and some lysine analogues like hydroxylysine and diaminopimelic acid (*9*). In the case of the enzyme from *Penicillium chrysogenum*, the inhibition by lysine was shown to be competitive with respect to α-ketoglutarate and pH dependent with only 20% inhibition by 1 mM lysine at pH 6.6-7.0 (*10*). It has been also reported that the HCS from *Thermus thermophilus* is highly sensitive to lysine (*11*). Regulation of HCS activity by CoA and divalent metal ions has also been reported (*12*).

In this paper, we make use of steady state kinetic and fluorescence binding studies to probe the kinetics of regulation of the cytosolic HCS from *Saccharomyces cerevisiae*. Our data suggest that lysine is a competitive inhibitor and the effects of lysine and Na^+ are independent of one another in the regulation of HCS. However, dependent on the concentration of the modulators and the concentration of substrates, the reaction can be either activated or inhibited. In an accompanying article (*24*), theory is developed for regulation by multiple effectors on the basis of studies presented in this manuscript.

4-2. Materials and methods

4-2-1. Materials

All chemicals were of the highest grade commercially available. α-Ketoglutarate, DCPIP, AcCoA, lysine and LiCl were obtained from Sigma. KCl, CsCl, $CaCl_2$ and $MnCl_2$ were purchased from Fisher Scientific, while $MgCl_2$ was from FisherBiotech. $(NH_4)_2SO_4$ was from Fluka, and NaCl was from EMD.

The concentration of AcCoA was adjusted spectrophotometrically (ε_{260}, 16.4 $mM^{-1}cm^{-1}$). The AcCoA solution in ddH_2O is stable, without any significant hydrolysis, for at least one month if kept at -21 °C. The concentration of DCPIP preparations was also adjusted spectrophotometrically ($\varepsilon_{600\ nm}$, 19.1 $mM^{-1}cm^{-1}$).

4-2-2. Assays of homocitrate synthase activity

Cell growth, HCS expression and purification were performed as previously described (*13*). A typical assay for HCS using the DCPIP method is as described with slight modifications (*13*). The final volume of the assay was 0.5 mL and contained 50 mM Hepes, pH 7.5 (adjusted by KOH), and variable concentrations of α-ketoglutarate and AcCoA (~K_m–20K_m) and 0.1 mM DCPIP. All assays were carried out at 25 °C. Reactions were thermally equilibrated to allow for completion of the reaction between CoA (in the AcCoA solution) with DCPIP before adding the enzyme to the reaction mixture.

In order to dissolve precipitated α-cyclodextrin in the stabilized HCS suspension (due to its interaction with other buffer components) (*13*) glycerol was added to a final

concentration of 10%. An enzyme solution prepared by this method is stable at room temperature for up to three to four hours after which, the enzyme begins to lose activity.

4-2-3. Initial velocity studies

Initial velocity patterns were obtained by measuring the initial rate as a function of AcCoA concentration (0.0125-0.125 mM) and a fixed concentration of α-Kg and the experiment was then repeated at several additional α-Kg concentrations (1-10 mM). An additional initial velocity pattern was also repeated using 0.0125-2.0 mM AcCoA at fixed concentrations of 0.5-10 mM α-Kg. The above initial velocity pattern was then repeated at several different fixed concentrations of the effector (including zero). In case of Na^+, concentrations of 0, 25, 100 and 250 mM were used, while concentrations of 0, 0.25, 0.5 and 1 mM were used for lysine. An initial velocity pattern was also repeated using high AcCoA concentration (0.5 mM) and 1-10 mM α-Kg at several additional lysine concentrations of 0, 0.25, 0.5, 1, 1.5, 2, 3, 4 and 5 mM.

To study the interaction between Na^+ and lysine, the initial rate was measured at a fixed concentration of α-Kg (1.46 mM≈0.5 $K_{\alpha\text{-Kg}}$) and a fixed concentration of AcCoA (0.0125 mM≈2 K_{AcCoA}, low, or 0.5 mM≈100 K_{AcCoA}, high) with the lysine concentration varied (0-1 mM) at different fixed concentrations of NaCl (0-250 mM).

4-2-4. Fluorescence binding studies

Fluorescence spectra were measured as previously described (*13*). Emission spectra (310-400 nm) were measured with the excitation monochromator fixed at 298 nm. Spectra were recorded on a Shimadzu RF-5301 PC spectrofluorometer equipped with a circulating water bath to maintain the temperature at 25°C. Fluorescence quartz cuvettes with a volume of 1 mL and a path length of 1 cm were used to measure sample and blank spectra. Excitation and emission slit widths were set to 1.5 nm and 5 nm, respectively. Because all of the reagents and buffer components have no absorbance above 310 nm, the inner filter effect is negligible under conditions used for taking the spectra.

The final buffer composition used to measure the spectra contained 55 mM Hepes (adjusted to pH 7.5 with KOH), 150 mM $(NH_4)_2SO_4$, 25 mM guanidinium chloride (GdmCl), 25 mM α-cyclodextrin, 8 mM KCl and 5 mM imidazole. All samples contained enzyme at a concentration of 55 μg/mL. Compounds used for fluorescence studies were α-Kg and lysine that were added sequentially from low to high concentration to both the blank and sample from a stock solution of 1 M for α-Kg, 1 M and 10 mM for lysine. The final total dilution in each case was 1.07 (α-Kg), 1.02 (10 mM stock solution) and 1.05 (1 M stock solution) (lysine), and all the data were corrected for dilution.

To calculate the K_d based on the fluorescence intensity, data were fitted to the equation for a rectangular hyperbola, eq 1:

$$\Delta F = \frac{\Delta F_{\max}\mathbf{L}}{K_{\mathrm{d}} + \mathbf{L}} \quad (1)$$

where ΔF is the change in intrinsic tryptophan fluorescence upon addition of ligand to enzyme, $\Delta F_{\max}$ is the maximum change in fluorescence at infinite ligand concentration, **L** is the ligand concentration, and K_{d} is the dissociation constant for the enzyme-ligand complex.

Due to nonlinearity of the lysine fluorescence data, they were fitted to eq 2, which represents the sum of two independent saturation curves indicating binding to non-interacting sites:

$$\Delta F = \frac{\Delta F_{\max 1}\mathbf{L}}{K_{\mathrm{d}1} + \mathbf{L}} + \frac{\Delta F_{\max 2}\mathbf{L}}{K_{\mathrm{d}2} + \mathbf{L}} \quad (2)$$

where **L** is the lysine concentration, and $\Delta F_{\max 1}$ and $\Delta F_{\max 2}$ are the maximum change in fluorescence intensity upon binding of lysine to the first and second binding sites, respectively. $K_{\mathrm{d}1}$ and $K_{\mathrm{d}2}$ are the dissociation constants associated with the binding of lysine to the aforementioned sites.

4-2-5. Effect of monovalent and divalent cations on HCS activity

Fixed concentration of α-Kg (5 mM≈$2K_{\alpha\text{-Kg}}$) and either low (0.031 mM≈$5K_{\mathrm{AcCoA}}$) or high (0.5 mM≈$100K_{\mathrm{AcCoA}}$) AcCoA concentrations were used at different

concentrations of monovalent and divalent cations (0-250 mM). Li^+, Na^+, K^+, Cs^+, Mn^{2+}, Mg^{2+}, Ca^{2+} were used as an additive to test their effects on HCS activity.

4-2-6. Data analysis

Data were fitted using the appropriate equations and the Marquardt-Levenberg algorithm supplied with the EnzFitter program from BIOSOFT, Cambridge, UK (www.biosoft.com). Rate, kinetic and dissociation constants and their corresponding standard errors were estimated using a simple, proportional or statistical robust weighing method (dependent on the maximum change in initial rate or ΔF observed in the experiment) for the activity or affinity of the enzyme by fitting the curves to the data either in the absence or presence of inhibitors or ligands. Some simple simulations for some of the equations were carried out using the *MATHEMATICA* version 5.0.1.0 from Wolfram Research, Inc., IL, USA (www.wolfram.com). Derivation of equations and theory are included in the accompanying article (*24*).

Data consistent with a sequential kinetic mechanism were fitted to eq 3.

$$\nu = \frac{\mathbf{VAB}}{K_{ia}K'_b + K'_a\mathbf{B} + K'_b\mathbf{A} + \mathbf{AB}} \qquad (3)$$

In eq 3, ν and V are initial velocity and maximum velocity, **A** (α-Kg) and **B** (AcCoA) are reactant concentrations, K'_a and K'_b are Michaelis constants for **A** and **B**,

and K_{ia} is the inhibition constant for **A** (the dissociation constant for E**A**, since HCS has an ordered kinetic mechanism (*14*)).

4-3. Results

4-3-1. Initial rate studies of lysine inhibition

In order to determine what forms of the enzyme bind lysine, the HCS reaction in the presence of lysine was treated as a terreactant (three reactants) reaction (*15*). Double reciprocal initial velocity patterns were obtained varying AcCoA at different fixed levels of α-Kg and zero lysine. This initial velocity pattern was then repeated at different lysine concentrations, Fig. 4-1A-D. The crossover points for all double reciprocal plots are to the left of the ordinate. Graphically, secondary plots were constructed by plotting the slopes (Fig. 4-2A) or intercepts (Fig. 4-2B) obtained from the plots in Fig. 4-1 against the reciprocal of the α-Kg concentration. Note that in Fig. 4-2A-B, there is no effect of lysine on the intercept of either the slope or intercept secondary plots. Finally, tertiary plots were constructed by plotting the slope from Figs. 4-2A and 4-2B vs. the concentration of lysine (Fig. 4-2C-D). Estimates of all of the kinetic parameters were obtained by fitting all of the data in Fig. 4-1 to eq 4 (see below). We present all of the data in this case, so that the method is clear to the reader; and so that it may be adapted to other systems. Kinetic parameters are summarized in Table 4-1. Values of $K_{i\ \alpha\text{-Kg}}$, $K_{\alpha\text{-Kg}}$, K_{AcCoA}, and V/E_t are within error identical to those reported previously (*14*).

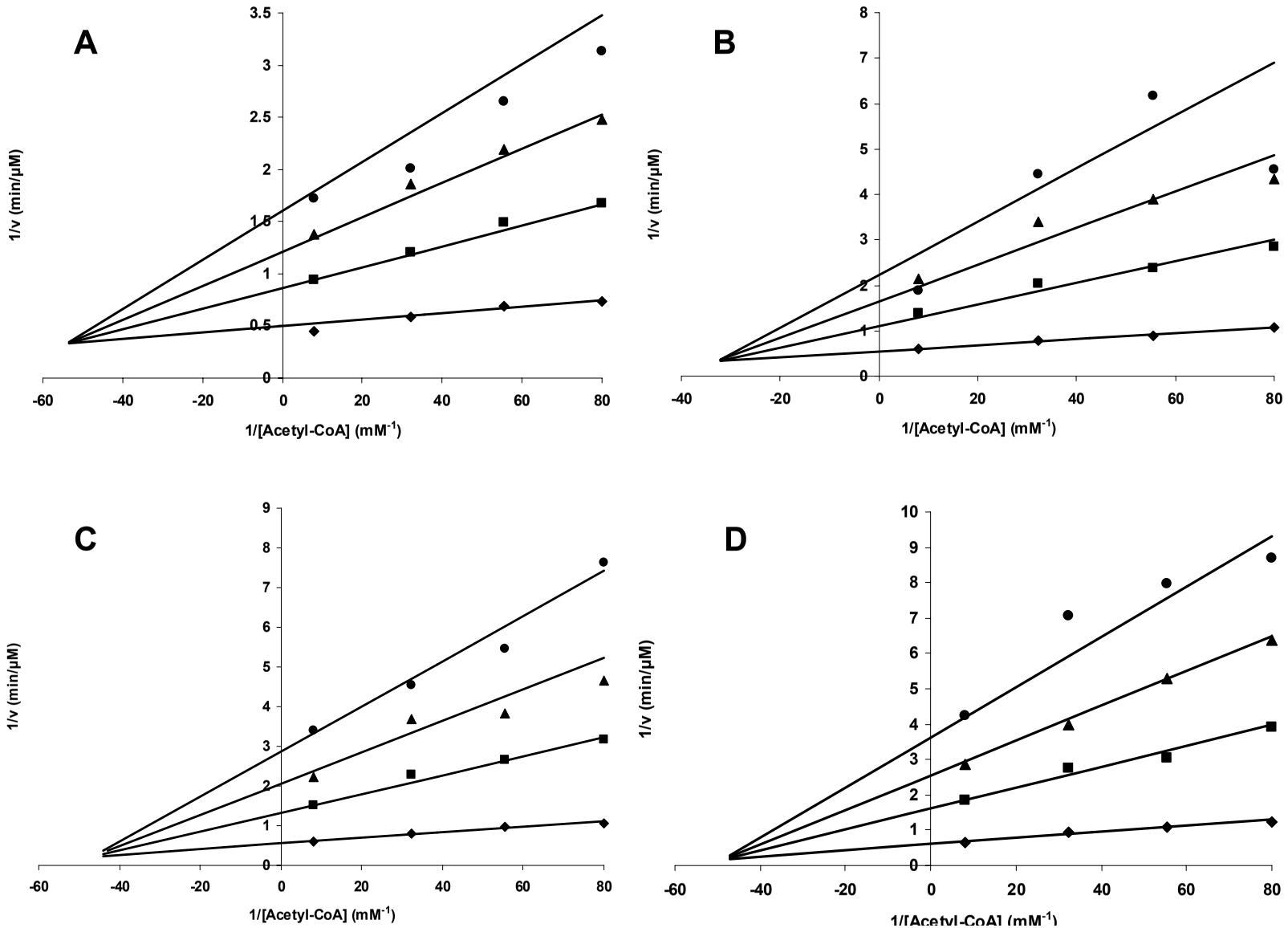

Fig. 4-1: Initial rate studies of lysine inhibition. Double reciprocal initial velocity patterns varying AcCoA at different fixed levels of α-Kg: 1 mM (●), 1.46 mM (▲), 2.5 mM (■), and 10 mM (◆) were measured in 50 mM Hepes, pH 7.5 and 25°C in the presence of the following lysine concentrations: (A) 0 mM, (B) 0.25 mM, (C) 0.5 mM, and (D) 1 mM. Points are experimental, while the solid lines are theoretical based on a fit to eq 3.

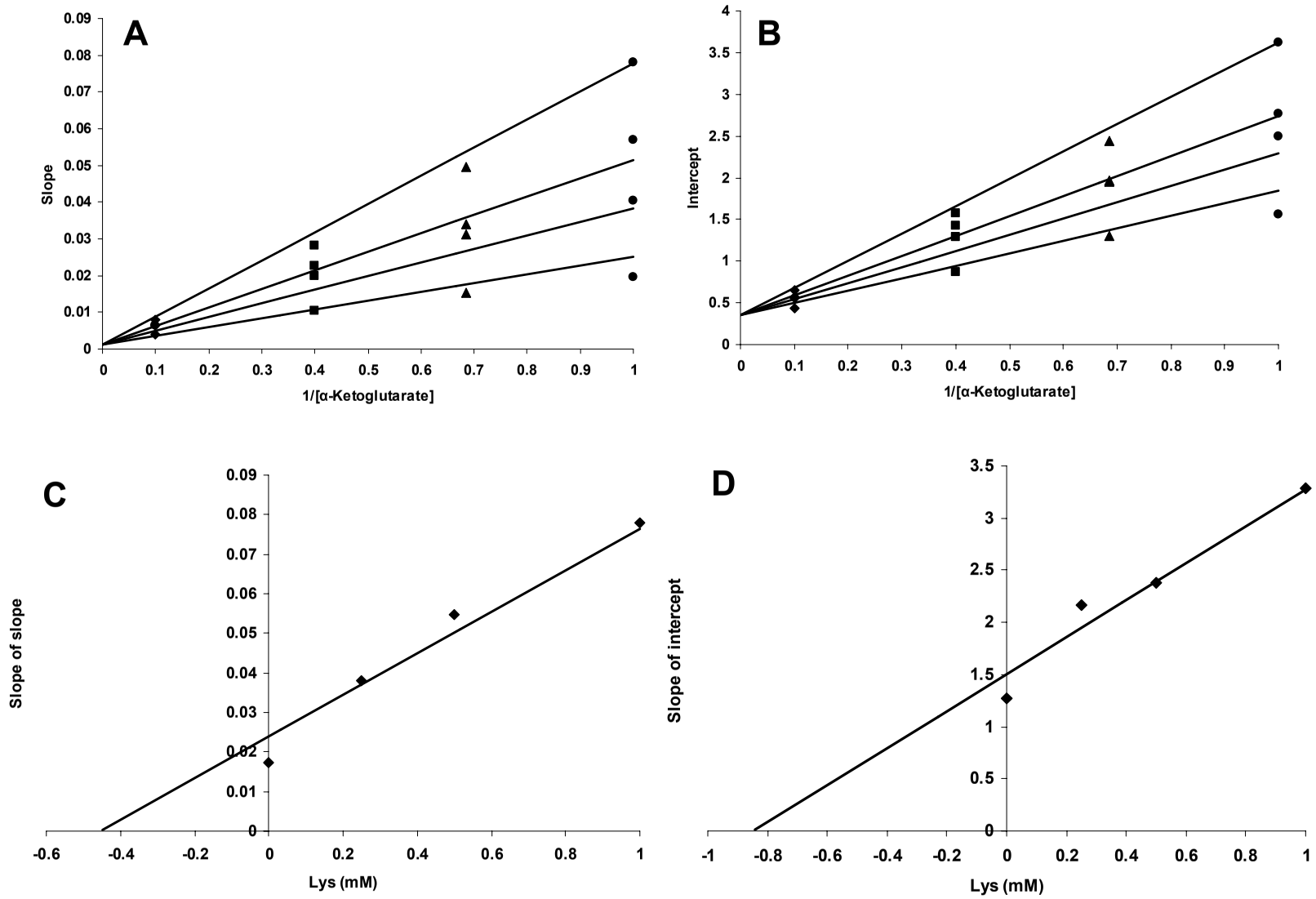

Fig. 4-2: Secondary and tertiary replots of the data in Fig. 4-1. A. Slope replot constructed from the slope of the lines in Figs. 4-1A-D vs. reciprocal of α-Kg concentration at each of the lysine concentrations indicated in Fig. 4-1A-D. B. Intercept replot constructed from the intercept vs. reciprocal of α-Kg concentration as in A. C. Tertiary replot of the slopes from Fig. 4-2A vs. lysine concentration. D. Tertiary replot of the slopes from Fig. 4-2B vs. lysine concentration. Points are from a graphical analysis, while the solid lines in A and B are theoretical based on a fit to the double reciprocal of eq 4, and the equation for a straight line in C and D.

Table 4-1: Kinetic parameters for inhibition patterns of HCS.

Kinetic parameter[a]	Lysine inhibition	Na^+ inhibition and activation	Na^+-lysine (low [AcCoA])	Na^+-lysine (high [AcCoA])
K_{ia} ($K_{i\ \alpha\text{-Kg}}$) (mM)	10.3 ± 0.4	3.9 ± 1.1	N/A	N/A
K'_a ($K_{\alpha\text{-Kg}}$) (mM)	4.6 ± 0.1	1.6 ± 0.3	N/A	N/A
K'_b (K_{AcCoA}) (μM)	7.7 ± 0.2	8.5 ± 2.3	N/A	N/A
K_{conf}	Included in K_{ia} and K_a	3.1 ± 0.4	Value of 3 included	Value of 3 included
K_{act} (mM)	N/A	12.2 ± 2.7	26.0 ± 4.0	83.0 ± 7.0
K''_{act} (mM)	N/A	N/A	18.0 ± 4.4	85.0 ± 19.0
$K_{i\ Na}$ (mM)	N/A	37 ± 9 (Graphical analysis)	27.0 ± 2.0	115.0 ± 5.0
$K_{i\ lys}$ (mM)	0.55 ± 0.02	N/A	0.42 ± 0.05	1.5 ± 0.2
k_p (μM/min)	N/A	N/A	3.4 ± 0.1	7.5 ± 0.2
V (μM/min)	3.37 ± 0.04	4.9 ± 0.2	N/A	N/A
V/E_t or k_p/E_t (s^{-1})	0.35 ± 0.01	0.47 ± 0.02	0.16 ± 0.01	0.36 ± 0.01

[a] The definition of kinetic parameters are as follows: K_{ia}, inhibition constant of α-Kg ($K_{i\ \alpha\text{-Kg}}$); K'_a, Michaelis constant of α-Kg ($K_{\alpha\text{-Kg}}$); K'_b, Michaelis constant of AcCoA (K_{AcCoA}); K_{conf}, conformational ratio constant; K_{act}, activation constant of Na^+; K''_{act}, activation constant of Na^+ for E′Lys complex; $K_{i\ Na}$, inhibition constant of Na^+; $K_{i\ lys}$, inhibition constant of lysine; k_p, overall enzymatic rate in the absence of inhibitors and activators; V, maximum velocity; V/E_t or k_p/E_t, turn-over number.

Partial inhibition by lysine was reported for the HCS from *Penicillium chrysogenum* (*10*). Thus, an initial velocity pattern was obtained at fixed AcCoA (0.5 mM≈100K_{AcCoA}) varying the concentration of α-Kg at different lysine concentrations (up to 5 mM). Data (see Appendix - Fig. A-5) indicates that in case of HCS from *S. cerevisiae*, lysine is a linear inhibitor over this concentration range. It should be also noted that initial rate measured for lysine inhibition studies is affected to some extent by the independent activatory effects of the monovalent cations present in the enzyme stock solution that introduce some (manageable) error in the data analysis.

4-3-2. Initial rate studies of sodium inhibition and activation

Initial velocity patterns were obtained as in Fig. 4-1, with the exception that Na^+ replaced lysine (see Appendix – Figs. A-6 and A-7). As for lysine, Na^+ does not affect the intercept of the secondary replots. Fig. 4-3 shows the tertiary replots of the slope of the slope replot (Fig. 4-3A) and the slope of the intercept replot (Fig. 4-3B). At low concentrations of both reactants (Fig. 4-3A), Na^+ exhibits complex behavior with activation at low concentrations and linear inhibition at high concentrations. At high AcCoA and low α-Kg, Na^+ exhibits only activation. Estimates of kinetic parameters are obtained by fitting all of the initial velocity data (see Appendix – Fig. A-6) to eq 5 (see below), and a summary of the estimates is given in Table 4-1.

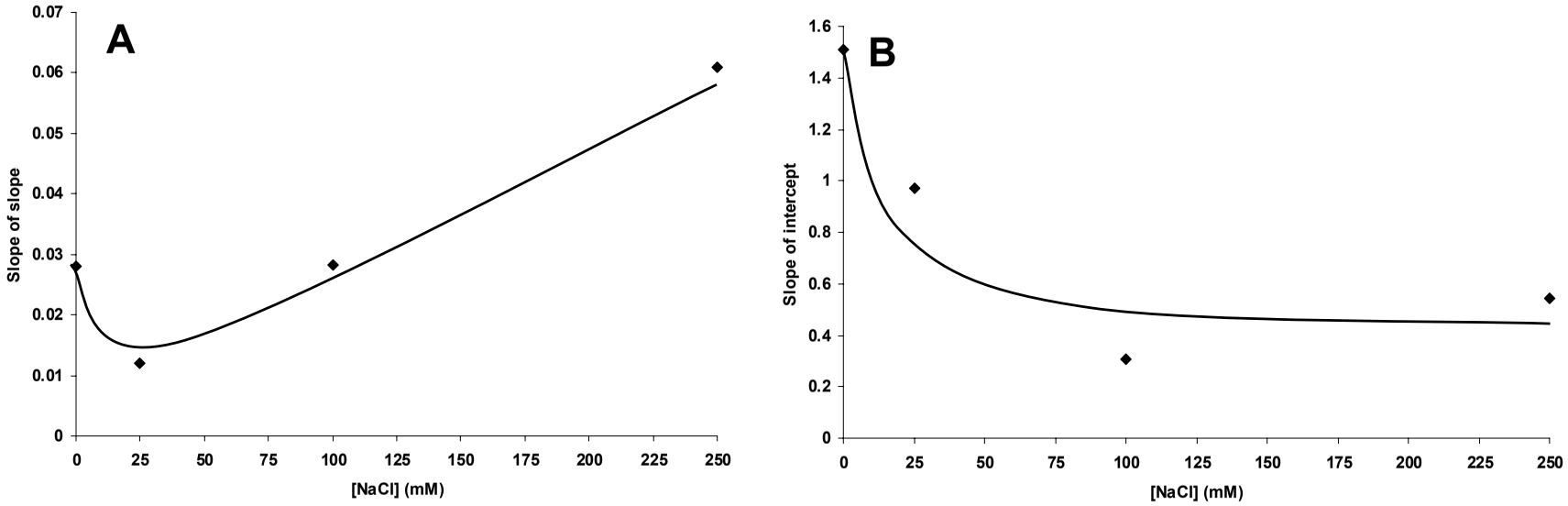

Fig. 4-3: Tertiary replots of the data (Fig. A-6) for Na^+ inhibition and activation studies. A. Tertiary replot of the slope of slope vs NaCl. B. Tertiary replot of the slope of intercept vs. NaCl. For both A and B, points are from a graphical analysis, while the solid lines are theoretical based on the kinetic parameters from a fit to eq 5.

4-3-3. Effect of lysine and Na^+

The behavior of the enzyme in the presence of both Na^+ and lysine is shown in Figs. 4-4 (low AcCoA) and 4-5 (high AcCoA). The rate in the absence of both Na^+ and lysine is the frame of reference in these studies. The effect of lysine in the absence of Na^+ is given at zero Na^+, while the effect of Na^+ in the absence of lysine is given as the intercepts of Figs. 4-4A and 4-5A and these are replotted in Figures 4-4C and 4-5C. For all conditions the effects of one of the modulators in the absence of the other is consistent with data obtained in Figs. 4-1 to 4-3. The interaction between the two modulators is given by the slope replots, Figs. 4-4B and 4-5B. The slope is, within error, independent of the concentration of Na^+ at high AcCoA concentration.

4-3-4. Fluorescence determination of the HCS-ligand dissociation constant

The binding of lysine to HCS as measured by fluorescence titration is biphasic, Fig. 4-6. Data were fitted to eq 2, which describes the sum of the two independent binding phenomenons. In addition, the K_d for α-Kg was measured in the absence and presence of lysine. Estimates of the K_d values are listed in Table 4-2.

4-3-5. Effect of monovalent and divalent cations on HCS activity

As shown in Fig. 4-7, monovalent cations activate HCS at low concentration, but inhibit at high concentrations when the activity is measured at low AcCoA and α-Kg concentrations. Monovalent cations other than Na^+ are less inhibitory at higher concentrations of AcCoA similar to the effect of Na^+ (see above). Among the

monovalent cations studied smaller cations (Li^+, 60 pm; Na^+, 95 pm, K^+, 133 pm; and Cs^+, 169 pm) show a greater inhibition and a lower activation. K^+ seems to be the best cation for HCS activity since it has the lowest inhibitory effect. The effect of NH_4^+ lie between the effects of Li^+ and Na^+ (data not shown).

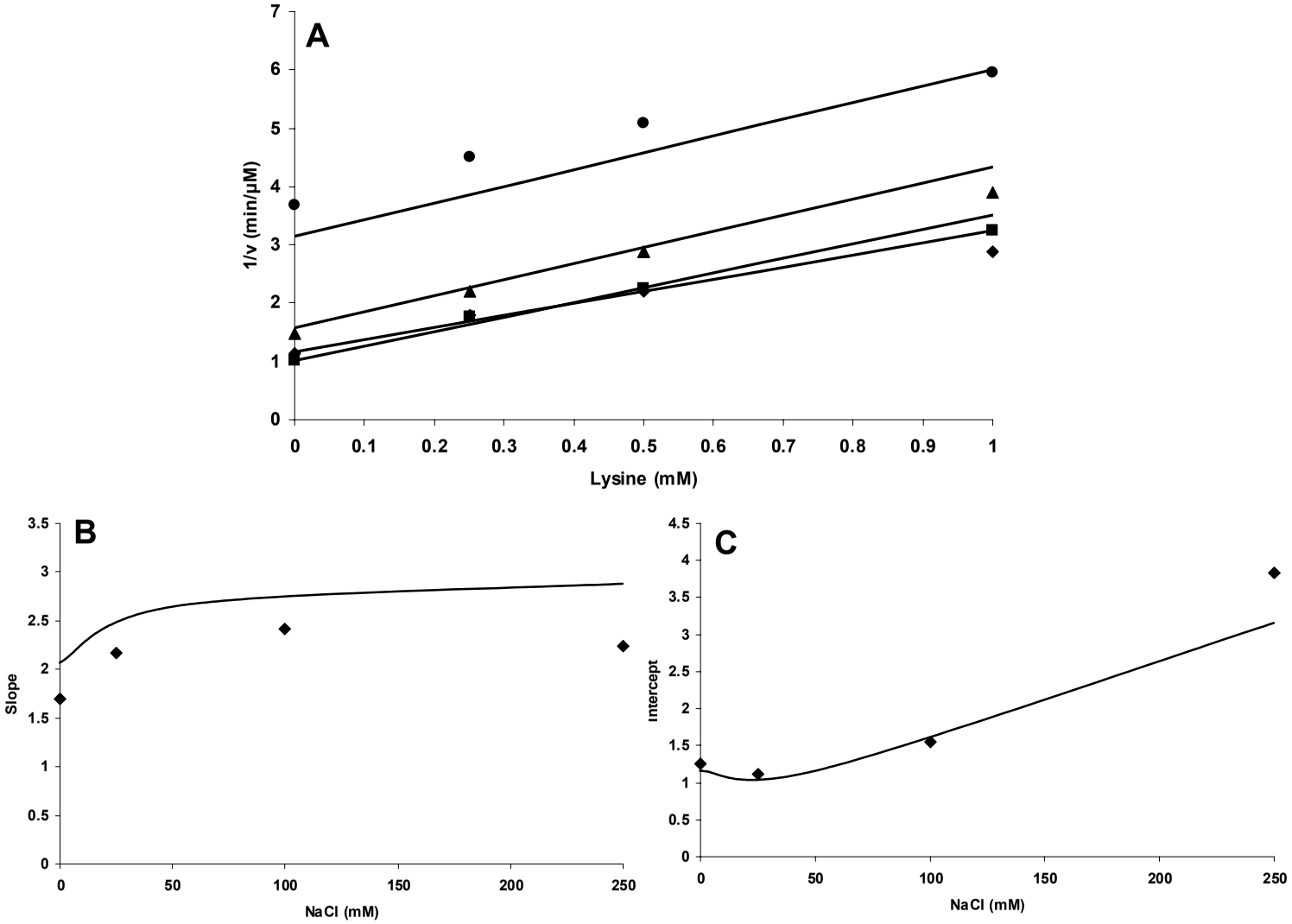

Fig. 4-4: Interactive effects of Na^+ and lysine at low AcCoA. A. Plot of reciprocal initial rate vs lysine concentration at different fixed concentrations of Na^+. Rates were measured in 50 mM Hepes, pH 7.5, 25°C at low concentrations of AcCoA (0.0125 mM) and α-Kg (1.46 mM) with the lysine concentration varied from 0-1 mM at different fixed concentrations of NaCl: 0 mM (◆), 25 mM (■), 100 mM (▲), and 250 mM (●). B. Replot of the slopes from A vs Na^+ concentration. The curvature arises from even the slight differences between K_{act} and K''_{act}. C. Replot of the intercepts from A vs Na^+ concentration. Points are the experimental, while the solid lines are for a fit of the data to eq 6.

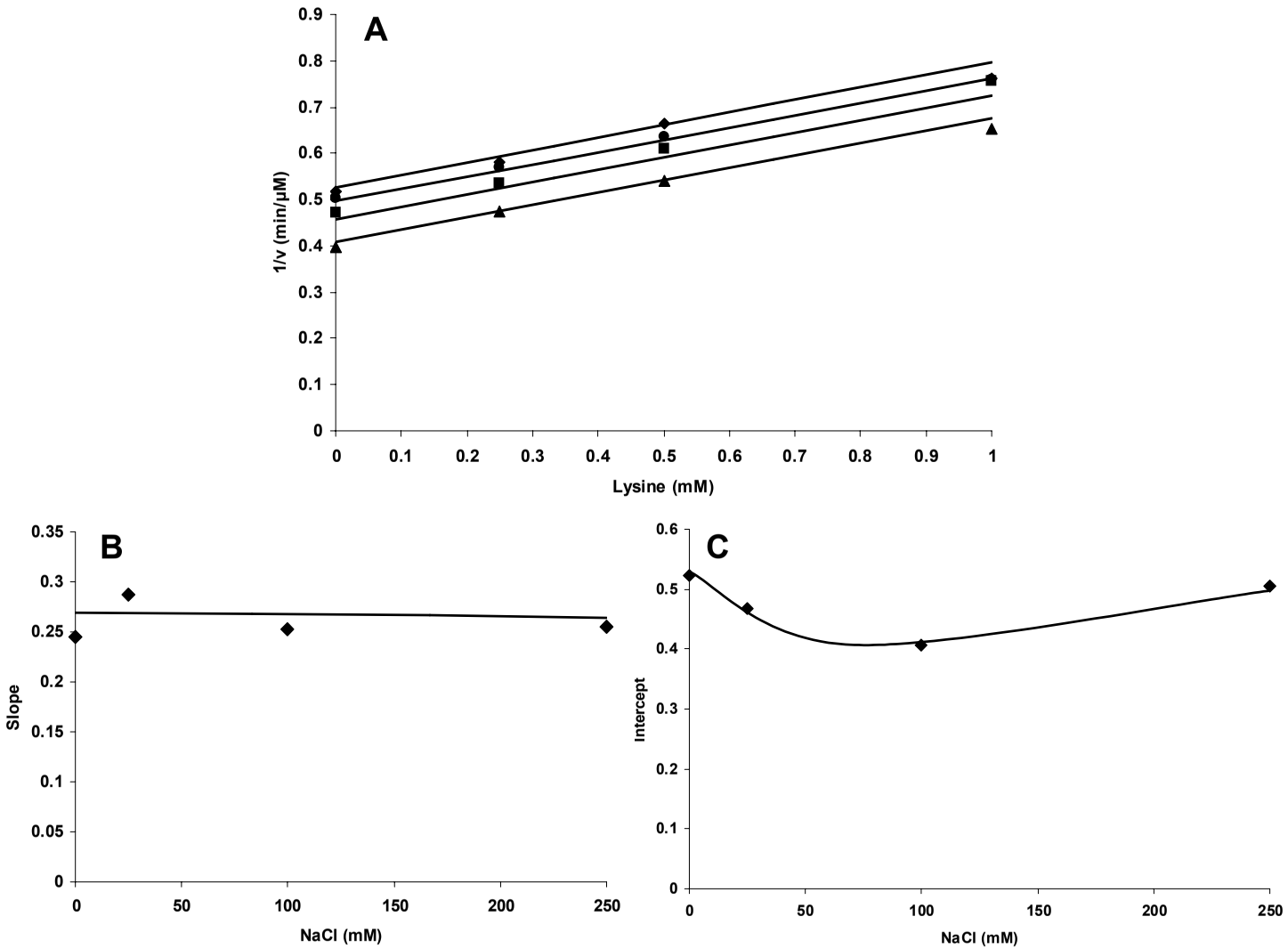

Fig. 4-5: Interactive effects of Na^+ and lysine at high AcCoA. A. Plot of reciprocal initial rate vs lysine concentration at different fixed concentrations of Na^+. Rates were measured in 50 mM Hepes, pH 7.5, 25°C at high concentration of AcCoA (0.5 mM) and low concentration of α-Kg (1.46 mM) with the lysine concentration varied from 0-1 mM at different fixed concentrations of NaCl: 0 mM (◆), 25 mM (■), 100 mM (▲), and 250 mM (●). B. Replot of the slopes from A vs Na^+ concentration. C. Replot of the intercepts from A vs Na^+ concentration. Points are the experimental, while the solid lines are for a fit of the data to eq 6.

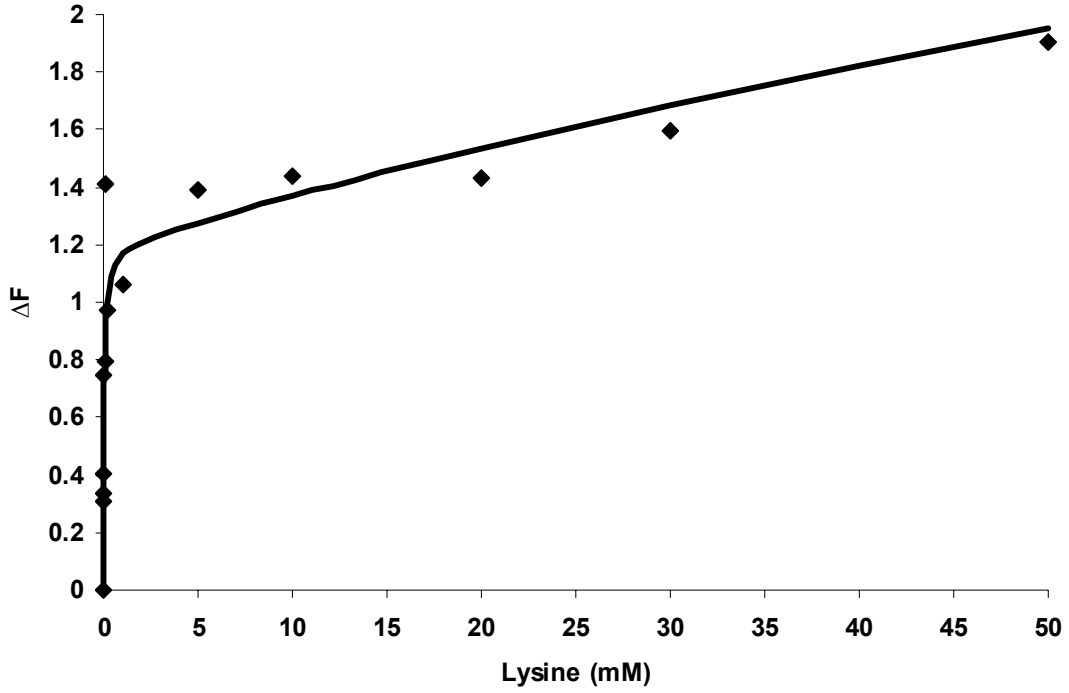

Fig. 4-6: Fluorescence titration of HCS with lysine. A plot of Δ*F* vs. the concentration of lysine is biphasic. Data were collected as discussed in Materials and Methods. Points are experimental, while the solid curve is theoretical based on a fit of the data to eq 2.

Table 4-2: Dissociation constants of ligand-HCS complexes by fluorescence titration.

Ligands	K_d (mM)
α-Ketoglutarate	26.1 ± 1.1
α-Ketoglutarate (+ 50 mM L-Lys)	34.8 ± 1.2
L-Lysine	0.04 ± 0.008, 255 ± 70

Of all of the divalent cations studied (Mn^{2+}, 75 pm; Mg^{2+}, 65 pm; and Ca^{2+}, 100 pm) smaller divalent cations exhibit a higher degree of inhibition, and are inhibitory at low AcCoA concentration. Experiments show that Mg^{2+} is much less inhibitory at lower concentration when used at high AcCoA concentration (Fig. 4-7 inset). In

general, it seems that the inhibitory effects of all of the monovalent and divalent cations are related to the density of the positive charge on the surface of the ion or

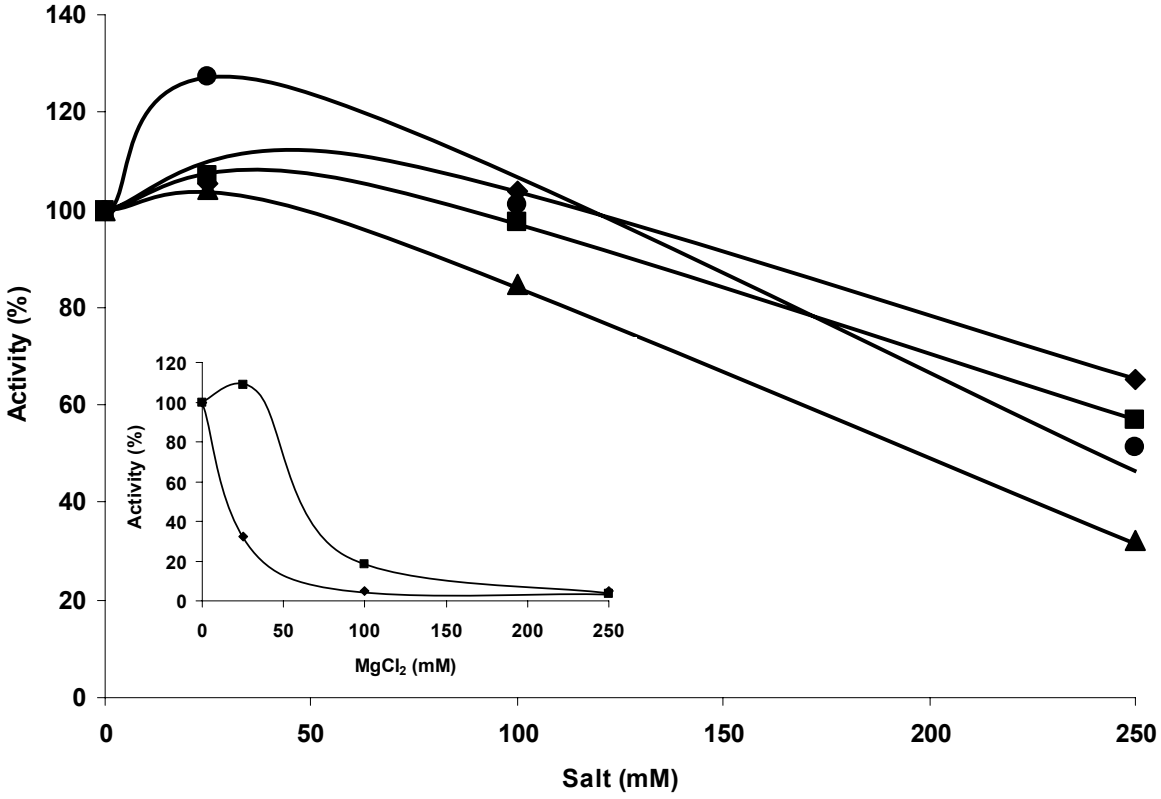

Fig. 4-7: Effect of monovalent and divalent cations on HCS activity at low reactant concentrations. Conditions were the same as those used in Fig. 4A. The concentration of the monovalent cations is as indicated for (◆) KCl, (■) NaCl, (▲) LiCl and (●) CsCl. Inset shows the effect of Mg^{2+} on HCS activity at (◆) low (0.031 mM) and (■) high (0.5 mM) AcCoA concentration. Curves are drawn by eye.

charge to mass ratio. The cations with more positive charge density show greater inhibitory effects on HCS activity.

4-4. Discussion

4-4-1. Inhibition by lysine

An ordered kinetic mechanism has been proposed for the HCS from *Saccharomyces cerevisiae* (*14*). As a result of the observation of an E:AcCoA complex, a possibility was raised that the HCS kinetic mechanism could be steady state random, and this will be addressed below under the Na^+ effect. The data in Fig. 4-1, can thus be interpreted in terms of the enzyme forms along the reaction pathway in an ordered mechanism. The data in Fig. 4-2 indicate that there is no effect of lysine on the intercept of the slope and intercept replots. The intercept of the slope replot represents the E:α-Kg form of the enzyme, while the intercept of the intercept replot represents whatever enzyme form or forms build up in the steady state with substrates at saturating concentration. The slopes of both replots, on the other hand represent free enzyme, and both reflect the inhibition by lysine. Thus, lysine binds to free enzyme to cause inhibition.

The overall rate equation for lysine inhibition (up to 5 mM) is given by eq 4, where ν and V are initial and maximum rates, the terms representing free enzyme, $K_{ia}K'_b$ and K'_a**B** (representing free enzyme under the conditions of the assay) are multiplied by (1 + **Lys**/$K_{i\ lys}$), where **A** and **B** are α-Kg and AcCoA, and K_{ia}, K'_a and K'_b are $K_{i\ \alpha\text{-Kg}}$, $K_{\alpha\text{-Kg}}$ and K_{AcCoA}, respectively. **Lys** is the concentration of lysine and $K_{i\ lys}$ is the dissociation constant for the E′lysine complex.

$$v = \frac{\mathrm{V}\mathbf{AB}}{\left(K_{\mathrm{ia}}K'_{\mathrm{b}} + K'_{\mathrm{a}}\mathbf{B}\right)\left(1 + \frac{\mathbf{Lys}}{K_{\mathrm{i\,lys}}}\right) + K'_{\mathrm{b}}\mathbf{A} + \mathbf{AB}} \qquad (4)$$

A fit of the all data in Fig. 4-1 to eq 4 gives kinetic parameters that are identical to those reported previously and a $K_{\mathrm{i\,lys}}$ for the E′lysine complex of 550 μM.

Lysine binding to HCS was also measured by fluorescence titration, but a difference is obtained in the magnitude of $K_{\mathrm{i\,lys}}$, with a value of 550 μM from kinetic studies, Table 4-1, and values of 40 μM and 255 mM from fluorescence titration, Table 4-2. The value of 255 mM likely reflects a nonspecific binding of some sort. The value of 40 μM reflects binding to a site with high affinity, but it is an order of magnitude lower than the value obtained from steady state kinetic studies. Quenching of HCS intrinsic tryptophan fluorescence by KI, CsCl and acrylamide exhibits downward curved Stern-Volmer plots consistent with at least two different environments for the single tryptophan in the HCS (*13*). If lysine binds to only one of the conformers, a difference in the $K_{\mathrm{i\,lys}}$ obtained from steady state studies and the K_{d} from fluorescence titration would be observed. Thus, the apparent competition between lysine and α-Kg likely arises from the two ligands binding with high affinity to the two different conformers of the enzyme with lysine stabilizing the inactive or less active form and α-Kg stabilizing the more active form. As a result $K_{\mathrm{i\,lys}}$, reflects the E′Lys complex.

The inhibition by lysine of the HCS from *P. chrysogenum* was reported to be partial (*11*). However, the inhibition of the HCS from *S. cerevisiae* by lysine appears

to be linear up to a concentration of 5 mM. The competitive inhibition by lysine vs α-Kg (at low concentration) is consistent with active site and not allosteric inhibition. However, there are several lines of evidence that argue against active site combination: 1) Mutant forms of HCS have been isolated that are insensitive to lysine feedback inhibition but are quite active (*16*); 2) α-Ketoglutarate is an α-ketodicarboxylic acid, while lysine is an α,ε-diamino acid, and their structures are inconsistent with direct competition for the same site; 3) The presence of lysine has no significant effect on the K_d for E:α-Kg consistent with an allosteric binding site for lysine.

4-4-2. The Na^+ effect

As for lysine inhibition, the effect of Na^+ is only observed on the secondary replots of slope and intercept vs α-Kg. Thus, as for lysine, the Na^+ effect is observed as a result of binding to free enzyme. Unlike the effect of lysine, however, the effect of Na^+ differs dependent on the concentration of AcCoA. When AcCoA is high, Na^+ is an activator, Fig. 4-3B, giving an overall activation of about 4-fold with a K_{act} of 12 mM. At low AcCoA, the effect of Na^+ is more complex. It is still an activator at low concentrations, but is a linear inhibitor at higher concentrations with a $K_{i\ Na}$ of 37 mM (from graphical analysis). At low AcCoA, the predominant form of the enzyme is E, but as its concentration approaches and exceeds the K_d for E:AcCoA (450 μM), E:AcCoA will predominate. The tertiary plot shown in Fig. 4-3B represents the limit where AcCoA is increased to infinite concentration and α-Kg is near zero

concentration. As a result all of the enzyme should be in the E:AcCoA form. Thus, inhibition likely occurs as a result of Na^+ binding to the AcCoA site, while activation occurs in the free enzyme form, likely as a result of binding to a site other than the active site. We suggest the combination is not to the active site as a result of the dianionic nature of α-Kg which apparently competes with Na^+ (the Na^+ effect is eliminated at saturating α-Kg).

The above discussion assumes the presence of an E:AcCoA complex. To probe the kinetic significance of the E:AcCoA complex, an initial velocity pattern was carried out with AcCoA varied over a wider range (12.5 μM to 2 mM) compared to that used in the previous study (12.5 μM to 125 μM) (*14*). The initial velocity pattern is shown in Fig. 4-8, and indicates competitive substrate inhibition by AcCoA vs α-Kg. Data thus indicate an ordered mechanism with formation of a dead-end E:AcCoA complex. Thus, α-Kg can not bind to E:AcCoA to give a productive E:AcCoA:α-Kg complex. The K_{Ib} for substrate inhibition by AcCoA is 0.93 ± 0.16 mM, similar to the value of about 0.45 mM obtained from fluorescence titration (*14*), especially given the standard error on K_{Ib}. An equation derived based on the above logic and Scheme 4-1 is given in eq 5, which includes Na^+ inhibition.

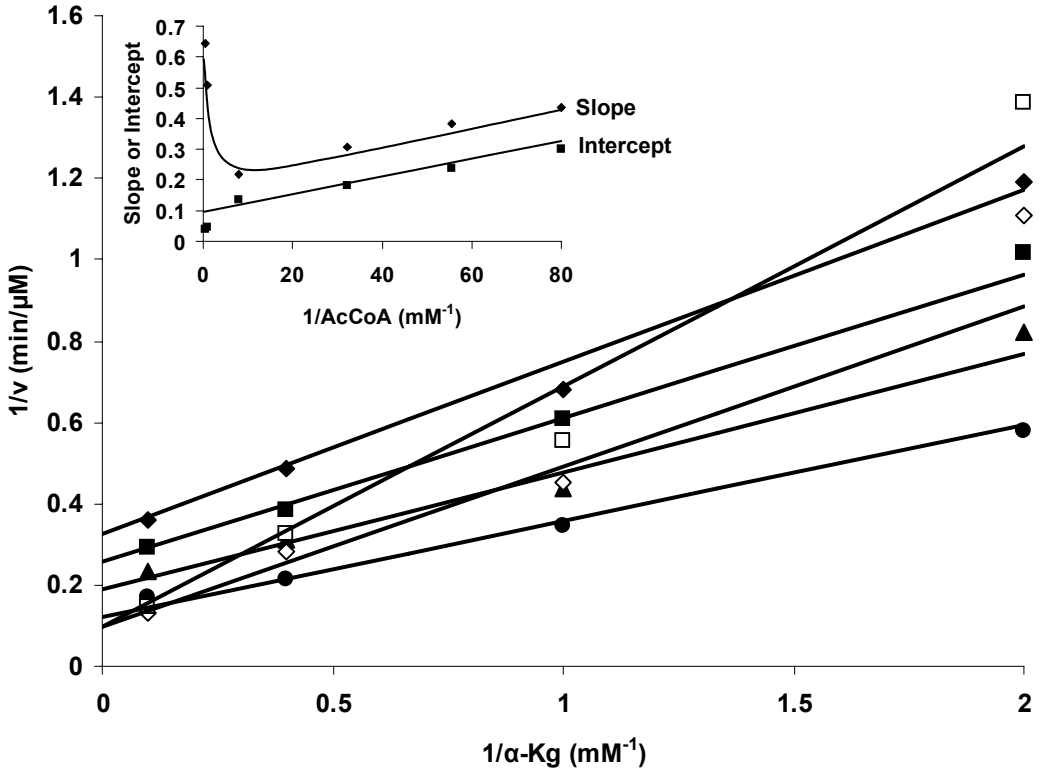

Fig. 4-8: Initial velocity pattern for HCS suggesting a competitive substrate inhibition by AcCoA. The concentration of AcCoA is as indicated for (◆) 0.0125 mM, (■) 0.018 mM, (▲) 0.031 mM, (●) 0.125 mM, (◊) 1 mM, and (□) 2 mM. Slope (low α-Kg) and intercept (high α-Kg) replots are shown in inset representing a substrate inhibition by AcCoA at low α-Kg. Points are experimental, while the solid curves are theoretical based on a fit of the data to $\nu = \dfrac{\mathbf{VAB}}{\left(K_{ia}K'_b + K'_a\mathbf{B}\right)\left(1+\dfrac{\mathbf{B}}{K_{Ib}}\right) + K'_b\mathbf{A} + \mathbf{AB}}$.

$$\nu = \frac{\mathrm{V}\left(1+\dfrac{\mathbf{Na}}{K_{act}}\right)\mathbf{AB}}{K_{ia}K'_b\left[\left(1+K_{conf}\right)+\left(1+K'_{conf}\right)\left(\dfrac{\mathbf{Na}}{K_{act}}\right)+\left(1+\dfrac{\mathbf{Na}}{K_{act}}\right)\left(\dfrac{\mathbf{Na}}{K_{i\,Na}}\right)\right] + K'_a\left[\left(1+K_{conf}\right)+\left(1+K'_{conf}\right)\left(\dfrac{\mathbf{Na}}{K_{act}}\right)\right]\mathbf{B} + \left(K'_b\mathbf{A}+\mathbf{AB}\right)\left(1+\dfrac{\mathbf{Na}}{K_{act}}\right)} \quad (5)$$

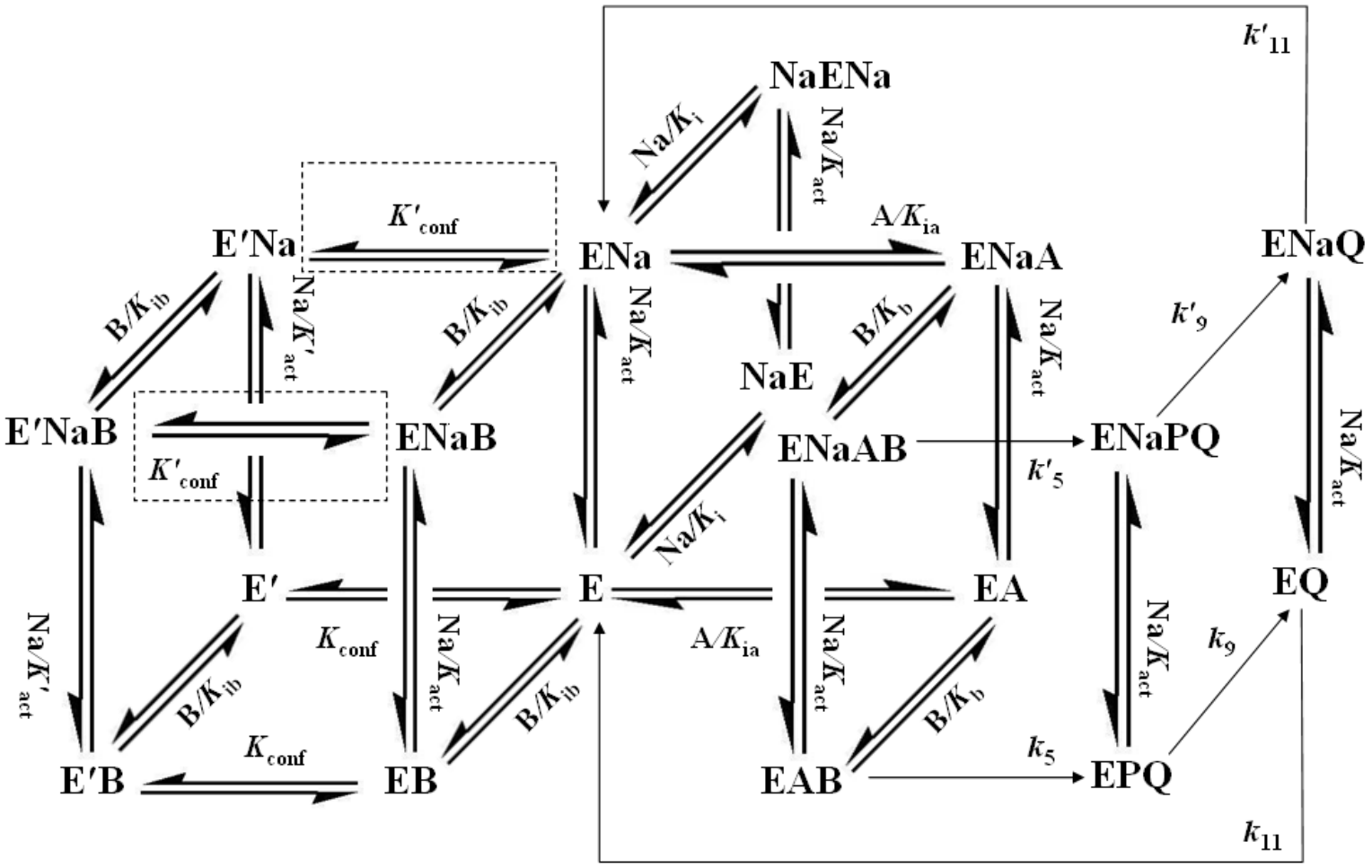

Scheme 4-1: Kinetic mechanism for activation and inhibition by Na^+. A, B, P, Q, Na, E, and E′ represent α-Kg, AcCoA, CoA, Hc, Na^+, active and less active forms of the enzyme, respectively. K_{conf} and K'_{conf} are the equilibrium constant between the free active and less active and Na^+-bound active and less active forms of the enzyme. K_{act} and K'_{act} are the activation constants of the Na^+ for active and less active forms of the enzyme. K_i is the inhibition constant for Na^+ ($K_{i\ Na}$). K_{ia} and K_{ib} are inhibition constants for α-Kg ($K_{i\ \alpha\text{-Kg}}$) and AcCoA ($K_{i\ AcCoA}$), respectively. The dotted box represents the equilibrium between sodium-bound E and E′ forms (either free or B-bound) of the enzyme. The value of K'_{conf} is kinetically zero (see text); however, it was considered for deriving the general equation for the Scheme (see chapter 5).

In eq 5, **A**, **B**, and **Na** are α-Kg, AcCoA, and Na^+ concentration, respectively, while K_{ia}, K'_a, K'_b, $K_{i\ Na}$ and K_{act} are the dissociation constant for α-Kg, the Michaelis constants for α-Kg and AcCoA, the inhibition and activation constants for Na^+, respectively. K_{conf} and K'_{conf} are equilibrium constants for the conformation change in E in the absence and presence of Na^+, respectively, which is E′/E, where E′ is the less active form. Equation 5, as written, did not give reasonable estimates of the kinetic parameters, unless K'_{conf} was set equal to zero. It thus appears that E′Na and ENa interconversion (Scheme 4-1) is very slow relative to enzymatic activity time scale (K'_{conf} can still be considered as equal to K_{conf}). Although a thermodynamically balanced model requires that $K_{conf} = K'_{conf} = 3$, the value of K'_{conf} is considered zero due to a slow interconversion. Therefore, from the point of view of the kinetic time scale, Na^+ does not bind to the inactive or less active form of the enzyme.

4-4-3. Interaction of Na^+ and lysine

Data obtained varying the concentrations of Na^+ and lysine indicate that Na^+ activates the HCS at any lysine concentration; therefore, Na^+ can bind to the E′Lys complex (see above) to form E′LysNa. The K_{act} values for Na^+ for both E and E′Lys (low AcCoA) are identical within error (Table 4-1). Equation 6 can be used to describe the enzymatic behavior of HCS in the presence of both Na^+ and lysine as represented in Scheme 4-2 with the assumption that $K'_{conf} = 0$ and $K_{conf} = 3$ (see above). A fit of the data to eq 6 shows that $K_{act} = K''_{act}$ at either low or high AcCoA (Table 4-1) indicating that Na^+ binds with equal affinity in the absence or presence of lysine (as

represented by K_{act} and K''_{act}) to the E and E′ forms of the enzyme. As suggested in Scheme 4-2, there is no evidence that lysine can bind to the E (active form) form of the enzyme.

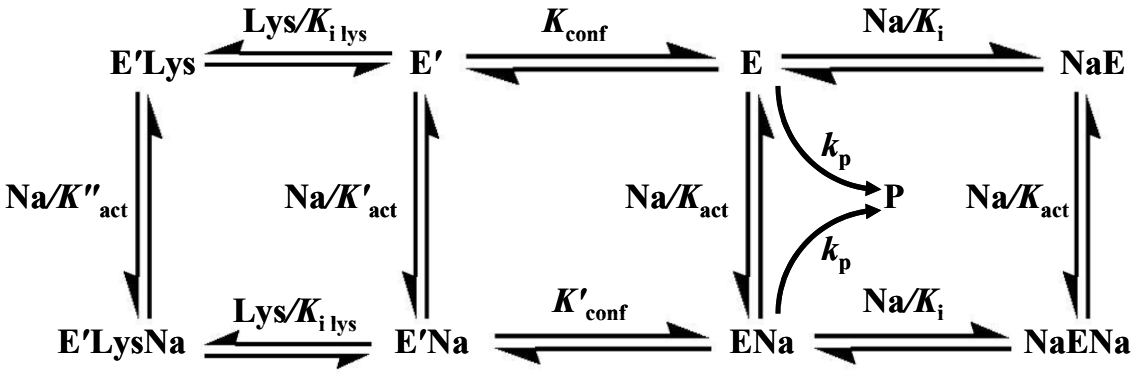

Scheme 4-2: Kinetic mechanism for interactive Na^+ and lysine effects. Na, E, and E′ represent Na^+, active, and less active forms of the enzyme, respectively. K_{conf} and K'_{conf} are the equilibrium constant between the free active and less active and Na^+-bound active and less active forms of the enzyme. K_{act}, K'_{act} and K''_{act} are the activation constants of the Na^+ for active and less active and lysine-bound less active forms of the enzyme. $K_{i\ lys}$ is the inhibition constant for lysine.

$$v = \frac{k_p\left(1+\frac{\mathbf{Na}}{K_{act}}\right)}{1+K_{conf}\left[1+\left(1+\frac{\mathbf{Na}}{K''_{act}}\right)\left(\frac{\mathbf{Lys}}{K_{i\ lys}}\right)\right]+\left(1+K'_{conf}\right)\left(\frac{\mathbf{Na}}{K_{act}}\right)+\left(1+\frac{\mathbf{Na}}{K_{act}}\right)\left(\frac{\mathbf{Na}}{K_{i\ Na}}\right)} \quad (6)$$

In eq 6, **Na**, **Lys**, $K_{i\ Na}$ and $K_{i\ lys}$ are the concentrations of Na^+ and lysine, and inhibition constants for Na^+ bound to E and lysine bound to E′, respectively. K_{act} and K''_{act} are the activation constant for Na^+ for the active and lysine-bound less active forms of the enzymes. k_p is the overall enzymatic rate in the absence of inhibitor and

activators. As shown in Table 4-1, the presence of lysine does not significantly change the values of kinetic parameters (K_{act} and $K_{i\ Na}$) for Na^+ at low AcCoA. The presence of high AcCoA increases the values of kinetic parameters by a factor of 2–5 consistent with the second substrate forcing the enzyme into the E:AcCoA form, which is apparently less active as compared to E. Thus, Na and or α-Kg are required to generate the E form of the enzyme. Simulations carried out in the accompanying article (*24*) using eq 6, provide more detailed information concerning the behavior of HCS in the presence of both lysine and Na^+. The overall regulation of HCS by Na^+ and lysine is illustratively shown in Fig. A-17 (see Appendix).

4-4-4. Effect of other monovalent cations and divalent cations on HCS activity

In general the mode of action of monovalent cations on enzyme activity is poorly defined. Two types of mechanism have been proposed to explain the effects of metal ion on catalytic activity (*17–18*). In the first mechanism, metal ion has a static structural role that activates the enzyme by stabilizing the catalytically active conformation of the enzyme. The second mechanism proposes a dynamic role for the metal ion that selectively assists the enzyme in specific conformational transitions essential to catalysis. Both mechanisms could be involved in the activation of HCS by cations with the first mechanism being more likely, but this aspect will require additional study.

4-4-5. Physiologic significance

The measured intracellular concentrations of α-Kg, AcCoA, lysine and Na^+ plus K^+ are 3, 0.3, 5 and 150 mM, respectively (*19–23*). On this basis, it appears that HCS is inhibited by lysine under physiological conditions. On the basis of the value for $K_{i\ lys}$ and the concentration of lysine inside the cell, the fraction of active HCS is almost 10% of the total enzyme and the enzyme is present as the E′Lys complex. Saturating levels (for HCS) of AcCoA in the cell diminish the inhibitory effects of Na^+ while maintaining its activatory effect. As shown in Fig. 4-3B, the increase in activity by Na^+ at high AcCoA is almost 3–4 fold. Therefore, the net active enzyme is equivalent to about 40%. However, as shown in Table 4-1, the physiological concentration of monovalent cations (150 mM) is the same as its $K_{i\ Na}$ value at high AcCoA giving an almost 50% decrease in HCS activity. Therefore, the net activity of HCS is 20%. It has been reported that variation in the α-Kg pool is responsible for changing flux through the lysine pathway (*23*). Since the concentration of α-Kg is around its K_m, it is the main determinant for the flux through the lysine biosynthetic pathway (*23*). The kinetic data reported in this study are consistent with this hypothesis. Although, variation in the concentrations of AcCoA and lysine are important to the flux through HCS, the reported data (*20*) generally indicate that variations in the concentrations of AcCoA and lysine (with respect to their kinetic parameters) are negligible for the HCS suggesting no significant effects on HCS activity by these modulators. Therefore, choosing strains containing HCS mutants insensitive to lysine inhibition are one of the several options required to increase the production of lysine at a commercial level.

Also, in the area of enzyme inhibitor design, theoretically, the most efficient inhibitors for HCS under physiological conditions, would be those that bind with high affinity to the α-Kg binding site.

4-5. Acknowledgements

We thank Dr. W. E. Karsten for his insightful discussion of the results. We also thank Dr. Corey M. Johnson for technical assistance on data analysis.

References

[1] Johansson, E., Steffens, J. J., Lindqvist, Y., and Schneider, G. (2000) Crystal structure of Saccharopine reductase from *Magnaporthe grisea*, an enzyme of the α-aminoadipate pathway of lysine biosynthesis, *Structure 8*, 1037-1047.

[2] Bhattacharjee, J. K. (1992) Evolution of α-aminoadipate pathway for the synthesis of lysine in fungi, in *Evolution of Metabolic Function* (Mortlock, R. P., Ed.), pp 47-80, CRC Press, Boca Raton.

[3] Bhattacharjee, J. K. (1985) α-aminoadipate pathway for the biosynthesis of lysine in lower eukaryotes, *Crit. Rev. Microbiol. 12*, 131-151.

[4] Umbarger, H. E. (1987) Amino acid biosynthesis and its regulation, *Annu. Rev. Biochem. 47*, 532-606.

[5] Vogel, H. J. (1960) Two modes of lysine synthesis among lower fungi: evolutionary significance, *Biochim. Biophys. Acta 41*, 172-173.

[6] Zabriskie, T. M. and Jackson, M. D. (2000) Lysine biosynthesis and metabolism in fungi, *Nat. Prod. Rep. 17*, 85-97.

[7] Ramos, F., Verhasselt, P., Feller, A., Peeters, P., Wach, A., Dubois, E., and Volckaert, G. (1996) Identification of a gene encoding a homocitrate synthase isoenzyme of *Saccharomyces cerevisiae*, *Yeast 12*, 1315-1320.

[8] Chen, S., Brockenbrough, J. S., Dove, J. E. and Aris, J. P. (1997) Homocitrate synthase is located in the nucleus in the yeast *Saccharomyces cerevisiae*, *J. Biol. Chem. 272*, 10839-10846.

[9] Gaillardin, G. M., Poirier, L. and Heslot, H. (1976) A kinetic study of homocitrate synthase activity in the yeast *Saccharomycopsis lipolytica*, *Biochim. Biophys. Acta 422*, 390-406.

[10] Jaklitsch W. M., and Kubicek, C. P. (1990) Homocitrate synthase from *Penicillium chrysogenum*, localization, purification of the cytosolic isoenzyme, and sensitivity to lysine, *Biochem. J. 269*, 247-253.

[11] Wulandari, A. P., Miyazaki, J., Kobashi, N., Nishiyama, M., Hoshino T., and Yamane, H. (2002) Characterization of bacterial homocitrate synthase involved in lysine biosynthesis, *FEBS Letters 522*, 35-40.

[12] Tracy, J., and Kohlhaw, G. (1975) Reversible, coenzyme-A-mediated inactivation of biosynthesis condensing enzymes in yeast: A possible regulatory mechanism, *Proc. Natl. Acad. Sci. USA 72*, 1802-1805.

[13] Andi, B., West, A. H., and Cook, P. F. (2004) Stabilization and characterization of histidine-tagged homocitrate synthase from *Saccharomyces cerevisiae*, *Arch. Biochem. Biophys. 421*, 243-254.

[14] Andi, B., West, A. H., and Cook, P. F. (2004) Kinetic mechanism of histidine-tagged homocitrate synthase from *Saccharomyces cerevisiae*, *Biochemistry 43*, 11790-11795.

[15] Cook, P. F. (1982) Kinetic studies to determine the mechanism of regulation of bovine liver glutamate dehydrogenase by nucleotide effectors, *Biochemistry 21*, 113-116.

[16] Feller, A., Ramos, F., Piérard, A., and Dubois, E. (1999) In *Saccharomyces cerevisiae*, feedback inhibition of homocitrate synthase isoenzymes by lysine modulates the activation of *LYS* gene expression by Lys14p, *Eur. J. Biochem. 261*, 163-170.

[17] Woehl, E. U., and Dunn, M. F. (1995) The roles of Na^+ and K^+ in pyridoxal phosphate enzyme catalysis, *Coord. Chem. Rev. 144*, 147-197.

[18] Liu, W., and Toney, M. D. (2004) Kinetic and thermodynamic analysis of the interaction of cations with dialkylglycine decarboxylase, *Biochemistry 43*, 4998-5010.

[19] Hans, M. A., Heinzle, E. and Wittmann, C. (2001) Quantification of intracellular amino acids in batch cultures of *Saccharomyces cerevisiae*, *Appl. Microbiol. Biotechnol. 56*, 776-779.

[20] Giuseppin, M. L. F. (2000) Metabolic modeling of *Saccharomyces cerevisiae* using the optimal control of homeostasis: A cybernetic model definition, *Metabolic Engineering 2*, 14-33.

[21] Hans, M. A., Heinzle, E. and Wittmann, C. (2003) Free intracellular amino acid pools during autonomous oscillations in *Saccharomyces cerevisiae*, *Biotechnology and Bioengineering 82*, 143-151.

[22] Ter Schure, E. G., Sillje, H. H. W., Verkleij, A. J., Boonstra, J. and Verrips, C. T. (1995) The concentration of ammonia regulates nitrogen metabolism in *Saccharomyces cerevisiae*, *Journal of Bacteriology 177*, 6672-6675.

[23] Feller, A., Ramos, F., Pierard, A. and Dubois, E. (1997) Lys80p of *Saccharomyces cerevisiae*, previously proposed as a specific repressor of LYS genes, is a pleiotropic regulatory factor identical to Mks1p, *Yeast 13*, 1337-1346.

[24] Andi, B., and Cook, P. F. (2005) Regulatory mechanism of histidine-tagged homocitrate synthase from *Saccharomyces cerevisiae*: II. THEORY, *J. Biol. Chem. 280*, 31633-31640.

CHAPTER 5

Regulatory mechanism of homocitrate synthase: II. THEORY

"Reproduced with automatic permission from [Andi, B., and Cook, P. F. (2005) Regulatory Mechanism of Histidine-tagged Homocitrate Synthase from *Saccharomyces cerevisiae* I. THEORY, *J. Biol. Chem. 280*, 31633-31640] Copyright [2005] The American Society for Biochemistry and Molecular Biology, Inc."

5-1. Introduction

Homocitrate synthase (HCS) [2-hydroxybutane-1,2,4-tricarboxylate 2-oxoglutarate-lyase (CoA-acetylating), EC 2.3.3.14] catalyzes the first and committed reaction in the α-aminoadipate pathway for the biosynthesis of lysine that is unique to higher fungi (*1–4*). Both cytosolic and mitochondrial isozymes of the HCS from *Saccharomyces cerevisiae* are feedback inhibited by lysine (*5*). It has also been reported that HCS activity can be affected by the presence of CoA and divalent metal ions (*6*).

In this paper, rate equations are derived to predict the regulatory effects of Na^+ and lysine on the activity of HCS, on the basis of experimental data presented in the accompanying article (*11*). Rate equations were derived using the King-Altman algorithm method (*7*) and Cha's rapid equilibrium assumption (*8*). The simulated data correlate well within error, with the experimental data and suggest that the activity of the HCS in the presence of Na^+ is simultaneously inhibited and activated. In the presence of lysine and Na^+, the kinetic behavior of HCS is complex, and the Na^+ effect is independent of lysine.

5-2. Materials and methods

5-2-1. Data analysis and simulation

Kinetic parameters used for simulation of kinetic behavior were obtained by fitting the experimental data presented in the previous article (*11*) using the appropriate rate equations and the Marquardt-Levenberg algorithm supplied with the EnzFitter program from BIOSOFT, Cambridge, UK (www.biosoft.com). All of the simulations were carried out using the appropriate derived equation and *MATHEMATICA* version 5.0.1.0 from Wolfram Research, Inc., IL, USA (www.wolfram.com).

5-3. Theory

On the basis of the experimental data presented in the accompanying article (*11*), a schematic of the regulatory kinetic mechanism of the HCS by Na^+ is shown in Scheme 5-1. The model is general in that it allows for binding of effector to all enzyme forms. As previously described a conformational equilibrium exists for HCS in the absence of reactants (*9*). The activation, affected by the cations, can be explained by stabilizing the E (active) form of HCS. In the case of HCS, Scheme 5-1 is reduced to a consideration of effector stabilizing only the E form, with no effect observed as reactants bind (see accompanying article (*11*)). The active form of the free enzyme is also subject to inhibition by the same effector that activates the enzyme. This phenomenon is separate from activation.

In deriving the equation, all steps for binding of Na^+ and the enzyme conformational change were assumed to be at equilibrium as shown in Scheme 5-1 and the mechanism is simplified as at the bottom of Scheme 1 (*8*). The simplified scheme was then used to derive the rate equation by the King-Altman method (*7*).

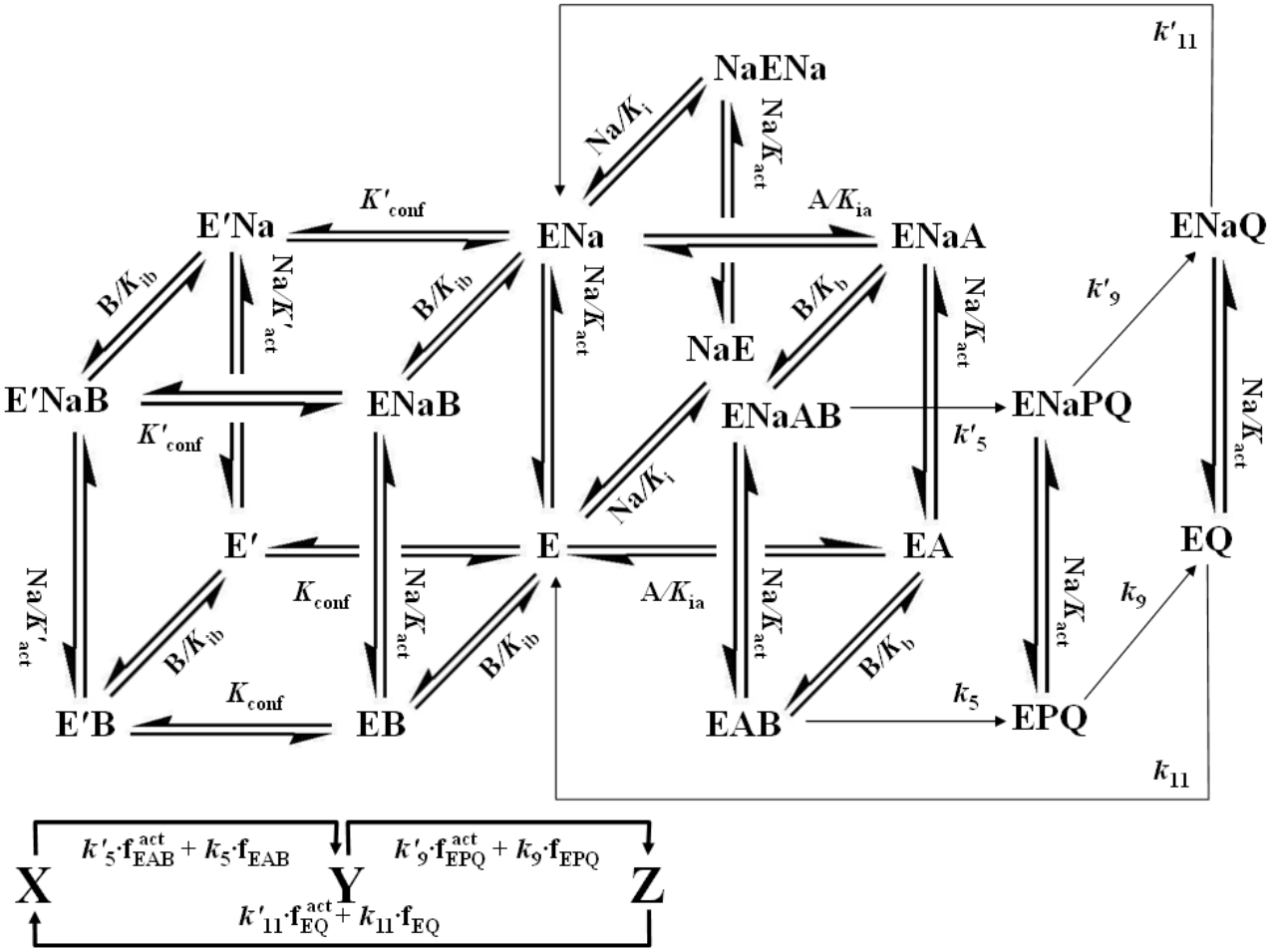

Scheme 5-1: (Top) Kinetic mechanism for activation by Na^+. A, B, P, Q, Na, E, and E′ represent α-Kg, AcCoA, CoA, Hc, Na^+, active, and less active forms of the enzyme, respectively. K_{conf} is the equilibrium constant between free enzyme in active and less active forms, while K'_{conf} is the same conformational equilibrium in the presence of Na^+. K_{act} and K'_{act} are the activation constants for Na^+ for active and less active conformers. (Bottom) Simplification of the Na^+ activation model using Cha's equilibrium assumption (*8*). According to the King-Altman algorithm (*7*), the simplified model contains three major enzyme-containing species represented as X, Y, and Z. Each major species of the enzyme contains other enzyme sub species in equilibrium. In the simplified model, f_J (J: enzyme forms) is the fraction of each enzyme form that contribute to the overall catalytic rate of the next major enzyme species.

The fractions of productive enzyme, *i.e.*, enzyme forms that go on to give product, at equilibrium within X are given as follows. Productive enzyme fractions are defined as $f_{EAB} = \frac{E\mathbf{AB}}{X}$ and $f_{EAB}^{act} = \frac{E\mathbf{NaAB}}{X}$, where

$$X = E + ENa + E' + E'Na + EA + ENaA + EB + E'B + ENaB + E'NaB + EAB + ENaAB + NaE + NaENa \quad (1)$$

Equilibrium dissociation constant can be written for each step and can be used to solve for the concentration of species in X in terms of effector concentration, dissociation constant and the concentration of E. Thus, $E\mathbf{Na} = E\left(\frac{\mathbf{Na}}{K_{act}}\right)$,

$E' = E(K_{conf})$, $E'\mathbf{Na} = E\left(\frac{\mathbf{Na}}{K_{act}}\right)(K'_{conf})$, $E\mathbf{A} = E\left(\frac{\mathbf{A}}{K_{ia}}\right)$, $E\mathbf{NaA} = E\left(\frac{\mathbf{Na}}{K_{act}}\right)\left(\frac{\mathbf{A}}{K_{ia}}\right)$,

$E\mathbf{B} = E\left(\frac{\mathbf{B}}{K_{ib}}\right)$, $E'\mathbf{B} = E\left(\frac{\mathbf{B}}{K_{ib}}\right)(K_{conf})$, $E\mathbf{NaB} = E\left(\frac{\mathbf{Na}}{K_{act}}\right)\left(\frac{\mathbf{B}}{K_{ib}}\right)$,

$E'\mathbf{NaB} = E\left(\frac{\mathbf{Na}}{K_{act}}\right)\left(\frac{\mathbf{B}}{K_{ib}}\right)(K'_{conf})$, $E\mathbf{AB} = E\left(\frac{\mathbf{A}}{K_{ia}}\right)\left(\frac{\mathbf{B}}{K_{b}}\right)$,

$E\mathbf{NaAB} = E\left(\frac{\mathbf{Na}}{K_{act}}\right)\left(\frac{\mathbf{A}}{K_{ia}}\right)\left(\frac{\mathbf{B}}{K_{ib}}\right)$, $\mathbf{Na}E = E\left(\frac{\mathbf{Na}}{K_{i}}\right)$, $\mathbf{Na}E\mathbf{Na} = E\left(\frac{\mathbf{Na}}{K_{act}}\right)\left(\frac{\mathbf{Na}}{K_{i}}\right)$. f_{EAB} is given below:

$$f_{EAB} = \frac{\mathbf{EAB}}{\begin{aligned} &E + E\mathbf{A} + E\mathbf{Na}\mathbf{A} + E\mathbf{B} + E\mathbf{Na}\mathbf{B} + E\mathbf{AB} + E\mathbf{Na}\mathbf{AB} + E' + E'\mathbf{B} + E'\mathbf{Na} + E'\mathbf{Na}\mathbf{B} \\ &+ E\mathbf{Na} + \mathbf{Na}E\mathbf{Na} + \mathbf{Na}E \end{aligned}}$$

(2)

Substitution for each of the enzyme forms in eq 2 with the parameters defined above gives eq 3.

$$f_{EAB} = \frac{\mathbf{AB}}{\begin{aligned} &K_{ia}K_b + \left[K_b\mathbf{A} + K_{ia}K_b\left(\frac{\mathbf{B}}{K_{ib}}\right) + \mathbf{AB}\right]\left(1 + \frac{\mathbf{Na}}{K_{act}}\right) + K_{ia}K_b\left(1 + \frac{\mathbf{B}}{K_{ib}}\right)\left[K_{conf} + K'_{conf}\left(\frac{\mathbf{Na}}{K_{act}}\right)\right] \\ &+ K_{ia}K_b\left(1 + \frac{\mathbf{Na}}{K_{act}}\right)\left(\frac{\mathbf{Na}}{K_i}\right) + K_{ia}K_b\left(\frac{\mathbf{Na}}{K_{act}}\right) \end{aligned}}$$

(3)

Eq 3 can be rearranged as shown in eq 4.

$$f_{EAB} = \frac{\mathbf{AB}}{\begin{aligned} &K_{ia}K_b\left[\left(1 + K_{conf}\right) + \left(1 + K'_{conf}\right)\left(\frac{\mathbf{Na}}{K_{act}}\right) + \left(1 + \frac{\mathbf{Na}}{K_{act}}\right)\left(\frac{\mathbf{Na}}{K_i}\right)\right] \\ &+ K_{ia}\left(\frac{K_b}{K_{ib}}\right)\left[\left(1 + K_{conf}\right) + \left(1 + K'_{conf}\right)\left(\frac{\mathbf{Na}}{K_{act}}\right)\right]\mathbf{B} \\ &+ \left(K_b\mathbf{A} + \mathbf{AB}\right)\left(1 + \frac{\mathbf{Na}}{K_{act}}\right) \end{aligned}} \qquad (4)$$

$$f^{act}_{EAB} = f_{EAB}\left(\frac{\mathbf{Na}}{K_{act}}\right) \qquad (5)$$

All of the other fractions (f_J) can be defined in the same way for Y and Z, Scheme 5-1. Therefore, the ENaPQ to EPQ and ENaQ to EQ equilibria are included in Y and Z, respectively. However, as long as the affinity for effector is independent of bound reactants, $f_{EQ} = f_{EPQ} = \left(\frac{1}{\left(1 + \frac{\mathbf{Na}}{K_{act}}\right)} \right)$ and $f_{EQ}^{act} = f_{EPQ}^{act} = \left(\frac{\left(\frac{\mathbf{Na}}{K_{act}}\right)}{\left(1 + \frac{\mathbf{Na}}{K_{act}}\right)} \right)$. The expression for E_t (total enzyme) is equal to the sum of all enzyme forms, *i. e.* X, Y and Z, and this gives the denominator of the final rate equation. X, Y, Z and v (the initial rate) can be defined as follows, where Δ is the sum of all of the numerator terms in X, Y and Z.

$$\frac{X}{E_t} = \frac{\left(k_9' f_{EPQ}^{act} + k_9 f_{EPQ}\right)\left(k_{11}' f_{EQ}^{act} + k_{11} f_{EQ}\right)}{\Delta} = \frac{\left[k_9'\left(\frac{\mathbf{Na}}{K_{act}}\right) + k_9\right]\left[k_{11}'\left(\frac{\mathbf{Na}}{K_{act}}\right) + k_{11}\right]\left(\frac{1}{\left(1 + \frac{\mathbf{Na}}{K_{act}}\right)^2}\right)}{\Delta} \quad (6)$$

$$\frac{Y}{E_t} = \frac{\left(k_5' f_{EAB}^{act} + k_5 f_{EAB}\right)\left(k_{11}' f_{EQ}^{act} + k_{11} f_{EQ}\right)}{\Delta} = \frac{\left[k_5'\left(\frac{\mathbf{Na}}{K_{act}}\right) + k_5\right]\left[k_{11}'\left(\frac{\mathbf{Na}}{K_{act}}\right) + k_{11}\right]\left(\frac{1}{\left(1 + \frac{\mathbf{Na}}{K_{act}}\right)}\right)(f_{EAB})}{\Delta} \quad (7)$$

$$\frac{Z}{E_t} = \frac{\left(k_5' f_{EAB}^{act} + k_5 f_{EAB}\right)\left(k_9' f_{EPQ}^{act} + k_9 f_{EPQ}\right)}{\Delta} = \frac{\left[k_5'\left(\frac{\mathbf{Na}}{K_{act}}\right) + k_5\right]\left[k_9'\left(\frac{\mathbf{Na}}{K_{act}}\right) + k_9\right]\left(\frac{1}{\left(1+\frac{\mathbf{Na}}{K_{act}}\right)}\right)(f_{EAB})}{\Delta} \quad (8)$$

$$v = \left(k_{11}' f_{EQ}^{act} + k_{11} f_{EQ}\right)Z = \frac{\left(k_5' f_{EAB}^{act} + k_5 f_{EAB}\right)\left(k_9' f_{EPQ}^{act} + k_9 f_{EPQ}\right)\left(k_{11}' f_{EQ}^{act} + k_{11} f_{EQ}\right)E_t}{\Delta} =$$

$$\frac{\left[k_5'\left(\frac{\mathbf{Na}}{K_{act}}\right) + k_5\right]\left[k_9'\left(\frac{\mathbf{Na}}{K_{act}}\right) + k_9\right]\left[k_{11}'\left(\frac{\mathbf{Na}}{K_{act}}\right) + k_{11}\right]\left(\frac{1}{\left(1+\frac{\mathbf{Na}}{K_{act}}\right)^2}\right)(f_{EAB})E_t}{\Delta} \quad (9)$$

Substitution of the expression for Δ in eq 9 gives

$$v = \frac{\left[k_5'\left(\frac{\mathbf{Na}}{K_{act}}\right) + k_5\right]\left[k_9'\left(\frac{\mathbf{Na}}{K_{act}}\right) + k_9\right]\left[k_{11}'\left(\frac{\mathbf{Na}}{K_{act}}\right) + k_{11}\right]E_t}{\frac{\left[k_9'\left(\frac{\mathbf{Na}}{K_{act}}\right) + k_9\right]\left[k_{11}'\left(\frac{\mathbf{Na}}{K_{act}}\right) + k_{11}\right]}{f_{EAB}} + \left[\left[k_5'\left(\frac{\mathbf{Na}}{K_{act}}\right) + k_5\right]\left[k_9'\left(\frac{\mathbf{Na}}{K_{act}}\right) + k_9\right] + \left[k_5'\left(\frac{\mathbf{Na}}{K_{act}}\right) + k_5\right]\left[k_{11}'\left(\frac{\mathbf{Na}}{K_{act}}\right) + k_{11}\right]\right]\left(1+\frac{\mathbf{Na}}{K_{act}}\right)} \quad (10)$$

Substitution of the expression for f_{EAB} into the eq 10 gives

$$\nu = \frac{\left[k_5'\left(\frac{\mathbf{Na}}{K_{act}}\right)+k_5\right]\left[k_9'\left(\frac{\mathbf{Na}}{K_{act}}\right)+k_9\right]\left[k_{11}'\left(\frac{\mathbf{Na}}{K_{act}}\right)+k_{11}\right]\mathbf{AB}E_t}{\left[k_9'\left(\frac{\mathbf{Na}}{K_{act}}\right)+k_9\right]\left[k_{11}'\left(\frac{\mathbf{Na}}{K_{act}}\right)+k_{11}\right]\begin{bmatrix} K_{ia}K_b\left[\begin{matrix}(1+K_{conf})+(1+K'_{conf})\left(\frac{\mathbf{Na}}{K_{act}}\right)\\ +\left(1+\frac{\mathbf{Na}}{K_{act}}\right)\left(\frac{\mathbf{Na}}{K_i}\right)\end{matrix}\right] \\ +K_{ia}\left(\frac{K_b}{K_{ib}}\right)\left[(1+K_{conf})+(1+K'_{conf})\left(\frac{\mathbf{Na}}{K_{act}}\right)\right]\mathbf{B} \\ +(K_b\mathbf{A}+\mathbf{AB})\left(1+\frac{\mathbf{Na}}{K_{act}}\right)\end{bmatrix}} \\ +\left[\left[k_5'\left(\frac{\mathbf{Na}}{K_{act}}\right)+k_5\right]\left[k_9'\left(\frac{\mathbf{Na}}{K_{act}}\right)+k_9\right]+\left[k_5'\left(\frac{\mathbf{Na}}{K_{act}}\right)+k_5\right]\left[k_{11}'\left(\frac{\mathbf{Na}}{K_{act}}\right)+k_{11}\right]\right]\left(1+\frac{\mathbf{Na}}{K_{act}}\right)\mathbf{AB}$$

(11)

In equation 11, if $k_j = k'_j$ (microscopic rate constants for binding and catalytic steps), as is true for Na^+ activation of HCS, then the equation reduces to eq 12 after rearrangement.

$$\nu = \frac{(k_5k_9k_{11})\left(1+\frac{\mathbf{Na}}{K_{act}}\right)\mathbf{AB}E_t}{\begin{matrix}K_{ia}K_b(k_9k_{11})\left[(1+K_{conf})+(1+K'_{conf})\left(\frac{\mathbf{Na}}{K_{act}}\right)+\left(1+\frac{\mathbf{Na}}{K_{act}}\right)\left(\frac{\mathbf{Na}}{K_i}\right)\right] \\ +K_{ia}\left(\frac{K_b}{K_{ib}}\right)(k_9k_{11})\left[(1+K_{conf})+(1+K'_{conf})\left(\frac{\mathbf{Na}}{K_{act}}\right)\right]\mathbf{B}+K_b(k_9k_{11})\left(1+\frac{\mathbf{Na}}{K_{act}}\right)\mathbf{A} \\ +(k_5k_9+k_5k_{11}+k_9k_{11})\mathbf{AB}\left(1+\frac{\mathbf{Na}}{K_{act}}\right)\end{matrix}} \quad (12)$$

The mechanism in the absence of Na^+ is sequential ordered (*10*). Thus, expressions for kinetic parameters can be generated from eq 12 at the limit where **Na** = 0, shown in eq 13.

$$\nu = \frac{(k_5 k_9 k_{11})\mathbf{AB}E_t}{K_{ia}K_b(k_9k_{11})(1+K_{conf}) + K_{ia}\left(\frac{K_b}{K_{ib}}\right)(k_9k_{11})(1+K_{conf})\mathbf{B} + K_b(k_9k_{11})\mathbf{A} + (k_5k_9 + k_5k_{11} + k_9k_{11})\mathbf{AB}} \quad (13)$$

Dividing the numerator and denominator of eq 13 by coefficient **AB** gives eq 14.

$$\nu = \frac{\left(\frac{k_5k_9k_{11}}{k_5k_9 + k_5k_{11} + k_9k_{11}}\right)\mathbf{AB}E_t}{K_{ia}\left(\frac{K_b(k_9k_{11})}{k_5k_9 + k_5k_{11} + k_9k_{11}}\right)(1+K_{conf}) + \left(\frac{K_{ia}\left(\frac{K_b}{K_{ib}}\right)(k_9k_{11})}{k_5k_9 + k_5k_{11} + k_9k_{11}}\right)(1+K_{conf})\mathbf{B} + \left(\frac{K_b(k_9k_{11})}{k_5k_9 + k_5k_{11} + k_9k_{11}}\right)\mathbf{A} + \mathbf{AB}} \quad (14)$$

Thus, $$\frac{\text{Coef } \mathbf{B}}{\text{Coef } \mathbf{AB}} = \left(\frac{K_{ia}\left(\frac{K_b}{K_{ib}}\right)(k_9k_{11})}{k_5k_9 + k_5k_{11} + k_9k_{11}}\right) = K'_a,$$

$\frac{\text{Coef } \mathbf{A}}{\text{Coef } \mathbf{AB}} = \left(\frac{K_b(k_9k_{11})}{k_5k_9 + k_5k_{11} + k_9k_{11}}\right) = K'_b$, where K_b is dissociation constant of AcCoA

for E**AB**, and K_{ia} and K_{ib} are the dissociaton constants of **A** and **B** for E**A** and E**B**, respectively. The limit of eq 14 where **A** and **B** tend to infinity gives V as $\left(\frac{k_5 k_9 k_{11}}{k_5 k_9 + k_5 k_{11} + k_9 k_{11}}\right)\mathrm{E_t}$, while the limit where **A** tends to infinity and **B** tends to zero gives $\left(\frac{\mathrm{V}}{K'_{\mathrm{b}}}\right)\mathbf{B}$, the limit where **B** tends to infinity and **A** tends to zero gives $\left(\frac{\mathrm{V}}{K'_{\mathrm{a}}}\right)\left(\frac{1}{1+K_{\mathrm{conf}}}\right)\mathbf{A}$, and the limit when **A** and **B** tend to zero gives $\left(\frac{\mathrm{V}}{K_{\mathrm{ia}}K'_{\mathrm{b}}}\right)\left(\frac{1}{1+K_{\mathrm{conf}}}\right)\mathbf{AB}$.

Substituting the above kinetic parameters into eqs 14 and 12 gives the eqs 15 and 16, respectively (eq 15 is basically equal to eq 16 with **Na** = 0).

$$\nu = \frac{\mathrm{V}\mathbf{AB}}{K_{\mathrm{ia}}K'_{\mathrm{b}}\left(1+K_{\mathrm{conf}}\right)+K'_{\mathrm{a}}\left(1+K_{\mathrm{conf}}\right)\mathbf{B}+K'_{\mathrm{b}}\mathbf{A}+\mathbf{AB}} \tag{15}$$

$$\nu = \frac{\mathrm{V}\left(1+\frac{\mathbf{Na}}{K_{\mathrm{act}}}\right)\mathbf{AB}}{\begin{aligned}&K_{\mathrm{ia}}K'_{\mathrm{b}}\left[\left(1+K_{\mathrm{conf}}\right)+\left(1+K'_{\mathrm{conf}}\right)\left(\frac{\mathbf{Na}}{K_{\mathrm{act}}}\right)+\left(1+\frac{\mathbf{Na}}{K_{\mathrm{act}}}\right)\left(\frac{\mathbf{Na}}{K_{\mathrm{i}}}\right)\right]\\&+K'_{\mathrm{a}}\left[\left(1+K_{\mathrm{conf}}\right)+\left(1+K'_{\mathrm{conf}}\right)\left(\frac{\mathbf{Na}}{K_{\mathrm{act}}}\right)\right]\mathbf{B}+\left(K'_{\mathrm{b}}\mathbf{A}+\mathbf{AB}\right)\left(1+\frac{\mathbf{Na}}{K_{\mathrm{act}}}\right)\end{aligned}} \tag{16}$$

In eq 16, for HCS, K_{ia}, K'_a and K'_b are the dissociation constant for α-Kg and the Michaelis constants for α-Kg and AcCoA, respectively, **A** and **B** represent the concentrations of α-Kg and AcCoA. K_{act}, K'_{conf} and K_i reflect the activation constant for Na^+, the conformational equilibrium between E and E′ in the presence of Na^+, and the inhibition constant for Na^+, respectively. K_{conf} is the equilibrium constant between E and E′ in the absence of Na^+. **Na** is Na^+ concentration. Table 5-1 gives the limits of equation 16.

In the presence of both lysine and Na^+ the behavior of the enzyme is more complicated due to the simultaneous activation and inhibition effects of Na^+ and inhibition by lysine. The kinetic mechanism in this case is shown in Scheme 5-2. However, there is no experimental evidence to suggest that any lysine-bound E form of the enzyme can be formed (see accompanying article (*11*)). In this case, all of the enzyme species shown are assumed to be at equilibrium, and the rate of the enzymatic reaction depicted in Scheme 5-2 is represented as $v = k_p[(E+ENa)/E_t]$. k_p is the overall enzymatic rate in the absence of inhibitors (not V since A and B are maintained at a fixed, low concentration), and activators. E_t is the sum of all enzyme species that are in equilibrium. The rate equation for prediction of the enzymatic behavior (derived as above) in this case is as follows:

$$\nu = \frac{k_p\left(1+\frac{\mathbf{Na}}{K_{act}}\right)}{1+K_{conf}\left[1+\left(1+\frac{\mathbf{Na}}{K''_{act}}\right)\left(\frac{\mathbf{Lys}}{K_{i\,lys}}\right)\right]+\left(1+K'_{conf}\right)\left(\frac{\mathbf{Na}}{K_{act}}\right)+\left(1+\frac{\mathbf{Na}}{K_{act}}\right)\left(\frac{\mathbf{Na}}{K_i}\right)} \qquad (17)$$

where K''_{act} is the activation constant of Na^+ for the E′Lys enzyme complex. When **Na** and **Lys** are at zero concentration, v is equal to $k_p/(1+K_{conf})$.

Table 5-1: Rate equations for HCS enzymatic activity in extreme cases.

Conditions	**A** (low), **B** (low)	**A** (high), **B** (low)
Na=0	$\nu = \dfrac{\mathrm{V}\mathbf{AB}}{\left(K_{\mathrm{ia}}K'_{\mathrm{b}} + K'_{\mathrm{a}}\mathbf{B}\right)\left(1+K_{\mathrm{conf}}\right)+K'_{\mathrm{b}}\mathbf{A}+\mathbf{AB}}$	$\nu = \dfrac{\mathrm{V}\mathbf{B}}{K'_{\mathrm{b}}+\mathbf{B}}$
$K_i > \mathbf{Na} > K_{act}$	$\nu = \dfrac{\mathrm{V}\left(1+\dfrac{\mathbf{Na}}{K_{\mathrm{act}}}\right)\mathbf{AB}}{K_{\mathrm{ia}}K'_{\mathrm{b}}\left[\left(1+K_{\mathrm{conf}}\right)+\left(1+K'_{\mathrm{conf}}\right)\left(\dfrac{\mathbf{Na}}{K_{\mathrm{act}}}\right)+\left(1+\dfrac{\mathbf{Na}}{K_{\mathrm{act}}}\right)\left(\dfrac{\mathbf{Na}}{K_{\mathrm{i}}}\right)\right] + K'_{\mathrm{a}}\left[\left(1+K_{\mathrm{conf}}\right)+\left(1+K'_{\mathrm{conf}}\right)\left(\dfrac{\mathbf{Na}}{K_{\mathrm{act}}}\right)\right]\mathbf{B}+\left(K'_{\mathrm{b}}\mathbf{A}+\mathbf{AB}\right)\left(1+\dfrac{\mathbf{Na}}{K_{\mathrm{act}}}\right)}$	
Na >>K_i, K_{act}	$\nu = 0$	
Conditions	**A** (low), **B** (high)	**A** (high), **B** (high)
Na=0	$\nu = \dfrac{\mathrm{V}\mathbf{A}}{K'_{\mathrm{a}}\left(1+K_{\mathrm{conf}}\right)+\mathbf{A}}$	$\nu = \mathrm{V}$
$K_i > \mathbf{Na} > K_{act}$	$\nu = \dfrac{\mathrm{V}\left(1+\dfrac{\mathbf{Na}}{K_{\mathrm{act}}}\right)\mathbf{A}}{K'_{\mathrm{a}}\left[\left(1+K_{\mathrm{conf}}\right)+\left(1+K'_{\mathrm{conf}}\right)\left(\dfrac{\mathbf{Na}}{K_{\mathrm{act}}}\right)\right]+\mathbf{A}\left(1+\dfrac{\mathbf{Na}}{K_{\mathrm{act}}}\right)}$	
Na >>K_i, K_{act}	$\nu = 0$	

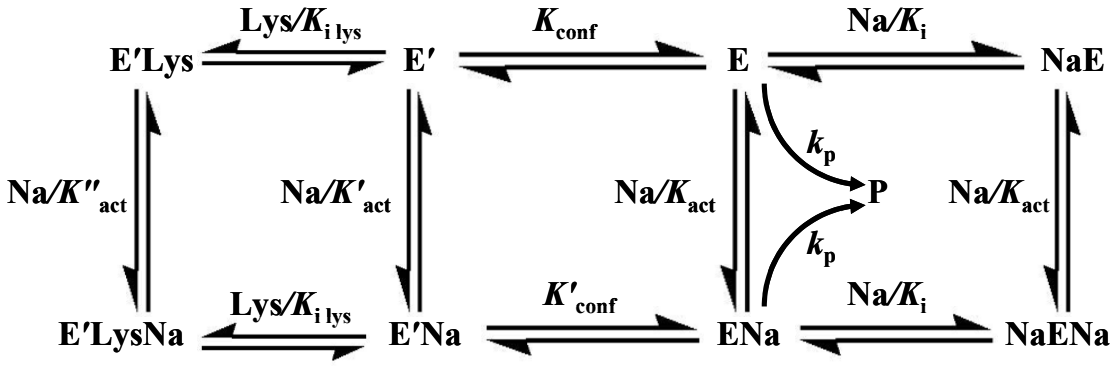

Scheme 5-2: Kinetic mechanism for interaction between Na^+ and lysine. Na, E, and E′ represent Na^+, and the active and less active forms of the enzyme, respectively. K_{conf} and K'_{conf} defined in the legend to Scheme 1. K_{act} and K'_{act} are defined in the legend to Scheme 5-1, while K''_{act} is the activation constant for Na^+ for E′ with lysine-bound. $K_{i\ lys}$ and K_i are the inhibition constants for lysine and Na^+.

5-4. Results and discussion

The effect of Na^+ on HCS activity is complex with activation and inhibition occurring simultaneously dependent on the concentration of Na^+. As shown in the accompanying article (*11*), the inhibitory effect is independent of its activation, and results from combination at the active site, competing with AcCoA. Graphically, the effects of Na^+ are observed in the tertiary replots of the initial rate data varying α-Kg, AcCoA and Na^+.

The double reciprocal plot of eq 16 with AcCoA varied at fixed levels of α-Kg is given in eq 18.

$$\frac{1}{v}=\left[\left\{\left(\frac{K_{ia}K'_{b}}{V}\right)\left[(1+K_{conf})+(1+K'_{conf})\left(\frac{\mathbf{Na}}{K_{act}}\right)+\left(1+\frac{\mathbf{Na}}{K_{act}}\right)\left(\frac{\mathbf{Na}}{K_{i}}\right)\right]\left(\frac{1}{\left(1+\frac{\mathbf{Na}}{K_{act}}\right)}\right)\right\}\frac{1}{\mathbf{A}}+\frac{K'_{b}}{V}\right]\frac{1}{\mathbf{B}}$$
$$+\left[\left(\frac{K'_{a}}{V}\right)\left[(1+K_{conf})+(1+K'_{conf})\left(\frac{\mathbf{Na}}{K_{act}}\right)\right]\left[\frac{1}{\left(1+\frac{\mathbf{Na}}{K_{act}}\right)}\right]\right]\frac{1}{\mathbf{A}}+\frac{1}{V}$$

(18)

On the basis of eq 18, expressions for slope and intercept are given in eqs 19 and 20.

$$\text{Slope}=\left[\left(\frac{K_{ia}K'_{b}}{V}\right)\left[(1+K_{conf})+(1+K'_{conf})\left(\frac{\mathbf{Na}}{K_{act}}\right)+\left(1+\frac{\mathbf{Na}}{K_{act}}\right)\left(\frac{\mathbf{Na}}{K_{i}}\right)\right]\left(\frac{1}{\left(1+\frac{\mathbf{Na}}{K_{act}}\right)}\right)\right]\frac{1}{\mathbf{A}}+\frac{K'_{b}}{V}$$

(19)

$$\text{Intercept}=\left[\left(\frac{K'_{a}}{V}\right)\left[(1+K_{conf})+(1+K'_{conf})\left(\frac{\mathbf{Na}}{K_{act}}\right)\right]\left[\frac{1}{\left(1+\frac{\mathbf{Na}}{K_{act}}\right)}\right]\right]\frac{1}{\mathbf{A}}+\frac{1}{V} \qquad (20)$$

If K'_{conf} is equal to zero as found experimentally for HCS, then on the basis of eqs 19 and 20, expressions for SOS and SOI are given in eqs 21 and 22. Tertiary replots are given by the slope of the secondary plot (slope vs 1/α-Kg) or SOS vs Na^+ (eq 21)

and the intercept of the secondary plot (intercept vs 1/α-Kg) or SOI vs Na^+ (eq 22) and are shown in Figs. 5-1 and 5-2.

$$\mathrm{SOS} = \left(\frac{K_{\mathrm{ia}} K'_{\mathrm{b}}}{\mathrm{V}}\right)\left[\left(1 + \frac{K_{\mathrm{conf}}}{\left(1 + \frac{\mathbf{Na}}{K_{\mathrm{act}}}\right)}\right) + \left(\frac{\mathbf{Na}}{K_{\mathrm{i}}}\right)\right] \tag{21}$$

$$\mathrm{SOI} = \left(\frac{K'_{\mathrm{a}}}{\mathrm{V}}\right)\left(1 + \frac{K_{\mathrm{conf}}}{\left(1 + \frac{\mathbf{Na}}{K_{\mathrm{act}}}\right)}\right) \tag{22}$$

The SOS/SOI ratio is given by eq 23, and is equal to the effective K_i for Na^+ at the AcCoA site.

$$\mathrm{SOS/SOI} = \left(\frac{K_{\mathrm{ia}} K'_{\mathrm{b}}}{K'_{\mathrm{a}}}\right)\left[1 + \left(\frac{\left(1 + \frac{\mathbf{Na}}{K_{\mathrm{act}}}\right)\left(\frac{\mathbf{Na}}{K_{\mathrm{i}}}\right)}{\left(1 + K_{\mathrm{conf}}\right) + \left(\frac{\mathbf{Na}}{K_{\mathrm{act}}}\right)}\right)\right] \tag{23}$$

As shown in Figures 5-1 and 5-2, the y-intercepts (y_1) represent SOS and SOI at zero NaCl, respectively, given by $y_{1\text{-SOS}} = \left(\frac{K_{\mathrm{ia}} K'_{\mathrm{b}}}{\mathrm{V}}\right)\left(1 + K_{\mathrm{conf}}\right)$ and $y_{1\text{-SOI}} = \frac{K'_{\mathrm{a}}}{\mathrm{V}}\left(1 + K_{\mathrm{conf}}\right)$.

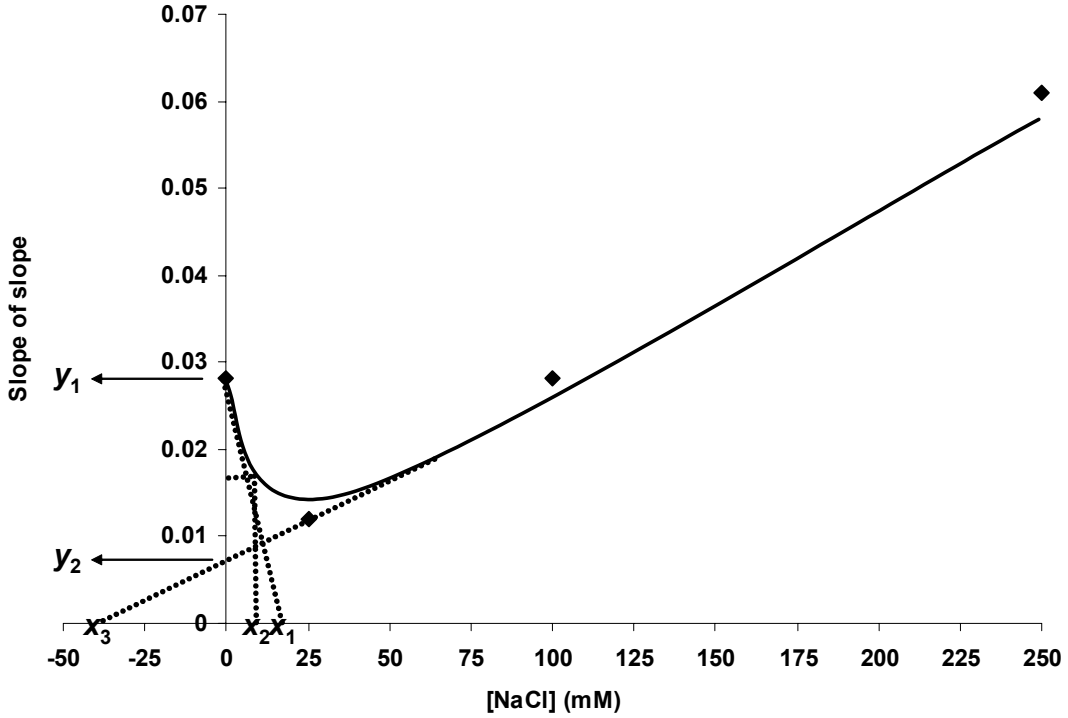

Fig. 5-1: Tertiary replot of slope of slope for the inhibition and activation by Na^+. x_2 and x_3 represent K_{act} and K_i, respectively. Values of x and y are defined in the text.

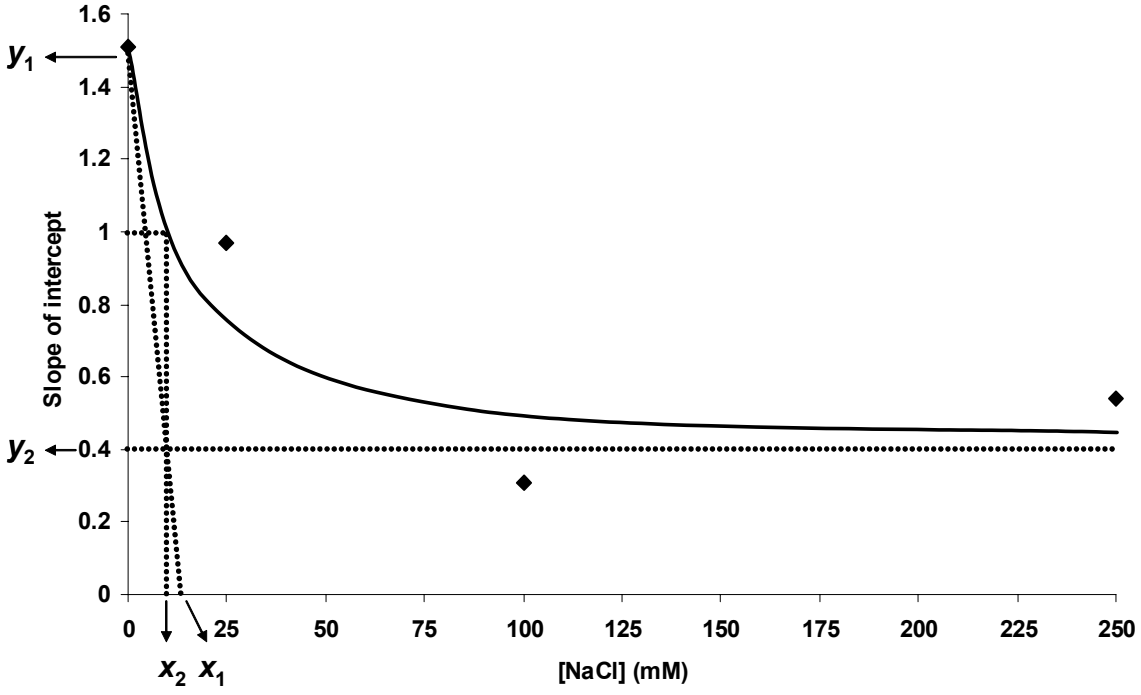

Fig. 5-2: Tertiary replot of slope of intercept for the inhibition and activation by Na^+. The values of x and y are defined in the text.

The point marked x_2 in the SOS and SOI tertiary replots is equal to K_{act}, *i.e.* the concentration of Na^+ that gives half maximal activation in the absence of Na^+ inhibition. In Fig. 5-1, y_2 is the maximal activity for the enzyme, in the absence of Na^+ inhibition. The value of y_2 is $\left(\frac{K_{ia}K'_b}{V}\right)$ (obtained from the y-intercept of eq 21 when **Na** tends to infinity in the absence of Na^+ inhibition).

The value of y_2 in the slope of intercept (SOI) plot is K'_a/V (Fig. 5-2), obtained from eq 22 at infinite **Na**. In both SOS and SOI plots, the ratio of y_1/y_2 is $1+K_{conf}$ (the fraction of activated enzyme). In Fig. 5-1, x_3 is $-K_i$ for Na^+ inhibition for the fully activated enzyme. If K_i goes to infinity (high AcCoA) then the value of x_1 (obtained using the derivative of eq 21) in Fig. 5-1, eq 24, is comparable to the value of x_1 in Fig. 5-2, eq 25, where x_1 is an apparent K_{act} value that depends on the values of K_{conf} and K_i. In other words, it determines the intrinsic effects of Na^+ inhibition and conformational changes on the K_{act} value. In the case of HCS the effect is negligible. If K_{act} goes to infinity and K_{conf} goes to zero, then the value of eq 24 is $-K_i$.

$$x_{1\text{-SOS}} = \frac{1}{\left(\frac{1}{1+K_{conf}}\right)\left[\frac{K_{conf}}{K_{act}} - \frac{1}{K_i}\right]} \tag{24}$$

$$x_{1\text{-SOI}} = K_{act}\left(1+\frac{1}{K_{conf}}\right) \tag{25}$$

As **Na** goes to infinity in eq 21, the equation will reduce to $\left(\frac{K_{ia}K'_b}{V}\right)\left(1+\frac{\mathbf{Na}}{K_i}\right)$, which is the equation for the dotted line that extrapolates to x_3 as SOS goes to zero. If there is no activation by Na^+, eq 21 is equal to $\left(\frac{K_{ia}K'_b}{V}\right)\left[\left(1+K_{conf}\right)+\left(\frac{\mathbf{Na}}{K_i}\right)\right]$. In this case, the experimentally measured K_i is equal to $K_i\left(1+K_{conf}\right)$. Between the two extremes, no activation as a result of an infinite K_{act} and completely activated enzyme as a result of infinite Na^+, a series of parallel lines is obtained for a plot of SOS vs Na^+, at constant K_i. The y-intercept depends on the value of K_{conf}. As the K_i for inhibition becomes greater than the K_{act} for activation by Na^+, then the SOS plot (Fig. 5-1) will show a lower minimum value, indicating a greater observed activation, and the linear part of the curve will have a greater slope as **Na** is increased.

Data simulation using the experimentally measured kinetic parameters (see accompanying article (*11*)) shows the dependence of activation on the K_{act}. If the K_{act} for Na^+ is much greater than K_i (37 mM), then as described in eq 21, the SOS vs Na^+ will approach linearity (Fig. 5-3A). If K_i increases, the plot shows less and less inhibition, Fig. 5-3B. A 3D plot of the above is shown in Fig. 5-3C.

The slope of intercept (SOI) (Fig. 5-4) represents a measure of enzyme activity at high AcCoA and low α-Kg, and exhibits no inhibition by Na^+. In other words, an infinite concentration of AcCoA eliminates the Na^+ inhibition by increasing its K_i to infinity. The percentage of the HCS enzymatic activity vs Na^+ based on the derived equations, is in a very good agreement with the experimental data (see accompanying

article (*11*)) indicating that the equations precisely predict the enzymatic behavior of HCS at different Na^+ concentrations, Fig. 5. Calculation of the percentage of the HCS activity is derived by dividing eq 16 by eq 16 when **Na** = 0 with the assumption that $K'_{conf} = 0$ and is shown in eq 26:

$$\%\text{Activity} = \frac{\left[\left(K_{ia}K'_b + K'_a\mathbf{B}\right)\left(1+K_{conf}\right) + \left(K'_b\mathbf{A} + \mathbf{AB}\right)\right]\left(1+\frac{\mathbf{Na}}{K_{act}}\right)}{K_{ia}K'_b\left[\left(1+K_{conf}\right) + \left(1+K'_{conf}\right)\left(\frac{\mathbf{Na}}{K_{act}}\right) + \left(1+\frac{\mathbf{Na}}{K_{act}}\right)\left(\frac{\mathbf{Na}}{K_i}\right)\right] + K'_a\left[\left(1+K_{conf}\right) + \left(1+K'_{conf}\right)\left(\frac{\mathbf{Na}}{K_{act}}\right)\right]\mathbf{B} + \left(K'_b\mathbf{A} + \mathbf{AB}\right)\left(1+\frac{\mathbf{Na}}{K_{act}}\right)} \times 100$$

(26)

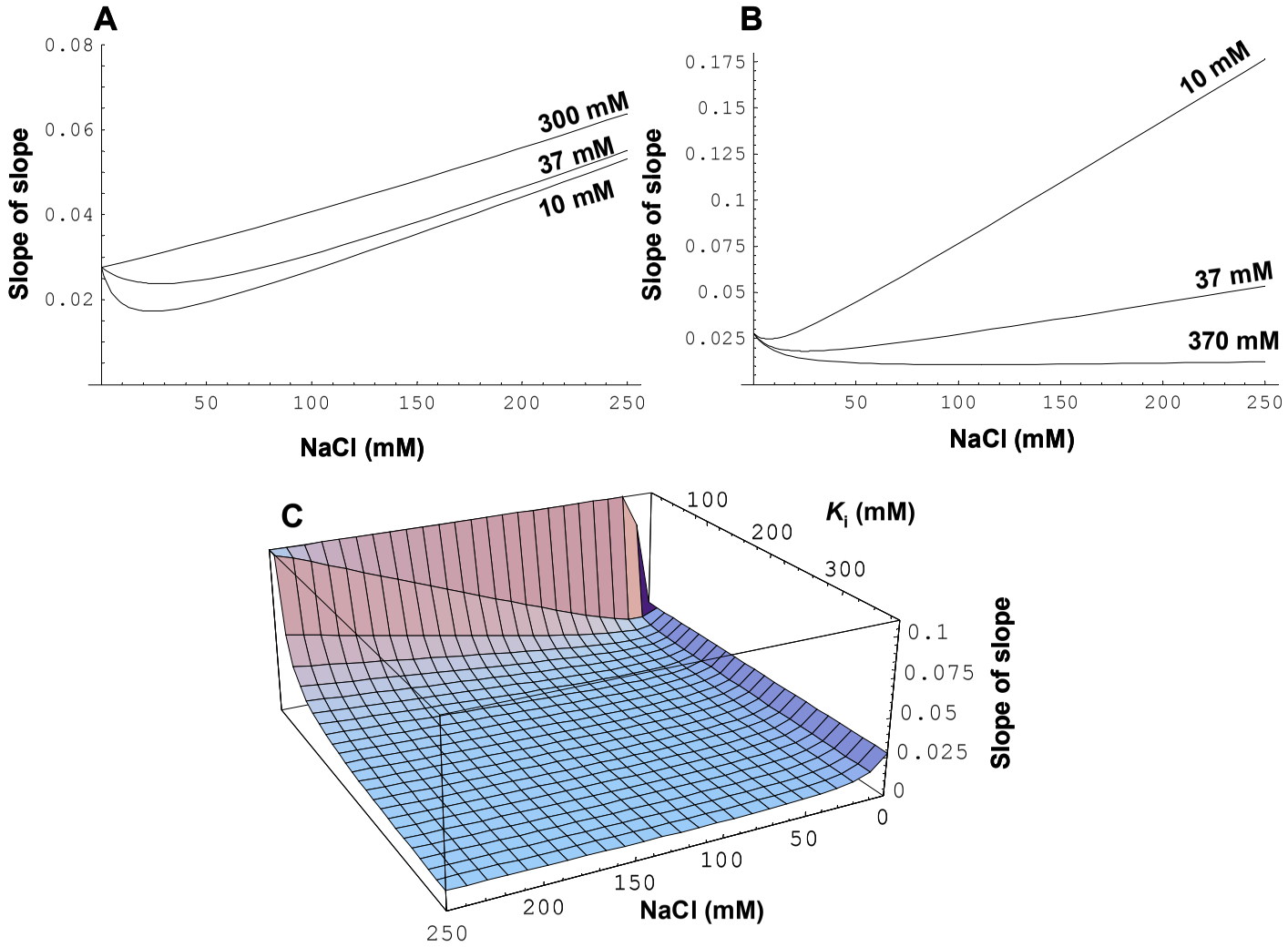

Fig. 5-3: Predicted slope of slope (SOS) replot for Na^+ activation and inhibition as a function of NaCl, K_{act} and K_i. A. Predicted plot at three different K_{act} values as recorded on the plot. When K_{act} >> K_i, the plot approaches linear. K_i was held constant at 37 mM. B. Predicted at three different K_i values as recorded on the plot. Note that the SOS at K_i = 370 mM is similar to slope of intercept (SOI) at K_{act} = 10 mM with no observed inhibition, suggesting that high AcCoA eliminates the Na^+ inhibition by increasing the K_i. K_{act} was held constant at 12 mM. C. 3D plot of B.

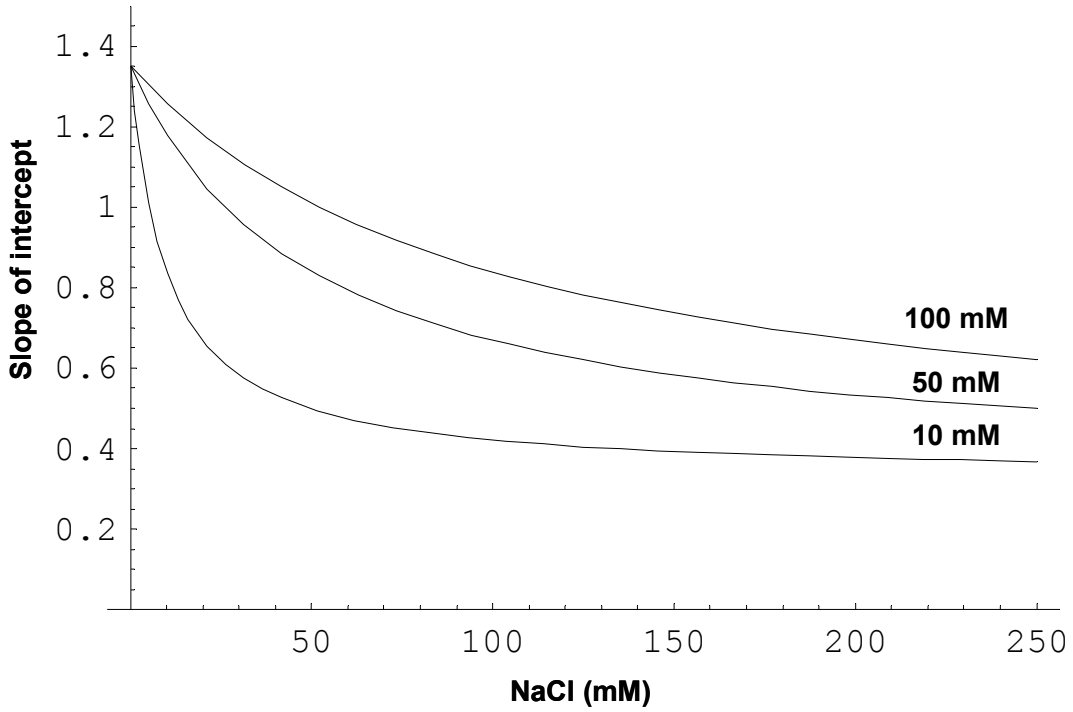

Fig. 5-4: Predicted slope of intercept (SOI) replot for Na^+ activation and inhibition as a function of NaCl and K_{act}. Prediction is shown at three different K_{act} values as recorded on the plot. At lower K_{act} values enzyme reaches the peak activity at lower Na^+ concentrations.

As shown in Figures 5-5A and 5-5C, increasing the α-Kg concentration decreases both activatory and inhibitory effects at all levels of Na^+. Interestingly, the common point for all of the curves in Fig. 5-5C is 150 mM Na^+, where the HCS activity remains at 100%, and this has physiological significance (see accompanying article (*11*)). In terms of equation 26, increasing the level of substrate A gives 100% activity. However, increasing AcCoA concentration (B goes to infinity) only eliminates the inhibitory effects of Na^+, while it has no effect on the activation by Na^+, Figs. 5-5B and 5-5D. The same mechanism can also be used to explain the behavior of other monovalent or divalent cations (see accompanying article (*11*)).

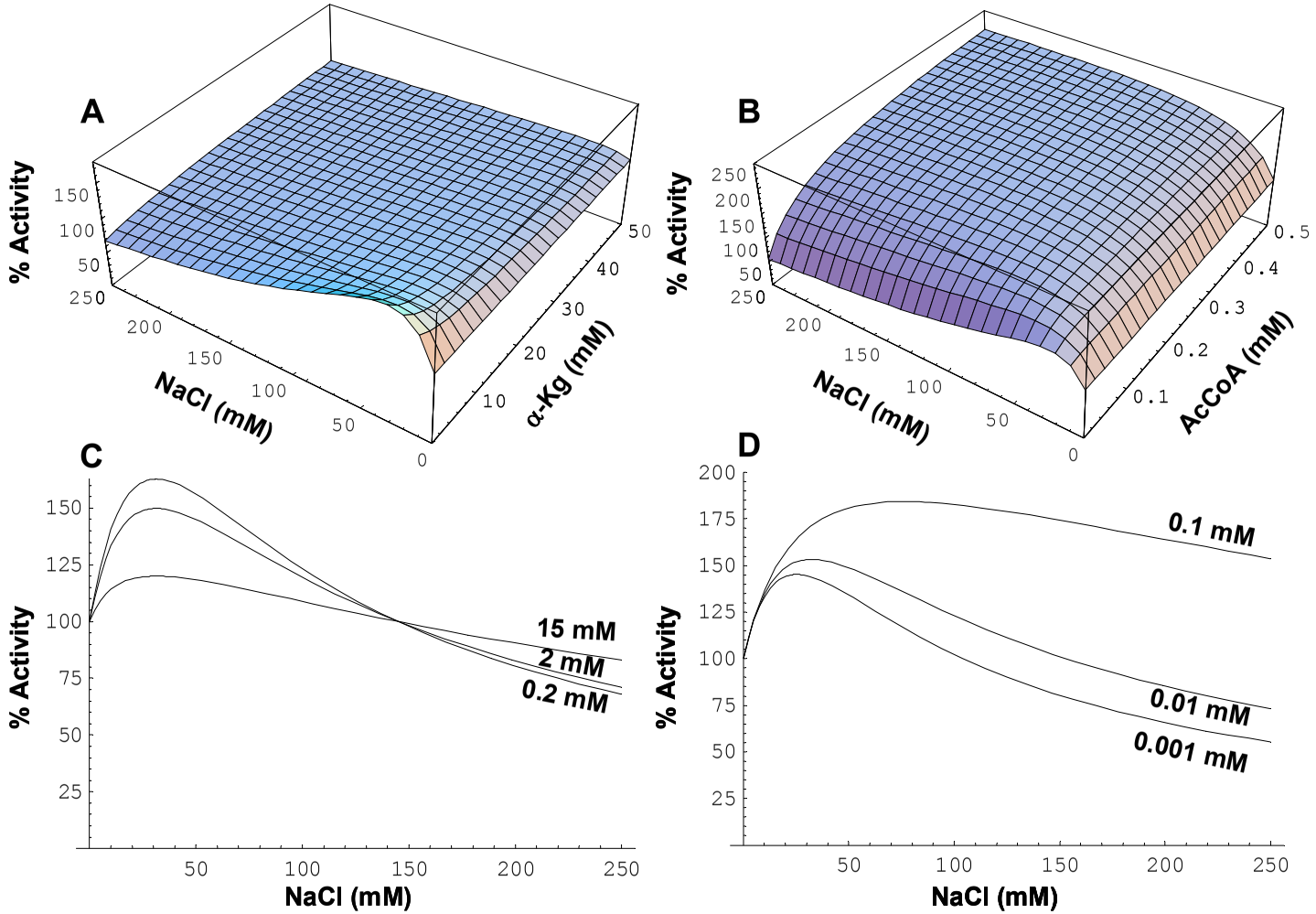

Fig. 5-5: Percentage of HCS activity as a function of NaCl and substrate concentration. A. 3D plot of the activity as a function of NaCl and α-Kg concentration. B. 3D plot of the activity as a function of NaCl and AcCoA concentration. C. Cross sections of A at three different α-Kg concentrations as plotted. Increasing the α-Kg concentration eliminates both activation and inhibition at all levels of Na^+ concentration. D. Cross sections of B at three different AcCoA concentrations as plotted. Increasing the AcCoA concentration eliminates the Na^+ inhibition at all levels of Na^+ concentration, while maintaining the activation.

The effects of lysine and Na^+, in the absence and presence of AcCoA is complex (see accompanying article (*11*)). The equation predicting enzyme activity in this case is as follows with the assumption that $K'_{conf} = 0$ (see accompanying article (*11*)):

$$\frac{1}{v} = \left(\frac{K_{conf}\left(1 + \frac{\mathbf{Na}}{K''_{act}}\right)}{k_p K_{i\,lys}\left(1 + \frac{\mathbf{Na}}{K_{act}}\right)} \right) [\mathbf{Lys}] + \left(\frac{(1 + K_{conf}) + \left(\frac{\mathbf{Na}}{K_{act}}\right) + \left(1 + \frac{\mathbf{Na}}{K_{act}}\right)\left(\frac{\mathbf{Na}}{K_i}\right)}{k_p\left(1 + \frac{\mathbf{Na}}{K_{act}}\right)} \right) \tag{27}$$

where **Na**, **Lys**, K_i and $K_{i\ lys}$ are the concentrations of Na^+, lysine, and inhibition constants for Na^+ and lysine, respectively. $\frac{k_p}{(1 + K_{conf})}$ is the overall enzymatic rate in the absence of inhibitors, activators, and a fixed concentration of α-Kg and AcCoA. The slope of the above equation when 1/v is plotted vs lysine concentration represents the enzyme activity as lysine tends to infinity. This equation can be used to explain HCS behavior in the presence of Na^+ and lysine at both low and high AcCoA concentrations. However, the K_i and K_{act} values differ at high and low AcCoA. As shown in Fig. 5-6, the slope of equation 27 vs Na^+ can be concave upward or downward depending on the values of K_{act} and K''_{act}. However, the values of K_{act} and K''_{act} affects the slope in opposite directions, and concentrations higher than 150 mM Na^+ (in the case of HCS), have almost no effect on the slope either at low or high AcCoA. As mentioned above, this phenomenon is thought to have physiological significance (see accompanying article (*11*)).

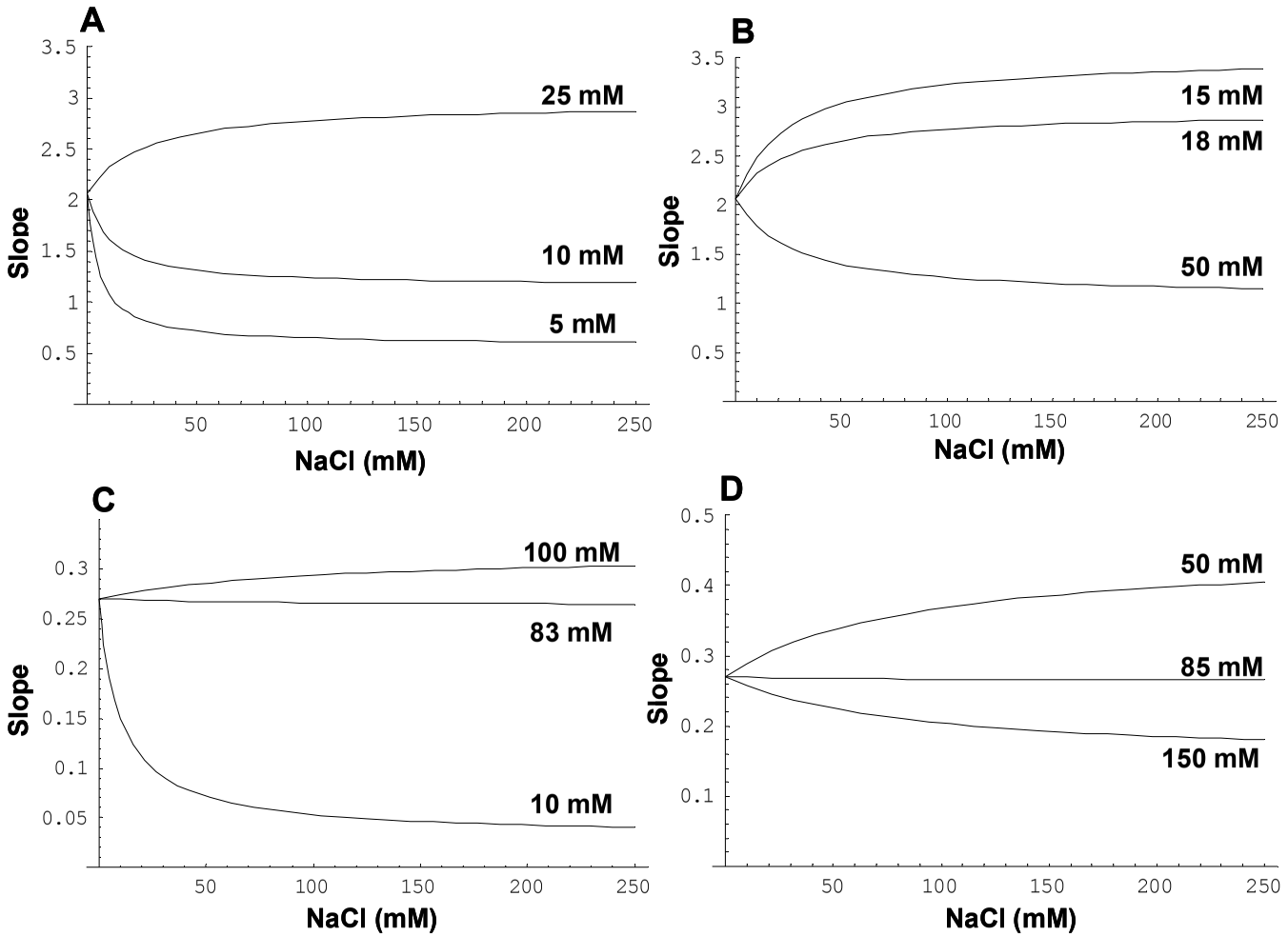

Fig. 5-6: Predicted slope for Na^+-lysine activation-inhibition as a function of lysine at low and high AcCoA. A. Plot of slope vs NaCl (low AcCoA) at three different K_{act} values as plotted. The slope is sensitive to slight changes in the K_{act} value. K''_{act} is held constant at 18 mM. B. Plot of slope vs NaCl (low AcCoA) at three different K''_{act} values as plotted. The slope is again sensitive to small changes in K''_{act}. K_{act} is held constant at 25 mM. C. Plot of slope vs NaCl (high AcCoA) at three different K_{act} values as plotted. The predicted slope is sensitive to changes in K_{act}. K''_{act} is held constant at 85 mM. D. Plot of slope vs NaCl (high AcCoA) at three different K''_{act} values as plotted. K_{act} is held constant at 83 mM.

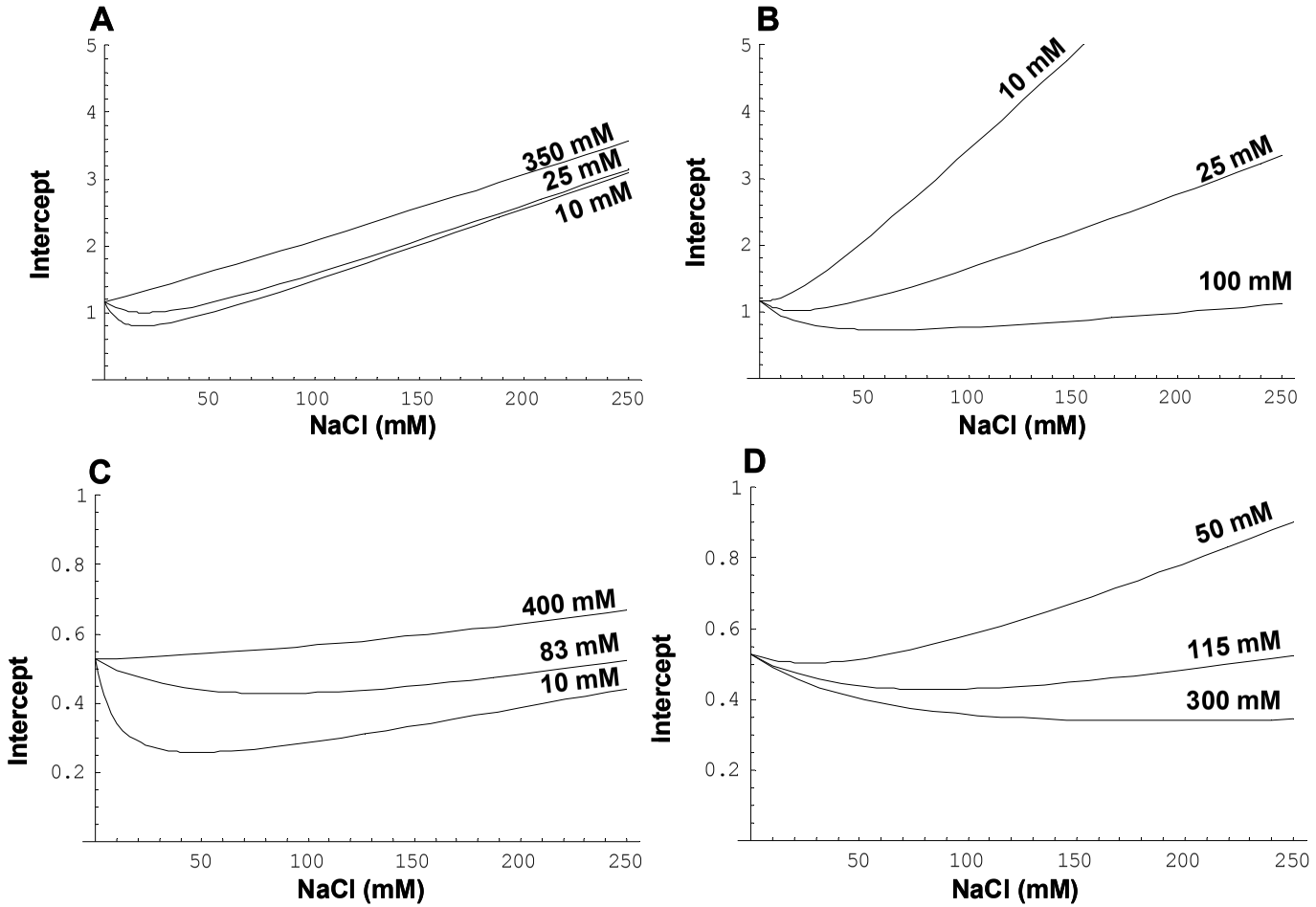

Fig. 5-7: Predicted intercept for Na^+-lysine activation-inhibition as a function of lysine at low and high AcCoA. A. Plot of intercept vs NaCl (low AcCoA) at three different K_{act} values as plotted. Note that K_{act} has little effect on the slope of the graph. Increasing K_{act} eliminates Na^+ activation only. K_i is held constant at 25 mM. B. Plot of intercept vs NaCl (low AcCoA) at three different K_i values as plotted. The slope is sensitive to slight changes in K_i. K_{act} is held constant at 25 mM. C. Plot of intercept vs NaCl (high AcCoA) at three different K_{act} values as plotted. Again, K_{act} has little effect on the slope. Increasing K_{act} eliminates Na^+ activation only. K_i is held constant at 115 mM. D. Plot of intercept vs NaCl (high AcCoA) at three different K_i values as plotted. As in B, the slope is sensitive to changes in K_i. K_{act} is held constant at 83 mM.

Fig. 5-7, shows the intercept of equation 27, *i.e.*, when lysine concentration is zero. In this case, the equation reflects the kinetic behavior of the enzyme in the presence of Na^+ as expected and the intercept effect depends on the values of K_{act} and K_i. Increasing the K_{act} value eliminates the Na^+ activation only and has little effect on the intercept values (low or high AcCoA), Fig. 5-7A. However, changing the K_i value dramatically changes the intercept (low and high AcCoA). Na^+ inhibition is eliminated at higher K_i values, while activation remains.

In conclusion, regulatory kinetic behavior of homocitrate synthase demonstrates the effect of a bifunctional activatory-inhibitory effector. In this context, the enzyme simultaneously senses the activatory and inhibitory effects of the effector and net catalytic outcome depends on the concentration of the effector and the activation and inhibition constants. The resulting expressions can be applied to enzyme systems that exhibit activation and inhibition as a result of interaction at different sites in free enzyme.

References

[1] Bhattacharjee, J. K. (1992) Evolution of α-aminoadipate pathway for the synthesis of lysine in fungi, in *Evolution of Metabolic Function* (Mortlock, R. P., Ed.), pp 47-80, CRC Press, Boca Raton.

[2] Bhattacharjee, J. K. (1985) α-aminoadipate pathway for the biosynthesis of lysine in lower eukaryotes, *Crit. Rev. Microbiol. 12*, 131-151.

[3] Umbarger, H. E. (1987) Amino acid biosynthesis and its regulation, *Annu. Rev. Biochem. 47*, 532-606.

[4] Vogel, H. J. (1960) Two modes of lysine synthesis among lower fungi: evolutionary significance, *Biochim. Biophys. Acta 41*, 172-173.

[5] Ramos, F., Verhasselt, P., Feller, A., Peeters, P., Wach, A., Dubois, E., and Volckaert, G. (1996) Identification of a gene encoding a homocitrate synthase isoenzyme of *Saccharomyces cerevisiae*, *Yeast 12*, 1315-1320.

[6] Tracy, J., and Kohlhaw, G. (1975) Reversible, coenzyme-A-mediated inactivation of biosynthesis condensing enzymes in yeast: A possible regulatory mechanism, *Proc. Natl. Acad. Sci. USA 72*, 1802-1805.

[7] King, E. L., and Altman, C. (1956) A schematic method of deriving the rate laws for enzyme-catalyzed reactions, *J. Phys. Chem. 60*, 1375-1381.

[8] Cha, S. (1968) A simple method for derivation of rate equations for enzyme-catalyzed reactions under the rapid equilibrium assumption or combined assumptions of equilibrium and steady state, *J. Biol. Chem. 243*, 820-825.

[9] Andi, B., West, A. H., and Cook, P. F. (2004) Stabilization and characterization of histidine-tagged homocitrate synthase from *Saccharomyces cerevisiae*, *Arch. Biochem. Biophys. 421*, 243-254.

[10] Andi, B., West, A. H., and Cook, P. F. (2004) Kinetic mechanism of histidine-tagged homocitrate synthase from *Saccharomyces cerevisiae*, *Biochemistry 43*, 11790-11795.

[11] Andi, B., West, A. H. and Cook, P. F. (2005) Regulatory mechanism of histidine-tagged homocitrate synthase from *Saccharomyces cerevisiae*: I. KINETIC STUDIES, *J. Biol. Chem. 280*, 31624-31632.

CHAPTER 6

Crystal structure of saccharopine reductase at 1.7 Å resolution*

"Reproduced with automatic permission from [Andi, B., Cook, P. F. and West A. H. (2005) Crystal Structure of the Histidine-tagged Saccharopine reductase from *Saccharomyces cerevisiae* at 1.7 Å Resolution, *Cell Biochem. Biophys.,* In press] Copyright [2005] Humana Press, Inc."

6-1. Introduction

The budding yeast, *Saccharomyces cerevisiae*, as well as some human pathogenic fungi such as *Candida albicans*, *Cryptococcus neoformans* and *Aspergillus fumigatus*, and plant pathogens like *Magnaporthe grisea* use the α-aminoadipate pathway for the biosynthesis of lysine (*1*). The human pathogens represent a major health threat for immunocompromised patients (cancer, transplant, and AIDS patients). In addition, *M. grisea* is among the most destructive pathogens in crop plants (rice blast) (*2*). The uniqueness of the α-aminoadipate pathway in fungal organisms thus makes it a potential target for the design of new antimycotic agents (*3*).

Saccharopine dehydrogenase (L-Glu forming) (SDH) or saccharopine reductase (SR), [N6-(L-1,3-dicarboxypropyl)-L-lysine:$NADP^+$ oxidoreductase (L-glutamate-forming) (E.C. 1.5.1.10)] catalyzes the penultimate reaction in the α-aminoadipate pathway, the reversible condensation of α-aminoadipate-δ-semialdehyde with L-glutamate and reduction by NADPH to give saccharopine (*4-7*).

The SR from *S. cerevisiae* consists of 446 amino acids with a calculated molecular weight of 48,917 (*Saccharomyces* Genome Database-

***The atomic coordinates have been deposited in the Protein Data Bank (PDB) with the accession code 2AXQ for the apo enzyme in the space group $P3_121$.**

www.yeastgenome.org). An apparent molecular weight of 67,000 has been reported using gel filtration chromatography (*8*), which is close to the value of 73,000 reported using sucrose density gradient centrifugation (*9*). Studies suggest a dimeric solution structure for fungal SRs with a molecular mass in the range of 70,000-90,000 (*3*, *10*).

The saccharopine reductase from *M. grisea* is 63% identical and 78% similar to the enzyme from *S. cerevisiae* in terms of sequence conservation. The crystal structure of the saccharopine reductase from *M. grisea* was recently solved (*3, 11*). The polypeptide chain of the saccharopine reductase from *M. grisea* folds into three domains. The first domain is a variant of the dinucleotide-binding domain known as a Rossmann fold (*12*) that binds to $NADP^+$ and NADPH. The second domain is an α/β fold known as a saccharopine reductase fold (*13*). The third domain is an all-helical domain that apparently moves upon binding of the substrates (*3*). The SR from *M. grisea* is reported to be a homodimer based on gel filtration and crystal structure (*3, 11*).

In this study, we report the crystal structure of the apo-histidine-tagged saccharopine reductase from *S. cerevisiae*. A comparative structural analysis with an emphasis on the active site is presented.

6-2. Materials and methods

6-2-1. Materials

All chemicals were of the highest grade commercially available. Ampicillin, isopropyl-β-D-1-thiogalactopyranoside (IPTG), KCl, $(NH_4)_2SO_4$, and Coomassie® Brilliant Blue G-250 were purchased from Amresco, Gold BioTechnology, Fisher, EMD, and BIO-RAD, respectively. Chloramphenicol, phenylmethylsulfonyl fluoride (PMSF), NAD^+, and saccharopine were obtained from Sigma. Tris-HCl and imidazole were purchased from Research Organics. Restriction enzymes were purchased from Invitrogen.

6-2-2. Construction of the saccharopine reductase expression plasmid

To amplify the *LYS9* gene (encoding the SR from *S. cerevisiae*), polymerase chain reaction (PCR) was performed on *S. cerevisiae* genomic DNA (200 ng) using Platinum® *Pfx* DNA polymerase purchased from Invitrogen (see Appendix – Fig. A-8). The following primers (Invitrogen) were used for PCR: 5′-CGT ATT ATA TAT TTT CAT ATG GGA AAG AAC G-3′ (forward primer) and 5′-GCG TTC TCG AGT TCT TCT TAT TTA AGC CAC TGT C-3′ (reverse primer). The forward and reverse primers contain the restriction endonuclease sites for *Nde* I and *Xho* I, respectively (underlined). The blunt-end PCR product was then ligated into the *Sma* I linearized pUC12 plasmid (see Appendix – Fig. A-9) to produce the pUC12-*LYS9* cloning vector (see Appendix – Fig. A-10) with which competent DH5α *Escherichia coli* cells were transformed by a 30 second heat shock at 42 °C. The vector was purified from the

DH5α *E. coli* cells, digested with the restriction enzymes *Nde* I and *Xho* I and the *LYS9* fragment was gel-purified using the GENECLEAN Turbo DNA purification kit purchased from QBIOgene. The *Nde* I and *Xho* I excised *LYS9* fragment was then ligated into the pET-16b vector from Novagen cut with the same restriction enzymes (see Appendix – Fig. A-11). The host cells used for expression of SR from the pET-16b-*LYS9* expression vector were BL21-Star™(DE3)-RIL from Stratagene. The *LYS9* gene of the expression vector was checked for accuracy by DNA sequencing (Microgen, University of Oklahoma Health Sciences Center) (see Appendix – Fig. A-12).

6-2-3. Expression and purification of saccharopine reductase

The BL21-Star™(DE3)-RIL cells containing the pET-16b-*LYS9* plasmid were grown at 30 °C in 1 L LB medium containing 100 μg/mL ampicillin and 25 μg/mL chloramphenicol. The expression of N-terminal $(His)_{10}$-tagged recombinant SR was induced by adding 1 mM isopropyl-β-D-1-thiogalactopyranoside (IPTG) at an $OD_{600\ nm}$ of 0.7-0.9 and incubation continued for an additional 4 hrs with shaking. The harvested cells were then suspended in 100 mM Tris-HCl pH 8.0 containing 300 mM KCl and disrupted using either sonication (4 × 15 sec. pulse-on followed by 4 × 30 sec. pulse-off intervals) or French press (800 psi). Because the SR protein is sensitive to proteases, 1 mM phenylmethylsulfonyl fluoride (PMSF) was added to the suspended cells prior to cell lysis. After removing cell debris by centrifugation at 12,000*g* for 10 min, the supernatant was applied to a Ni-NTA column (Qiagen) and

eluted using a linear imidazole gradient of 30-180 mM dissolved in the sonication buffer. The purity of the protein was monitored using SDS-PAGE with the gel stained with Coomassie® Brilliant Blue G-250.

6-2-4. Enzyme assay

Enzyme assays were performed spectrophotometrically at 25 °C by following the reduction of NAD^+ (substituted for $NADP^+$) (*14*) and measuring the increase of absorbance at 340 nm ($\varepsilon_{340\ nm}$ 6.22 $mM^{-1}cm^{-1}$) using a Beckman DU-640 spectrophotometer. The reaction mixture contained 100 mM Tris buffer (pH 9.0), 3 mM saccharopine, and 0.2 mM NAD^+ in a 1 mL quartz cuvette. One unit (U) of SR enzyme activity is equivalent to one μmole of product (in this case NADH) formed per min (at pH 9.0, 25 °C).

6-2-5. Protein crystallization

Crystal Screen kit and Crystal Screen 2 kit from Hampton Research were used for initial crystallization trials using the hanging-drop vapor diffusion method. The following home-made screening kits were also used to explore a range of precipitants and buffer pH: 1) A range of 6-18% PEG 4000 vs pH (50 mM buffer solutions: sodium citrate pH 3.0, sodium acetate pH 5.0, imidazole pH 7.0, sodium borate pH 9.0), 2) A range of 2.2-2.6 M ammonium sulfate vs pH (50 mM buffer solutions: sodium citrate pH 3.0, sodium formate pH 4.0, sodium acetate pH 5.0, Bis-Tris pH 6.0, imidazole pH 7.0, Tris-HCl pH 8.0, sodium borate pH 9.0) and 3) A range of 2.3-

2.6 M ammonium sulfate vs pH (100 mM buffer solutions: Bis-Tris pH 6.5, Tris-HCl pH 7.0, Tris-HCl pH 7.5, Tris-HCl pH 8.0, Tris-HCl pH 8.5, Tris-HCl pH 9.0). Crystallization trials were performed by mixing 2 μL of the enzyme solution (13-14 mg/mL in 100 mM Tris-HCl pH 8.0, 300 mM KCl, and 150 mM imidazole) with the same amount of reservoir (precipitant) solution equilibrated over 1 mL reservoir solution at 25 °C using 24 well-VDX™ plates (Hampton Research).

6-2-6. Data collection and processing

For data collection, crystals were flash-frozen in a stream of nitrogen gas at a temperature of 100 K (Oxford Series 700 cryosystem) in mother liquor containing 10% glycerol as a cryoprotectant. X-ray diffraction data were collected using CuKα radiation (λ = 1.5418 Å) produced from a Rigaku/MSC RU-H3R rotating anode X-ray generator operated at 50 kV/100 mA and R-Axis IV^{++} image plate detectors. The crystal to detector distance was set at 120 mm, and 303 frames of data (see Appendix – Fig. A-16) were collected using an oscillation angle of 0.5°. The exposure time was set to 5 min per image. All data were processed with the d*TREK® data processing package (version 9.2D) (*15*).

6-2-7. Molecular replacement, model building, structure refinement and validation

The software program *Phaser* (version 1.3.1) was used for molecular replacement using maximum-likelihood techniques (*16-18*). The candidate model for molecular

replacement was the apo-saccharopine reductase from *M. grisea* (PDB code: 1E5L) in monomer form with side chains removed. For the $P3_1$ and $P3_2$ space groups, two copies of the candidate model were searched as a single component of the asymmetric unit such that the output is a dimer. However, only one copy of the candidate model was searched as a single component of the asymmetric unit for the $P3_121$ and $P3_221$ space groups. A medium-range resolution dataset of 8.0-3.0 Å was used for both rotation and translation searches using the fast rotation function (FRF) and fast translation function (FTF), respectively. The Euler angles for the solutions output from the rotation function were automatically input into the *Phaser* module for the translation search.

Automated model building was carried out using *ARP/wARP* (*19, 20*) (version 6.1) starting from the model obtained from molecular replacement. The initial model was refined by ten cycles of auto-building along with five refinement sub-cycles (total 50 cycles) of *REFMAC* (*21*) (version 5.0) using the *CCP4* program suite (version 5.0.1) (*22*). After removing the residues outside the main domains of the protein, manual model building was performed for missing residues using *XtalView/Xfit* software (version 4.1) (*23*), followed by 20 cycles of maximum-likelihood refinement using *REFMAC*. The *ARP/wARP* program was used to add solvent atoms. The quality of the structure factor data and stereochemical properties of the final model were checked using the *SFCHECK* (*24*) and *PROCHECK* (*25*) programs implemented in the *CCP4* program suite (*22*).

6-2-8. Molecular graphics

All of the figures in this paper were prepared and rendered using *PyMOL*™ version 0.97 (*26*) or *XtalView* (*23*).

6-3. Results

6-3-1. Expression and purification of saccharopine reductase

The SR produced in the BL21-Star™(DE3)-RIL cells using the pET expression system was very high, about 22% of the total soluble proteins. The elution profile of SR from the Ni-NTA column shows that the enzyme begins to elute at an imidazole concentration of 90 mM with the highest concentration in fractions eluted between 150 and 180 mM imidazole (data not shown). The purity of the eluted SR was estimated to be ≥ 98% based on Coomassie-stained SDS-PAGE gels (see Appendix – Fig. A-13). The amount of purified enzyme obtained is 10-12 mg from 150 mL of cell culture.

6-3-2. Protein crystallization

No crystals were observed using Crystal Screen kit and Crystal Screen 2 kit from Hampton Research. Further studies showed that these sparse matrix screens do not contain the minimal appropriate conditions (see below) for promotion of the crystal growth.

Home-made screen #1 did not show any sign of crystal growth. However, diffraction-quality single crystals were obtained using home-made screen #2 (see

Appendix – Fig. A-14). Crystals usually appeared within 5-7 days with average dimensions of 0.14 × 0.14 × 0.18 mm. The diffraction quality single crystals can be morphologically categorized as truncated hexagonal prisms (see Appendix – Fig. A-15). Checking the final pH of the screening solutions (as an additional internal control), showed that SR crystallizes within a narrow pH range of 7.0-7.5, with the highest number of single crystals obtained in 50 mM Bis-Tris (pH 7.2) containing 2.4 M ammonium sulfate. Using home-made screen #3, a pH range of 7.0-7.5 and ammonium sulfate concentration of 2.4-2.5 M and freshly purified enzyme appeared to be optimal for crystallization of SR.

6-3-3. Activity

To check the activity of the crystallized enzyme, four medium-sized crystals were transferred to the mother liquor for washing. The crystals were then dissolved in 100 mM Tris buffer (pH 9.0) and used for enzyme assay. The SR enzyme remains active in crystalline form at room temperature for a long period. The results of an enzyme assay (*14*) performed on crystals 60 days after the preparation of the crystallization screen, showed that the enzyme in crystalline form was almost as active as the enzyme stored at -80 °C. Under the conditions used for enzyme assay, specific activities of 2.6 and 4.0 U/mg were calculated for the enzyme that was in the crystalline form and the enzyme solution stored at -80 °C, respectively.

6-3-4. Data collection and processing

Initial processing of the dataset revealed that four possible trigonal space groups ($P3_1$, $P3_2$, $P3_121$, $P3_221$) should be considered. The data collection statistics seemed reasonable when processed in these space groups and all four space groups represent the general $l = 3n$ reflection condition that was obvious as systematic absences in the scaled reflection file. Space groups $P3_2$ and $P3_221$ were ruled out as they did not give reasonable molecular replacement solutions. Molecular replacement and model refinement were successful in the $P3_121$ and $P3_1$ space groups with the asymmetric unit as a monomer or dimer, respectively. In the case of the $P3_1$ space group, the SR dimer interface is coincident with a crystallographic axis in the $P3_121$ space group. Therefore, the higher symmetry space group ($P3_121$) with the asymmetric unit as monomer was the space group of choice (Table 6-1). In this case, the crystal packing shows the dimeric form of the SR. A Matthews' coefficient (*27*) of 2.90 Å^3/Da was calculated for both space groups (asymmetric unit as dimer for $P3_1$ and as a monomer for $P3_121$) corresponding to a solvent content of 57.5%.

Table 6-1: Summary of data collection statistics

Space group	$P3_1$	$P3_121$
$a = b$ (Å)	85.28	85.28
c (Å)	141.97	141.98
Resolution (Å)	40.0-1.70	40.0-1.70
Number of observations	459,467	465,261
Unique reflections	120,831	64,787
Completeness (%)	95.1 (92.3)[b]	97.6 (95.9)
Mean $I/\sigma(I)$	12.7 (3.2)	15.8 (4.3)
R_{sym}[a] (%)	5.2 (28.3)	5.6 (36.8)

[a] $R_{sym} = \frac{\sum\left(I_j - \bar{I}_j\right)}{\sum\left(\bar{I}_j\right)}$, **where** I_j **is the intensity measurement for a given reflection, and** $\bar{I}_j$ **is the average intensity for multiple measurements of this reflection.**

[b] **Values in parentheses correspond to the highest resolution shell (1.76-1.70 Å).**

6-3-5. Molecular replacement, model building, structure refinement and validation

As shown in Table 6-2, the value of LLG (Log-Likelihood Gain) as reported by the *Phaser* program is an indication of the success of a candidate model used for macromolecular phasing in a specific space group. No solution could be found for either $P3_2$ or $P3_221$ space groups suggesting that $P3_1$ and $P3_121$ were the most probable space groups. In the case of the $P3_121$ space group, the initial model had an R factor of 51.5% (R_{free} = 50.3%) and 434 out of 446 residues were built in 6 chains at the end of cycle eight with a connectivity index of 0.97 and an R factor of 19.4% (R_{free} = 28.7%). Missing residues were built using *XtalView* and four sulfate anions were added to positions with high F_o-F_c electron density and proper geometry. The first methionine residue of the protein as well as the 21 residue deca-histidine tag could not be built because of missing electron density. Also, part of the electron density for the side chains of the surface-located residues Phe12 and Lys44 is missing. The final model was refined using *REFMAC*. The final protein model, which is the monomer form ($P3_121$) contains 445 residues, 349 water molecules and 4 sulfate anions. Pro126 and Pro414 adopt a *cis* conformation and surprisingly, Trp173 was also found to be in *cis* conformation (see below). The refinement statistics of the final model are summarized in Table 6-3.

Table 6-2: Results of molecular replacement

Space group	Asymmetric unit	LLG[a] (Initial)	LLG (Refined)
$P3_1$	Dimer	619.26	685.19
$P3_121$	Monomer	332.69	366.24

[a] LLG: Log-Likelihood Gain.

Table 6-3: Summary of the refinement statistics for the $P3_121$ space group.

Resolution (Å)	40.0-1.70
R_{cryst} (R_{free}[a]) (%)	19.8 (24.0)
Avg. B factor (all) (Å^2)	26.7
Avg. B factor (main) (Å^2)	25.2
Avg. B factor (side) (Å^2)	28.3
Asymmetric unit	Monomer
No. of protein atoms	3444
No. of solvent molecules	(349 H_2O + 4 SO_4^{2-})
RMS deviation	
Bond length (Å)	0.014
Bond angle (°)	1.41
Ramachandran plot (% residues in)	
Most favored regions	94.4
Additional allowed regions	5.6
Generously allowed regions	0.0
Disallowed regions	0.0

[a] **R_{free} was calculated using 5% of the diffraction data.**

6-3-6. Overall structure

Similar to the enzyme from *M. grisea* (*3*), the SR from *S. cerevisiae* folds into three domains. The overall structure of the enzyme and a topology diagram (www.tops.leeds.ac.uk) is presented in Fig. 6-1. Domain I (residues 1-124 and 387-438), which is a variant of Rossmann fold (*12*), consists of a seven-stranded β-sheet (β1-6 and β15), sandwiched between three helices (α3-5) on one side and four helices (α1-2, α17-18) on the other side. Domain II (residues 125-247, 351-386, 439-446) which is composed of an α/β fold, contains a central seven-stranded mixed β-sheet (β7-9, β12-14 and β16). The β-sheet of domain II is surrounded by helices α6 and α10 on one side and helices α7-9, and strands β10-11 on the other side. The loop connecting the β10 and β11 strands is involved in dimer interaction. Domain II has a

unique fold that is known as saccharopine reductase fold (*3*). Domain III (residues 248-350) is an all-helical domain composed of helices α11-16.

The dimer interface for the SR from *S. cerevisiae* is similar to the interface reported for the SR from *M. grisea* (*3*) (Fig. 6-2A). The two subunits of the homodimer enzyme are related by twofold symmetry. The interface residues consist of 45% polar and 55% nonpolar residues. The loop connecting the β10 and β11 strands has the highest contribution to the dimer interface interaction (Fig. 6-2B). Also, the residues from helices α7 and α15, and β strands β14 and β16 participate in dimer interface interactions. The total buried surface area in both subunits is 2213 $Å^2$ (calculated using a probe with a radius of 1.4 Å) (www.biochem.ucl.ac.uk/bsm/PP/server), which is 5.6% of the total surface area of the enzyme. Fourteen hydrogen bonds are responsible for the subunit-subunit interactions in the homodimer enzyme molecule (Table 6-4).

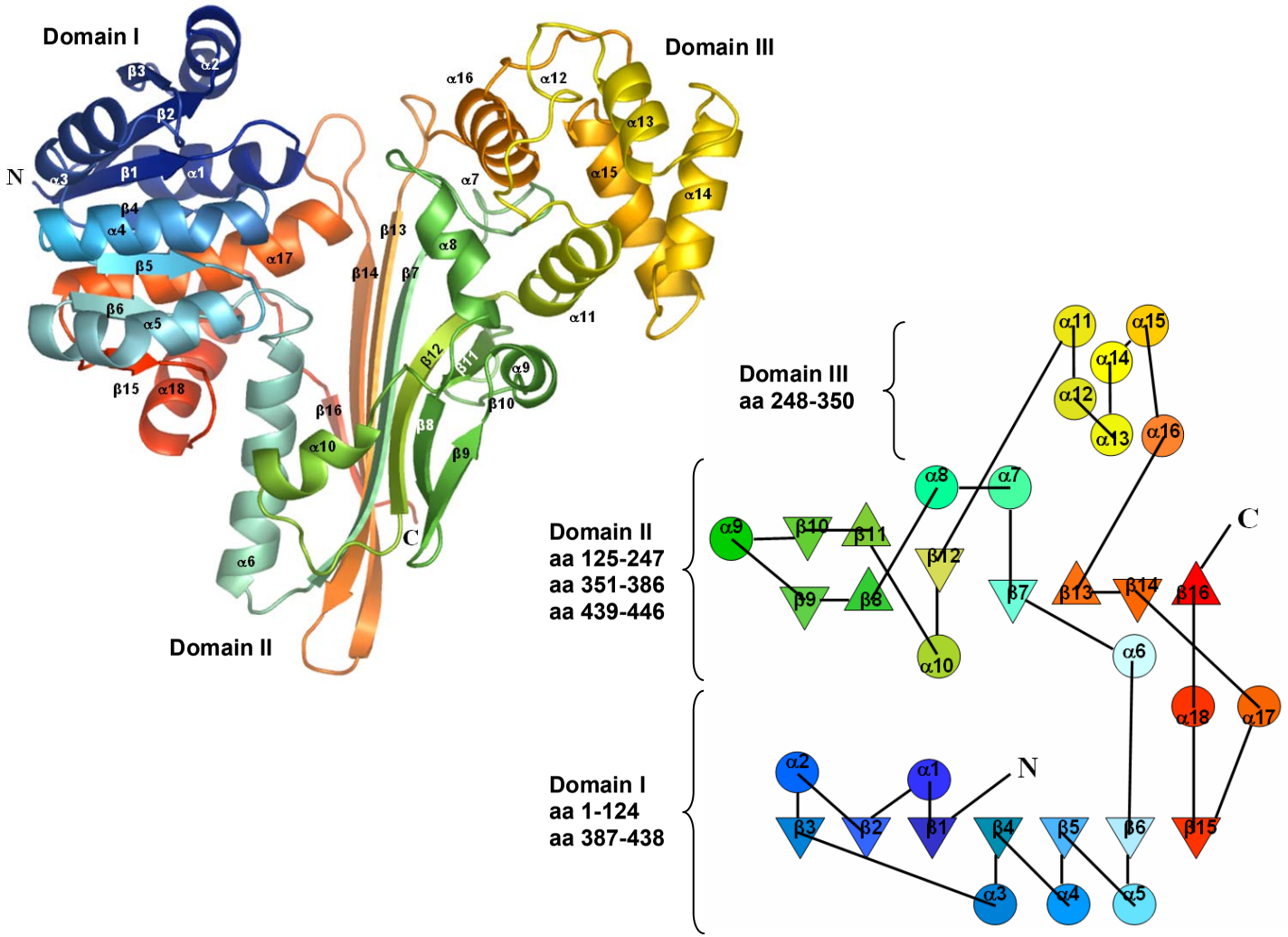

Fig. 6-1: Saccharopine reductase from *S. cerevisiae*. A ribbon representation of the enzyme monomer shows that it consists of three domains: domain I is a modified Rossmann fold, domain II is an α/β fold with central seven-stranded mixed β-sheet flanked by α-helices, domain III in an all-helical fold. The topology diagram of the enzyme with residue assignments is also given.

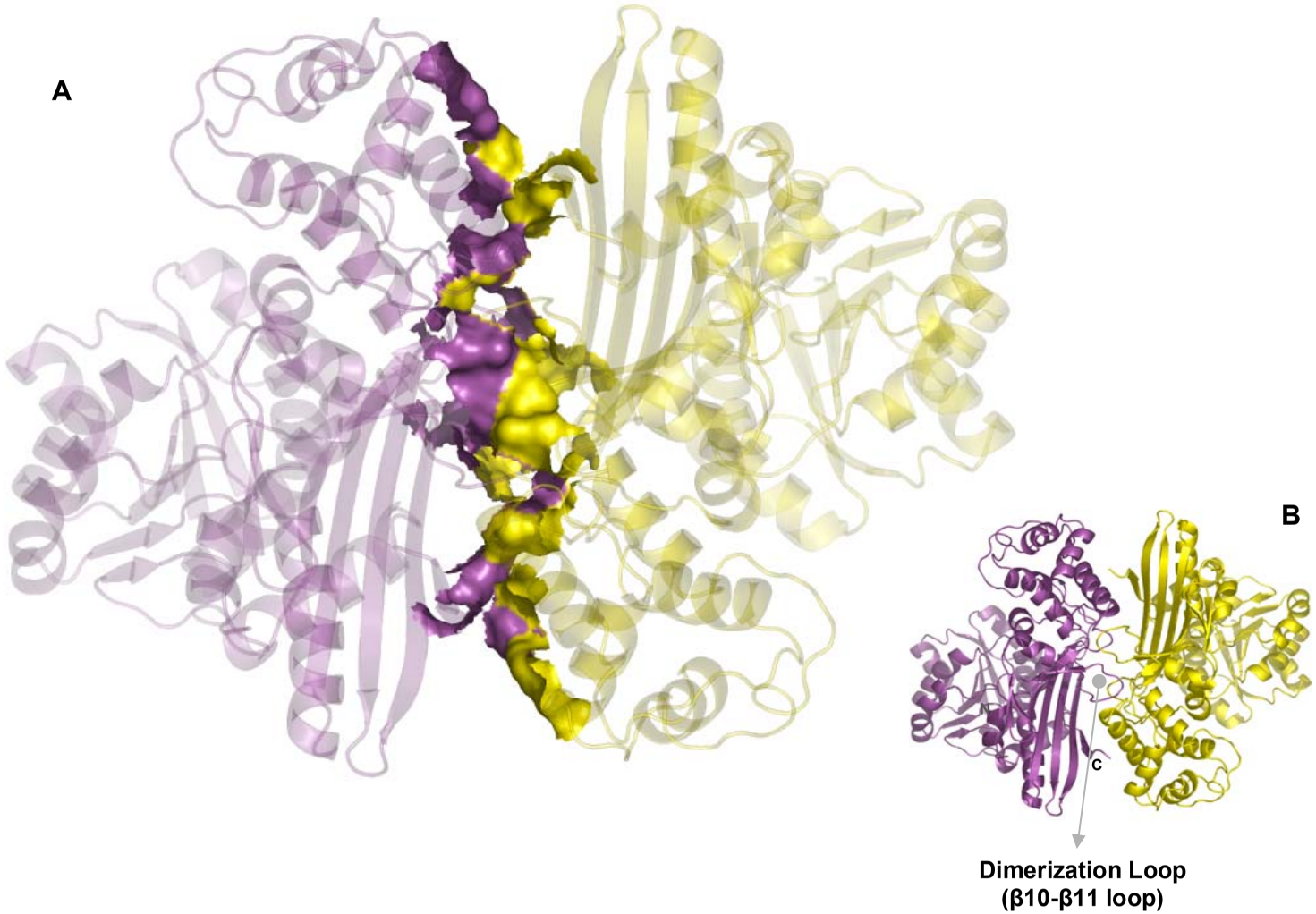

Fig. 6-2: Dimer interface of the SR enzyme. The total buried surface area involving in forming the dimer interface is 2213 Å^2 highlighted in molecular surface representation in panel A. Monomer A and B are shown in ribbon representation in yellow and magenta, respectively. The molecular two-fold axis of symmetry is perpendicular to the page. The loop connecting β10 and β11 strands is called the dimerization loop (panel B).

Table 6-4: Hydrogen bond interactions in homodimer interface

Subunit A/Subunit B intermolecular contacts (hydrogen bond interactions[a])				
Chain A residues	Location	Chain B residues	Location	Distance (Å)
Glu161 Oε1	α7	Tyr382 Oη	β14: C-term	2.91
Ser163 Oγ	α7	Gly214 N	β10-11 loop	2.97
Asp164 Oδ2	α7	Lys443 Nζ	β16: C-term	2.71
Pro213 O	β10-11 loop	Gln248 Nε2	β12: C-term	2.98
Gly214 N	β10-11 loop	Ser163 Oγ	α7	3.00
Gly214 O	β10-11 loop	Ala216 N	β10-11 loop	2.96
Tyr215 O	β10-11 loop	Gln248 Nε2	β12: C-term	2.70
Ala216 N	β10-11 loop	Gly214 O	β10-11 loop	3.03
Gln248 Nε2	β12: C-term	Tyr215 O	β10-11 loop	2.81
Gln248 Nε2	β12: C-term	Pro213 O	β10-11 loop	2.93
Ser316 Oγ	α15	Ala446 O	β16: C-term	2.84
Arg354 Nη2	β13: N-term	Arg354 Nη2	β13: N-term	2.94
Tyr382 Oη	β14: C-term	Glu161 Oε1	α7	2.90
Ala446 O	β16: C-term	Ser316 Oγ	α15	2.88

[a]Identified using the CONTACT program implemented in CCP4 program suite with donor-acceptance cutoff distance of ≤3.2 Å, and by visual inspection.

6-4. Discussion

On the basis of structural comparisons and alignment between the SR from *S. cerevisiae* and the SR from *M. grisea*, the two structures have small differences in the relative positions of the domains (Fig. 6-3). The superposition of the two apo enzymes (performed using *LSQKAB* implemented in the *CCP4* program suite (*22*)) yields a main chain RMS displacement of 4.7 Å. Individual domain superposition for domains I, II, and III give the RMS values of 4.8, 4.1 and 3.5 Å, respectively. The molecular packing of SR in space group $P3_121$ brings part of domain II from one SR molecule into close proximity of the active site of another SR molecule resulting in the active site being partially buried. This kind of interaction is different from the molecular packing interaction observed for SR from *M. grisea* in space group $C222_1$ in which the

active site is completely open to solvent (*3*). The relative location of the active site based on SR from *M. grisea* is shown in Fig. 6-3.

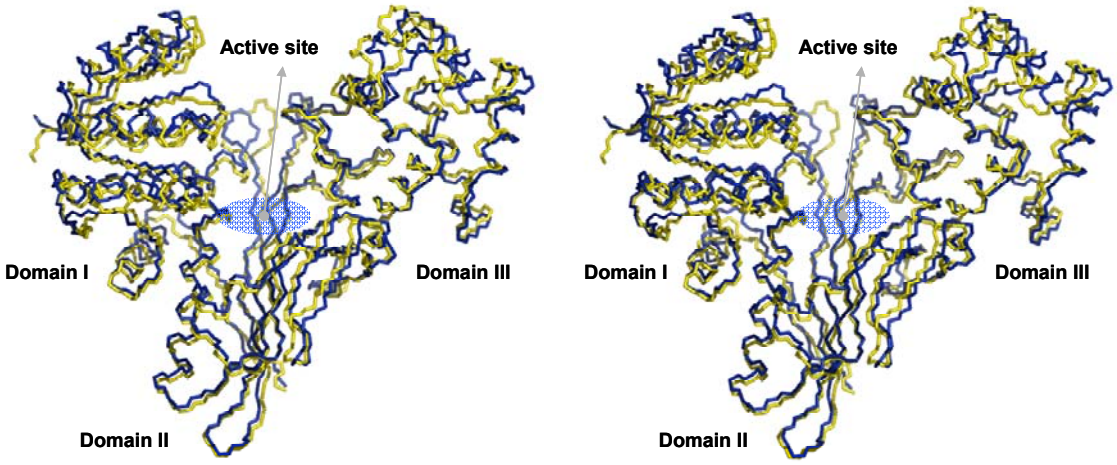

Fig. 6-3: Stereoview of structural superposition of the apo-SR molecules from *M. grisea* (yellow) and *S. cerevisiae* (blue). Overall RMS deviation for main chain atoms is 4.7 Å. The position of the active site of the SR from *M. grisea* is also shown (blue oval).

In the *S. cerevisiae* SR, Trp173 is in close contact with Gly144 from a symmetry-related molecule suggesting that the *cis* conformation of Trp173 is an induced conformation, due to close molecular packing in the $P3_121$ space group. In the structure of the SR from *M. grisea* *trans*-Trp174 is the equivalent residue to the Trp173 of the SR from *S. cerevisiae*. The two amino acids can be superposed at the same location in terms of the structural position. However, the side chain conformation of the two amino acids is different (Fig. 6-4). It has been reported that in the case of the SR from *M. grisea*, Trp174 forms a hydrophobic contact against the active site allowing the enzymatic reaction to occur. Trp174 is also in close contact to

the nicotinamide ring of the NADPH thus influencing the geometric position of the cofactor (*3*).

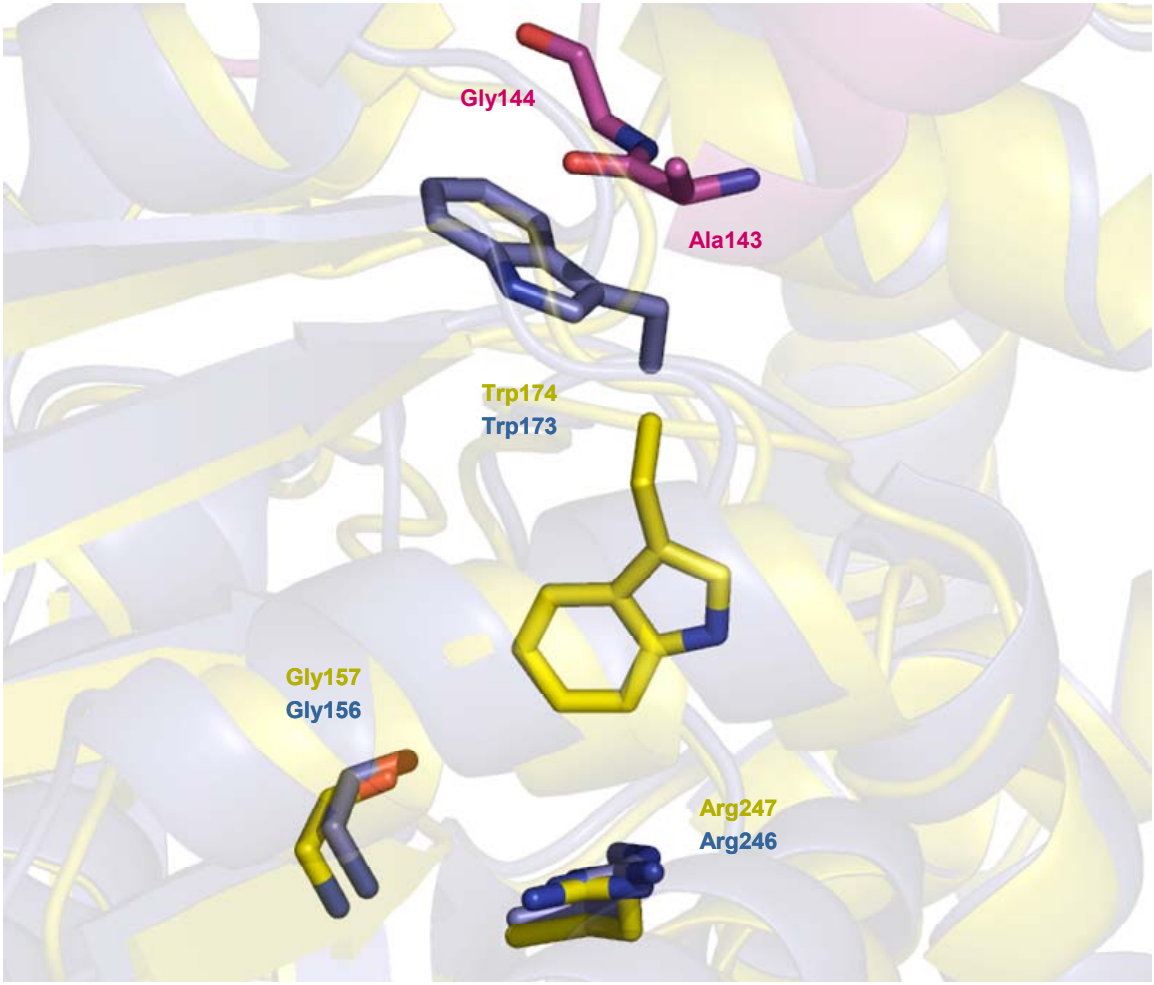

Fig. 6-4: Structural superposition of the apo-SR molecules from *M. grisea* (yellow) and *S. cerevisiae* (blue) focusing on the positions of Trp173 and Trp174. Trp174 (*M. grisea*) maintains a *trans* conformation while Trp173 (*S. cerevisiae*) exists as an induced *cis* conformation due to the molecular packing interactions. The interaction between Trp173 and the residues (Ala 143 and Gly 144) from a symmetry-related SR molecule is also shown.

The *cis*-Pro126 of SR from *S. cerevisiae* is equivalent to *cis*-Pro127 of SR from *M. grisea*. The carbonyl group of the Pro127 forms a hydrogen bond to the amine

group of the amide of the nicotinamide ring of the NADPH which requires the proline to be in *cis* conformation (*3*). A similar role is suggested for the Pro126 of the SR from *S. cerevisiae*. These two prolines are located in the same structural position when the two SR enzymes are superposed. *cis*-Pro414 is part of a loop in domain I connecting the helix α17 to strand β15 .The equivalent residue to *cis*-Pro414 in the SR from *M. grisea* is Arg418. The functional role of this replacement is unknown.

The ternary complex of the SR from *M. grisea* with the bound saccharopine and NADPH, shows that Arg247, Arg224, and Ser99 interact with the carboxylate of the lysine moiety of saccharopine, carboxylate of the glutamate moiety of saccharopine, and side chain carboxylate of the glutamate moiety of saccharopine, respectively (*3*). The same roles in binding to saccharopine are suggested for the Arg246, Arg223, and Ser98 residues for the SR from *S. cerevisiae*. As shown in Fig. 6-5, the residues involved in the active site of the SR from *M. grisea* superpose very well to their equivalent residues in the SR from *S. cerevisiae*, strongly suggesting that the same residues are involved in forming the active site of SR from *S. cerevisiae*. The largest difference is in the side chain positions of Tyr99 and Tyr100. However, since the main chain of the Tyr residues are involved in substrate (saccharopine) binding (*3*), the difference in side chain position does not seem to be significant.

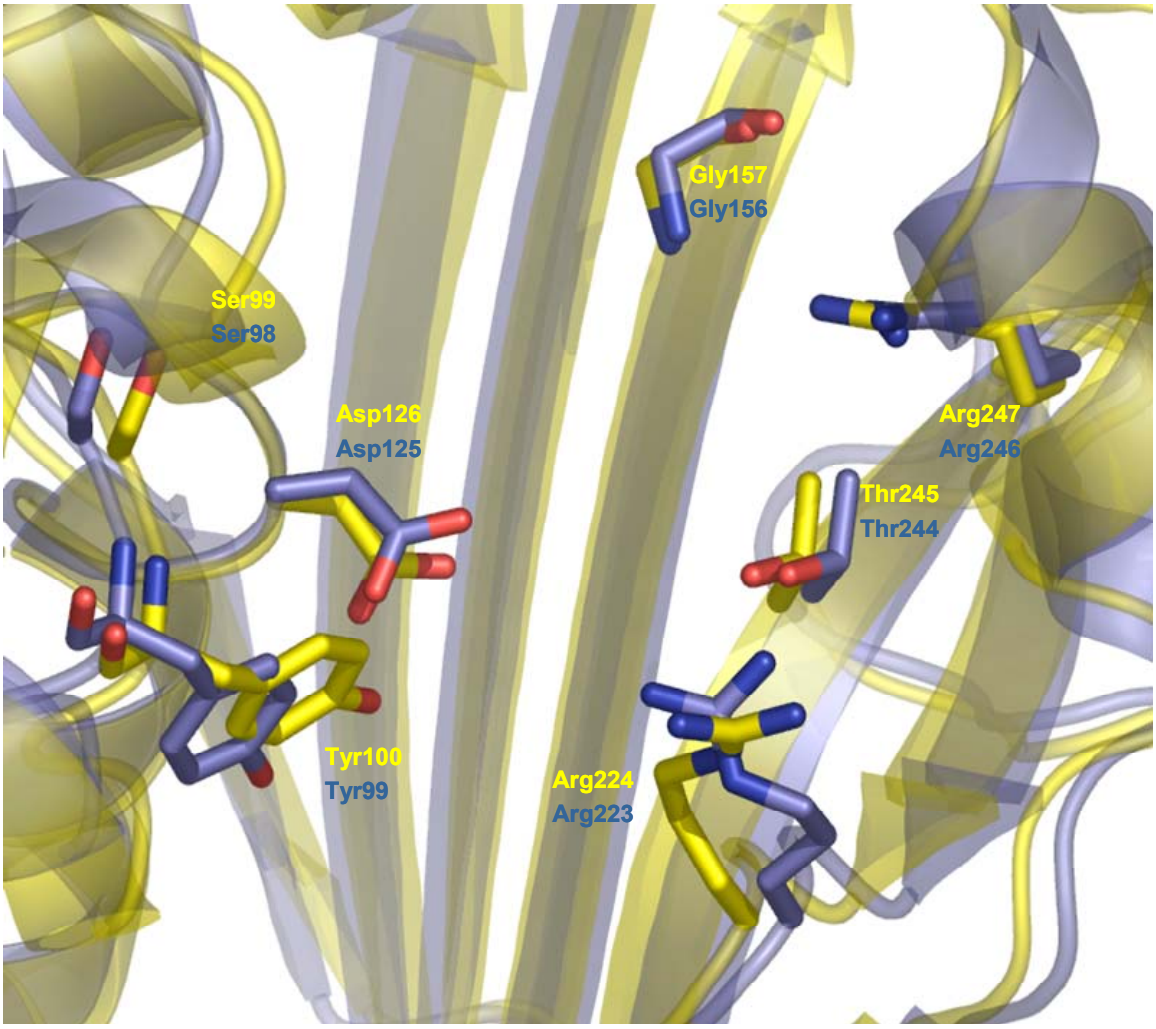

Fig. 6-5: Structural superposition of the apo-SR molecules from *M. grisea* (yellow) and *S. cerevisiae* (blue) focusing on the residues around the active site. The relative spatial positions of the residues and side chain orientation involved in the active site are well conserved.

Fig. 6, shows the superposition of the NADPH:Saccharopine:Enzyme ternary complex from *M. grisea* to the apo enzyme from *S. cerevisiae* (main chain RMS: 4.7 Å) suggesting that the substrates (saccharopine and NADPH) may bind in a similar manner to the active site of the enzyme from *S. cerevisiae*.

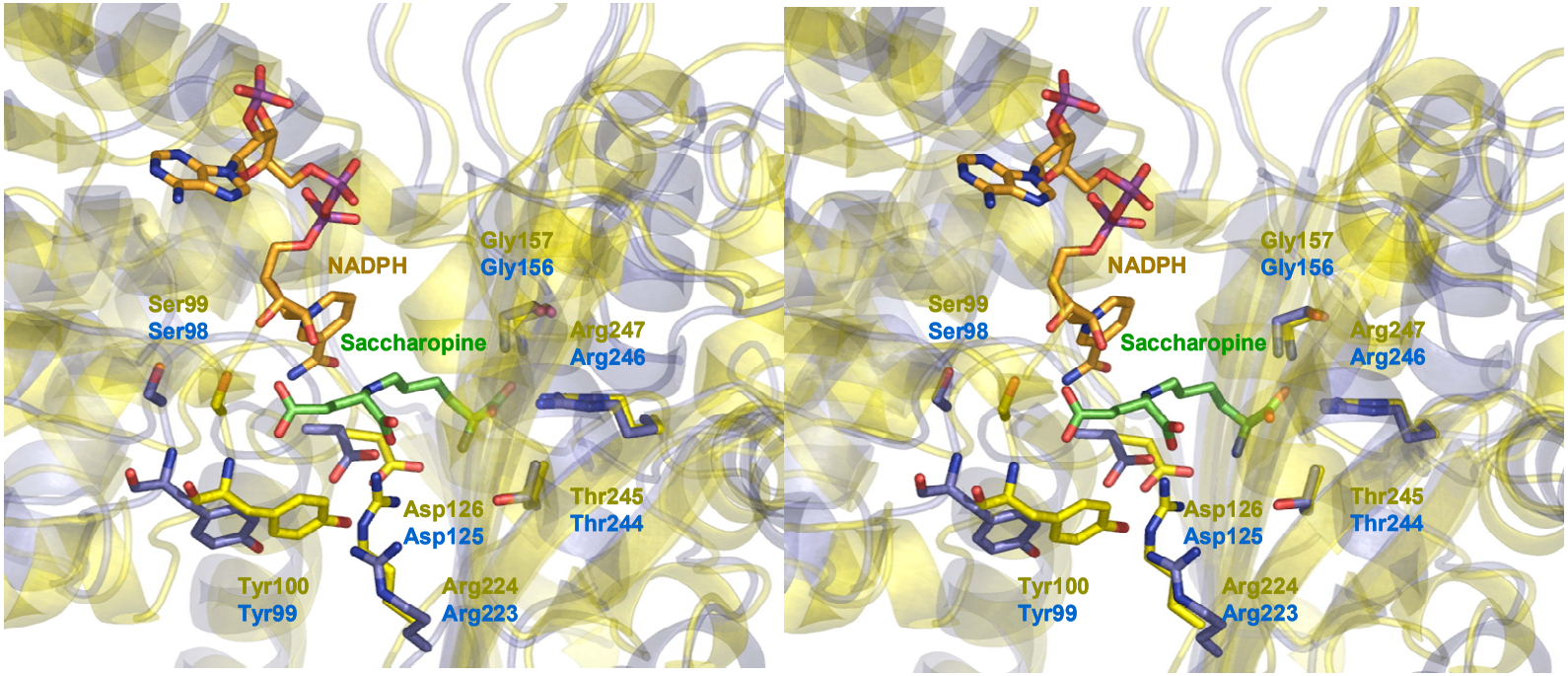

Fig. 6-6: Stereo diagram of the structural superposition of the apo SR molecule from *S. cerevisiae* (blue) with the NADPH:Saccharopine:SR ternary complex from *M. grisea* (yellow). The bound saccharopine molecule is shown in green.

Four sulfate anions (per monomer), likely originating from the crystallization solution, interact with residues of SR from *S. cerevisiae* (Fig. 6-7). Three of the four sulfate molecules are positioned to occupy the saccharopine carboxylate binding sites of SR from *M. grisea*. Arg246 interacts with one sulfate molecule as indicated by a very well-defined electron density for the sulfate. Arg246 is inside a hydrophobic core surrounded by Tyr169, Phe250, Val178, and Leu167 contributing to the rigidity of the Arg side chain that facilitate its interaction with sulfate molecule. A tetrahedral-shaped electron density map was interpreted as the second sulfate molecule interacting with Ser98 and the main chain nitrogen of Tyr77 (relative occupancy of 50%) (not shown). The third sulfate molecule interacts with both Arg223 and Arg242 with a relative occupancy of 50% (not shown). The fourth sulfate molecule (50% relative occupancy) binds in a position that brings together the side chains of the Arg354 from both chains A and B (not shown). The side chain of Arg354 from both chains A and B exist as two conformers.

Mapping the non-conserved residues between the SRs from *M. grisea* and *S. cerevisiae*, shows that a total of 92 out of 446 amino acids (21%) are different (Fig. 6-8). In terms of individual domains, 42 out of 176 residues differ within domain I (24%), 24 out of 167 residues are different within domain II (14%), and 26 out 103 residues differ within domain III (25%). Domain II shows the highest degree of conserved residues, suggesting that the fold is important for proper substrate binding as well as to keep the domain I and domain III in an appropriate spatial orientation for closing and opening the active site. However, the residues that differ do not impose

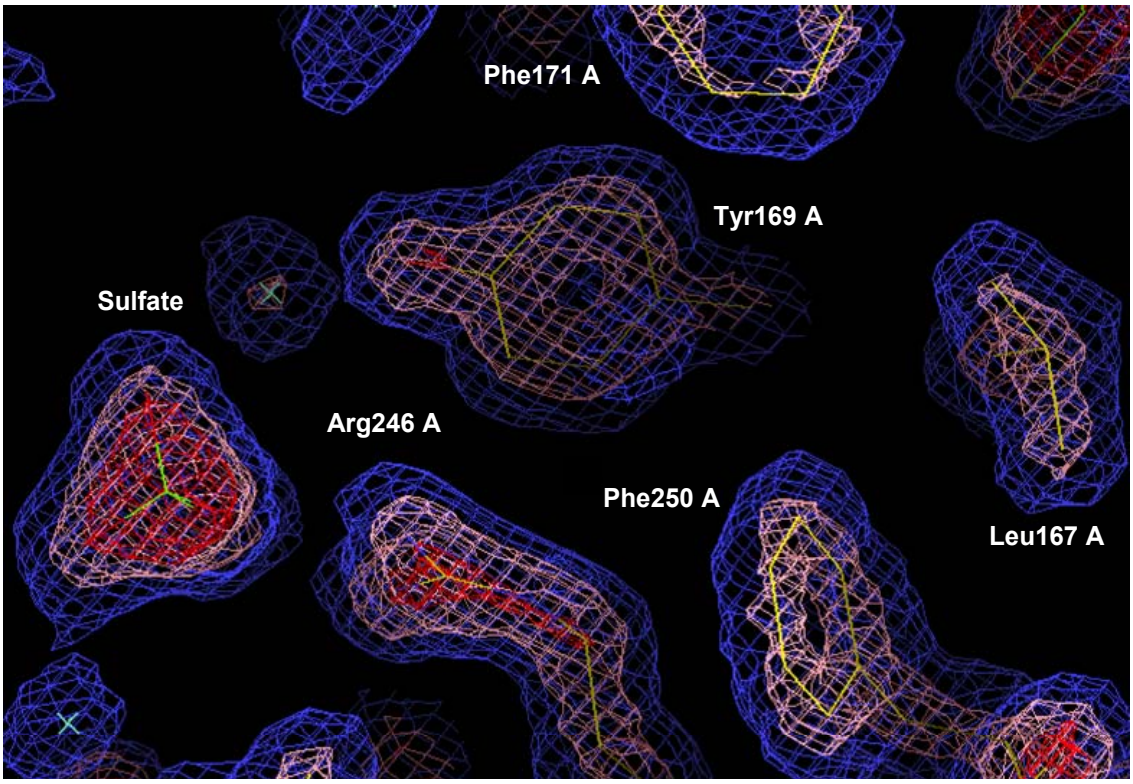

Fig. 6-7: Electron density of a sulfate molecules in the vicinity of Arg246. This residue has a rigid side chain because of the surrounding hydrophobic residues and hydrogen bond interactions to the sulfate molecule (Blue, 1σ; Pink, 3σ; Red, 5σ).

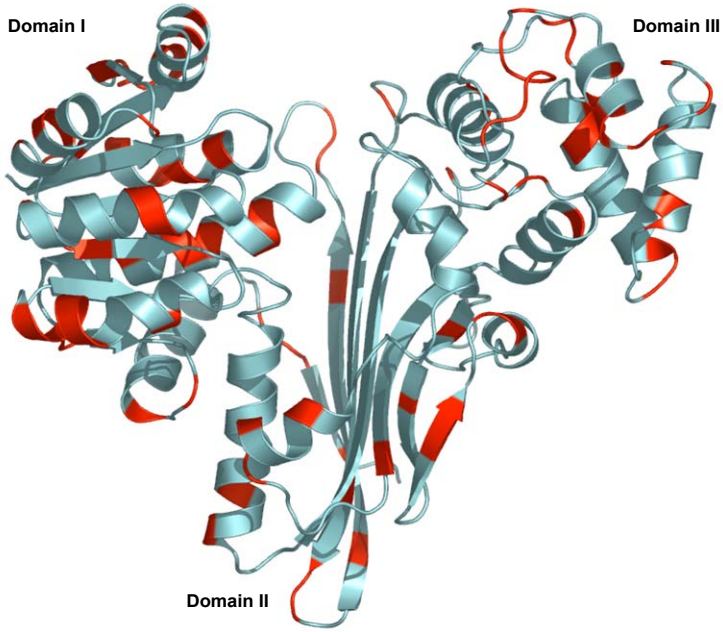

Fig. 6-8: Location of the non-conserved residues between SRs from *S. cerevisiae* vs. *M. grisea*. Areas depicted in red represent non-conserved residues. Domain II has the highest ratio of conserved residues.

any significant change to the total accessible surface area (calculated using *AREAMOL*

implemented in the *CCP4* program suite (*22*)) for the apo SRs, which are 19,789 and 19,680 $Å^2$, for the enzymes from *S. cerevisiae* and *M. grisea*, respectively.

Most of the enzymes similar to saccharopine reductase from *S. cerevisiae* and *M. grisea* belong to the aspartate family of amino acid biosynthesis pathways suggesting that some of these enzymes evolved from a common ancestor (*3*). The SR from *S. cerevisiae* shares significant similarities to the SR from *M. grisea* suggesting that the same evolutionary pathways are applicable in this case. The uniqueness of the α-aminoadipate pathway for the biosynthesis of lysine, make it a potential pathway for the structure-based drug design once the three-dimensional structures of the enzymes are in hand. The known structures of the saccharopine reductases from *M. grisea* (*3*) and *S. cerevisiae* could be the starting point for this endeavor.

6-5. Acknowledgements

We are grateful to Dr. Eric Enwall for assistance in data collection. We thank Dr. Lillian Chooback and Daniel M. Copeland for their technical assistance on crystallization and structure determination, respectively. We also wish to thank Dr. Fabiola Janiak-Spens, Dr. Stace Porter and Hui Tan for their helpful discussions on molecular biology experiments.

References

[1] Zabriskie, T. M., and Jackson, M. D. (2000) Lysine biosynthesis and metabolism in fungi, *Nat. Prod. Rep. 17*, 85-97.

[2] Talbot, N. J. (1995) Having a blast: exploring the pathogenicity of *Magnaporthe grisea*, *Trends Microbiol. 3*, 9-16.

[3] Johansson, E., Steffens, J. J., Lindqvist, Y., and Schneider, G. (2000) Crystal structure of saccharopine reductase from Magnaporthe grisea, an enzyme of the alpha-aminoadipate pathway of lysine biosynthesis, *Structure Fold Des. 8*, 1037-1047.

[4] Bhattacharjee, J. K. (1985) alpha-Aminoadipate pathway for the biosynthesis of lysine in lower eukaryotes, *Crit. Rev. Microbiol. 12*, 131-151.

[5] Broquist, H. P. (1971) Lysine biosynthesis (yeast), *Methods Enzymol. 17B*, 112-129.

[6] Jones, E. W., and Fink, G. R. (1982) Regulation of amino acid and nucleotide synthesis in yeast, in *Molecular biology of the yeast Saccharomyces, metabolism and gene regulation* (Strathern, J. N., Jones, E. W., and Broach, J. R., Eds.) pp 181-299, Cold spring harbor laboratory, Cold spring harbor, NY.

[7] Xu, H., Andi, B., Qian, J., West, A. H. and Cook, P. F. (2005) The α-aminoadipate pathway for lysine biosynthesis in fungi, *Cell Biochem. Biophys*., Manuscript submitted.

[8] Storts, D. R., and Bhattacharjee, J. K. (1987) Purification and properties of saccharopine dehydrogenase (glutamate forming) in the Saccharomyces cerevisiae lysine biosynthetic pathway, *J. Bacteriol. 169*, 416-418.

[9] Jones, E. E., and Broquist, H. P. (1966) Saccharopine, an intermediate of the aminoadipic acid pathway of lysine biosynthesis. 3. Aminoadipic semialdehyde-glutamate reductase, *J. Biol. Chem. 241*, 3430-3434.

[10] Bhattacharjee, J. K. (1992) Evolution of α-aminoadipate pathway for the synthesis of lysine in fungi, in *Evolution of metabolic function* (Mortlock, R. P., Ed.) pp 47-80, CRC Press, Boca Raton, Fla.

[11] Johansson, E., Steffens, J. J., Emptage, M., Lindqvist, Y., and Schneider, G. (2000) Cloning, expression, purification and crystallization of saccharopine reductase from Magnaporthe grisea, *Acta Crystallogr. D Biol. Crystallogr. 56 (Pt 5)*, 662-664.

[12] Rossmann, M. G., Liljas, A., Branden, C. I., and Banaszak, L. J. (1975) Evolutionary and structural relationship among dehydrogenases, *Enzymes 11*, 51-102.

[13] Pearl, F. M., Bennett, C. F., Bray, J. E., Harrisson, A. P., Martin, N., Shepherd, A., Sillitoe, I., Thornton, J., and Orengo, C. A. (2003) The CATH database: an extended protein family resource for structural and functional genomics, *Nucleic Acids Res. 31*, 452-455.

[14] Storts, D. R. and Bhattacharjee, J. K. (1987) Purification and properties of saccharopine dehydrogenase (glutamate forming) in the Saccharomyces cerevisiae lysine biosynthetic pathway, *J. Bacteriol. 169*, 416-418.

[15] Pflugrath, J. W. (1999) The finer things in X-ray diffraction data collection, *Acta Crystallogr. D Biol. Crystallogr. 55*, 1718-1725.

[16] Read, R. J. (2001) Pushing the boundaries of molecular replacement with maximum likelihood, *Acta Crystallogr. D Biol. Crystallogr. 57*, 1373-1382.

[17] Storoni, L. C., McCoy, A. J., and Read, R. J. (2004) Likelihood-enhanced fast rotation functions, *Acta Crystallogr. D Biol. Crystallogr. 60*, 432-438.

[18] McCoy, A. J., Grosse-Kunstleve, R. W., Storoni, L. C., and Read, R. J. (2005) Likelihood-enhanced fast translation functions, *Acta Crystallogr. D Biol. Crystallogr. 61*, 458-464.

[19] Lamzin, V. S., and Wilson, K. S. (1993) Automated refinement of protein models, *Acta Crystallogr. D Biol. Crystallogr. 49*, 129-147.

[20] Perrakis, A., Morris, R., and Lamzin, V. S. (1999) Automated protein model building combined with iterative structure refinement, *Nat. Struct. Biol. 6*, 458-463.

[21] Murshudov, G. N., Vagin, A. A., Lebedev, A., Wilson, K. S., and Dodson, E. J. (1999) Efficient anisotropic refinement of macromolecular structures using FFT, *Acta Crystallogr. D Biol. Crystallogr. 55 (Pt 1)*, 247-255.

[22] (1994) The CCP4 suite: programs for protein crystallography, *Acta Crystallogr. D Biol. Crystallogr. 50*, 760-763.

[23] McRee, D. E. (1999) XtalView/Xfit--A versatile program for manipulating atomic coordinates and electron density, *J. Struct. Biol. 125*, 156-165.

[24] Vaguine, A. A., Richelle, J., and Wodak, S. J. (1999) SFCHECK: a unified set of procedures for evaluating the quality of macromolecular structure-factor data and their agreement with the atomic model, *Acta Crystallogr. D Biol. Crystallogr. 55 (Pt 1)*, 191-205.

[25] Laskowski, R. A., MacArthur, M. W., Moss, D. S., and Thornton, J. M. (1993) PROCHECK: a program to check the stereochemical quality of protein structures, *J. Appl. Cryst. 26*, 283-291.

[26] Delano, W. L. (2004) The PyMOL molecular graphics system (San Carlos, CA: Delano Scientific).

[27] Matthews, B. W. (1968) Solvent content of protein crystals, *J. Mol. Biol. 33*, 491-497.

APPENDIX

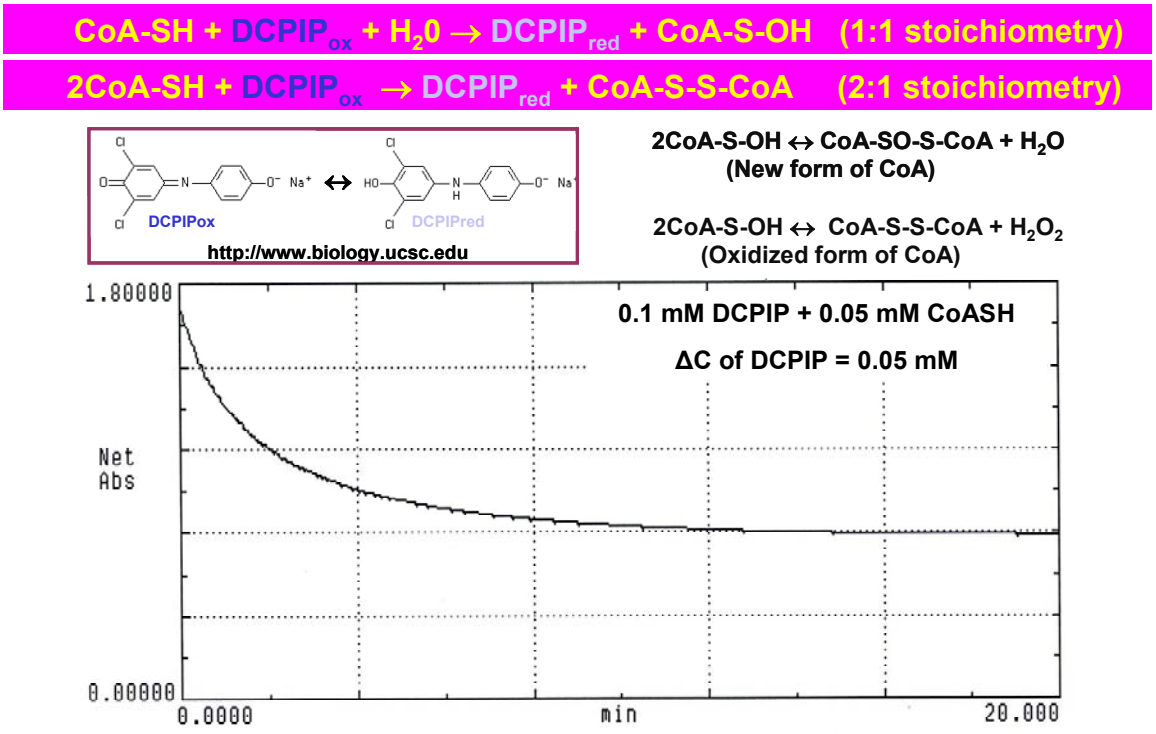

Fig. A-1: Stoichiometry of the reaction of DCPIP with CoA based on the spectroscopic assay.

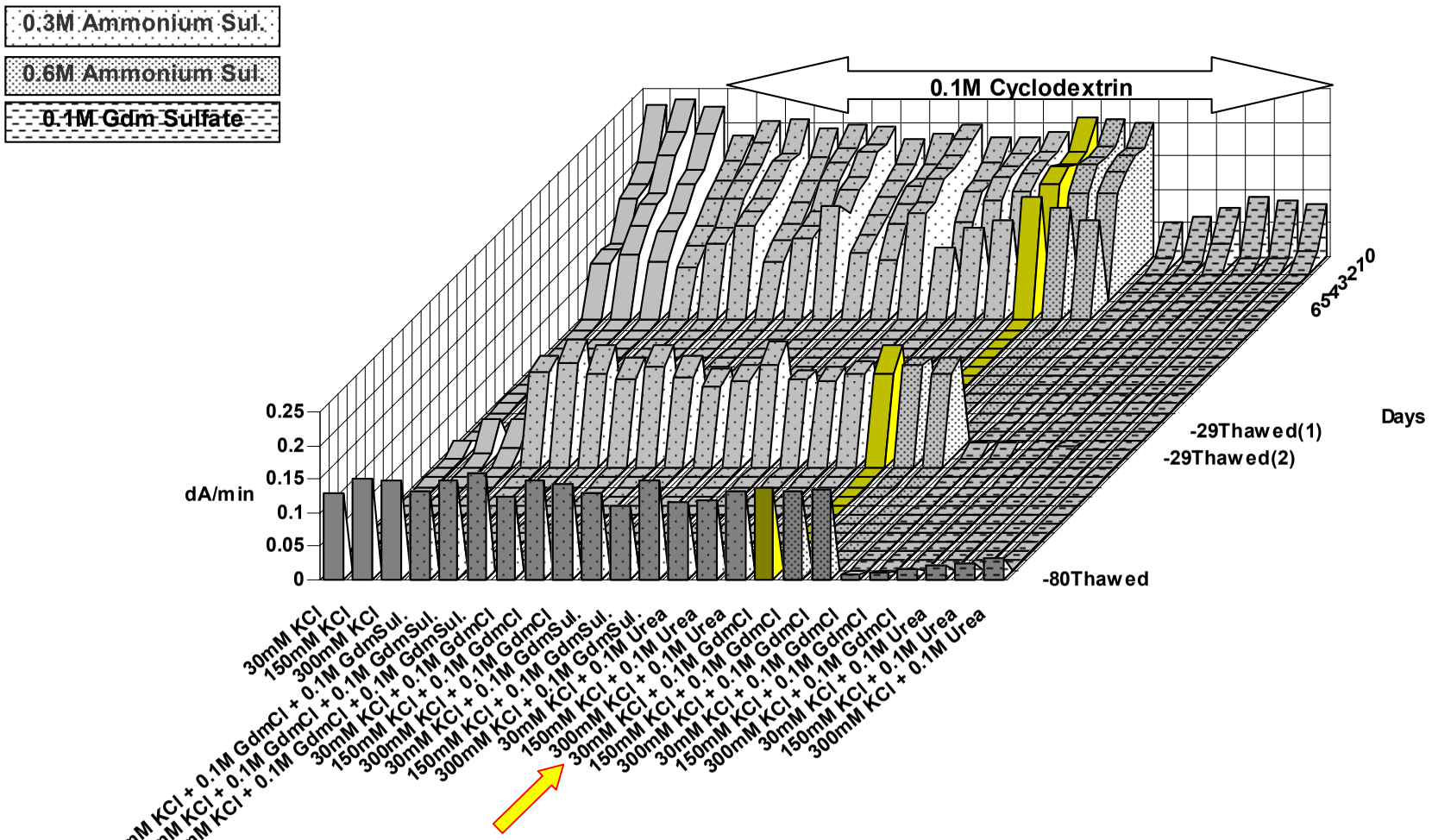

Fig. A-2: Effects of the different stabilization buffers on homocitrate synthase activity. Arrow shows the best condition for the HCS stabilization.

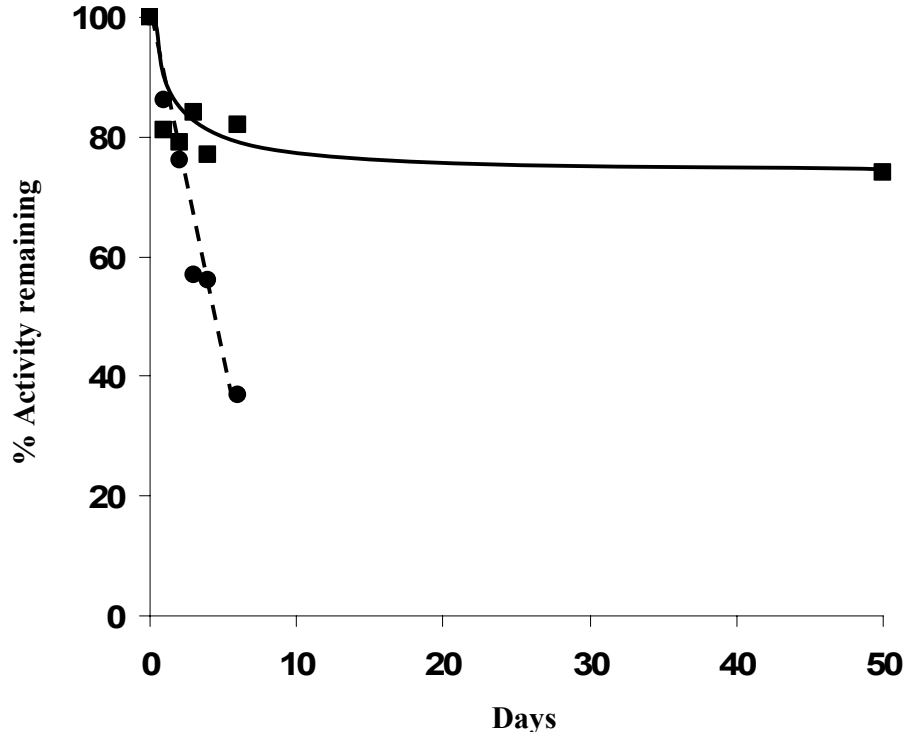

Fig. A-3: Activity of the homocitrate synthase in the absence (•) and presence of the stabilization buffer (100 mM α-cyclodextrin, 600 mM ammonium sulfate, 100 mM GdmCl) as the function of day.

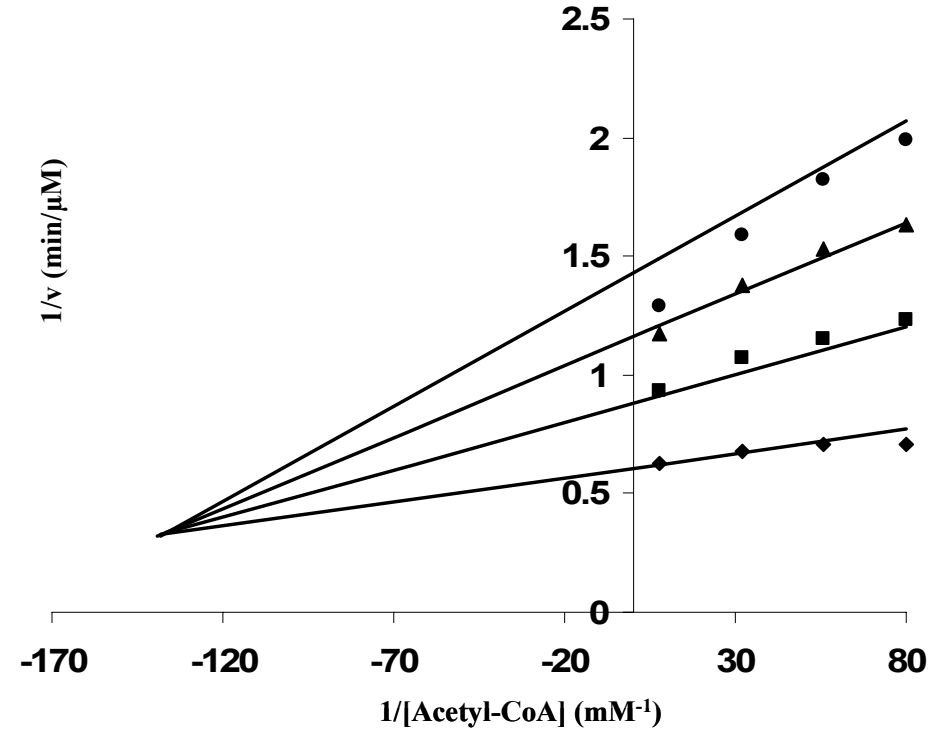

Fig. A-4: Initial velocity double-reciprocal plot for the HCS reaction using OAA as substrate. The concentrations of AcCoA are as plotted, while OAA is fixed at 50 mM (◆), 21.4 mM (■), 13.6 mM (▲), and 10 mM (•). The solid lines are drawn based on a fit to eq. 3, while the points are experimental.

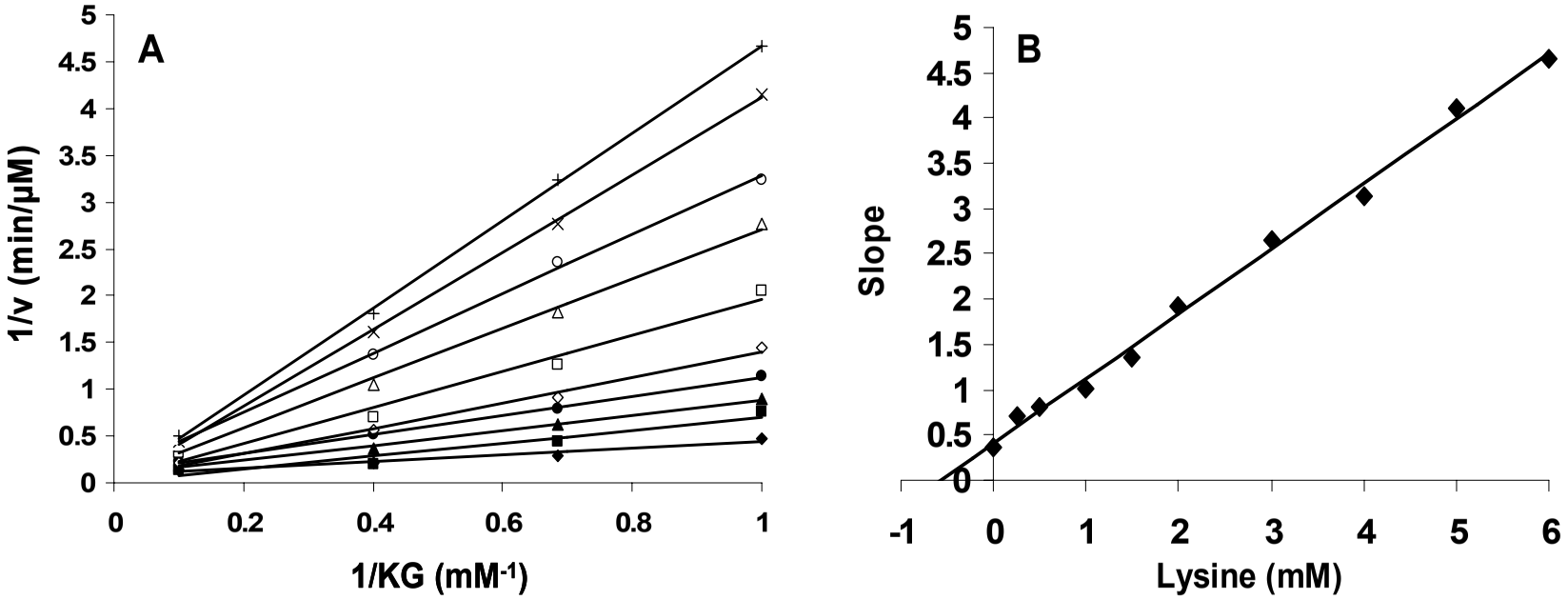

Fig. A-5: A. Inhibition of HCS by lysine. Concentrations of KG are as plotted, while AcCoA is fixed at 0.5 mM. Lysine concentrations are as follows: 0 mM (◆), 0.25 mM (■), 0.5 mM (▲), 1.0 mM (●), 1.5 mM (◊), 2.0 mM (□), 3.0 mM (Δ), 4.0 mM (○), 5.0 mM (×), and 6 mM (+). The solid lines are drawn based on the graphical analysis, while the points are experimental. B. The slope of the lines in A vs lysine concentration showing a linear inhibition with a $K_{i\,lys}$ of 0.5 mM.

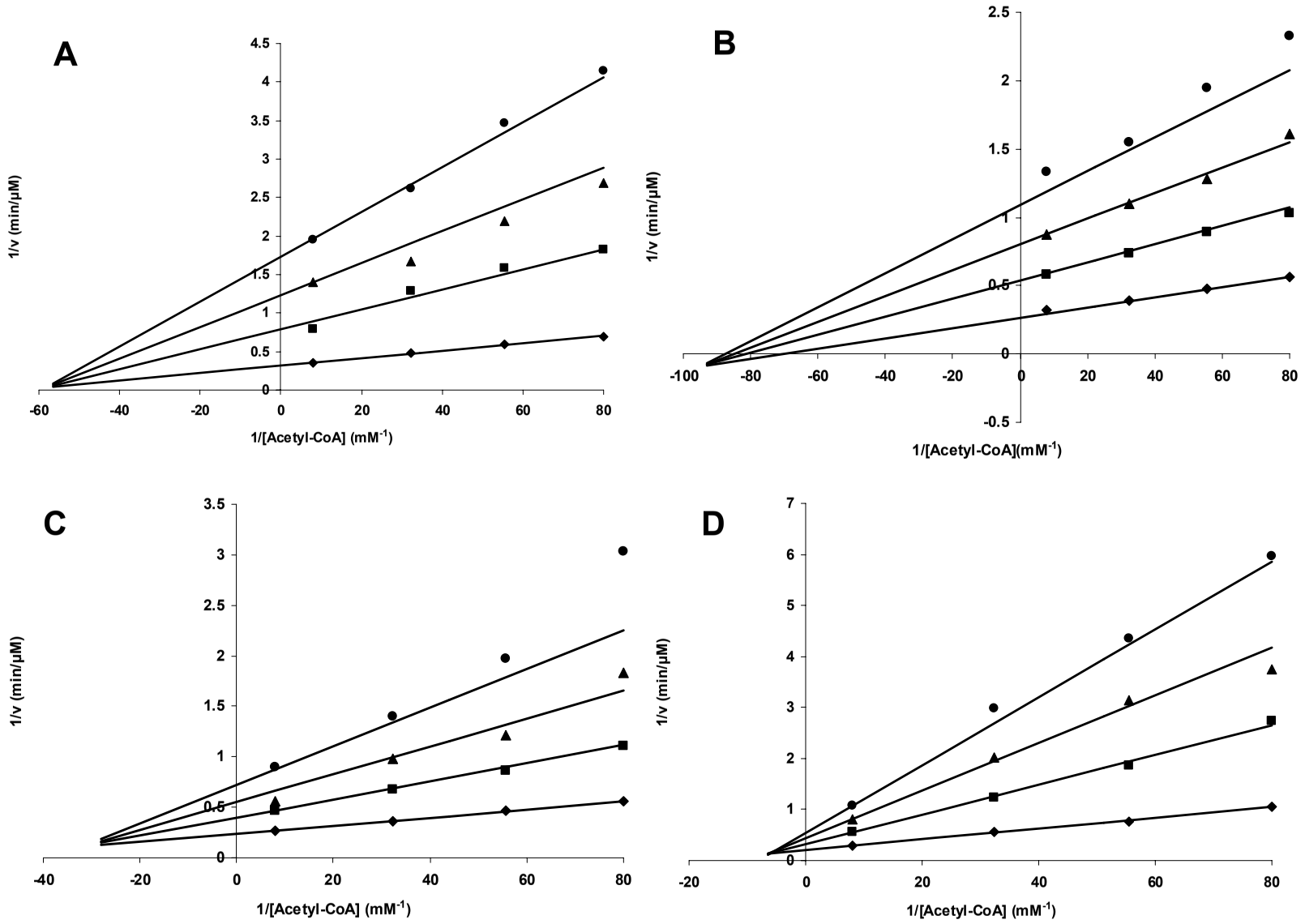

Fig. A-6: Initial rate studies of Na^+ inhibition and activation. Double reciprocal initial velocity patterns varying AcCoA at different fixed levels of α-Kg: 1 mM (●), 1.46 mM (▲), 2.5 mM (■), and 10 mM (◆) were measured in 50 mM Hepes, pH 7.5 and 25°C in the presence of the following Na^+ concentrations: (A) 0 mM, (B) 25 mM, (C) 100 mM, and (D) 250 mM. Points are experimental, while the solid lines are theoretical based on a fit to eq 3.

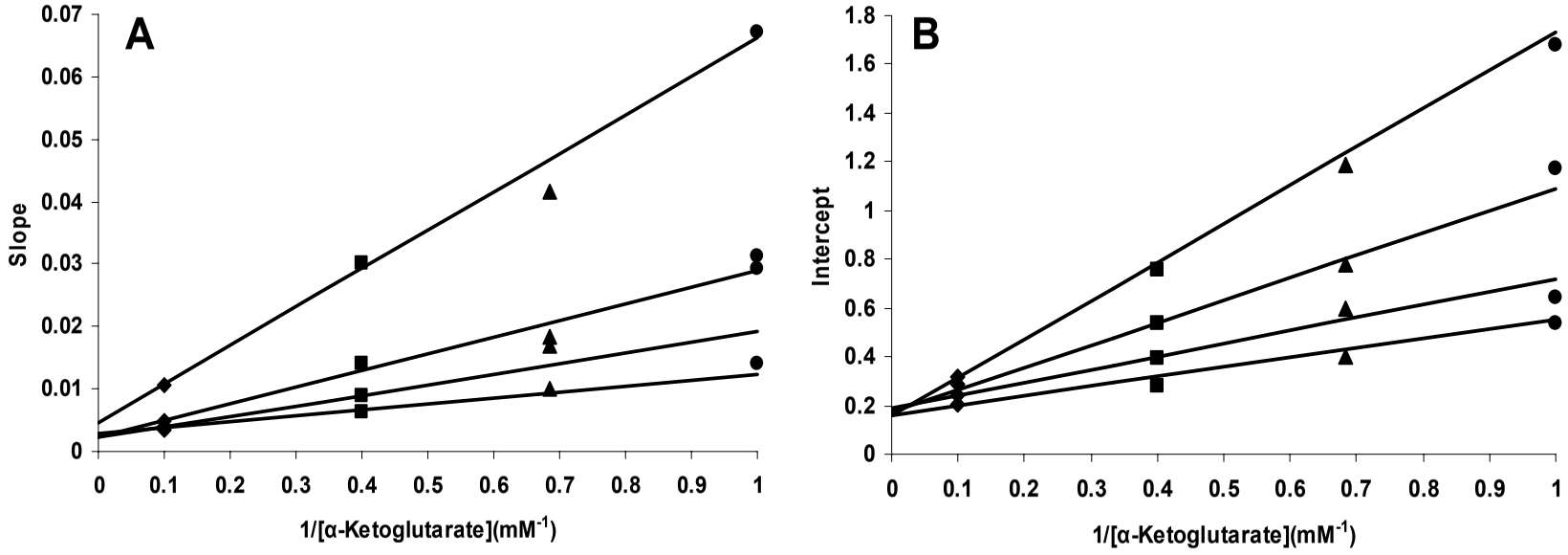

Fig. A-7: Secondary replots of the data in Fig. A-6. A. Slope replot constructed from the slope of the lines in Figs. A-6A-D vs. reciprocal of α-Kg concentration at each of the Na^+ concentrations indicated in Fig. A-6A-D. B. Intercept replot constructed from the intercept vs. reciprocal of α-Kg concentration as in A. Points are from a graphical analysis, while the solid lines in A and B are theoretical based on a fit to eq 3 (Chapter 4).

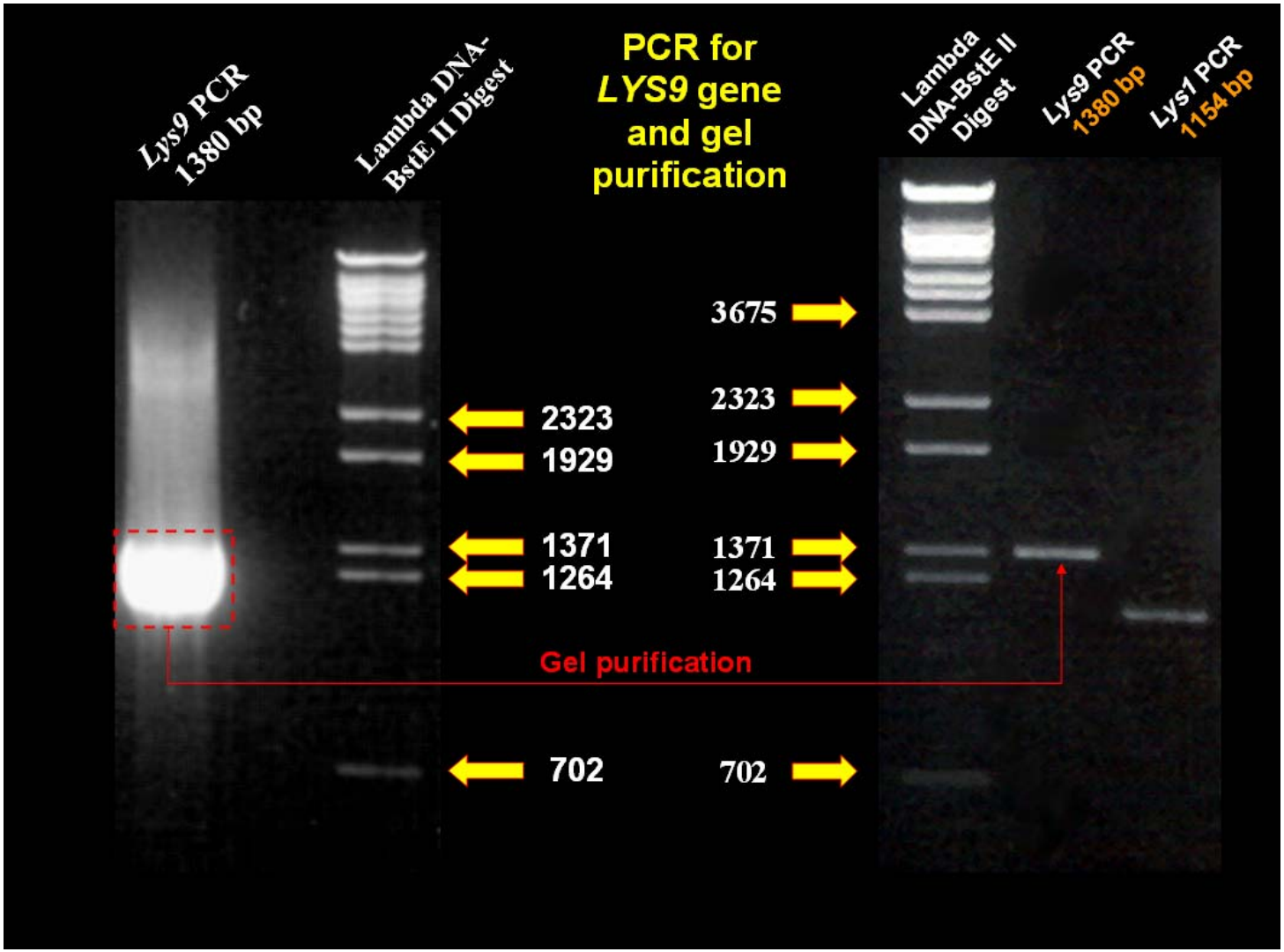

Fig. A-8: PCR for the *LYS9* gene (1341 bp) from *Saccharomyces cerevisiae* and gel purification. The PCR product is 1380 bp.

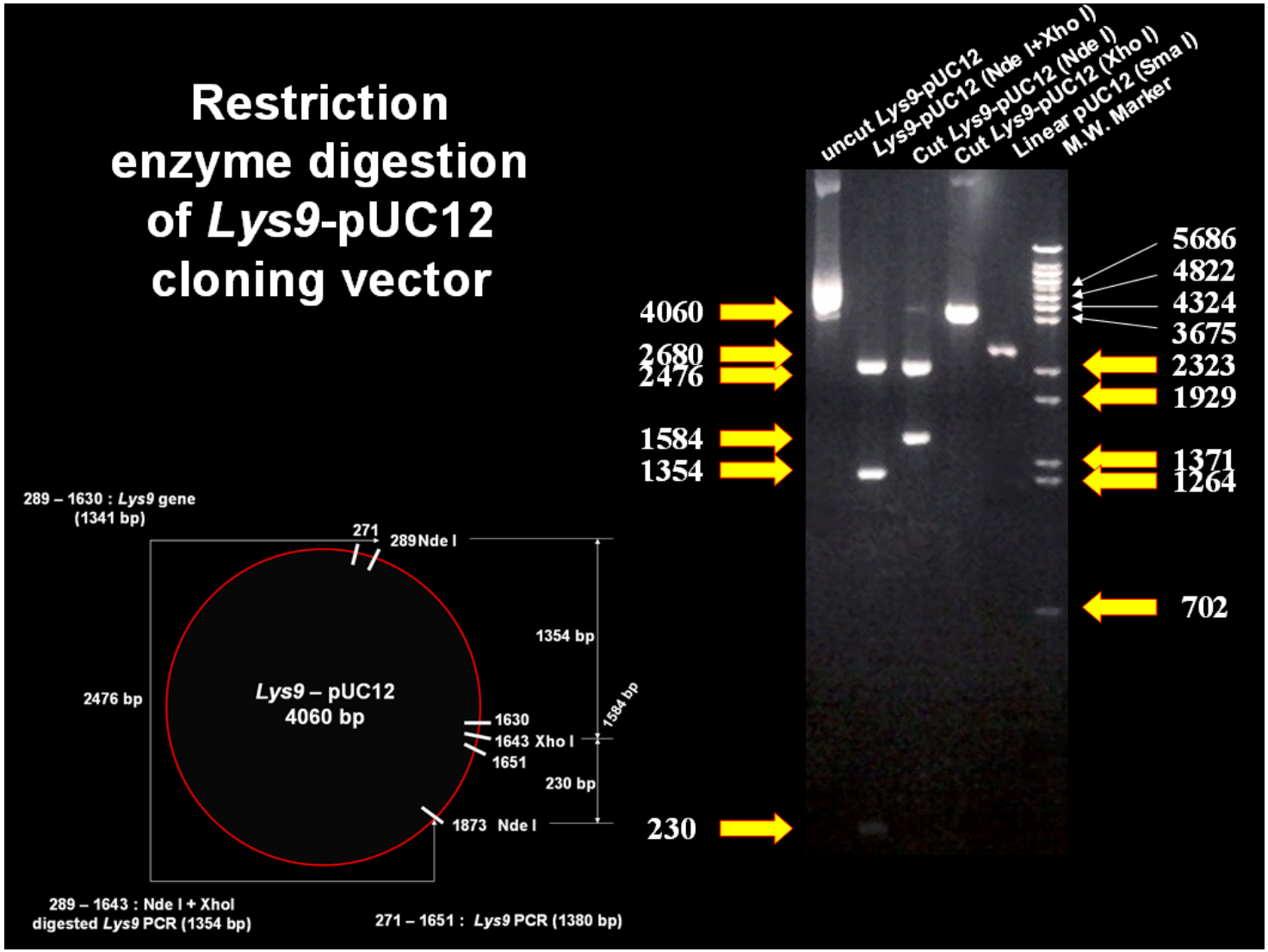

Fig. A-9: *LYS9*-pUC12 cloning vector (4060 bp). *Nde* I and *Xho* I cut *LYS9* segment is 1354 bp.

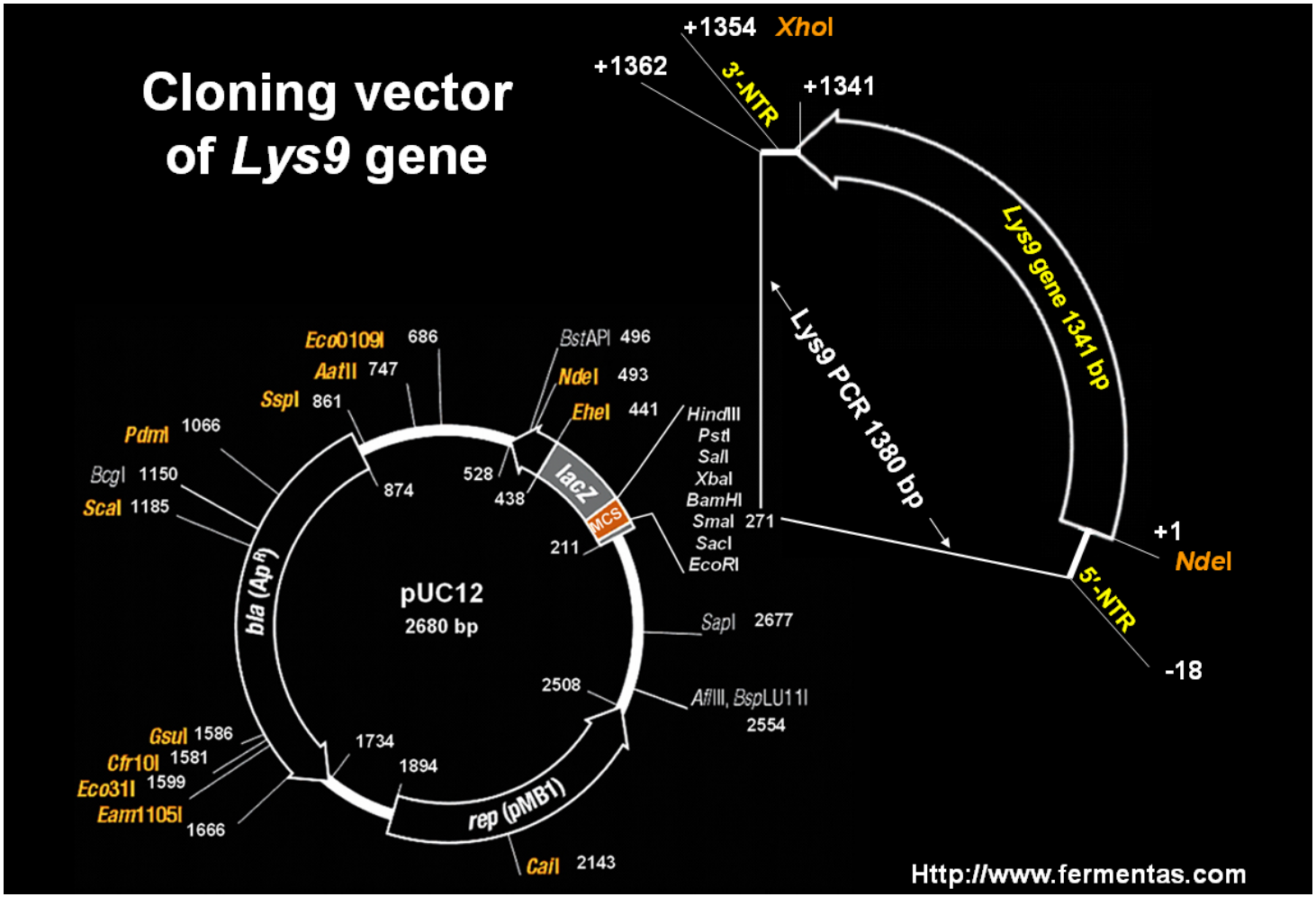

Fig. A-10: Construction of the *LYS9*-pUC12 cloning vector.

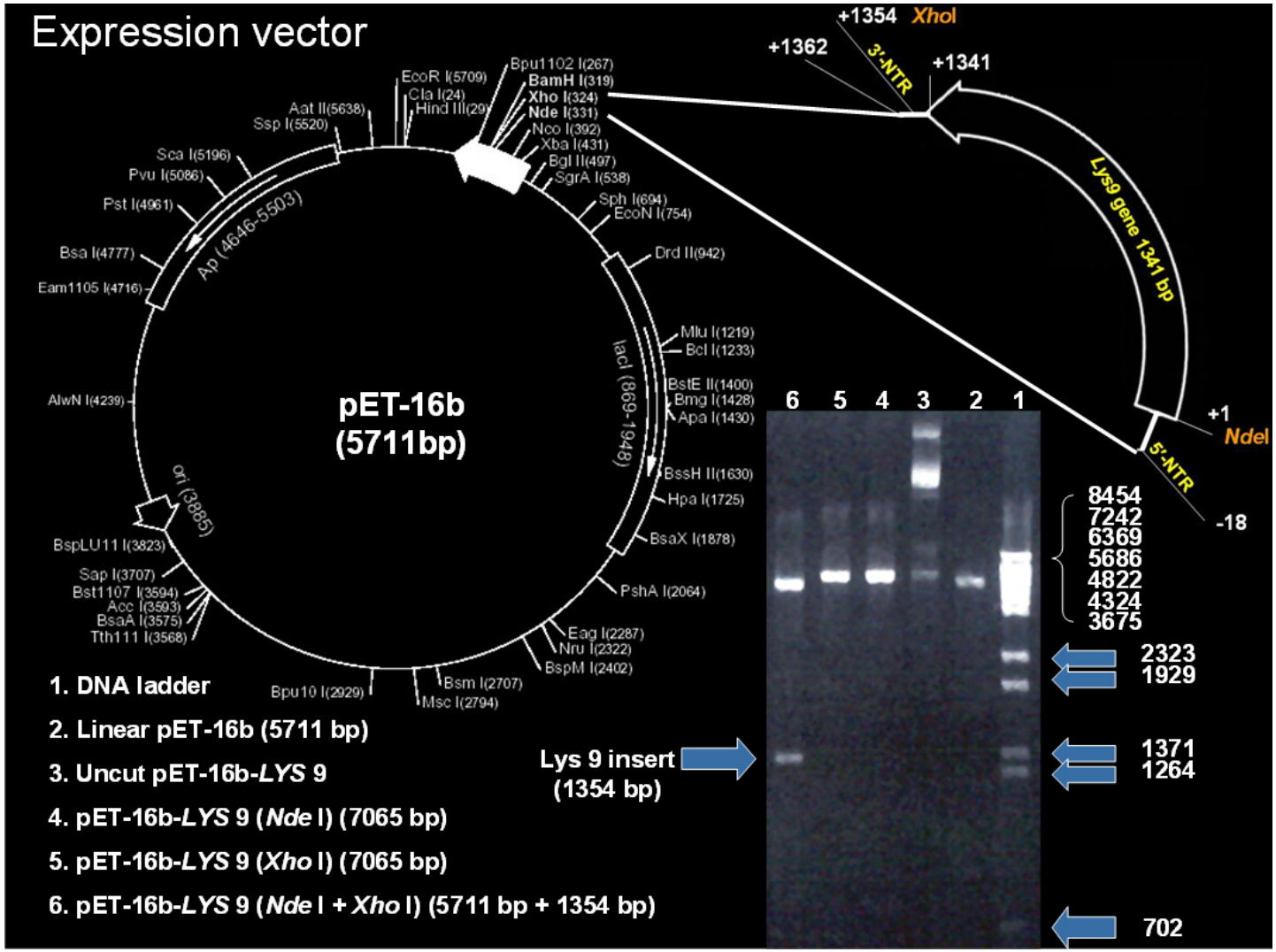

Fig. A-11: ***LYS9*-pET-16b expression vector (7065 bp).** ***Nde* I and *Xho* I cut vector shows the *LYS9* insert (lane 6).**

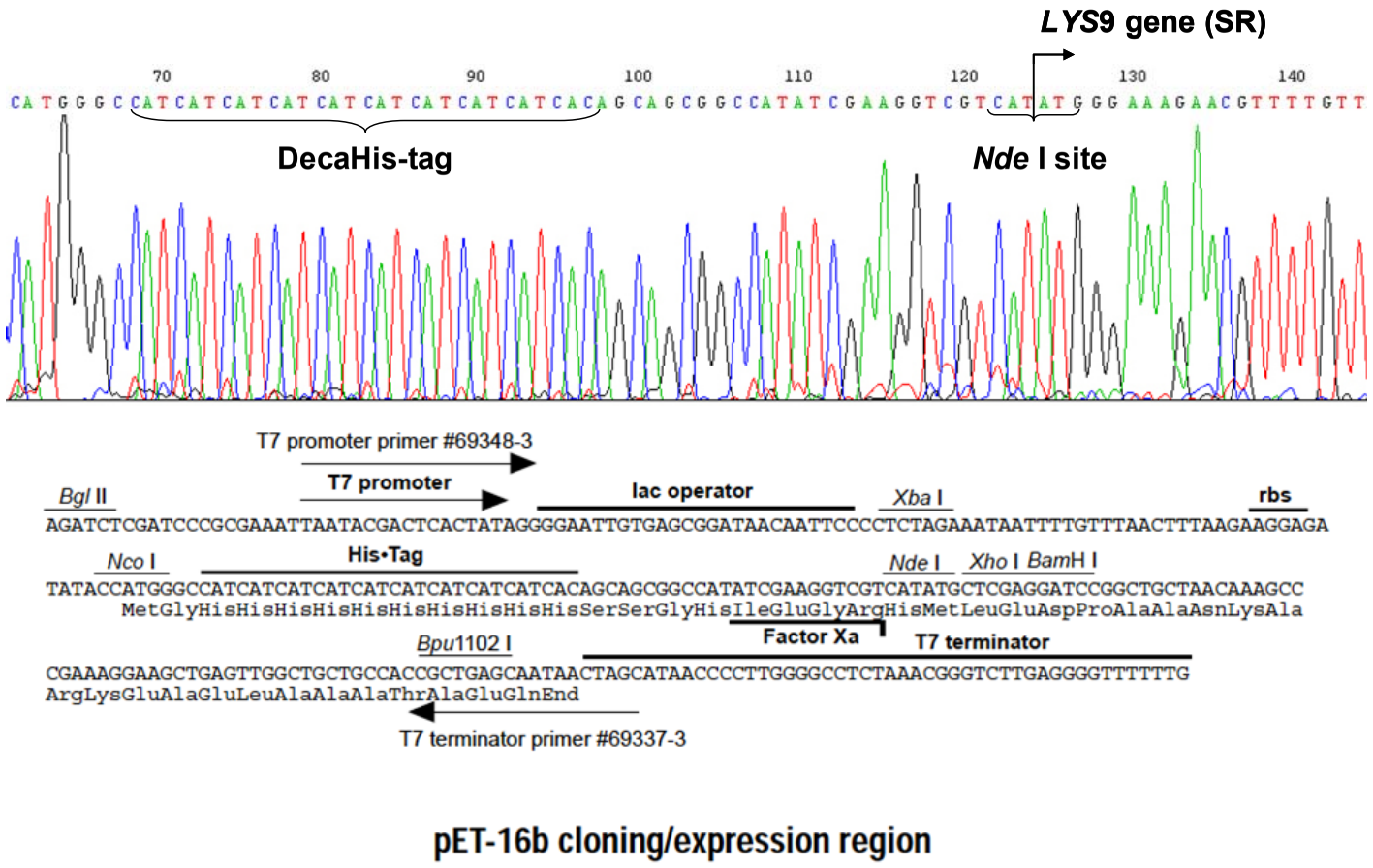

Fig. A-12: Sequencing of the *LYS9* fragment of the *LYS9*-pET-16b expression vector. The sequence of the 21 amino acid in the His-tag is shown. The arrow shows the beginning of the *LYS9* gene.

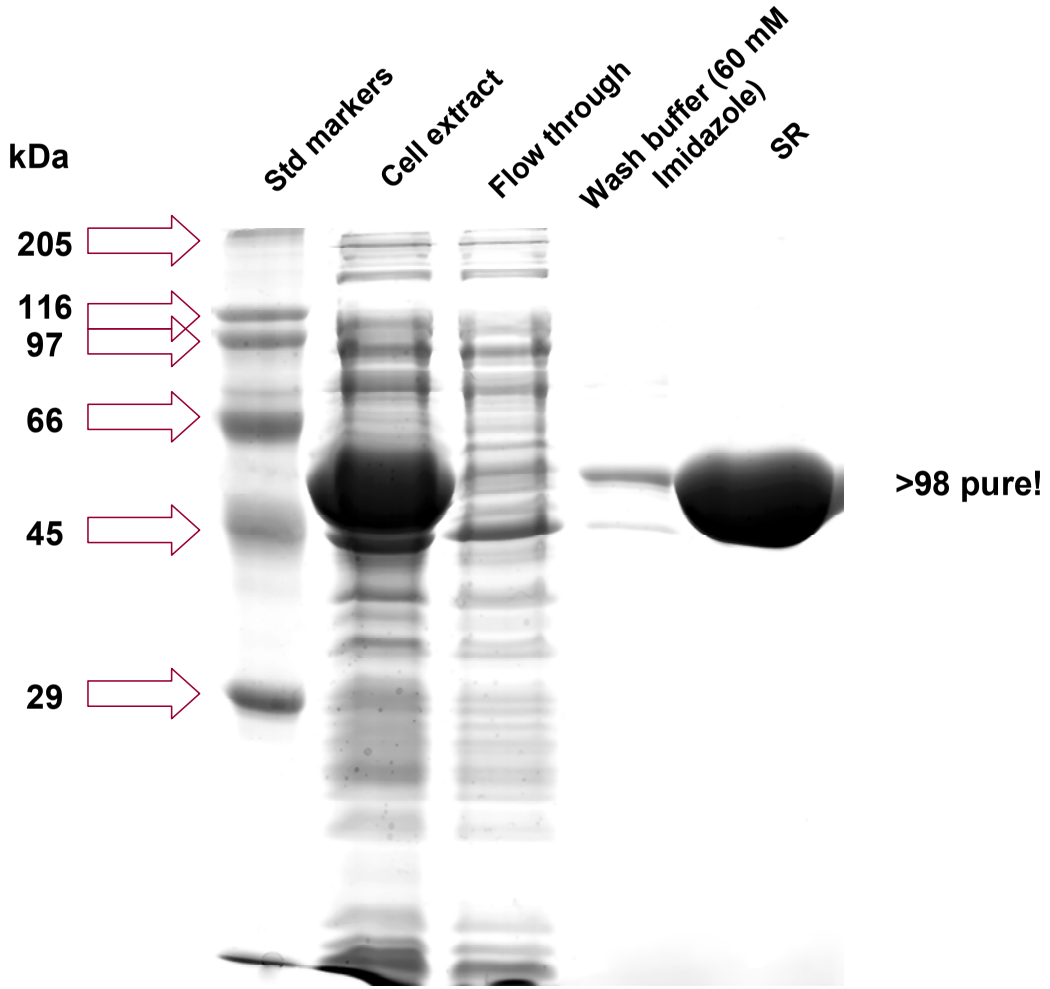

Fig. A-13: Purification of the SR using Ni-NTA resin. The enzyme is more than 98% pure based on the Coomassie-blue staining.

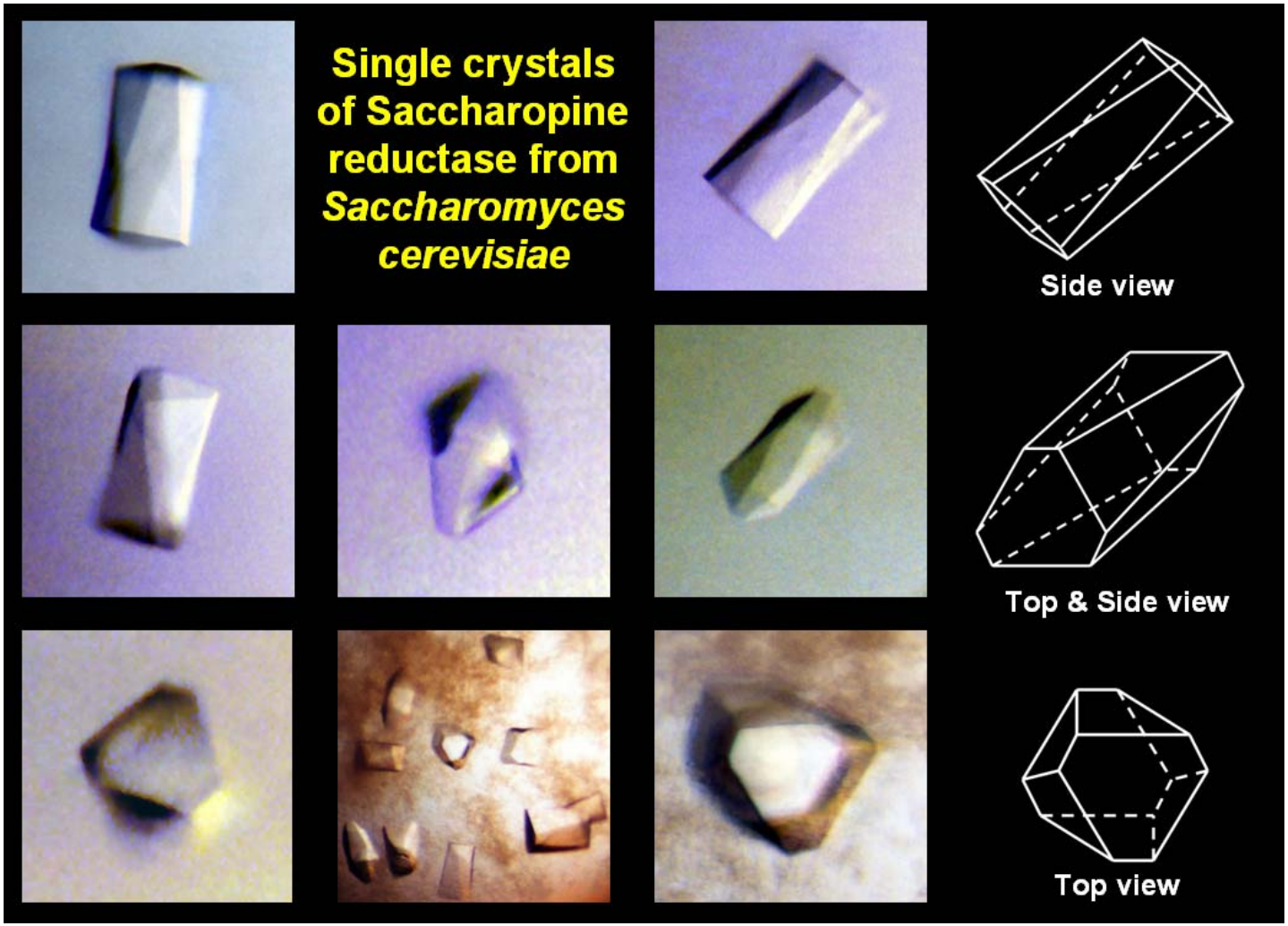

Fig. A-14: Single crystals of SR from *Saccharomyces cerevisiae* from different views. Crystals can be morphologically categorized as truncated hexagonal prism.

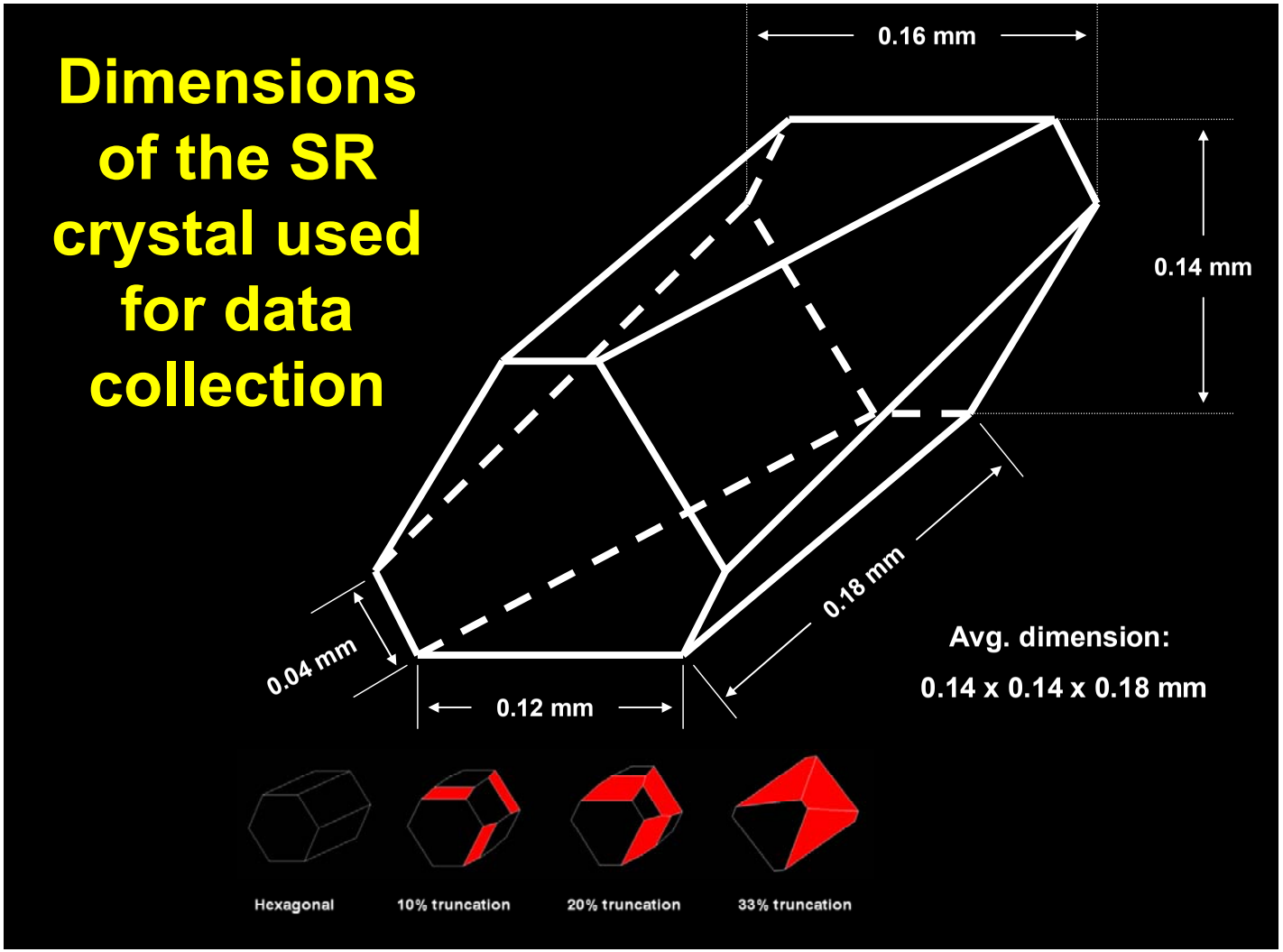

Fig. A-15: Dimensions of the SR crystal used for data collection. Average dimensions of the crystal is 0.14 × 0.14 × 0.18 mm.

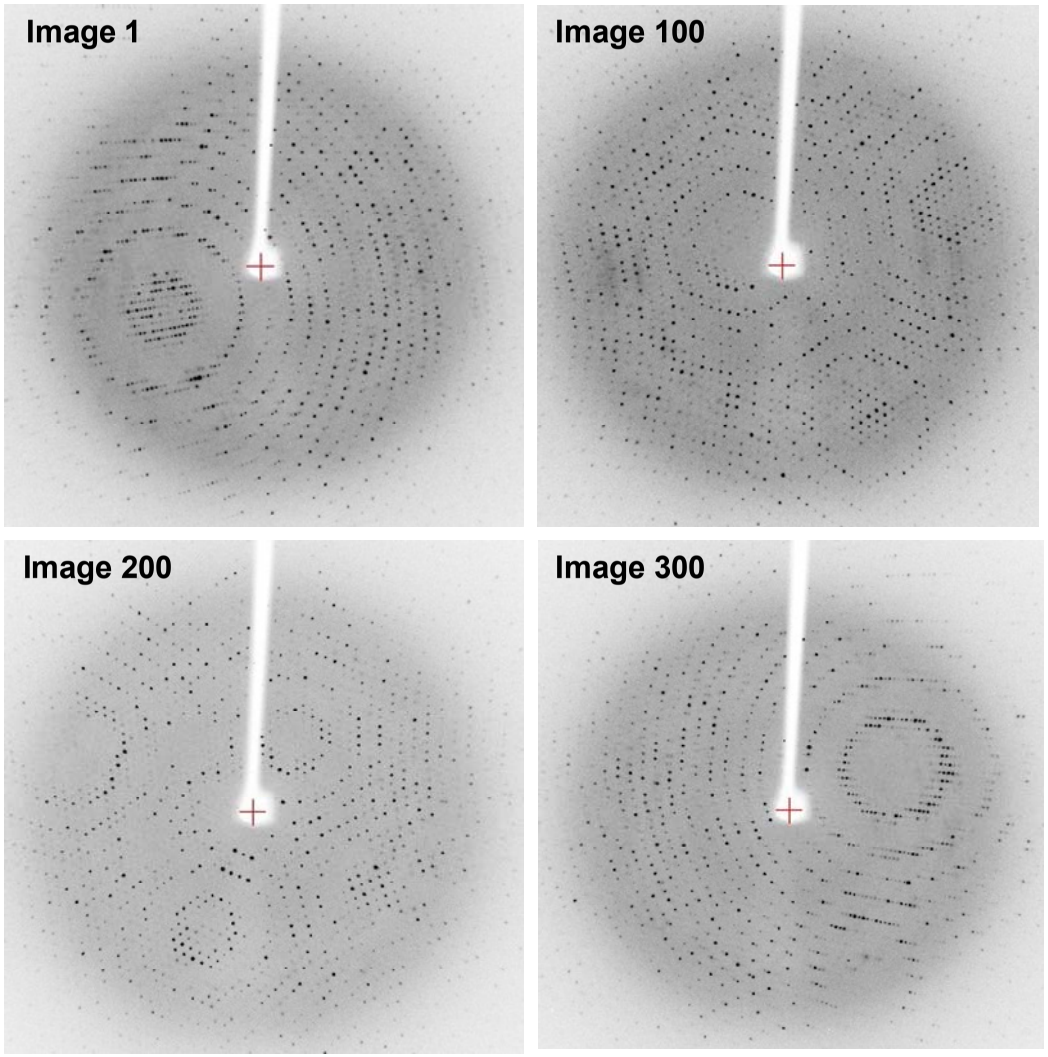

Fig. A-16: Reflection images of the SR crystals taken at different crystal orientations.

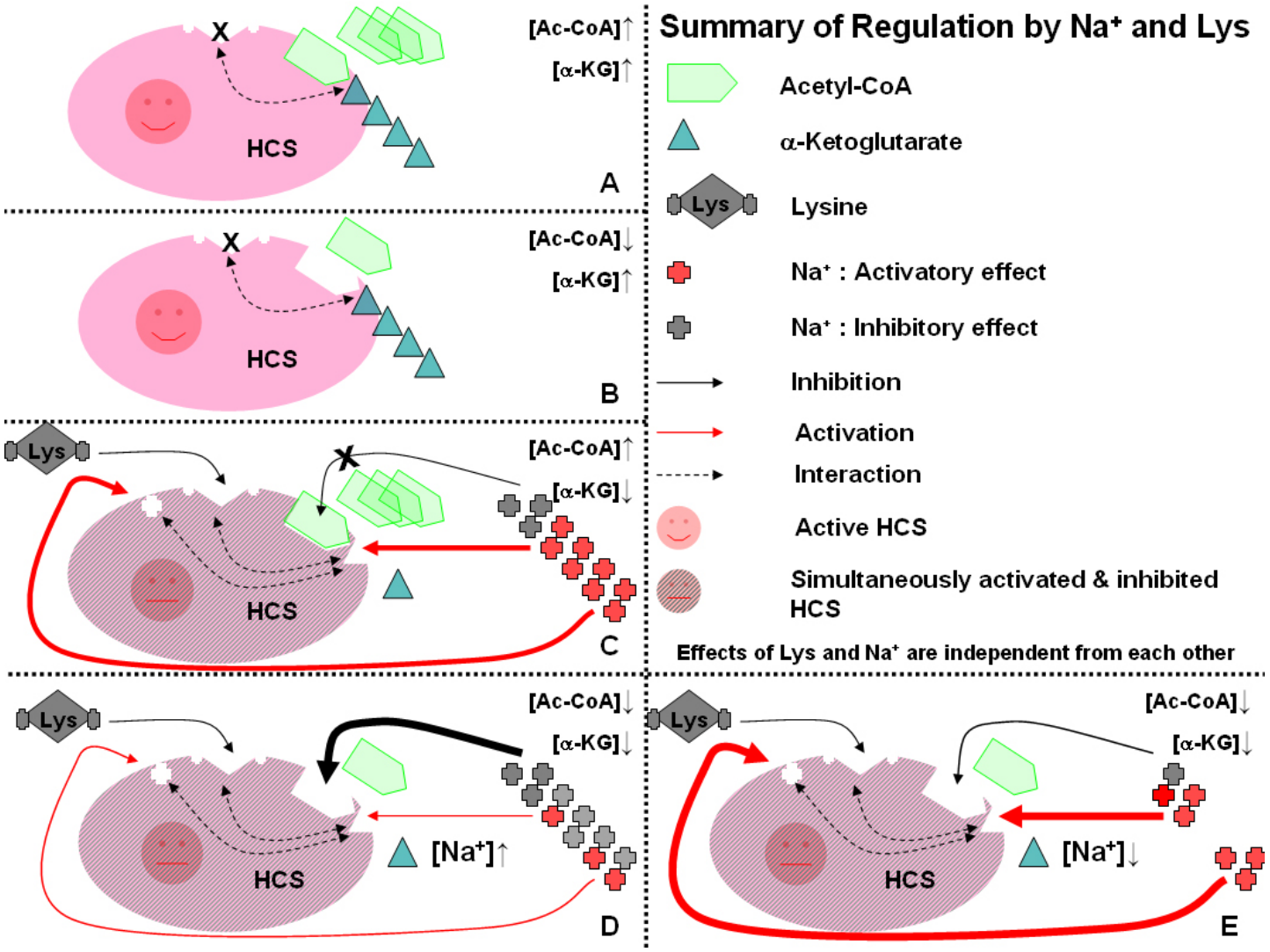

Fig. A-17: Schematic diagram for the regulation mechanism of HCS by Na^+ and lysine.

THE END